

N64-28462

(ACCESSION NUMBER)

255

(PAGES)

NASA CR-54112

(NASA CR OR TMX OR AD NUMBER)

(THRU)

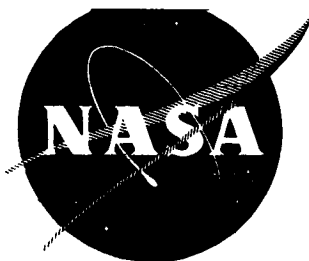
1

(CODE)

27

(CATEGORY)

NASA-CR-54112



DEVELOPMENT OF A 30 KW THREE-PHASE AC ARC JET PROPULSION SYSTEM

FINAL REPORT

Period : January 18, 1963 Thru January 17, 1964

OTS PRICE

XEROX

\$

16.50ph

MICROFILM

\$

2

By

ROBERT RICHTER

prepared for
NATIONAL AERONAUTICS AND SPACE ADMINISTRATION
CONTRACT NAS 3-2523

SPACE POWER AND PROPULSION SECTION
MISSILE AND SPACE DIVISION

GENERAL  ELECTRIC

CINCINNATI, OHIO 45215

NOTICE

This report was prepared as an account of Government sponsored work. Neither the United States, nor the National Aeronautics and Space Administration (NASA), nor any person acting on behalf of NASA:

- A.) Makes any warranty or representation, expressed or implied, with respect to the accuracy, completeness, or usefulness of the information contained in this report, or that the use of any information, apparatus, method, or process disclosed in this report may not infringe privately owned rights; or
- B.) Assumes any liabilities with respect to the use of, or for damages resulting from the use of any information, apparatus, method or process disclosed in this report.

As used above, "person acting on behalf of NASA" includes any employee or contractor of NASA, or employee of such contractor, to the extent that such employee or contractor of NASA, or employee of such contractor prepares, disseminates, or provides access to, any information pursuant to his employment or contract with NASA, or his employment with such contractor.

Requests for copies of this report
should be referred to:

National Aeronautics and Space Administration
Office of Scientific and Technical Information
Washington 25, D.C.
Attention: AFSS-A

CASE FILE COPY

NASA-CR-54112

FINAL REPORT
Covering the period
January 18, 1963 to January 17, 1964

DEVELOPMENT OF A 30 KW THREE-PHASE AC ARC JET PROPULSION SYSTEM

by
Robert Richter

prepared for

NATIONAL AERONAUTICS AND SPACE ADMINISTRATION

August 4, 1964
Contract NAS 3-2523

Program Manager
NASA - Lewis Research Center
Cleveland, Ohio
Mr. H. Ferguson

SPACE POWER AND PROPULSION SECTION
RE-ENTRY SYSTEMS DEPARTMENT
MISSILE AND SPACE DIVISION
GENERAL ELECTRIC COMPANY
CINCINNATI, OHIO 45215

TABLE OF CONTENTS

	<u>Page No.</u>
SUMMARY.....	1
INTRODUCTION.....	3
1. TESTING OF MODIFIED THREE-PHASE PLASMA ARC JET ENGINE.....	5
1.1 Determination of the Effect of Electrode and Nozzle Configuration on the Electrical Characteristic of a Three-Phase Arc Jet Engine.....	5
1.2 Testing of Modified Engine #6.....	10
2. DESIGN OF ADVANCED THREE-PHASE PLASMA ARC JET ENGINE.....	13
2.1 Engine Design.....	13
2.2 Testing of 30 KW Three-Phase Plasma Arc Jet Engine Y16-1.....	25
2.3 Investigation of the Effect of the Magnitude of the Reactive Impedance in the Electrical Circuit on Engine Operation.....	49
2.4 Effect of Firing Order on Arc Operation.....	50
2.5 Performance Testing of the Three-Phase Plasma Arc Jet Engine (Y16-1).....	55
3. THE PLASMA ARC JET ENGINE Y16-2.....	59
3.1 Design of Engine Y16-2.....	59
3.2 Testing of Engine Y16-2.....	59
3.3 Performance Testing of Engine Y16-2.....	70
3.4 Long Duration Operation of Engine Y16-2.....	72
4. LONG DURATION OPERATION OF ENGINE Y16-1.....	77
4.1 Initial Long Duration Test.....	77
4.2 250 Hour Duration Run With Repeated Restarts.....	77
5. SINGLE PHASE ENGINE TESTING.....	89

Table of Contents (continued)

	<u>Page No.</u>
5.1 Modification of the Single Phase Plasma Arc Jet Engine Facility.....	89
5.2 Checkout Testing of Single Phase Plasma Arc Jet Engine.....	92
5.3 Design of the Single Phase AC Plasma Arc Jet Engine...	96
5.4 Power Control for an AC Plasma Arc Jet Engine.....	101
5.5 Testing of the Single Phase Arc Jet Engine.....	109
5.6 Conclusions.....	133
6. CONCLUSIONS AND RECOMMENDATIONS FOR FUTURE EFFORTS.....	135
6.1 Conclusions.....	135
6.2 Recommendations.....	136
 APPENDICES	
I. INSTRUMENTATION OF THREE-PHASE PLASMA ARC JET ENGINE FACILITY.....	137
II. EFFECT OF NON-UNIFORM ENERGY DISTRIBUTION IN THE PROPELLANT GAS.....	171
III. ABLATION RATE OF THE ELECTRODES IN A PLASMA ARC JET ENGINE.	177
IV. SELECTION OF OPTIMUM NOZZLE AND ELECTRODE MATERIALS.....	203
V. HEAT CONDUCTION THROUGH THE ELECTRODE.....	207
VI. MAXIMUM HEAT CONDUCTION THROUGH A GAS.....	211
VII. THE PERFORMANCE ANALYSIS OF ENGINE Y16-2.....	215
VIII. 30 KW THREE-PHASE PLASMA ARC JET ENGINE DESIGN.....	221
REFERENCES.....	241

LIST OF ILLUSTRATIONS

<u>Fig. No.</u>		<u>Page No.</u>
1.1	Arc Characteristics of Three-Phase Arc Jet Engines of Different Designs.....	6
1.2	Arc Chamber Configuration and Electrode Setting of Engine #4.....	7
1.3	Electrical Test Data of Engine #4 (Power vs Current).	8
1.4	Arc Voltage and Arc Current of Engine #4.....	9
1.5	Assembly of Engine #6.....	11
1.6	Arc Chamber Configuration and Electrode Setting of Engine #6.....	12
2.1	Original Three-Phase Plasma Arc Jet Engine Design....	14
2.2	Advanced 30 KW Three-Phase Plasma Arc Jet Engine.....	15
2.3	Relation Between Area Ratio, Nozzle Length, and Maximum Divergent Angle for Optimum Nozzle Length....	17
2.4	Parametric Study of Nozzle Configuration.....	18
2.5	Effect of Area Ratio on Specific Impulse and Thermodynamic Efficiency (Nozzle Y16-1).....	19
2.6	Effect of Area Ratio on the Specific Impulse (Nozzle Y16-1).....	20
2.7	Parametric Study of Nozzle Configuration for Engine Y16.....	21
2.8	Parametric Study of Nozzle Configuration for Engine Y16.....	22
2.9	Parametric Study of the Effect of Nozzle Length and Maximum Divergent Angle on the Specific Impulse.....	23
2.10	30 KW Three-Phase Plasma Arc Jet Engine Nozzle.....	24
2.11	30 KW Three-Phase Plasma Arc Jet Engine (Y16-1) - Assembled.....	26
2.12	Exploded View of 30 KW Three-Phase Plasma Arc Jet Engine (Y16-1).....	27

List of Illustrations (continued)

<u>Fig. No.</u>		<u>Page No.</u>
2.13	Advanced 30 KW Three-Phase Plasma Arc Jet Engine (Y16-1, Assembly).....	28
2.14	Arc Chamber Configurations and Electrode Setting of the 30 KW Three-Phase Plasma Arc Jet Engine (Y16-1)..	29
2.15	Electrical System of the Three-Phase Plasma Arc Jet Engine.....	30
2.16	Center Electrodes of Engine Y16-1 (May 17, 1963).....	33
2.17	Converging Section of Nozzle After Testing (Y16-1)...	34
2.18	Electrical Test Data of Engine Y16-1 (Power vs Line Current).....	35
2.19	Electrical Test Data of Engine Y16-1 (May 1963) (Arc Voltage vs Line Current).....	36
2.20	Design Operating Curve for 30 KW Three-Phase Plasma Arc Jet Engine (Y16-1).....	37
2.21	Correlation of Test Data with Analytical Data (Y16-1) (Power vs Arc Chamber Pressure).....	38
2.22	Center Electrodes After 220 Minutes of Continuous Operation and Approximately 4 Hours of Checkout Runs.	41
2.23	Converging Section of 30 KW Three-Phase Plasma Arc Jet Engine Nozzle After 220 Minutes Continuous Operation and Approximately 4 Hours of Checkout Runs (June 14, 1963) (Y16-1).....	42
2.24	Center Electrodes After 500 Minutes of Continuous Oper- ation and Approximately 4 Hours of Checkout Runs (June 24, 1963).....	43
2.25	Converging Section of 30 KW Three-Phase Arc Jet Engine Nozzle After 500 Minutes Continuous Operation and Approximately 4 Hours of Checkout Runs (June 24, 1963)	44
2.26	Diverging Section of 30 KW Three-Phase Plasma Arc Jet Engine Nozzle After 500 Minutes of Continuous Opera- tion and Approximately 4 Hours of Checkout Runs (June 24, 1963).....	45

List of Illustrations (continued)

<u>Fig. No.</u>		<u>Page No.</u>
2.27	Center Electrodes in Their Electrode Holder After 500 Minutes Continuous Operation and Approximately 4 Hours of Checkout Runs (June 24, 1963).....	46
2.28	Ablation Rate of Center Electrodes as a Function of Total Arc Power.....	48
2.29	Effect of Inductance on the Power-Current Relation of a Three-Phase Plasma Arc Jet Engine (Engine #4).....	51
2.30	Effect of Inductance on the Voltage-Current Relations of a Three-Phase Plasma Arc Jet Engine (Engine #4)...	52
2.31	Effect of Inductance on the Relation Between Indicated Voltage and Current (Electrodynamometer Readings, Engine #4).....	53
2.32	Schematic of Electrode Firing.....	54
2.33	Line Currents and Arc Voltages of a Stable Operating Three-Phase Arc Jet Engine.....	56
3.1	Electrodes and Electrode Holder Assemblies of Engines Y16-1 and Y16-2.....	60
3.2	Advanced 30 KW Three-Phase Plasma Arc Jet Engine (Y16-2).....	61
3.3	30 KW Three-Phase Plasma Arc Jet Engine (Y16-2) Assembled.....	62
3.4	30 KW Three-Phase Plasma Arc Jet Engine (Y16-2) Exploded View.....	63
3.5	Y16-2 Electrode Setting (Double Scale).....	66
3.6	Flow Passages in the Y16-2 Engine.....	70
3.7	Vortex Slot Width as a Function of Upstream Critical Pressure for a Flow Rate of 5×10^{-4} lb/sec.....	67
3.8	Electrodes of Engine Y16-2 After 15 Hours Continuous Operation.....	73

List of Illustrations (continued)

<u>Fig. No.</u>		<u>Page No.</u>
3.9	The Instability of Arc Operation in the Y16-2 Three-Phase Plasma Arc Jet Engine Design.....	74
4.1	Ablation Rate as Affected by Currents.....	78
4.2	Center Electrodes of 30 KW Three-Phase Engine After 250 Hours Operation (Y16-1).....	81
4.3	Electrode Tips of 30 KW Three-Phase Engine After 250 Hours Operation (Y16-1).....	81
4.4	Center Electrodes of 30 KW Three-Phase Engine Before Operation (Y16-1).....	82
4.5	Nozzle of 30 KW Three-Phase Engine After 250 Hours Operation (Y16-1).....	83
4.6	Nozzle of 30 KW Three-Phase Engine Before Operation (Y16-1).....	84
4.7	Performance of Engine Y16-1 After 250 Hour Test.....	86
4.8	Operating Points of Y16-1 Engine at Start of 250 Hour Test Run.....	87
4.9	Analytical Predicted Effect of Nozzle Deterioration on the Performance of the Engine Y16-1.....	88
5.1	Electrical System for Single Phase AC Plasma Arc Jet Engine Test Facility.....	90
5.2	Propellant Supply System for Single Phase AC Plasma Arc Jet Engine Test Facility.....	91
5.3	Design Operating Curve for Single Phase Plasma Arc Jet Engine.....	98
5.4	Single Phase AC Plasma Arc Jet Engine.....	99
5.5	Exploded View of Single Phase Plasma Arc Jet Engine...	102
5.6	Single Phase Plasma Arc Jet Engine.....	103
5.7	Arc Characteristic of a DC Plasma Arc Jet Engine.....	104

List of Illustrations (continued)

<u>Fig. No.</u>		<u>Page No.</u>
5.8	Electrical System for Single Phase AC Plasma Arc Jet Engine.....	105
5.9	Hall Effect Device with Meter.....	107
5.10	Automatic Power Level Control for a Single Phase Arc Jet Engine (Step Control Method) Air Cored Reactor System.....	108
5.11	Automatic Power Level Control for a Single Phase Arc Jet Engine (Step Control Method) Saturable Reactor System.....	110
5.12	Electrical System for Single Phase AC Plasma Arc Jet Engine (Saturable Reactor).....	111
5.13	Electrical System for a Three-Phase Plasma Arc Jet Engine.....	112
5.14	Electrical Characteristics of External Impedance Stabilized Arcs.....	113
5.15	Orifice Calibration for Hydrogen (18 mils).....	114
5.16	Inductance - Capacitance Graph for Unity Power Factor.	117
5.17	Power-Current Characteristic of a DC Arc Engine.....	118
5.18	Power-Current Characteristics for an AC Arc Engine....	119
5.19	Ablation Rate of Electrode - Single Phase Engine (AC Data).....	120
5.20	Ablation Rate of Electrode - Single Phase Engine (DC Data).....	122
5.21	Temperature of Electrode and Nozzle Body, 30 mil gap, single phase engine (AC).....	124
5.22	Measured Temperatures of DC Arc Cathode.....	125
5.23	Schematic Diagram of Circuit used for Frequency Testing.....	127

List of Illustrations (continued)

<u>Fig. No.</u>		<u>Page No.</u>
5.24	Effects of Frequency on Electrical Characteristics of an Arc Jet Engine.....	129
5.25	Effect of Frequency on AC Arc Current.....	130
5.26a	Current and Voltage Traces of an AC Arc at Different Frequencies.....	131
5.26b	Current and Voltage Traces of an AC Arc at Different Frequencies.....	132
 <u>APPENDICES</u>		
I.1	Thrust Measuring System.....	138
I.2	Thrust Measuring Device (Side View).....	139
I.3	Schematic of Thrust Measuring System.....	142
I.4	Thrust Measuring Device with Tank Removed (Side View). ..	144
I.5	Thrust Measuring Device Installed in Test Tank with Engine.....	145
I.6	30 KW Three-Phase Plasma Arc Jet Engine Model.....	141
I.7	Radiation Cooled Engine Design Model.....	146
I.8	Model of Thrust Measuring Device.....	147
I.9	Simplified Model of Thrust Measuring Device.....	148
I.10	Relation of Forces Between Electrical Leads for a Current of 150 Amps.....	150
I.11	Calibration of Displacement Transducer of Thrust Measuring Device (August 30, 1963).....	153
I.12	Test Setup for Checking of Currents Effect on the Indicated Displacement of Thrust Measuring Device.....	154
I.13	Test Setup for Determination of the Effect of a Shift of the Center of Gravity of a Plasma Arc Jet Engine on the Thrust Indicator of the Thrust Measuring Device. ..	157

List of Illustrations (continued)

<u>Fig. No.</u>		<u>Page No.</u>
I.14	Effect of Shift of Center of Gravity on the Indicated Thrust Meter Displacement ($W = 18$ lb).....	156
I.15	Propellant Flow Measuring System.....	161
I.16	Calibration Test Setup of Propellant Flow Measuring System.....	163
I.17	Electronic Wattmeter Calibration Circuit.....	165
I.18	Calibration Circuit for the Hall Effect Wattmeter.....	168
I.19	Calibration Curve for Three-Phase Hall Effect Wattmeter System (May 15, 1963).....	169
II.1	Effect of Non-Uniform Energy Distribution in the Exhaust of a Plasma Arc Jet Engine on the Effective Specific Impulse (Stagnation Temperature of Low Energy Hydrogen).....	172
II.2	Effect of Non-Uniform Energy Distribution in the Exhaust of a Plasma Arc Jet Engine on the Effective Specific Impulse (Stagnation Temperature of Low Energy Hydrogen).....	173
II.3	Effect of Non-Uniform Energy Distribution in the Exhaust of a Plasma Arc Jet Engine on the Effective Specific Impulse (Stagnation Temperature of High Energy Hydrogen).....	174
II.4	Effect of Non-Uniform Energy Distribution in the Exhaust of a Plasma Arc Jet Engine on the Effective Specific Impulse (Stagnation Temperature of High Energy Hydrogen).....	175
III.1	Ablation Rate of Center Electrodes as a Function of Total Arc Power.....	178
III.2	Energy Balance at the Cathode.....	179
III.3	Electrical Test Data of Engine Y16-1 (Arc Voltage vs Line Current).....	180
III.4	Ablation Rate of Tungsten Electrodes.....	183

List of Illustrations (continued)

<u>Fig. No.</u>		<u>Page No.</u>
III.5	Evaporation Rate of Tungsten.....	188
III.6	Evaporation Rate of Thoriated Tungsten.....	189
III.7	Electron Emission Rate for Tungsten.....	190
III.8	Electron Emission Rate for Thoriated Tungsten.....	191
III.9	Energy Balance at the Electrode of an AC Arc.....	192
III.10	Ablation Rate of a Tungsten Electrode in an AC Arc at Stagnation Pressure One Atmosphere.....	194
III.11	AC and DC Ablation Rates of the Center Electrodes Three-Phase Engine, Atmospheric Stagnation Pressure...	195
III.12	Ablation Rates of Tungsten and Thoriated Tungsten Electrodes, Three-Phase Engine, Atmospheric Pressure..	197
III.13	Effect of Pressure on Ablation Rate (Tungsten Electrode)	199
III.14	Relative Emission Factor for Tungsten and Tantalum....	200
III.15	Ablation Rates for an AC Arc with Different Size Tungsten Electrodes.....	202
IV.1	Electrodes of Engine Y16-2 After 3 Hours, 19 Minutes Operation.....	206
VII.1	Test Accuracy of Y16-2 Performance Test.....	219
VII.2	Analytically Predicted Performance of Engine Y16-2 Design.....	220

LIST OF TABLES

<u>Table No.</u>		<u>Page No.</u>
1	Voltage Measurements Between Electrodes.....	54
2	Test Data for Engine Y16-1 (September 18, 1963).....	57
3	Effect of Electrode Setting on the Power-Current Relation of Engine Y16-2.....	68
4	Test Data for Engine Y16-2 (October 18, 1963).....	71
5	Restarts During the 250 Hour Duration Run.....	79
6	Test Data of Single Phase Plasma Arc Jet Engine.....	93
7	Test Data of Single Phase Plasma Arc Jet Engine.....	94
8	Test Data of Single Phase Arc Jet Engine.....	95
9	Thermodynamic and Fluid Dynamic Data of Single Phase Plasma Arc Jet Engine.....	97
10	Chemical Composition of Climelt Molybdenum Metal (TZM Molybdenum).....	100
11	Effect of a Shift of Center of Gravity of an 18 lb Weight on the Indicated Displacement of the Thrust Measuring Device.....	155
12	Calibration of Electronic Wattmeter (John Fluke Model 101, VAW Meter, No. 793).....	166
13	Effects of Ambient Pressure on Engine Performance.....	217
14	Test Data of Engine Y16-2 (November 15, 1963) (36.97 mils/0.5 lb).....	218

SUMMARY

28462

This is the final report of the program "Development of a 30 KW Three-Phase AC Arc Jet Propulsion System", performed for the National Aeronautics and Space Administration under Contract NAS 3-2523. The program was executed by the Space Power and Propulsion Section, Re-Entry Systems Department, of the General Electric Company. The period of performance was from 18 January 1963 through 17 January 1964. The NASA Program Manager was Mr. Harold Ferguson, NASA-Lewis Research Center, Cleveland, Ohio.

Author
28462

A 30 kw, three-phase ac hydrogen arc jet engine was designed and operated for 250 hours. The nominal design point was 0.5 lb thrust at 1000 seconds specific impulse. The engine produced a thrust of .57 lb and a specific impulse of 1076 seconds.

After 250 hours and ten subsequent restarts the engine performance in terms of efficiency, thrust and specific impulse had changed by less than five percent.

The participants in this program were Dr. M. L. Bromberg as Program Manager, R. Richter as Project Engineer, B. C. Merten and H. Williams as Test Engineers, and N. P. Jeffries as analyst.

AP-5T

INTRODUCTION

This report presents the results of a research and development program aimed at the development of a 30 kilowatt three-phase ac plasma arc jet engine. The primary objective was to design a 30 kw three-phase engine for operation with hydrogen as propellant performing at a minimum specific impulse of 1000 seconds and a minimum thrust of 0.5 pounds for a minimum duration of 250 hours. To accomplish this goal development work was carried out on many phases of plasma arc jet technology. The following sections of this report will explain the work performed during the overall program.

In Section 1 the operation of a modified three-phase plasma arc jet engine design is discussed. This was an interim experimental investigation necessitated by experience gained from operating the first generation of three-phase engines. This engine was later in the program superseded by the advanced engines Y16-1 and Y16-2.

A complete discussion of Engine Y16-1 is given in Section 2. The design, checkout testing, modifications and performance testing are presented. This engine was ultimately used to achieve the stated goals of the program, as will be shown in Section 4.

In Section 3, Engine Y16-2 is discussed. This engine is similar to Engine Y16-1 except that larger electrodes are used. It was expected that this engine would have a considerably longer lifetime than engine Y16-1 since the lifetime of a three-phase plasma arc jet engine is determined by the extent of electrode erosion. An unexpected instability in the arc operation that occurred with this engine is discussed.

In Section 4, the long duration engine test is described. The engine performed for 250 hours at values greater than 1000 seconds specific impulse and 0.5 lb thrust at 30 kw power. Shutdown was voluntary. The engine was restarted a number of times thereafter with no decrease in performance.

In Section 5, a single phase ac plasma arc jet engine is described. This engine was designed to operate with ac or dc under a wide range of conditions. The test facility for this engine is described and the tests performed are presented. The purpose of this investigation was to explore basic arc phenomena so that the information gained therefrom could be applied to improve the design of the three-phase engine. This sub program was carried out with beneficial results for the overall program.

The appendices of this report present a number of technical efforts which were carried out in support of the main goals of the program. Appendix I describes the instrumentation in support of the three-phase engine operation. The survey of the effect of non-uniform energy distribution in the exhaust is presented in Appendix II. This is followed by an initial attempt to determine the parameters that affect the ablation rate of electrodes. The difference in

Arthur
530

behavior of several materials is discussed in Appendix IV. Consideration of heat conduction through an electrode is given in Appendix V, while the limit of convective heat transfer from the gas to the electrode is investigated in Appendix VI. Performance measurements are evaluated in Appendix VII and the 30 kw three-phase plasma arc jet engine is presented in Appendix VIII.

1. TESTING OF MODIFIED THREE-PHASE PLASMA ARC JET ENGINES

Several modified three-phase plasma arc jet engines were tested to obtain data for the redesign of a 30 kw three-phase engine. These engines, when operated in their original configuration, exhibited a voltage-current relation with a rather strong effect of the current on the arc voltage. This unfavorable arc characteristic is shown in Fig. 1.1. To stabilize an arc with a steep negative slope a large external impedance is required. This, in turn, calls for a high supply voltage for the system. It had been observed that changes in the gap setting between the electrodes could improve the arc characteristic. Two existing engines were modified to investigate the effect of the physical configuration of the arc chamber on the arc characteristic.

Engine #4 with two 1/4 inch diameter center electrodes was made first. The second engine, #6, had two 3/8 inch diameter center electrodes. This engine had been manufactured after it had become apparent that 1/4 inch diameter tungsten electrodes would not be heavy enough to carry the current load of 150 amp at 30 kw power.

1.1 Determination of the Effect of Electrode and Nozzle Configuration on the Electrical Characteristic of a Three-Phase Arc Jet Engine

An existing 30 kw three-phase plasma arc jet engine (engine #4) was modified by enlarging the constrictor entrance and moving the center electrodes into the converging section of the constrictor. This new configuration is indicated in Fig. 1.2. The test results were very encouraging. The indications were that it is possible to flatten the arc characteristic of the engine such that the effective arc voltage becomes almost independent of the current. The test data obtained with this configuration are shown in Figs. 1.3 and 1.4. The effective arc voltage which is calculated from the relation $P/\sqrt{3} \times I = V$ varied only between 111 and 120 volts over a wide range of power and current. The arc voltages, A-B, B-C, and A-C were measured by the electrodynamicometer voltmeter which has been calibrated for a sinusoidal voltage. They are apparently distinctly dependent on the current. This difference between the effective arc voltage and the arc voltage measured by an electrodynamicometer voltmeter indicates that the arc voltage shape is affected by the current and power level.

Initially, the engine was operated only up to a power level of 24 kw. There were reasons to believe that the two center electrodes which are made of 1/4 inch tungsten rods are too small to carry a load of 150 amps which apparently is required to reach a power input of 30 kw. It was intended to obtain all needed information about the arc characteristic before taking a chance of damaging the engine by going to higher power levels. After all pertinent data had been obtained, the engine was disassembled for inspection. There were no visible signs of ablation either of the center electrodes or of the nozzle.

The engine was reassembled and the power raised to 30 kw. Failure of the engine occurred after a short run. Upon disassembly, it was found that one electrode had lost its tip completely, apparently by a fracture. The damage to

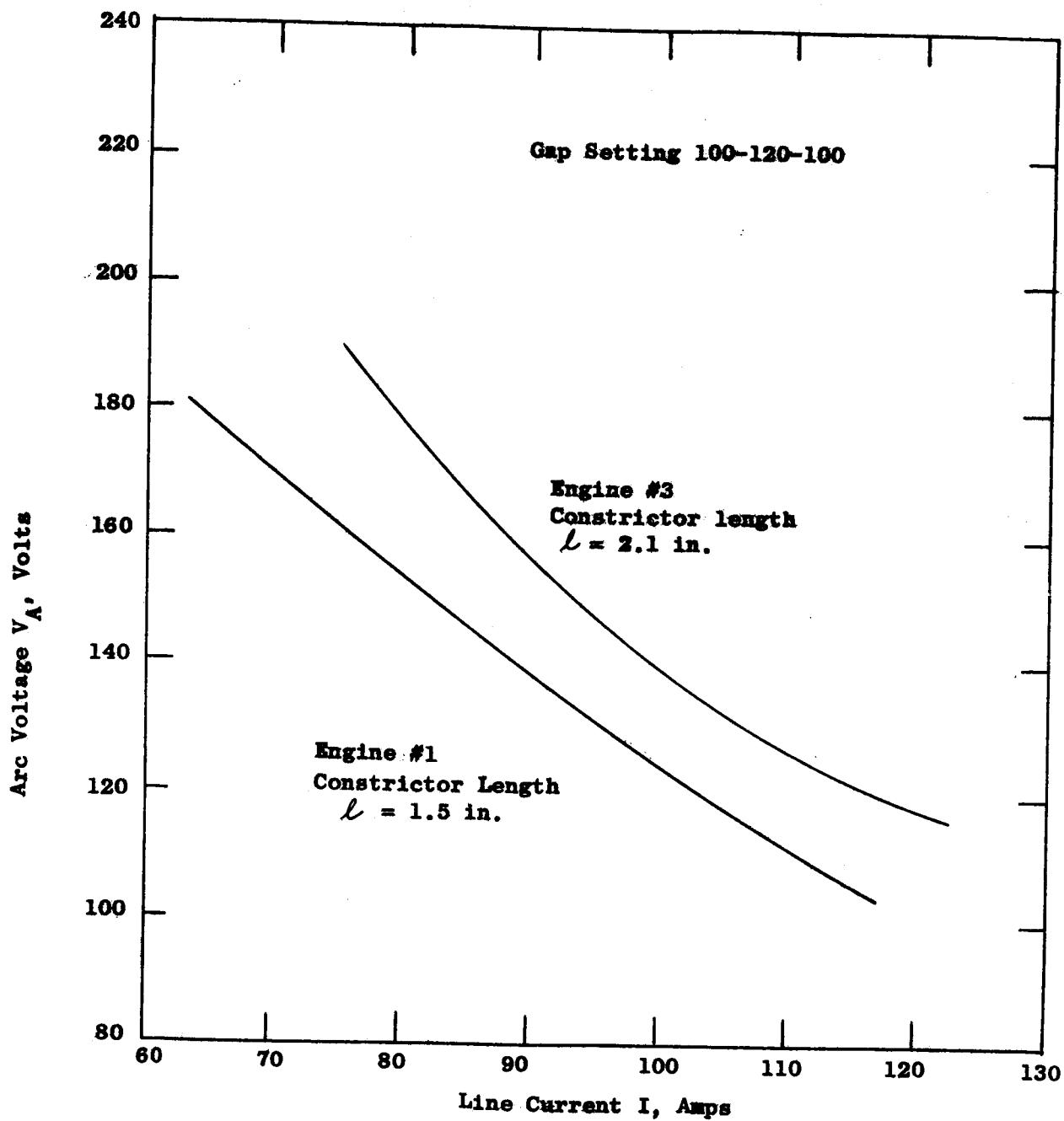


Fig. 1.1.1: Arc Characteristic of Three-Phase Plasma Arc Jet Engines of Different Designs

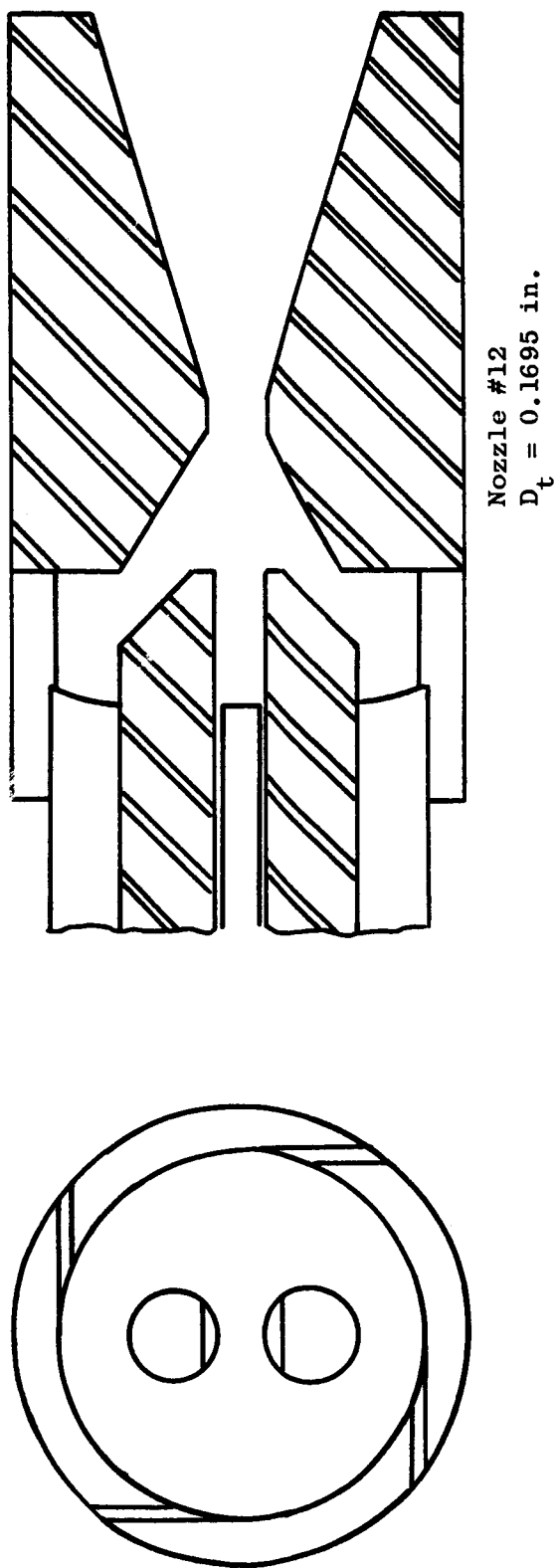


Fig. 1.1.2: Arc Chamber Configuration and Electrode Setting of Engine #4

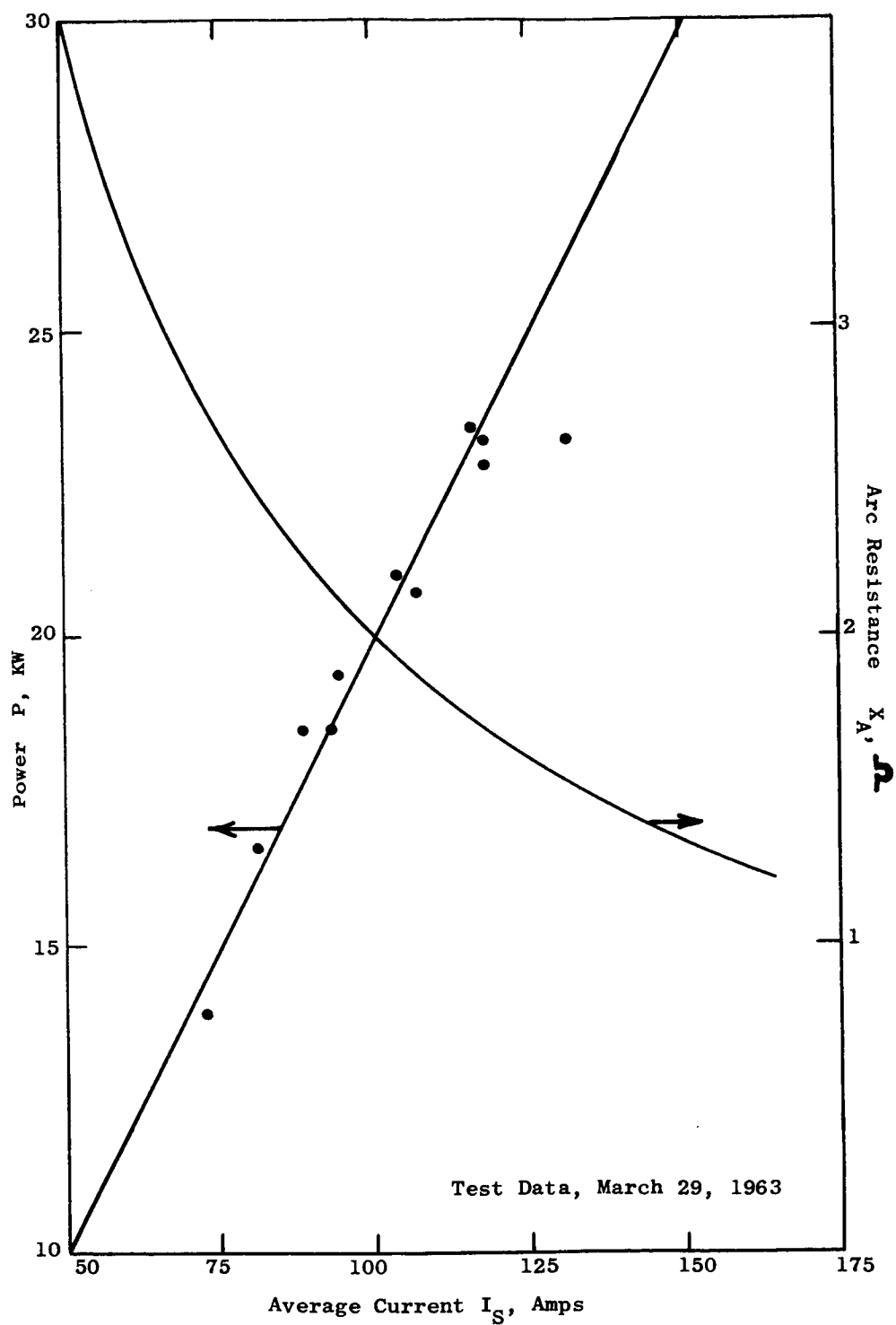


Fig. 1.3: Electrical Test Data of Engine #4 (Power vs Current)

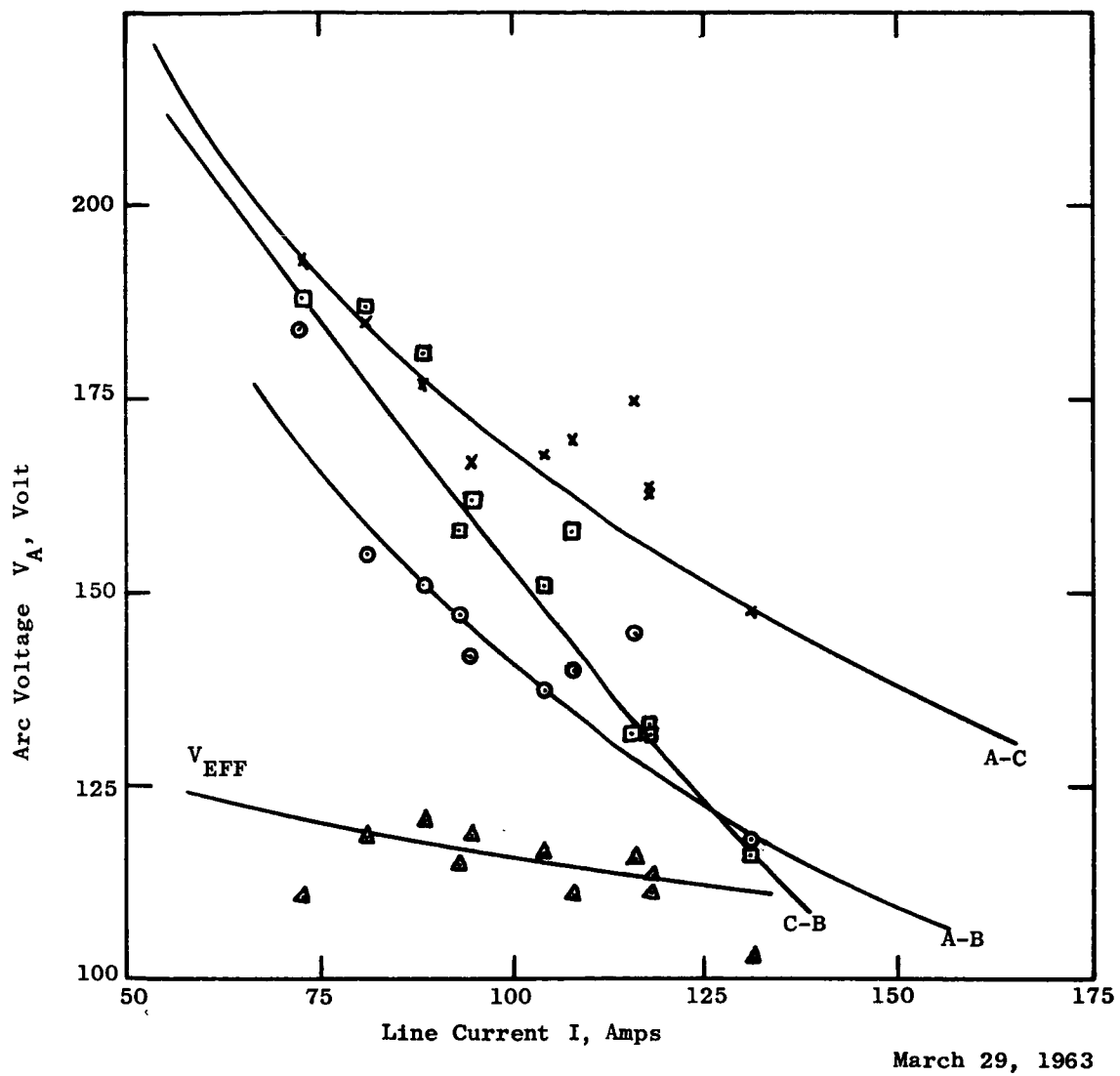


Fig. 1.4: Arc Voltage and Arc Current of Engine #4

the engine was minor. The electrode material which was plugging up the nozzle was easily removed.

1.2 Testing of Modified Engine #6

Engine #6 was built under a previous contract with the center electrodes made of 3/8-inch diameter tungsten rods. To accommodate the larger center electrodes, the nozzle body had to be manufactured from a 1.5-inch diameter tungsten bar. The original configuration of this larger engine is shown in Fig. 1.5. After the successful operation of Engine #4 with the arc chamber configuration which was shown in Fig. 1.2, it was decided to apply the same modification to Engine #6. The arc chamber and electrode configuration resulting from this change is shown in Fig. 1.6.

The program for testing the modified engine was designed to furnish the most information on the operation without running the danger of extensive damage to the engine. The first run lasted only 20 seconds after which the engine was disassembled for inspection. The arc was very diffuse during the short operation as no distinct point of arc attachment could be detected. The second run lasted 130 seconds during which there were occasional indications of ablation. Signs of melting and ablation were visible in the entrance of the restrictor where distinct large areas of arc attachment could be recognized. These molten areas were strong indications that the two arcs had stagnated at the entrance of the constrictor. The stagnation of the two arcs could be attributed to either a weak vortex or no vortex at all. Absence of the vortex could have been due to a loose seat of the vortex sleeve on the nozzle permitting the gas to enter the arc chamber radially. The test was repeated after special attention was given to the seating of the vortex sleeve during assembly. The third run lasted 133 seconds. It ended in a failure which was indicated by signs of ablation and a gradual increase in arc chamber pressure followed by a sudden sharp surge of the pressure. Inspection revealed that the two arcs had stagnated again causing more localized melting. The molten tungsten was dislodged into the throat where it solidified and caused the nozzle area to plug up.

The results obtained by testing Engine #6 indicate that the increase in the nozzle chamber required with the larger center electrodes present a problem with respect to the strength of the vortex required to rotate the arc. It was necessary to test new configurations of the center electrodes. They are described under the design of the three-phase plasma arc jet engine.

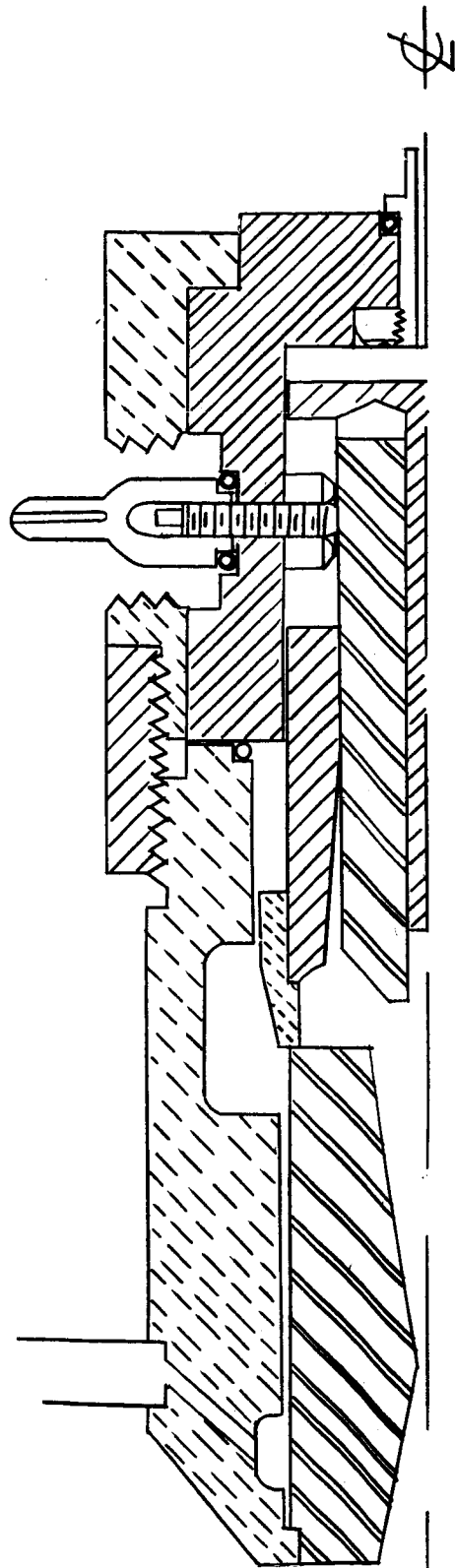
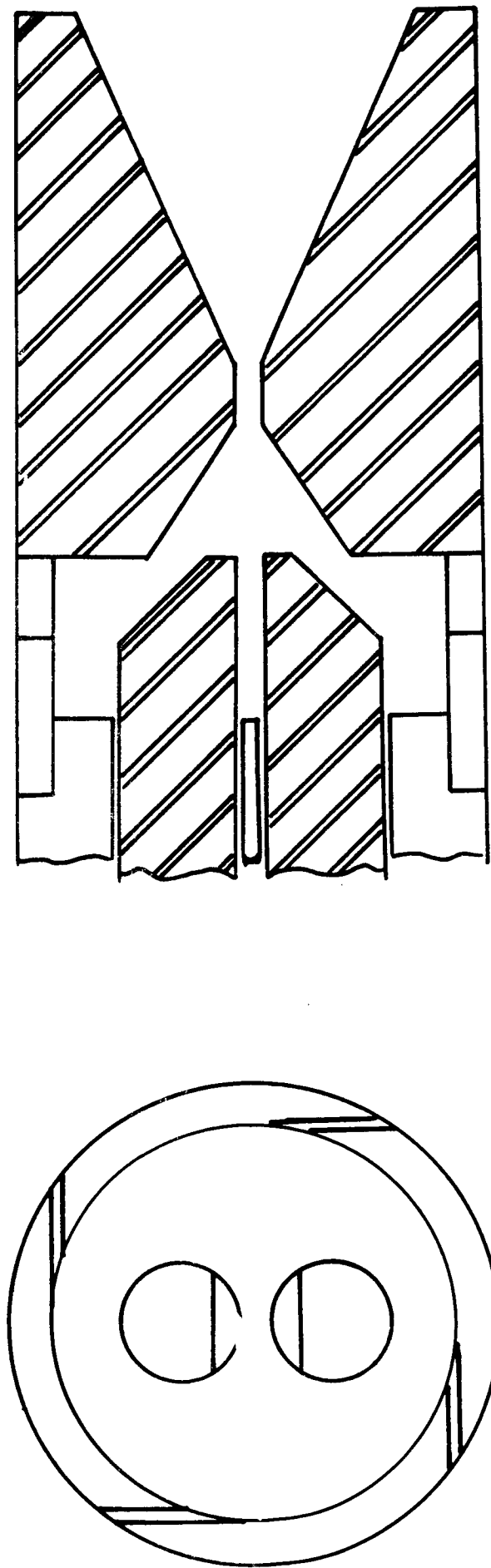


Fig. L.5 - Assembly of engine #6



Arc Chamber of Engine #6

Fig. 1.6: Arc Chamber Configuration and Electrode Setting of Engine #6

2. DESIGN OF ADVANCED THREE-PHASE PLASMA ARC JET ENGINE, Y16-1

2.1 Engine Design

Two basic three-phase plasma arc jet engines have been operated up to this date. The design of the first is shown in Fig. 2.1 while the configuration of the second engine was shown in Fig. 1.5. Difficulties were experienced with both configurations that pointed out that a redesign was indicated.

From the heat transfer analysis it had been determined that for effective regenerative cooling, a single propellant path along the nozzle is sufficient. Based on this consideration, the engine configuration shown in Fig. 2.1 evolved, two major shortcomings of this design became apparent in testing. Several times after sudden breakdowns of the engine there were indications that one of the electrodes had failed. The real cause of engine failure was difficult to determine. The damage to the arc jet engine was such that the cause and result of a failure could not be determined. During the few occasions when the operator was able to terminate a test during the crucial moment of impending total failure, one of the electrodes always showed the loss of a substantial amount of material while the other electrode had an additional tungsten blub on its tip. Tungsten not missing from any part of the nozzle body was found in the nozzle throat.

The above described failure pattern pointed out apparent weakness of the 1/4 inch center electrodes and the need for center electrodes of larger diameter. The engine design shown in Fig. 1.5 incorporates center electrodes made of 3/8 inch tungsten rod. The arc chamber had to be enlarged with the increased size of the center electrodes to prevent arcing from the electrodes to the chamber walls. The arc chambers of Engine #4 and Engine #6 can be compared in Figs. 1.2 and 1.6. It was realized that the enlarged arc chamber of Engine #6 might cause a problem due to a decrease in the vortex strength, which is a function of the vortex slots, the arc chamber size, and the flow rate. However, since absolute values have not been established for the vortex strength required for the rotation of the arc, the feasibility of Engine #6 design had to be established by an experimental evaluation.

Tests of Engines #4 and #6 at power levels above 23 kw also indicated that the temperatures at the main seal exceeded the allowable temperature for the sealing material. This problem can only be resolved by using the incoming propellant for cooling. For this purpose the gas has to enter the engine at the sealing area which is located above the arc chamber. To effect also cooling of the nozzle body by the propellant in such a design, two gas paths are required.

The engine design which evolved from these considerations is shown in Fig. 2.2. The propellant is fed into the rear of the engine and flows through a path in the boron nitride. The heat transfer to the gas from the insulator is not appreciable since the insulator temperature is low and in a tubular path the heat transfer coefficient is inherently low. A relatively cool gas reaches the area of the main seal where the cooling path becomes annular. The propellant flows to the nozzle exit area where it returns in the inner path and enters the arc chamber through the tangential vortex slots in the molybdenum vortex ring.

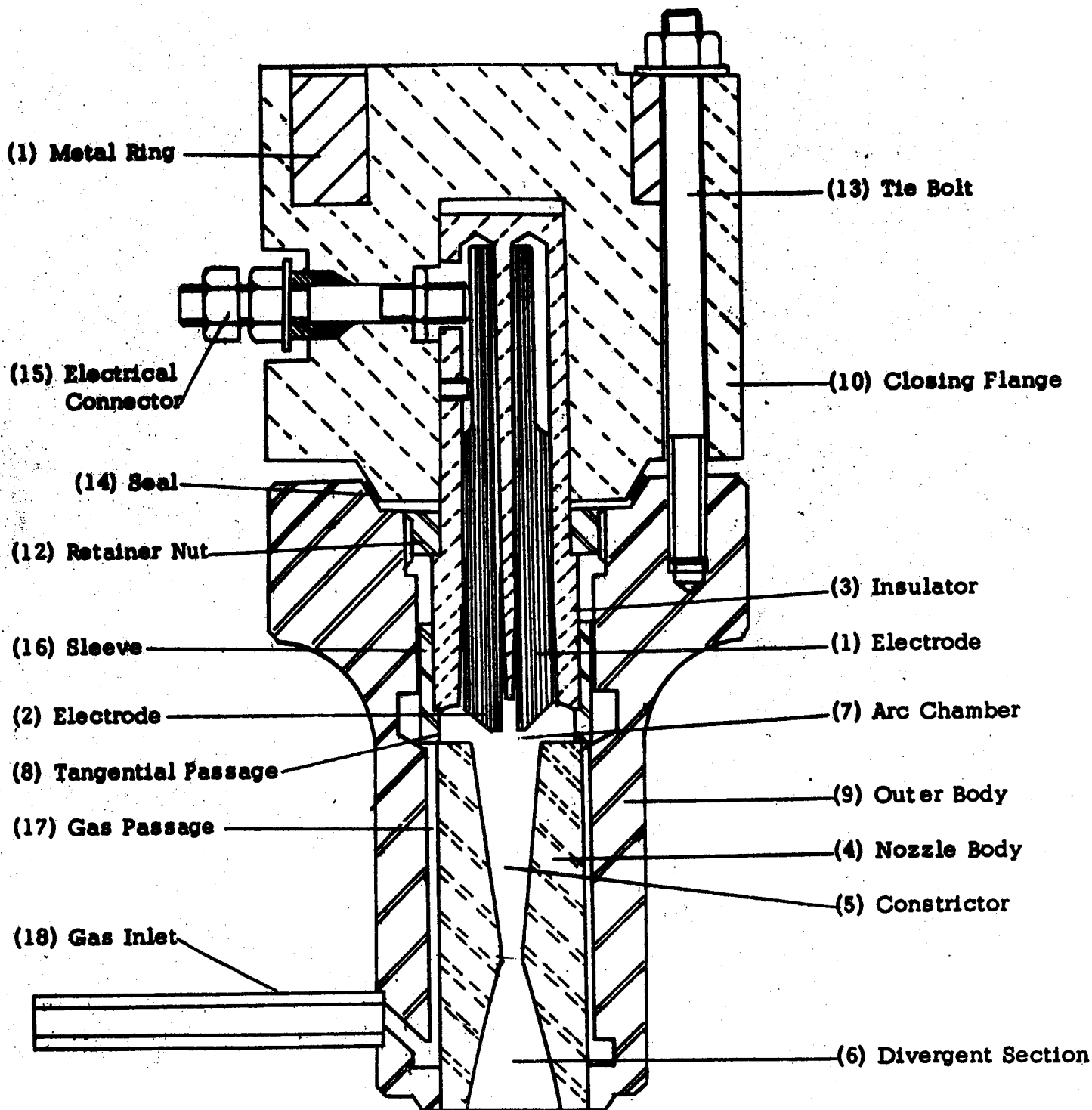


Fig. 2 1. Original Three-Phase Plasma Arc Jet Engine Design.

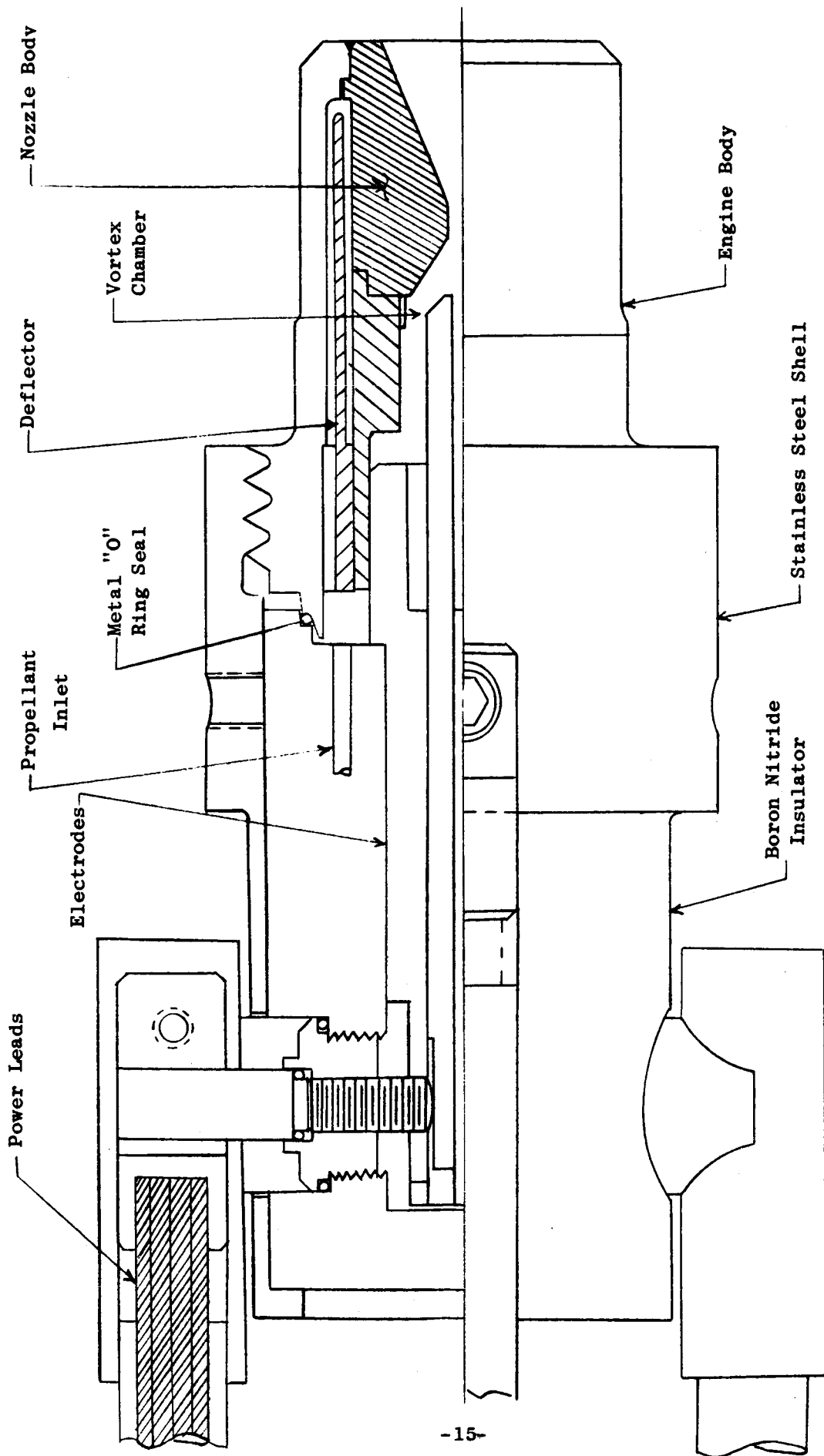


Fig. 2.2: Advanced 30 KW Three-Phase Plasma Arc Jet Engine

Little change has been made in the design of the electrical connections. An electrical connection with a small flat contact is not very desirable because of an inherently high electrical contact resistance and the difficulty in keeping the contact tight during the heating and cooling cycles. Since for the test engines the absolute position of the two center electrodes had not been finalized, it is still desirable to be able to adjust the center electrode position with ease.

2.1.1 Nozzle Design

The nozzle design for the new 30 kw engine is based on a stagnation pressure of one atmosphere and a stagnation temperature of 6400°R. The throat diameter is 0.1685 in. These design values are based on an effective power of 28.5 kw which makes an allowance for a radiation and conduction heat loss of 1.5 kw. The ideal thrust at an ambient pressure of 1 mm Hg is then determined from the ideal thermodynamic data to be 0.52 lb.

The optimum design of the divergent section of the nozzle was obtained from a parametric study. First, the thrust efficiency was determined for a number of maximum divergent angles as a function of the length of the divergent section and area ratio. This study is based on the relations between the area ratio, nozzle length, and maximum divergence angle of optimum nozzle designs for ideal fluids. These relations are shown in Fig. 2.3. The dependency of the thrust efficiency of a real fluid on these parameters is indicated in Fig. 2.4. The thrust efficiency is defined as the ratio between the actual thrust to the ideal thrust.

$$\eta_{TH} = \frac{T_{actual}}{T_{ideal}}$$

Deviations from the ideal thrust are due to under-expansion or over-expansion, momentum loss in the boundary layer, and heat transfer. Under-expansion will occur if the nozzle length is too short for a given maximum divergent angle. The opposite is true for over-expansion. Loss of momentum in the boundary layer increases with boundary layer growth and heat transfer through the nozzle. Hence, there exists a nozzle design point at which the efficiency improvement due to an increased expansion ratio becomes less than the increase in the losses in the boundary layer. This is the point of optimum thrust efficiency which can never reach unity. Assuming an effective nozzle wall temperature of 4000°R which was determined from a heat transfer study, the optimum nozzle efficiency for the stated operating conditions was found to be 91.9%. This maximum efficiency is obtained with an area ratio of 20 which corresponds to a pressure ratio of only 475.33, though the optimum expansion ratio based purely on thermodynamic considerations is 760. In Figs. 2.5 and 2.6 only the effect of under-expansion on the thrust efficiency is shown. A comparison of the data of Fig. 2.4 with the data of Fig. 2.6 gives an indication of the boundary layer effect. To convey an appreciation of the effect of the nozzle wall temperature on the thrust efficiency, Figs. 2.7 and 2.8 are presented. The data of these two parametric studies are based on nozzle wall temperatures of 2000°R and 6000°R. Based on the thrust efficiencies shown in Fig. 2.4 the effective specific impulse at the operating conditions and an ambient pressure of 1 mm Hg is shown in Fig. 2.9 in parametric form. Three nozzle contours are shown in Fig. 2.10. The nozzle contour for an ideal fluid assumes frictionless flow. It has an area ratio of 20. An adjusted nozzle contour is obtained by adding the displacement thickness to the ideal nozzle

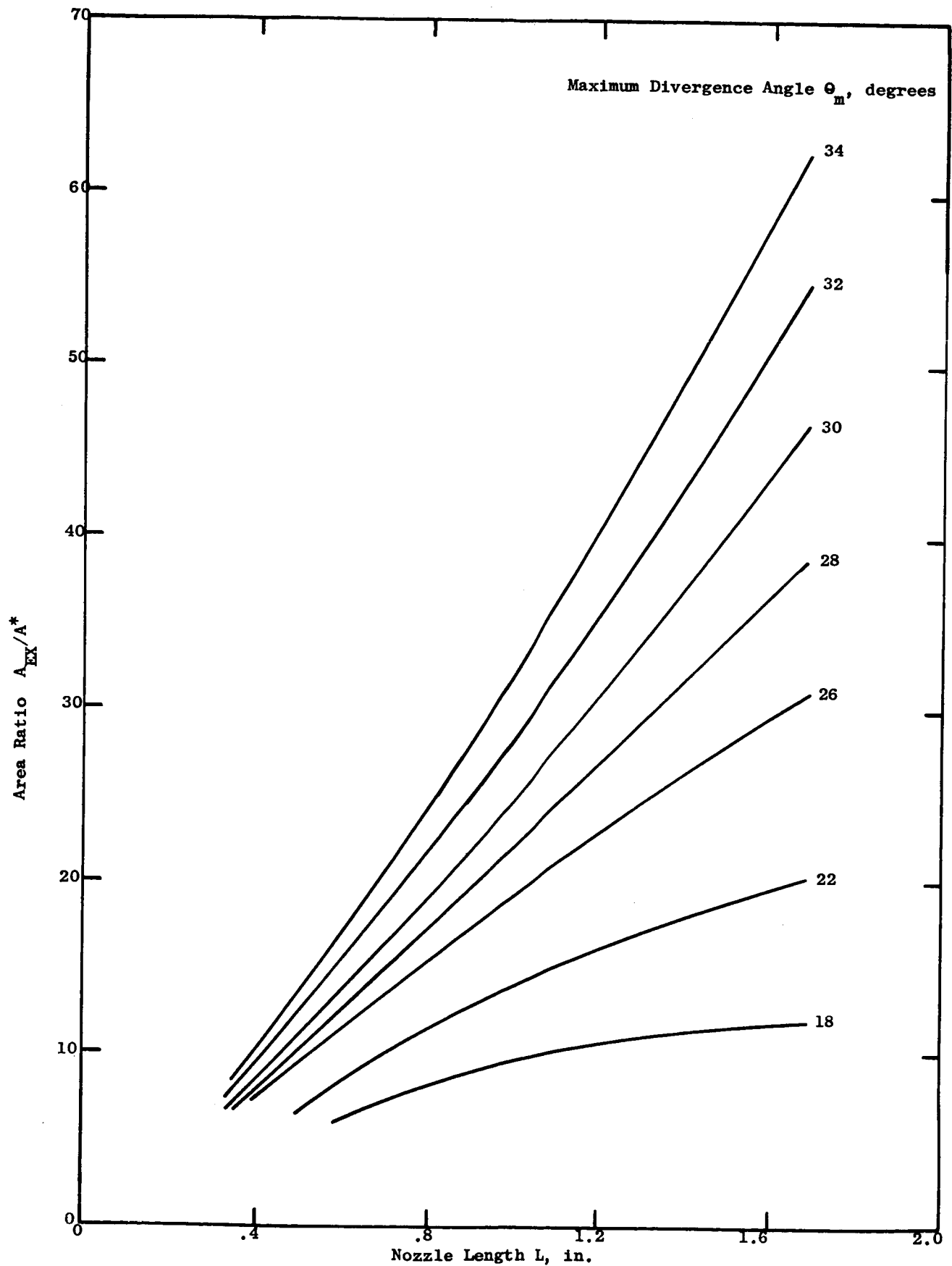


Fig. 2.3 Relation Between Area Ratio, Nozzle Length, and Maximum Divergent Angle for Optimum Nozzle Design

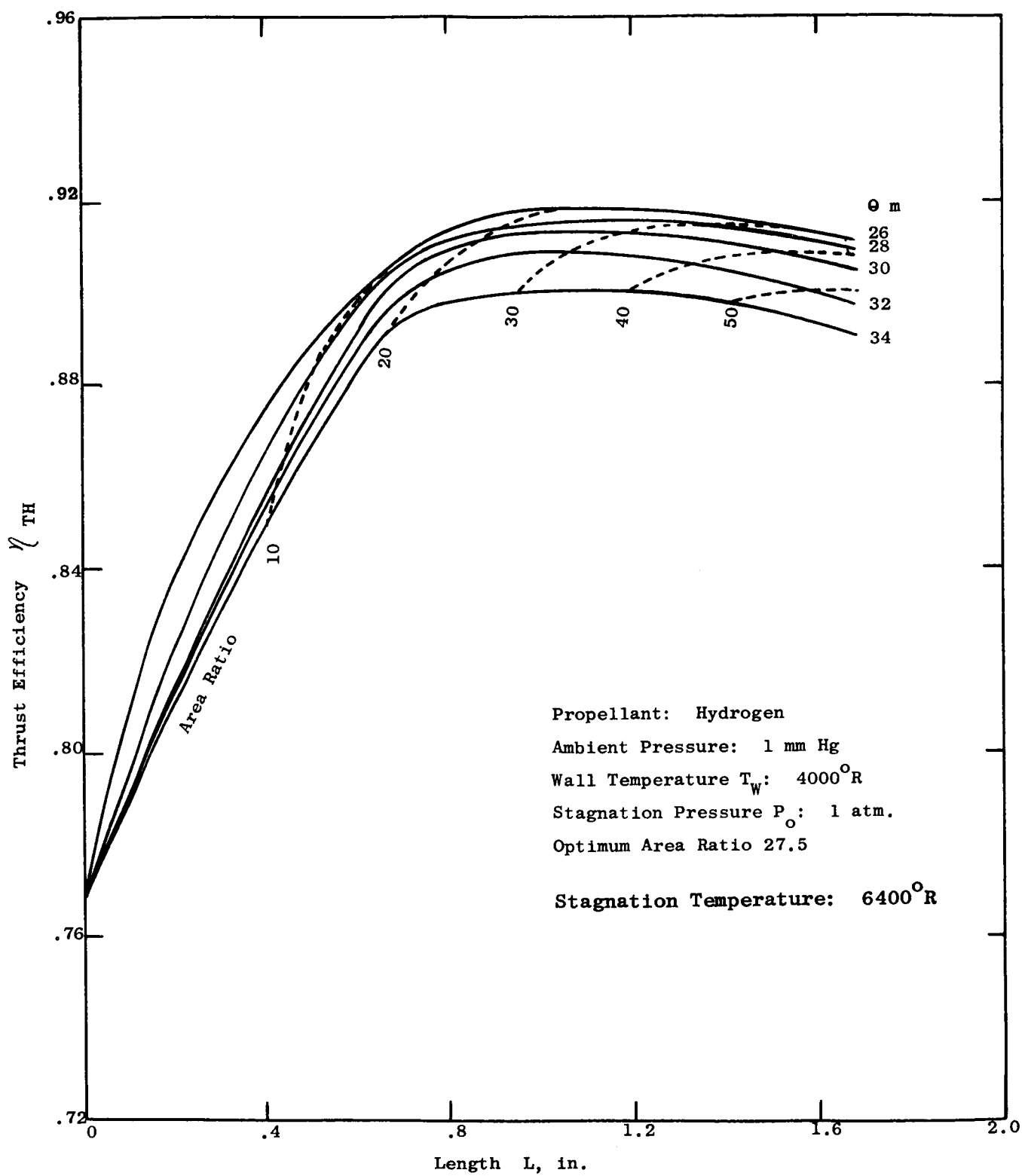


Fig. 2.4: Parametric Study of Nozzle Configuration

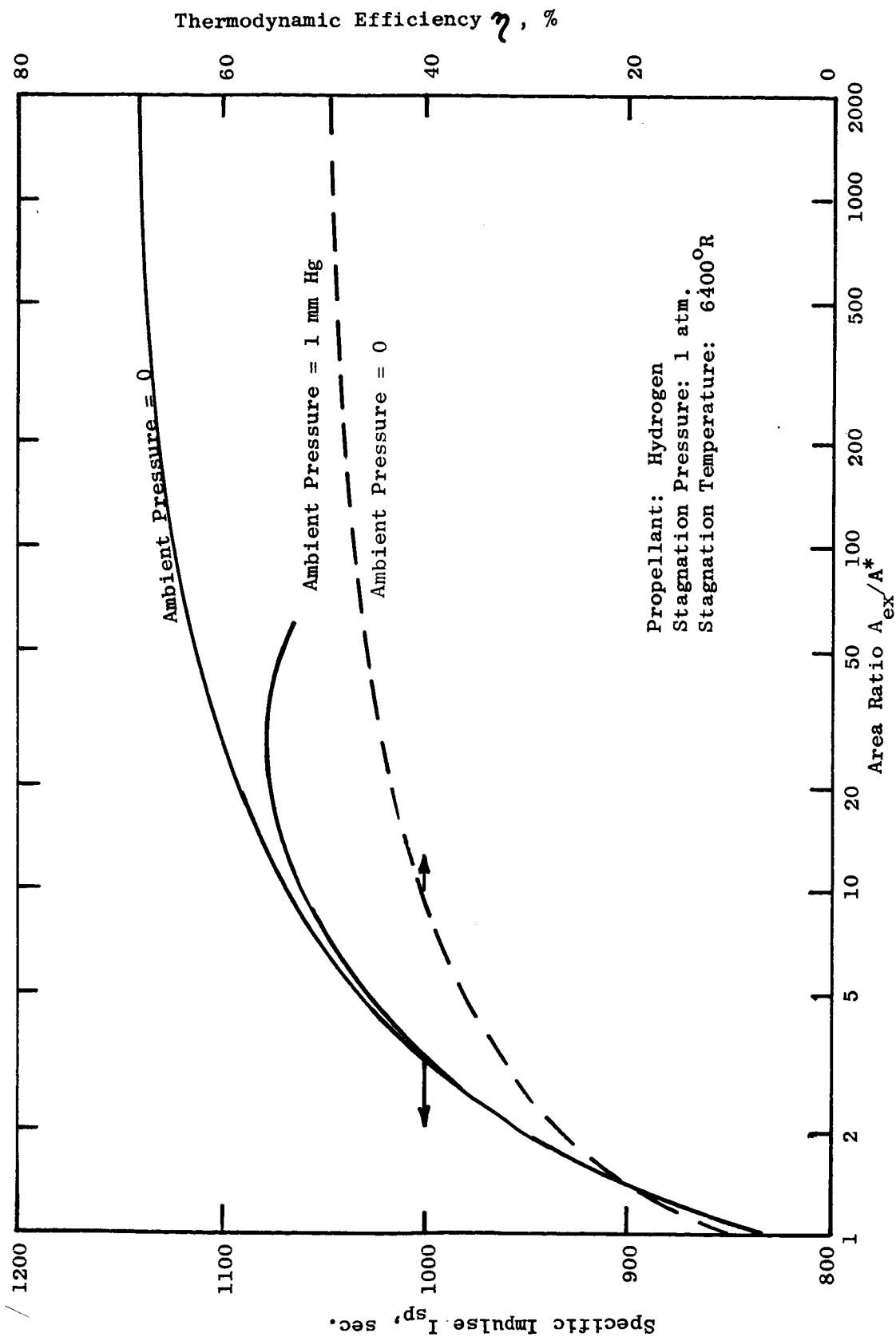


Fig. 2.5: Effect of Area Ratio on Specific Impulse and Thermodynamic Efficiency (Nozzle Y16-1)

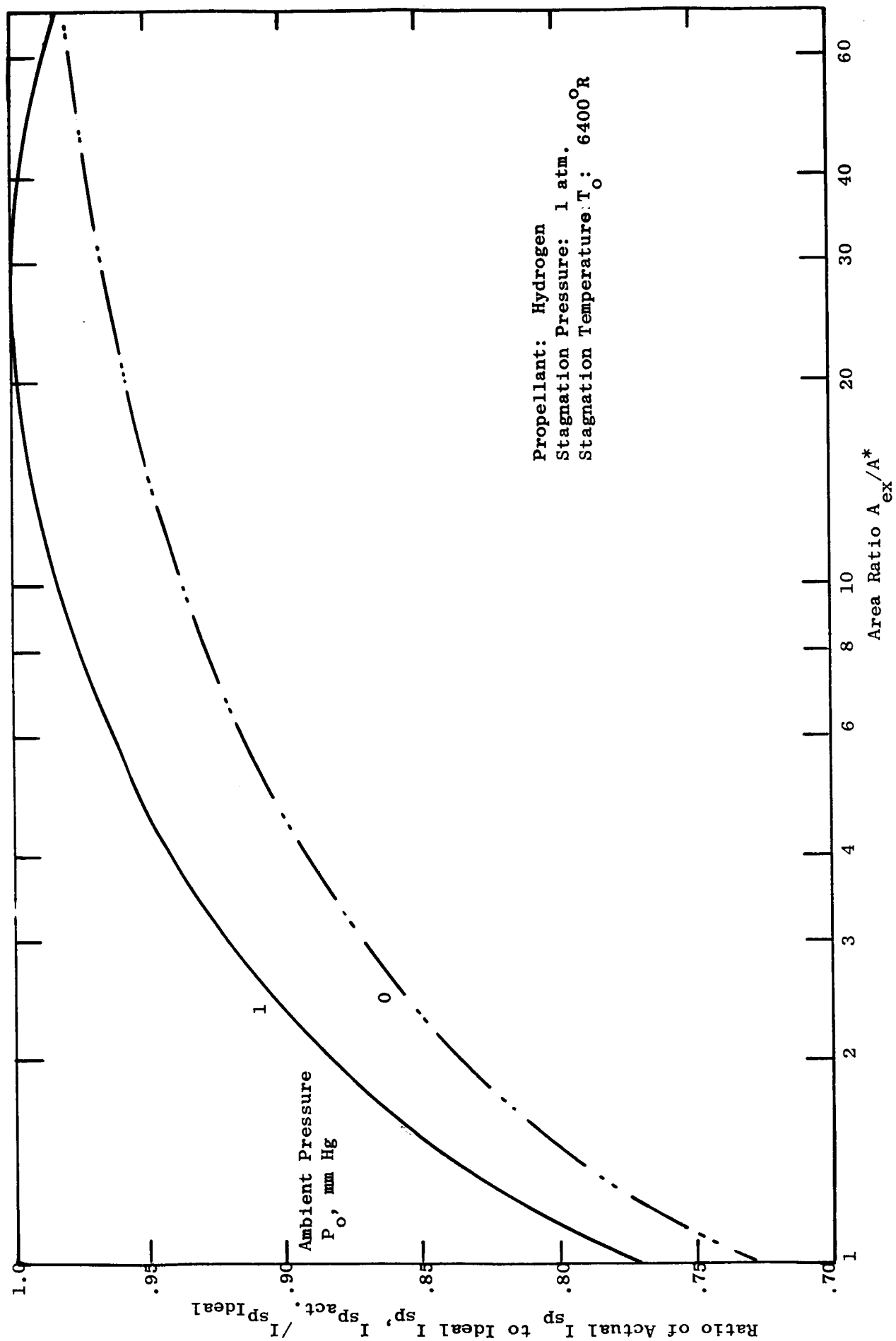


Fig. 2.6: Effect of Area Ratio on the Specific Impulse (Nozzle Y16-1)

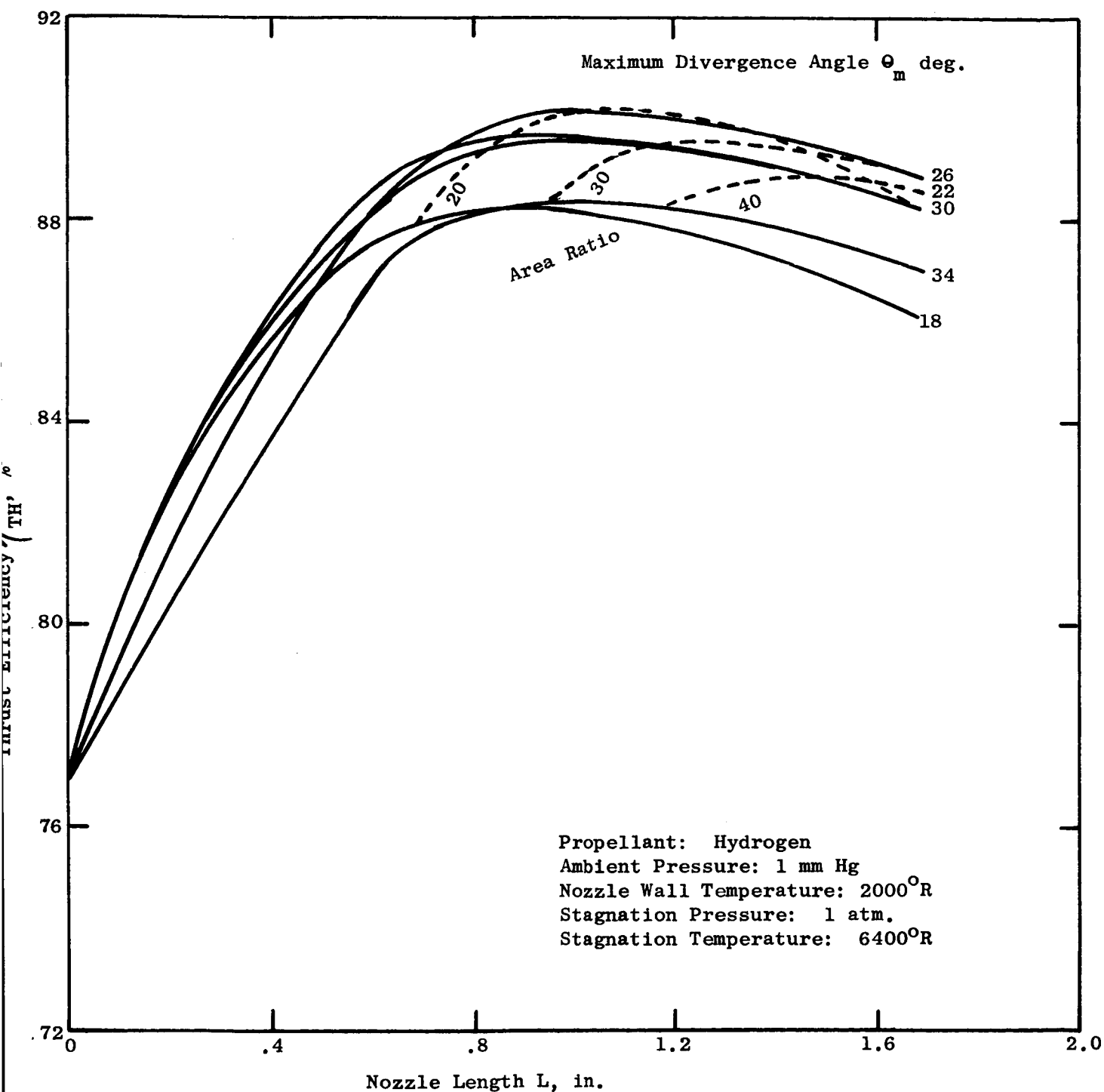


Fig. 2.7: Parametric Study of Nozzle Configuration for Engine Y16

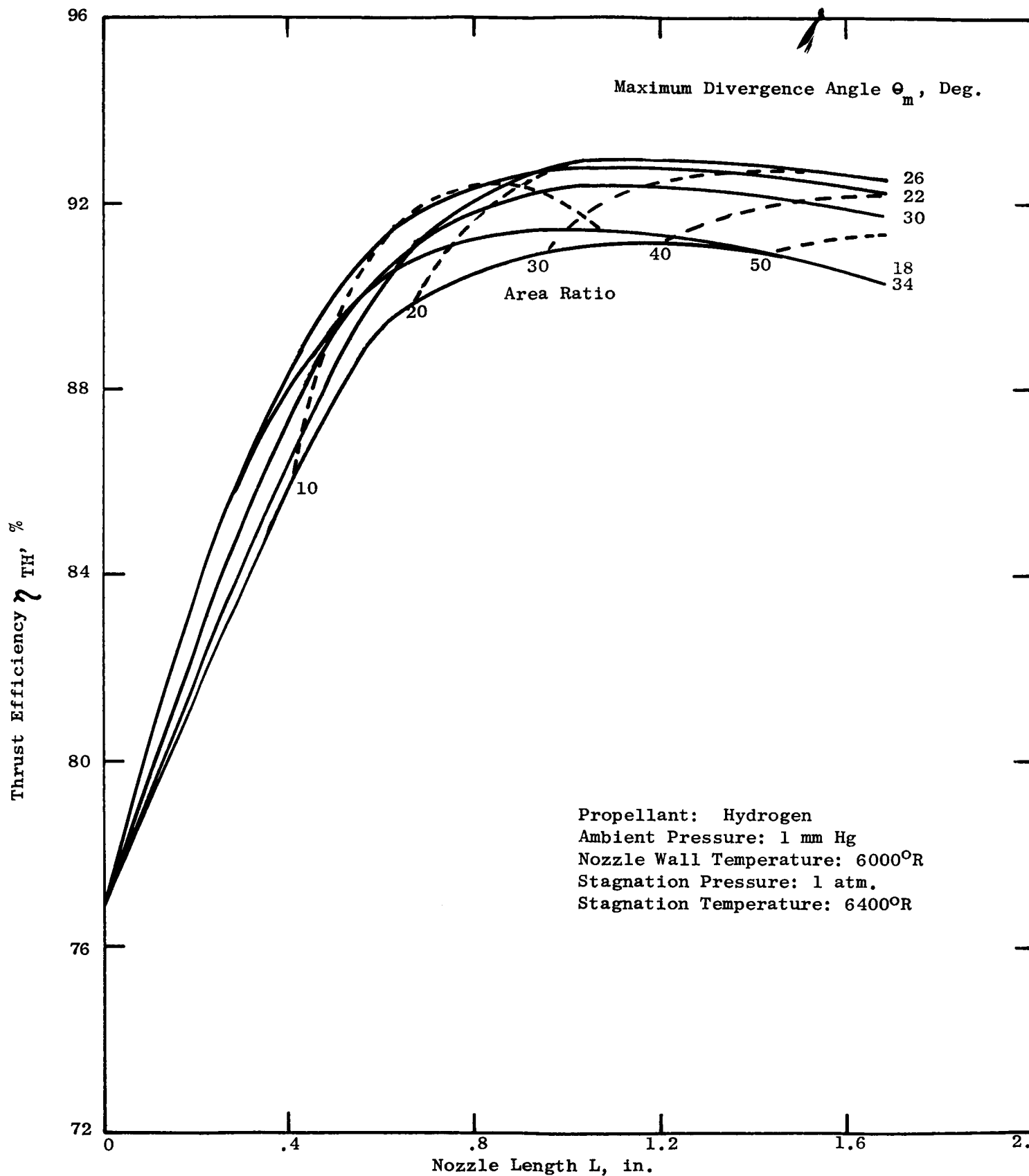


Fig. 2.8: Parametric Study of Nozzle Configuration for Engine Y16

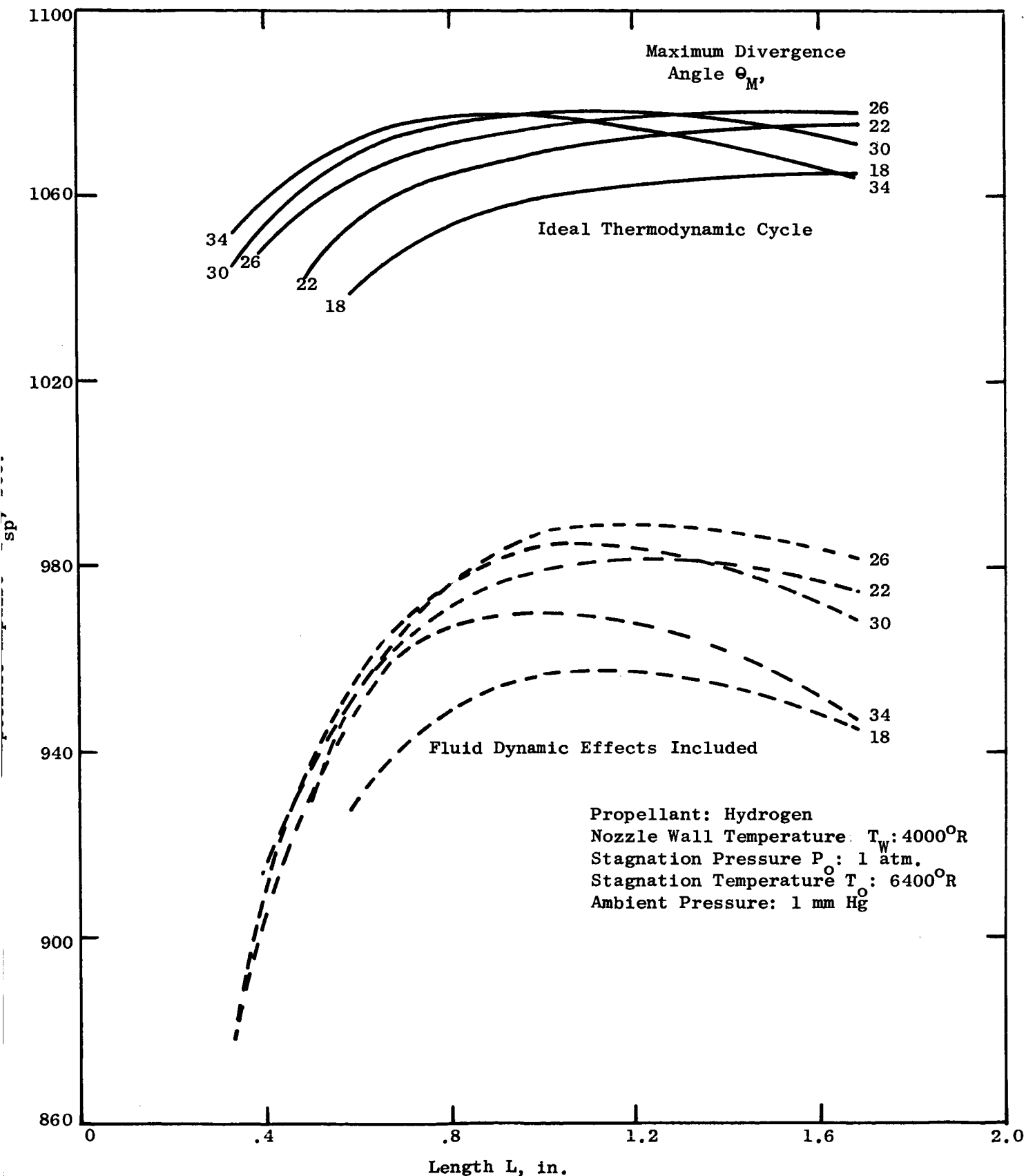


Fig. 2.9: Parametric Study of the Effect of Nozzle Length and Maximum Divergent Angle on the Specific Impulse

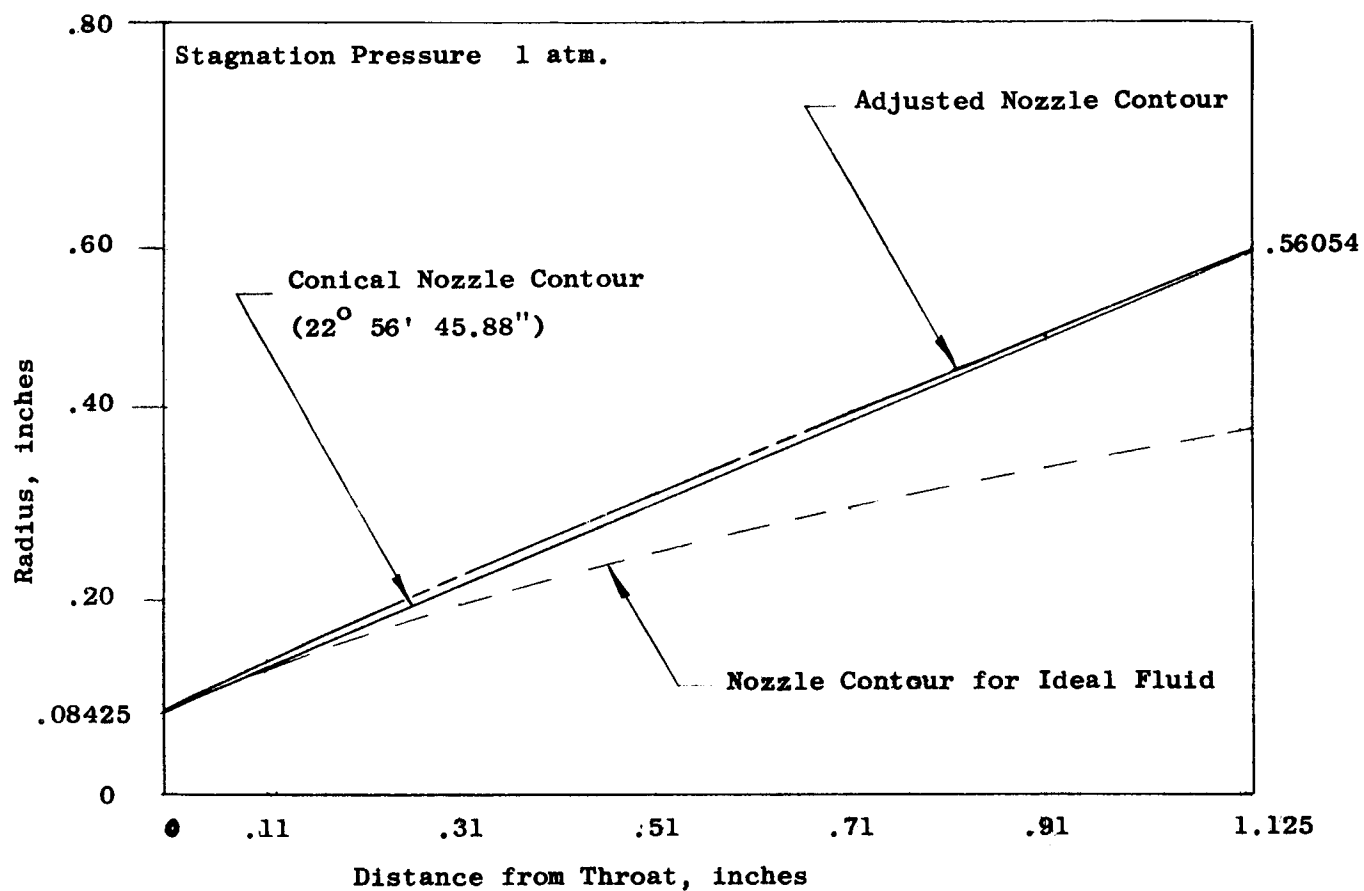


Fig. 2.10: 30 KW Three-Phase Plasma Arc Jet Engine Nozzle

contour. The final nozzle specified for the engine has a conical nozzle contour since the deviations from the ideal nozzle contour were never larger than the machining tolerance that can be realistically specified for manufacturing of test engines.

2.2 Testing of 30 KW Three-Phase Plasma Arc Jet Engine Y16-1

2.2.1 Initial Testing of Engine Y16-1

At the beginning of the second quarter of this program the new 30 kw three-phase plasma arc jet engine (Y16-1) was received from the shop. The assembly was completed without modifications or corrections. All parts of the engine were manufactured according to specifications. The assembled engine is shown in Fig. 2.11 while an exploded view is shown in Fig. 2.12 and the assembly drawing in Fig. 2.13. The initial arc chamber configuration and electrode setting was based on the most successful configuration which had evolved during operation of Engine #4. This configuration is shown in Fig. 2.14a.

2.2.1.1 Test Schedule

The test schedule for engine Y16-1 was designed to obtain the greatest amount of information with the least amount of damage to the engine in the event of an error in the design. The engine was, therefore, to be initiated with a very short run lasting not longer than 15 seconds. During this run the engine would not reach steady state operating conditions. But it also would not permit excessive damage to the nozzle and electrodes if the arc should stagnate. After this initial run, the engine was to be taken apart and thoroughly inspected in order to determine the location of the arc attachment and condition of the nozzle body after its first thermal shock.

The second run was to last about 100 seconds, a time duration which was known to be just short of steady state operating conditions. This run would again be followed by a complete inspection of the engine. Only after completion of these two initial tests would an attempt be made to reach full power of 30 kw and to obtain the electrical characteristic of the engine.

2.2.1.2 Electrical Circuit

The electrical system shown in Fig. 2.15 was set up with a reactive impedance, X_L , of 0.575 ohms in each line of the primary circuit, a transformer ratio of 2/1 and a capacitance of $75 \mu F$ across the primary lines. The primary voltage was set at 260 volts for starting.

2.2.1.3 Testing

The engine ignited immediately without any additional starting procedure. The power level reached by the engine without adjustment of the primary voltage was 24.3 kw. The first run lasted 13 seconds and was terminated before the engine reached stable operating conditions. After disassembly and upon inspection no



Fig. 2.11: 30 KW Three-Phase Plasma Arc Jet Engine (YL6-1) -
Assembled

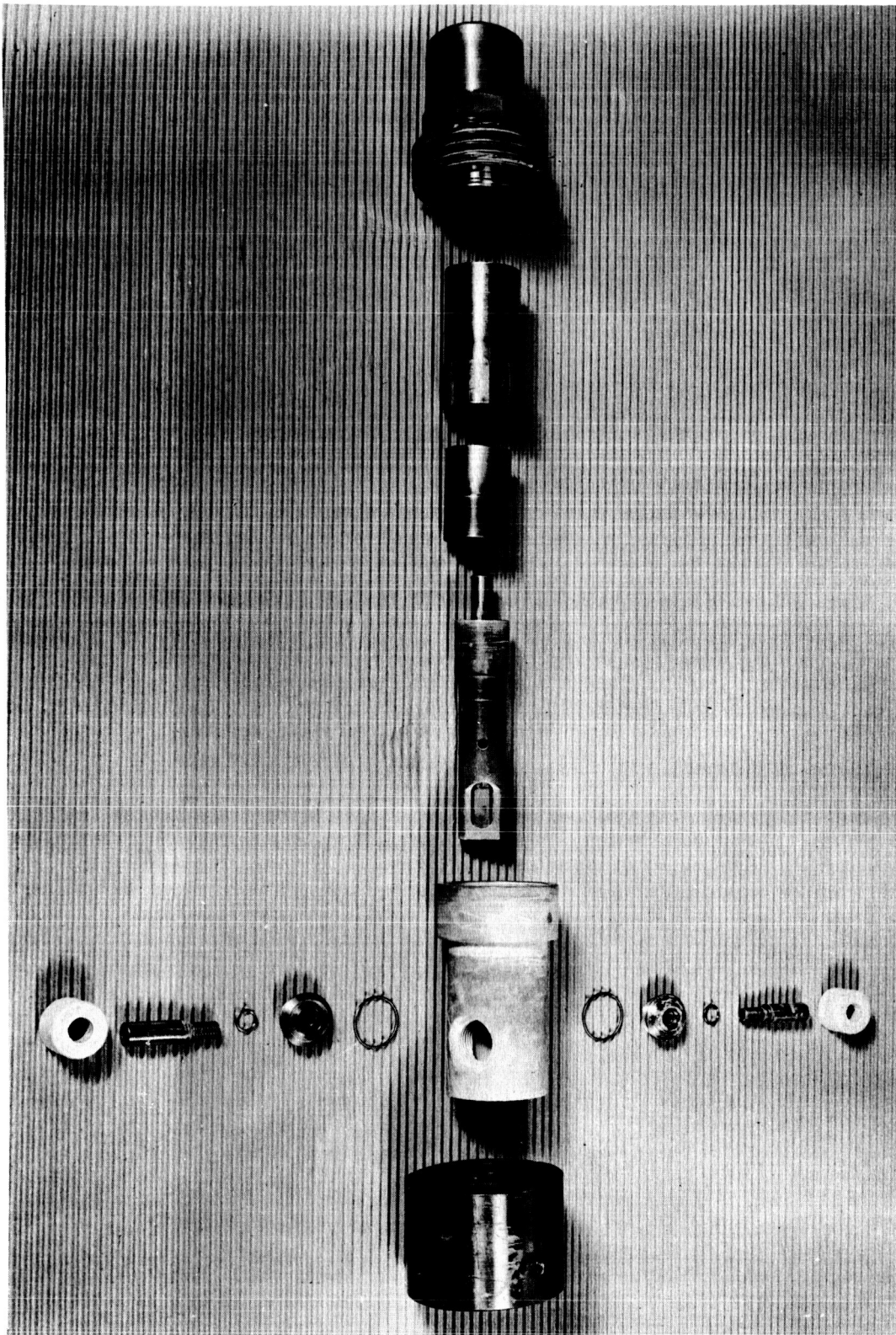
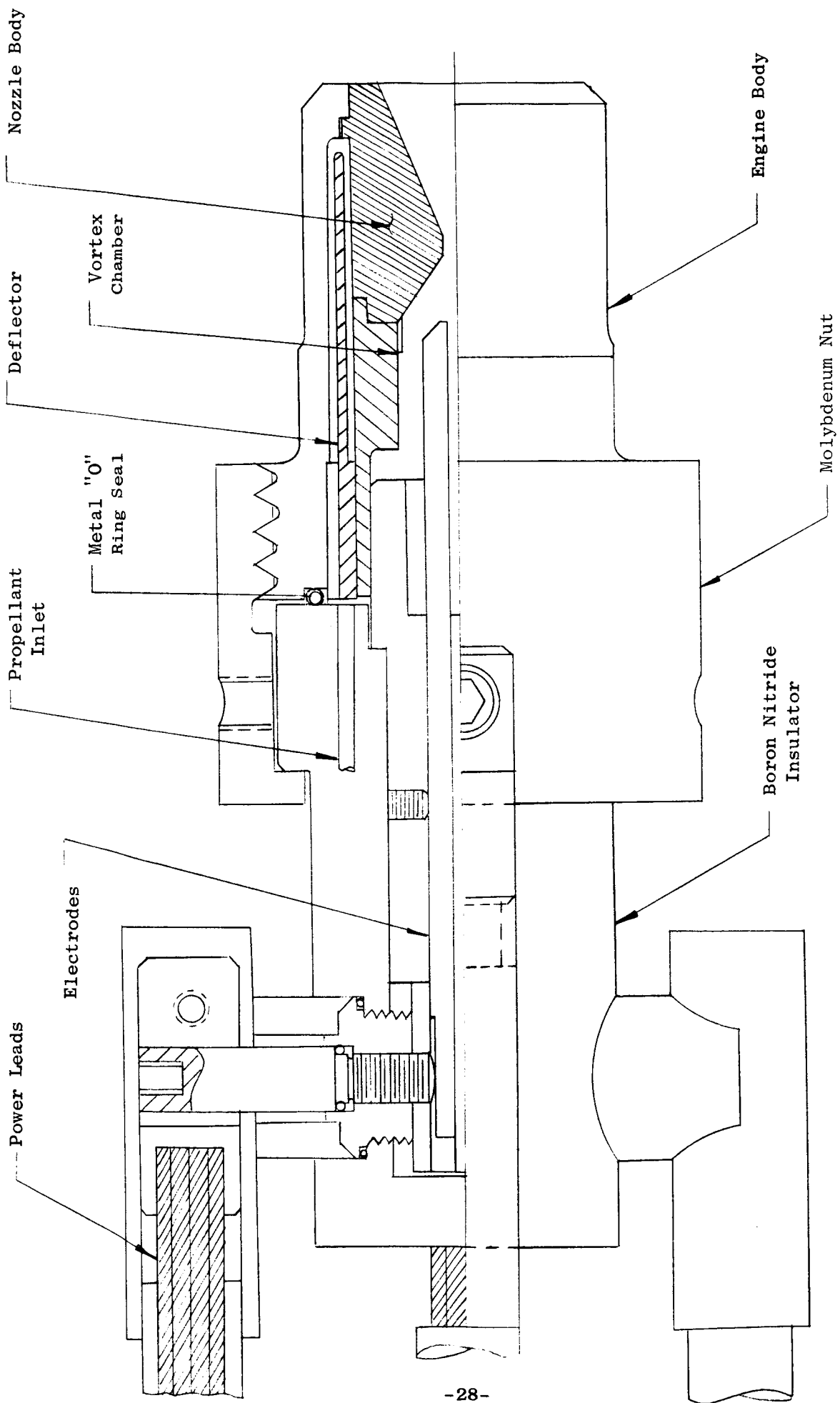


Fig. 2.12: Exploded View of 30 KW Three-Phase Plasma Arc Jet
Engine (Y16-1)



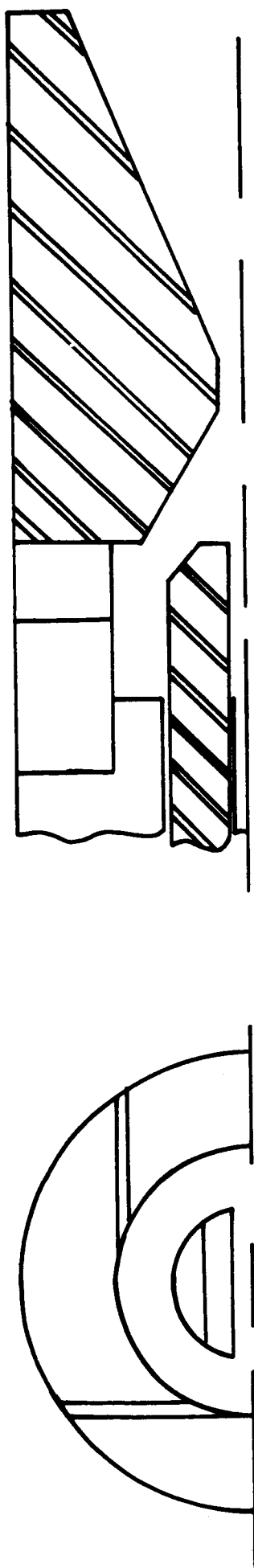


Fig. 2.14 a INITIAL ARC CHAMBER CONFIGURATION

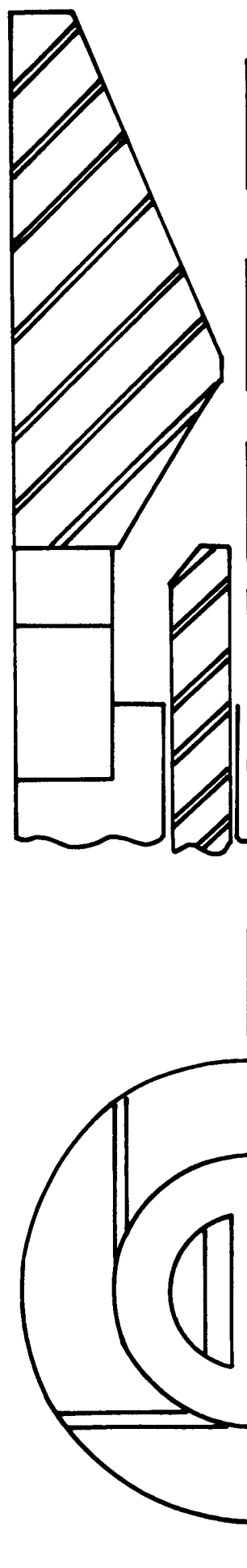


Fig. 2.14b ARC CHAMBER CONFIGURATION AFTER REPAIR

Fig.2.14;Arc Chamber Configurations and Electrode Setting of the 30 KW Three-Phase Plasma Arc Jet Engine (Y16--1)

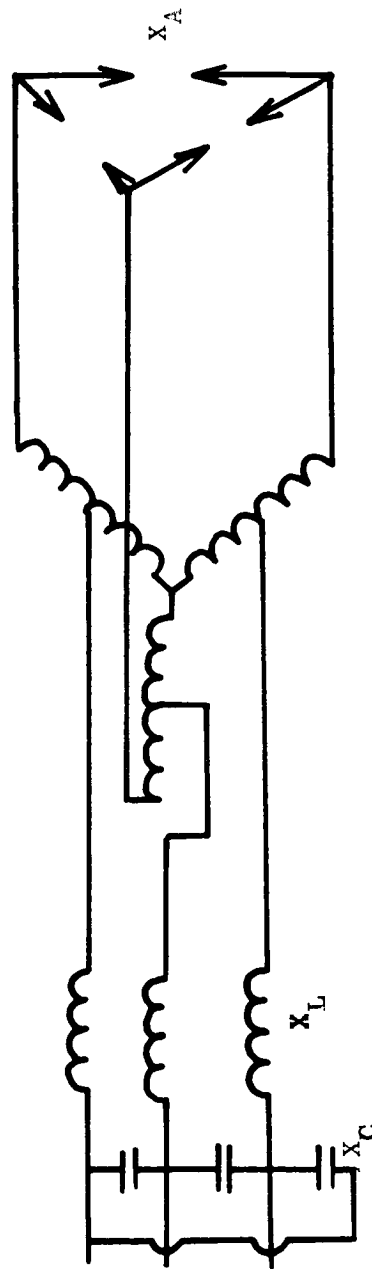


Fig. 2.15: Electrical System of the Three-Phase Plasma Arc Jet Engine

visible signs of arc attachment could be observed at the convergent section of the nozzle. The surface appearance of the tungsten indicated that very diffused arcing must have occurred over the entire exposed area of the converging section of the nozzle. Each center electrode had a small indented spot on the tip from where the arc must have originated. No signs of diffuse arc attachment was found on the electrodes.

The second test run was performed with exactly the same electrode setting indicated in Fig. 2.14. Starting was normal. After 25 seconds the arc had stabilized as could be determined from the arc voltage and current traces on the oscilloscope. At this time, the arc chamber pressure was still rising. After complete stabilization of all operating condition had occurred, intermittent ablation was observed. The arc chamber pressure on the Sanborn recorder and on the Taber read-out indicator were closely observed in order to immediately detect plugging of the nozzle if it should occur. The run was terminated after 105 seconds, before any indications of nozzle plugging was detected. Sporadic signs of ablation had continued through the entire test run. After disassembly of the engine, the inspection of the nozzle indicated that the two arcs originating from the two center electrodes had stagnated in the convergent section of the nozzle. The two areas of the arc attachment were the origin of the tungsten material which was found in the nozzle throat. This material was easily removed without the use of special tools.

The results of the second run had indicated that the vortex strength of the propellant was too weak to rotate the arc at the area of arc attachment. This could be attributed either to the vortex slot design or the arc chamber design. The vortex slots were enlarged from 12 mils to 17 mils. This slot design approached that previously employed in other engines. After this modification the engine was operated for 440 seconds. The run was terminated because of a sudden complete loss of chamber pressure indicating a large propellant leakage. Unfortunately, the arc had continued to operate for about 3 seconds after the loss of flow. During this short time there were strong indications of ablation. The cause of the pressure drop was traced to a failure of a connection in the pressure pickup line. Upon inspection of the engine, deep indentations due to material loss were found in the nozzle throat. Due to the failure of the pressure line, and the following complete loss of the vortex in the arc chamber, it was not possible to establish the real cause of the damage found in the convergent section of the nozzle after this test. It was, therefore, not possible to determine whether the vortex slot modification had solved the problem of arc stagnation. A close inspection of the Sanborn recording indicated that in this run the arc required 75 seconds to stabilize. This compares with 25 seconds recorded with the 12 mil slot design. This difference in the time required for arc stabilization in itself could be considered an indication of a stronger arc diffusion with the larger slots. The arc chamber pressure and the arc power reached their stable operating point after 200 seconds. The arc power during this run was 28.5 kw.

The converging section of the nozzle was repaired by enlarging this section until the indentations caused by the loss of material disappeared. The resulting arc chamber configuration is shown in Fig. 2.14b. During the following

runs no ablation was observed. The runs had to be terminated after 10 to 30 minutes of operation due to failure in the pressure pickup or flow lines. These failures had never been experienced previously with other engines and could only be attributed to a faulty piece of material that was used to make the new gas lines for the new engine. All test runs were made at a power level of at least 29.5 kw. Evaluation of the data indicated operation at a power level of 31.7 kw over a substantial length of time.

In Figs 2.16 and 2.17 the engine parts mostly affected by the arc operation are shown. The first set of electrodes which were used in all the tests are compared with a new set of electrodes in Fig. 2.16. The tips of the electrodes had melted locally after the first tests as was expected. No apparent change in the electrode tip configuration could be observed after the following extended tests. The surface in the convergent section of the nozzle as shown in Fig. 2.17 was roughened by the arc but was free of indentations or other indications of local material loss.

The first electrical data of the engine produced some unexpected power relations between arc voltages, and line currents. These data are shown in Figs. 2.18 and 2.19.

With Engine Y16-1 a power level of 30 kw can be reached with a line current of less than 130 amps as shown in Fig. 2.18. The effective arc voltage at this power was 135 volts. The power of each line which is recorded continuously on the Sanborn recorder, confirmed that the engine was operating stably at these voltage and current relations. From the electrical data which were obtained with Engine #4, the line current was expected to reach 150 amps at a power of 30 kw. The slight variations in the effective voltages for the different test runs, which are shown in Fig. 2.19, have to be attributed to the minor changes in the gap setting between the center electrodes and the nozzle which occurred with each reassembly of the engine.

As an added check on the measured power, the measured arc chamber pressure and the measured power were correlated with analytically predicted values. Fig 2.20 is the calibration curve for the nozzle design used in Engine Y16-1. In Fig. 2.21 the measured power values are superimposed on the analytical locus for a propellant flow rate of 5×10^{-4} lb/sec. It can be seen that the test points agree well with the analytical predictions.

2.2.1.4 Initial Evaluation of Engine Y16-1

At the conclusion of the initial testing of Engine Y16-1, several minor modifications of the engine were indicated. The radial O-ring seals proved impractical because of the large tolerances on the metal O-rings as they were received from the manufacturer. The engine was, therefore, modified to accept an axial O-ring seal. The problem encountered with an axial seal, due to differential thermal expansion, was resolved by making the shell out of molybdenum. The possible galling between the threads of the shell and the engine body which was anticipated to be a serious problem was alleviated by coating the engine body threads with alumina.

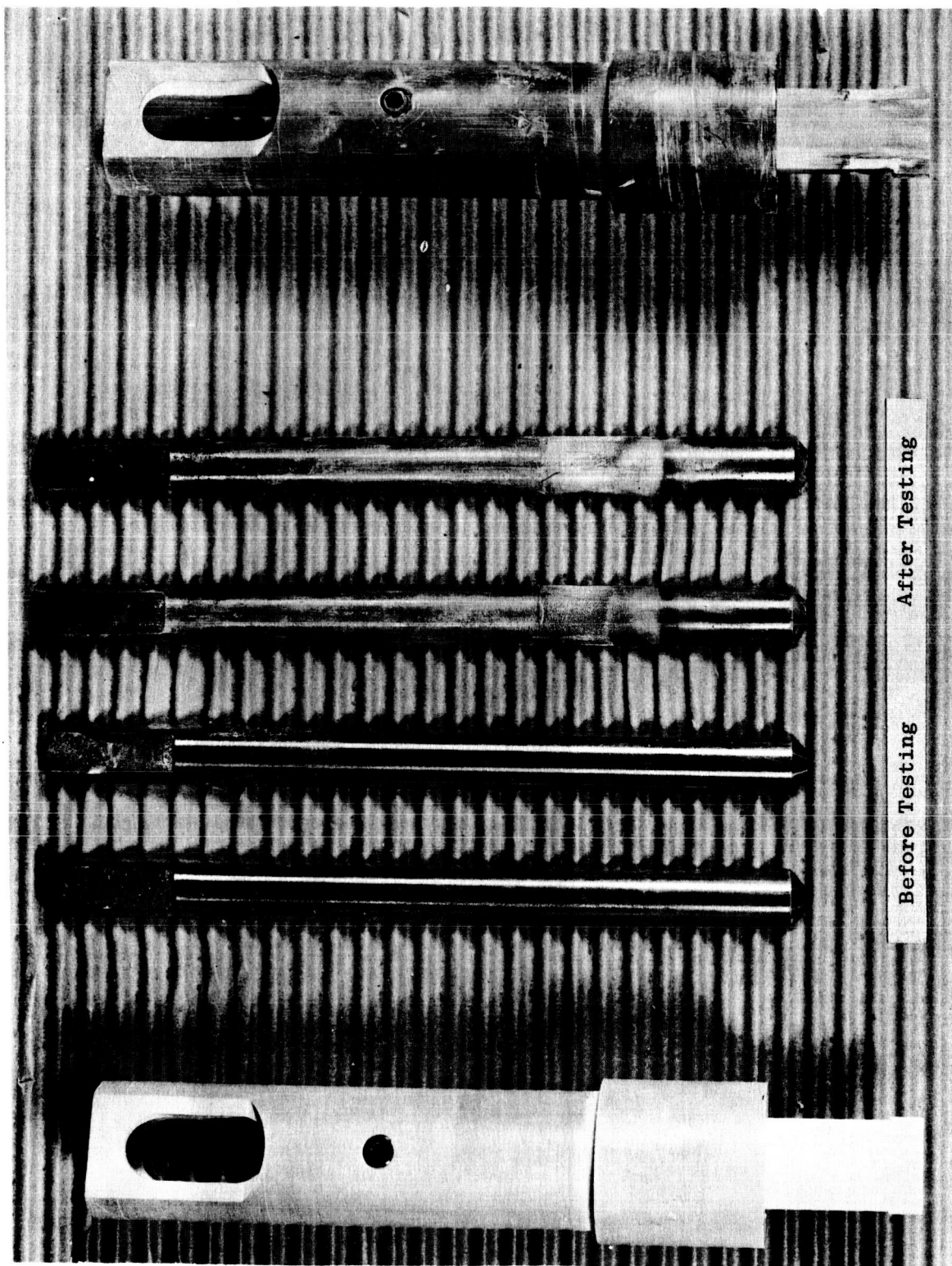


Fig. 2.16: Center Electrodes of Engine Y16-1 (May 17, 1963)

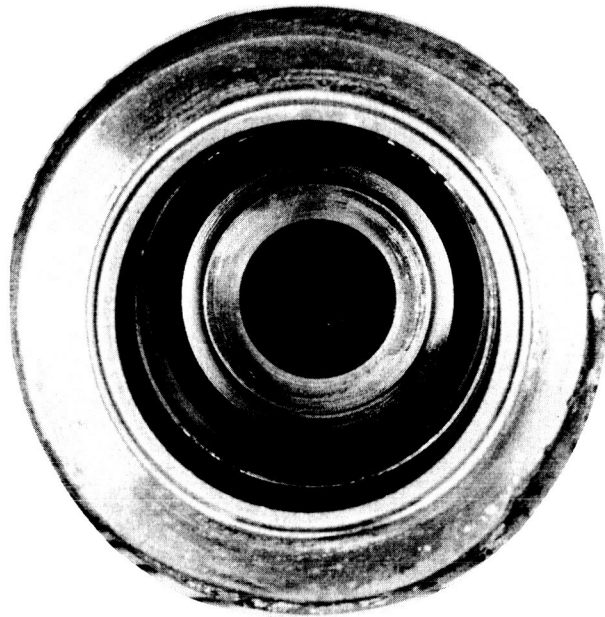


Fig. 2.17: Converging Section of Nozzle After Testing (Y16-1)

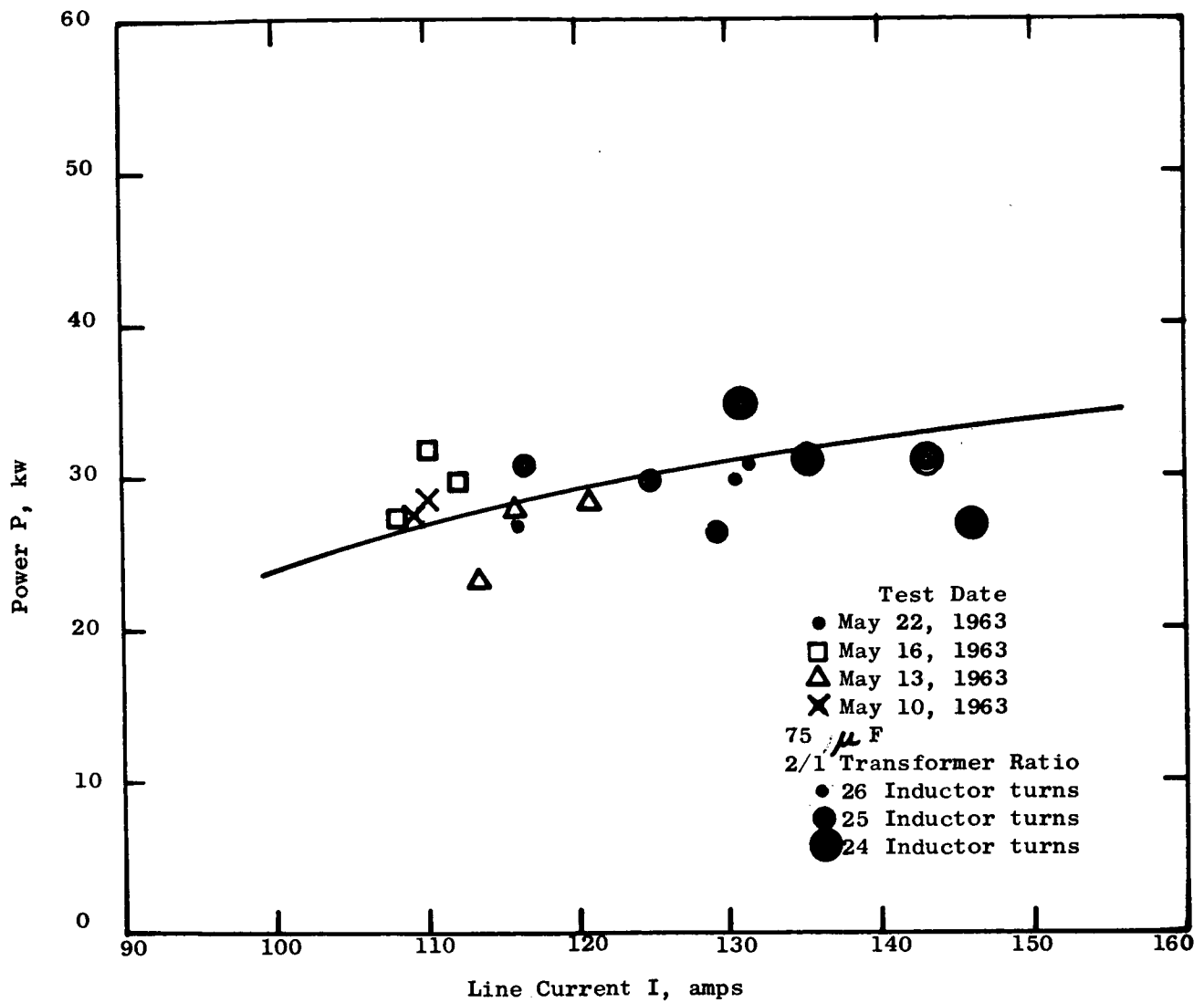


Fig. 2.18: Electrical Test Data of Engine Y16-1 (Power vs Line Current)

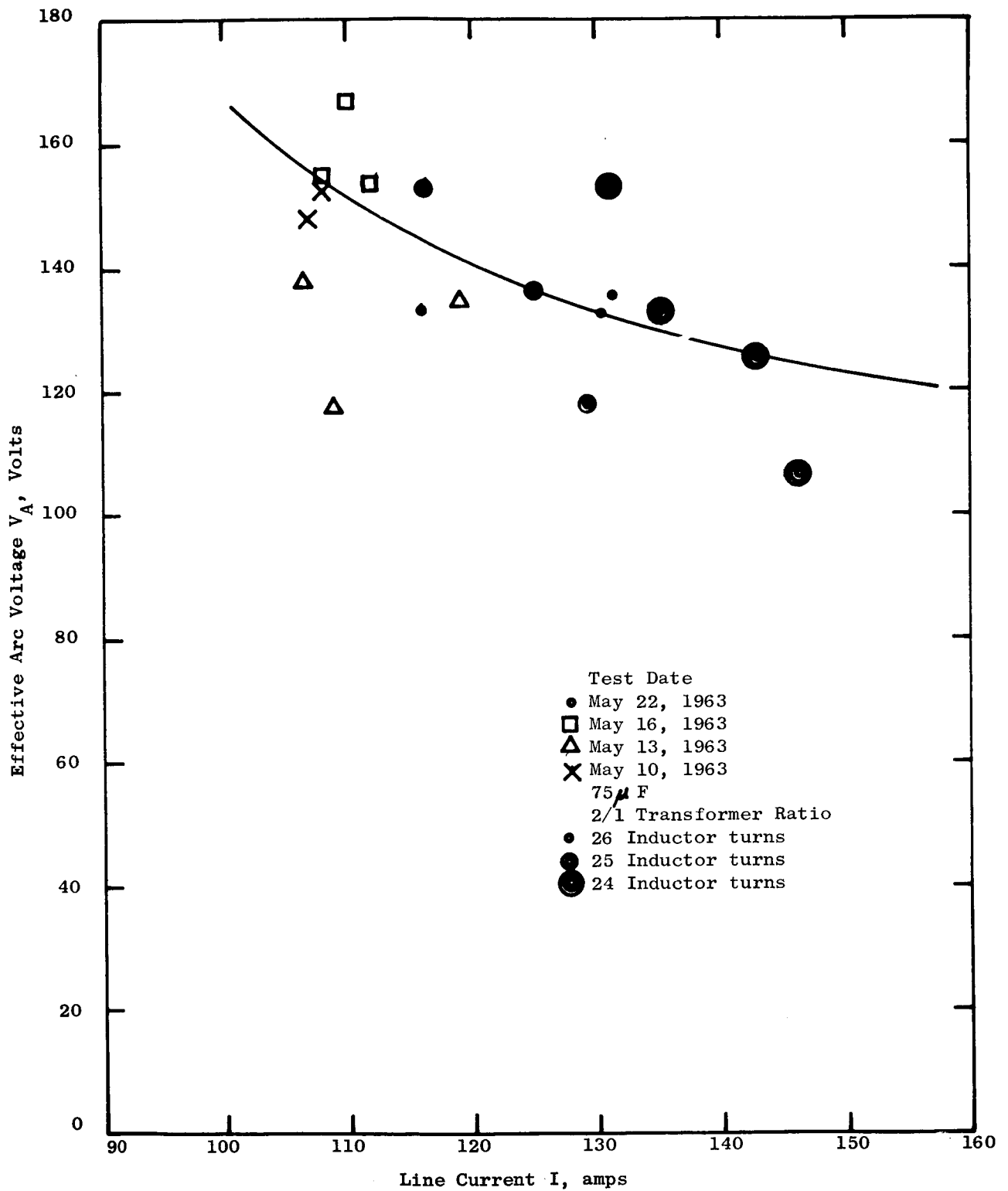


Fig. 2.19: Electrical Test Data of Engine Y16-1 (May 1963) (Arc Voltage vs Line Current)

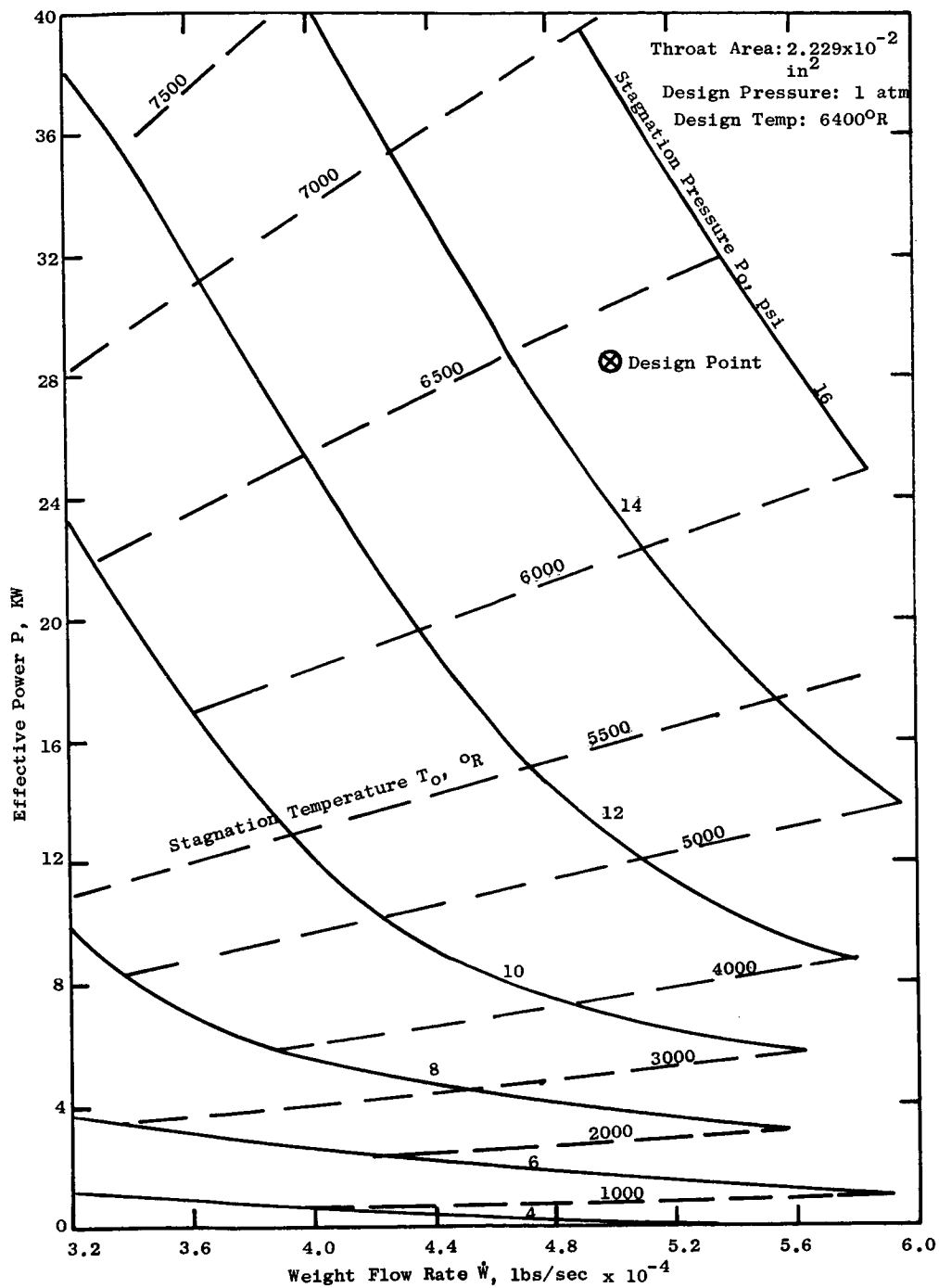


Fig. 2.20: Design Operating Curve for 30 KW Three-Phase Plasma Arc Jet Engine (Y16-1)

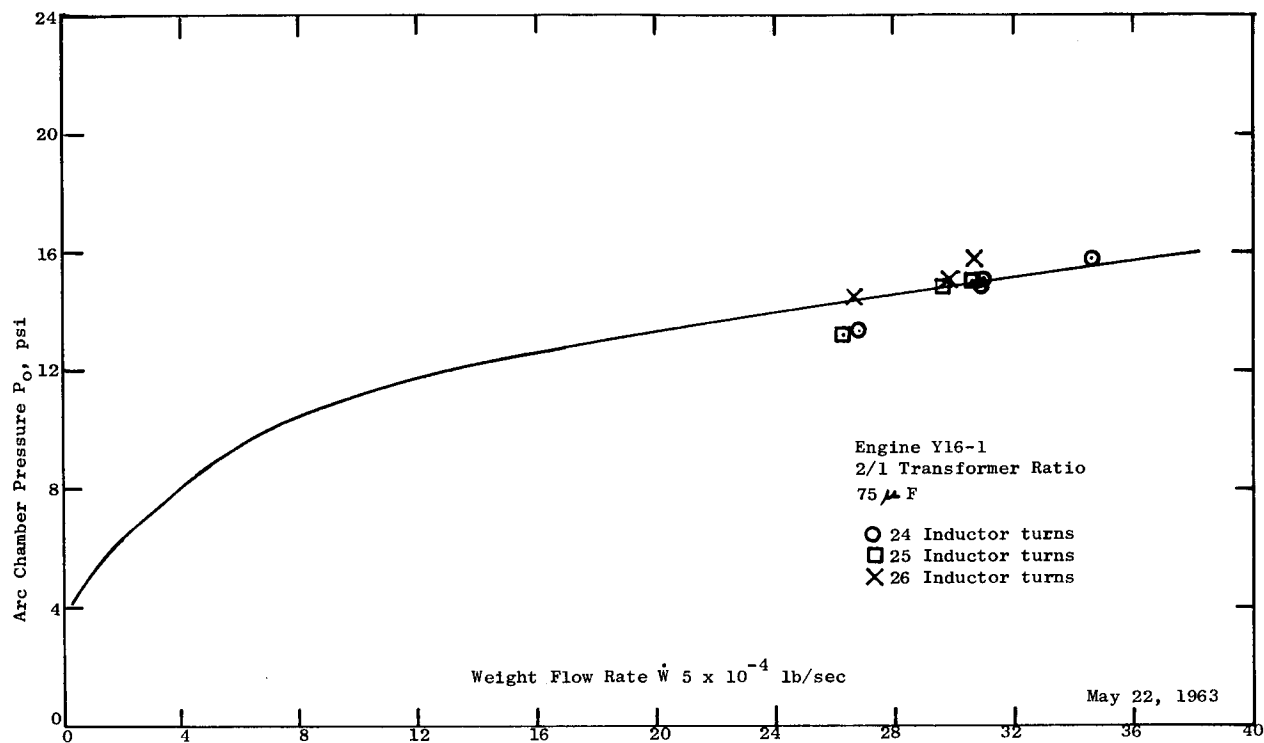


Fig. 2.21: Correlation of Test Data with Analytical Data (Y16-1)
(Power vs Arc Chamber Pressure)

Because of the repeated assembly and disassembly of the engine, problems were encountered wherever parts were threaded in boron nitride. It was just not possible to prevent loosening of the joints during disassembly. Stripping of the threads in the boron nitride insulator made several temporary fixes on the engine necessary.

2.2.2 Endurance Testing of Engine Y16-1

After completion of the initial testing of engine Y16-1, testing for endurance and stability over long duration was started. The electrical circuit for the long duration runs was selected from the results of the initial tests. The most stable arc operation had been found to prevail with a transformer ratio of 2:1, a stabilizing inductance of 0.575 ohms in each primary line, and a capacitance of $75 \mu F$ across the primary lines. The main objectives of the endurance tests were to establish possible relations between the ablation rate, the frequency of starting, and the power level.

The first long duration run was started June 6, 1963. The engine had been operated for 82 minutes at a power level of 30 kw when external arcing necessitated shutdown. On inspection, it was found that the insulation of all electrical connectors in the vacuum tank had melted and that the observed arc was the beginning of a general impending breakdown of the electrical leads to the engine. On disassembly and inspection of the engine all parts were found to be in perfect operating condition. The electrodes had lost some more material at their tips in such a way that they appeared more evenly worn over the entire tip area. This indicated that the previously observed preferred ablation as was seen in Fig. 2.16 did not constitute a wearing in of the electrodes. The boron nitride electrode holder was in perfect condition, showing no loss of material at all.

The electrical wiring in the tank had to be completely replaced. All connectors were eliminated and only Geoprene insulated wire was used as leads. A thermal shield was immediately installed behind the engine to shield some of the wiring in the tank from the direct radiation of the exhaust plume.

Before initiating the next long duration run, the center electrodes were weighed and marked. The second extended run lasted 2 hours and 20 minutes. This run was terminated because of the breakage of optical glass in one of the port holes of the tank. No damage occurred to the engine or any other component since the second glass in the port hole remained intact, maintaining the vacuum in the tank.

On disassembly of the engine it was found that the Geoprene insulated leads had suffered substantially. The insulation near the engine had become charred and brittle and was fractured at several locations. All engine parts were in operating condition. There were visible indications that the electrodes had lost further material at their tips, but no unusual arc attachment could be detected along the electrodes. The electrodes lost 0.128 g and 0.126 g respectively due to ablation. Based on this material loss, the combined ablation rate for both center electrodes was 3.024×10^{-5} g/sec. The surface of the convergent section of the nozzle showed a uniform roughness over the entire area of arc

attachment. Some new tungsten material was located in the throat. The two initial cracks in the nozzle were enlarged. It appeared as if material had actually broken out of the cracks. However, the cracks had not penetrated any further to the outside. Pictures of the two center electrodes as they appeared after this run are shown in Fig. 2.22. At this time these original electrodes had accumulated over 220 minutes of continuous operation and approximately 4 hours of check-out runs. The same amount of operating time was also accumulated by the nozzle shown in Fig. 2.23.

The broken glass in the port hole of the test tank was replaced by a Pyrex glass. All electrical leads were retaped with glass tape to safeguard against possible failure of the insulation. The next long duration run was planned to last exactly double the time of the previous run. The run proceeded completely uneventful. The engine operated stably at its power level with only an occasional variation in the voltage-current relation. At the time of shutdown, all components were operating perfectly. The combined ablation rate for the two center electrodes was 3.5774×10^{-5} g/sec for this 280 minute operation. The material loss of each electrode was .33 g and .271 g respectively. Visually, no difference could be detected between the appearance of the two electrode tips as can be seen in Fig. 2.24. It was quite obvious that the converging section of the nozzle had deteriorated further. The two cracks in the nozzle were enlarged. On close inspection it appeared that material has been lost from the cracks due to breaking off. No sign of arc attachment could be found along the cracks although the sharp corners would be expected to furnish preferred points of attachment (Fig. 2.25). Looking into the diverging section of the nozzle, one of the cracks was seen to have penetrated to this side of the throat. Some material was deposited in the nozzle throat, but not more than there had been seen before from the previous runs (Fig. 2.26). The complete electrode holder assembly with the vortex sleeve is shown in Fig. 2.27. The holder and the sleeve remained in perfect condition.

In order to confirm the measured ablation rate, another 2 hour run was scheduled. The test was run in a routine fashion. The total ablation for each electrode was 0.089 g and 0.125 g respectively. The ablation rate for this run was 2.94×10^{-5} g/sec. A close check of the recorded data showed that the average power during this run was not quite 30 kw.

At the end of 620 minutes continuous operation the two center electrodes had lost 0.547 g and 0.522 g respectively. The combined average ablation rate was 3.2993×10^{-5} g/sec for the two electrodes. The ablation rate of each electrode varied only by 2.3% from the average ablation rate. This very slight variation of the total ablation between the two center electrodes suggests that the loss of material at the electrodes is a continuous process and that it had not occurred due to fracturing off.

To determine whether a relation exists between the ablation rate and the power level, tests at power levels below the 30 kw design point were scheduled. These tests were to last for two hours each, a duration that had proven to be sufficient to produce consistent reproducible data. The first of these tests

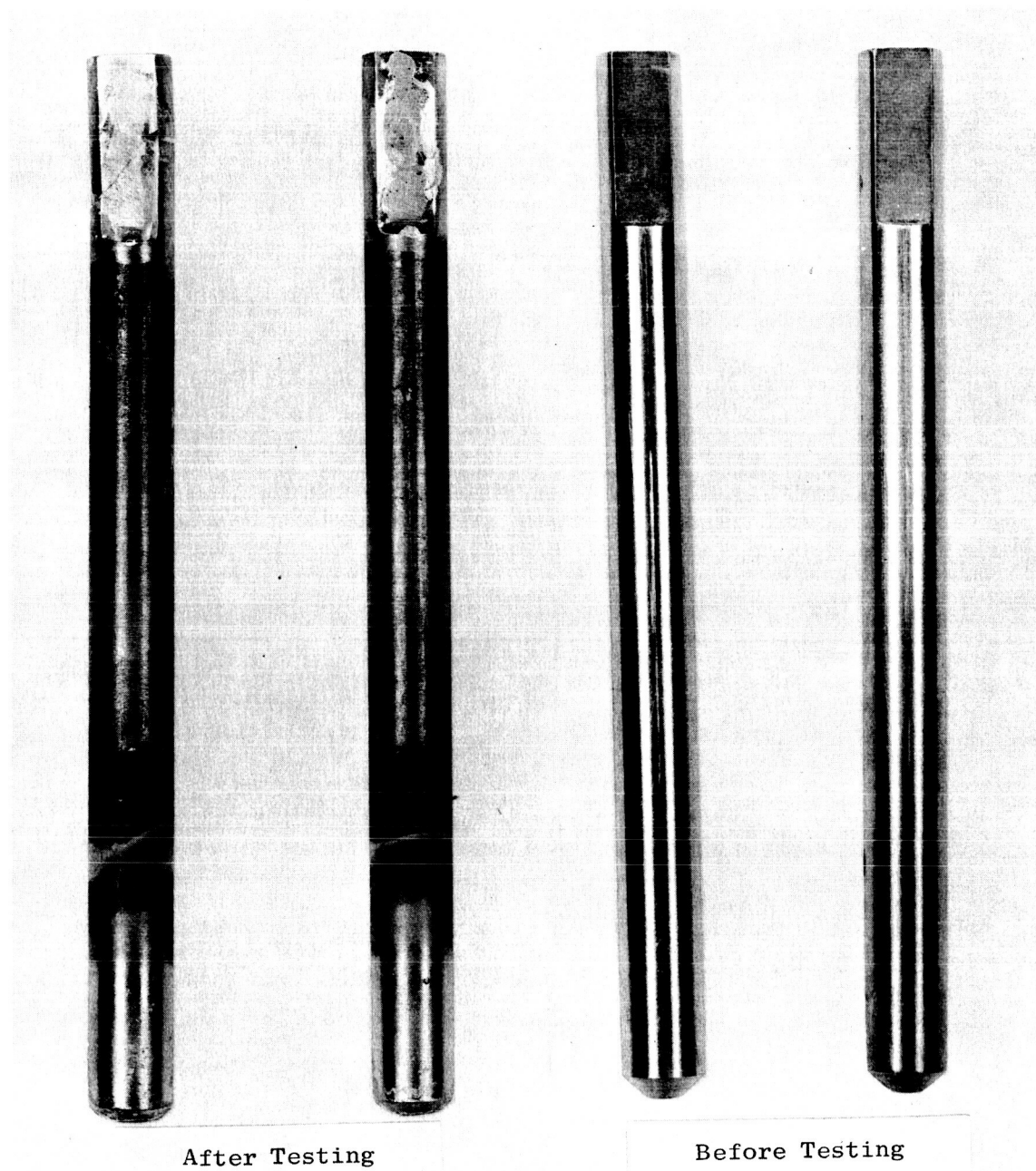


Fig. 2.22: Center Electrodes After 220 Minutes of Continuous Operation and Approximately 4 Hours of Checkout Runs

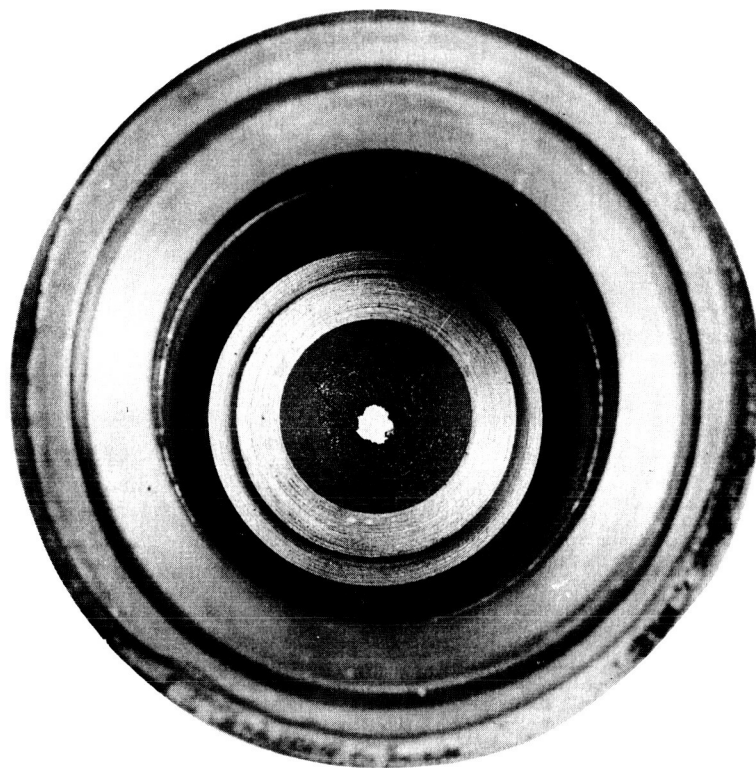


Fig. 2.23: Converging Section of 30 KW Three-Phase Plasma Arc Jet Engine Nozzle After 220 Minutes Continuous Operation and Approximately 4 Hours of Checkout Runs (June 14, 1963) (Y16-1)

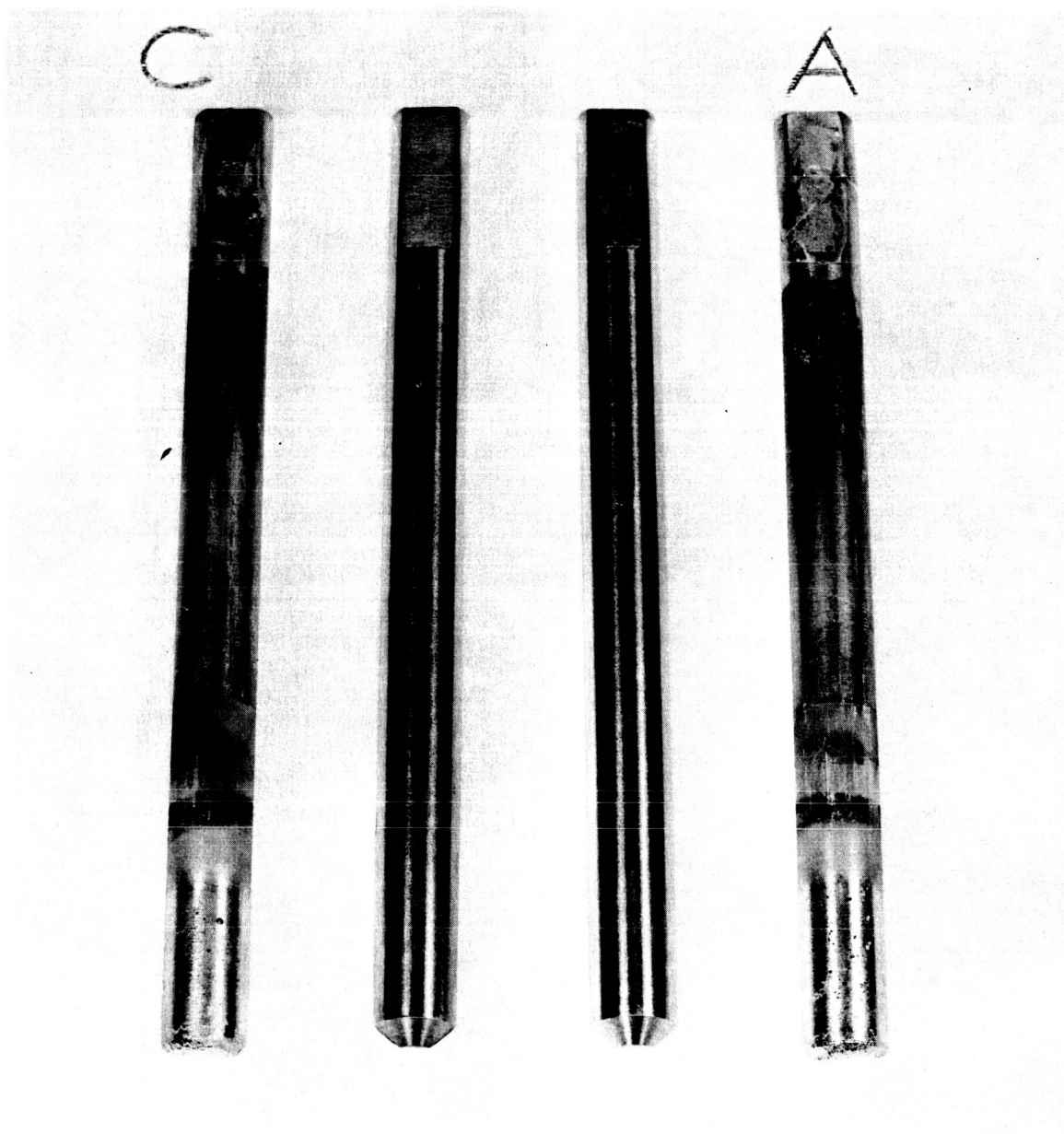


Fig. 2.24: Center Electrodes After 500 Minutes of Continuous Operation and Approximately 4 Hours of Checkout Runs (June 24, 1963)

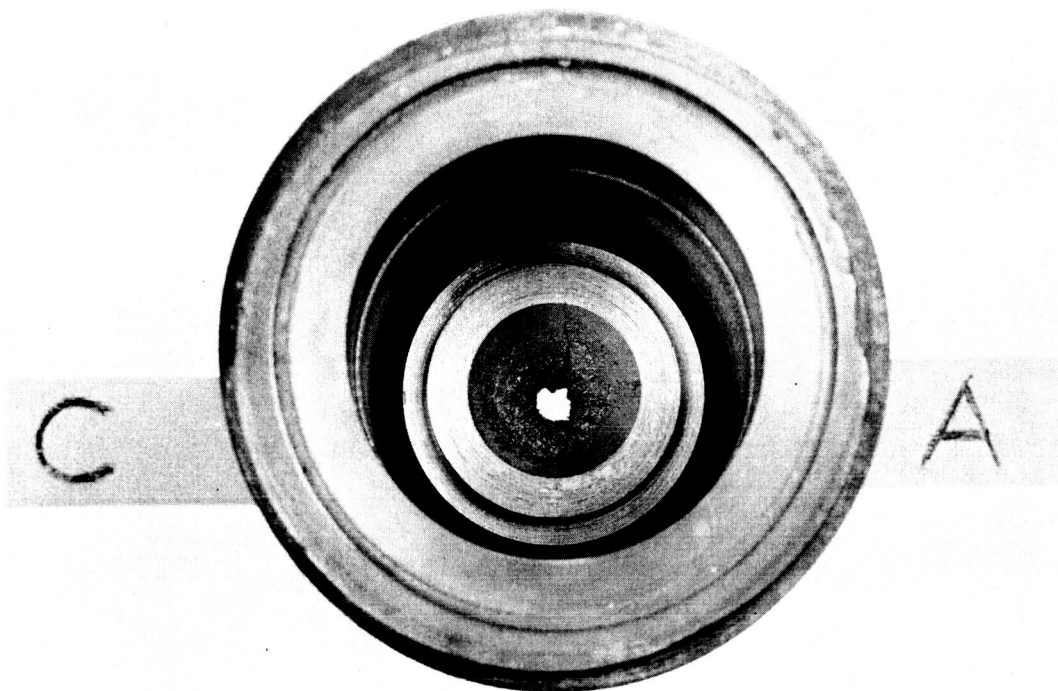


Fig. 2.25: Converging Section of 30 KW Three-Phase Arc Jet Engine Nozzle After 500 Minutes Continuous Operation and Approximately 4 Hours of Checkout Runs (June 24, 1963)



Fig. 2.26: Diverging Section of 30 KW Three-Phase Plasma Arc Jet Engine Nozzle After 500 Minutes of Continuous Operation and Approximately 4 Hours of Checkout Runs (June 24, 1963)

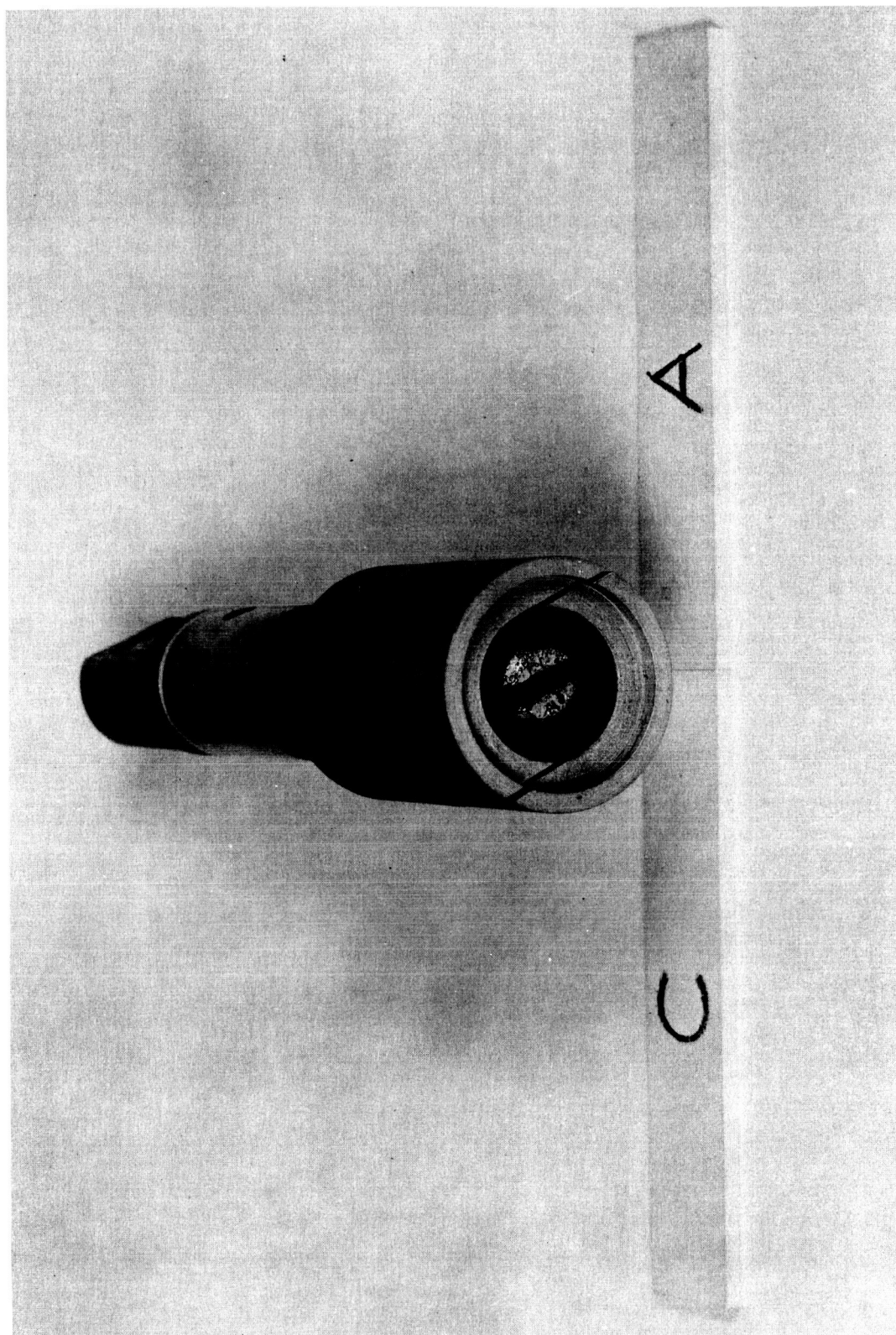


Fig. 2.27: Center Electrodes in Their Electrode Holder After
500 Minutes Continuous Operation and Approximately
4 Hours of Checkout Runs (June 24, 1963)

was run at a power level of 24.8 kw. The measured ablation rate was 2.53×10^{-5} g/sec. The second test run conducted at a power level of 21 kw, produced an ablation rate of the electrodes of 1.319×10^{-5} g/sec. These data and previously obtained data are plotted in Fig. 2.28. The results indicated that there is a distinct dependency between ablation rate and power level and that the ablation rate can be modified by changes in the design of the electrodes.

With these results the effect of the ablating electrode material on the specific impulse can be determined. For an ablation of 3.3×10^{-5} g/sec, the total contribution of the tungsten material to the expelled mass is only 0.0146%. This indicates that the error in the specific impulse due to ablation is outside of the accuracy with which the specific impulse will be determined.

2.2.2.1 Results of the Endurance Testing of Engine Y16-1

The long duration test runs have provided ablation rate data for full power operation and some correlation between power level and ablation rate. It was found that the ablation rate apparently is a function of the power level and that starting does not have any pronounced effect on the material loss from the electrodes. The ablation rates remained effectively constant regardless of the duration of each individual run. The combined ablation rate at a 30 kw power level operation is about 3.3×10^{-5} g/sec for both center electrodes. Using this ablation rate to extrapolate to 250 hours continuous operation, total weight loss of 29.7 g or about 15 g per electrode can be expected. A six inch electrode weighs about 117 gr. The increase in gap after 250 hours of operation would be approximately 0.77 inch.

2.2.3 Evaluation of Engine Design

2.2.3.1 Performance of the Tested Engine

At the end of the testing phase of Engine Y16-1 lasting from the beginning of May to the beginning of July, a re-evaluation of the design was timely. Engine Y16-1 had been designed to operate at a power level of 30 kw for 250 hours continuously. Testing of the engine has shown that the ablation from the center electrodes is the limiting process in the life of the three-phase plasma arc jet engine. Extrapolating the test results showed that the Y16-1 engine should be capable of operating for approximately 100 hours. After about 100 hours of continuous operation, the electrode gap will have increased by about .31 inch. The arc would then become unstable and will break towards the vortex ring. This will result in a failure of the engine. These predictions all assumed that the ablation rate did not change significantly with time. Later results indicated otherwise.

If the ablation of the center electrodes can be reduced, the nozzle becomes the limiting component in the design of Engine Y16-1. The nozzle has shown continuous deterioration during the long duration operation. Cracks developed and increasing roughness of the metal surface in the convergent section of the nozzle could be observed. Neither of these two kind of deteriorations has any

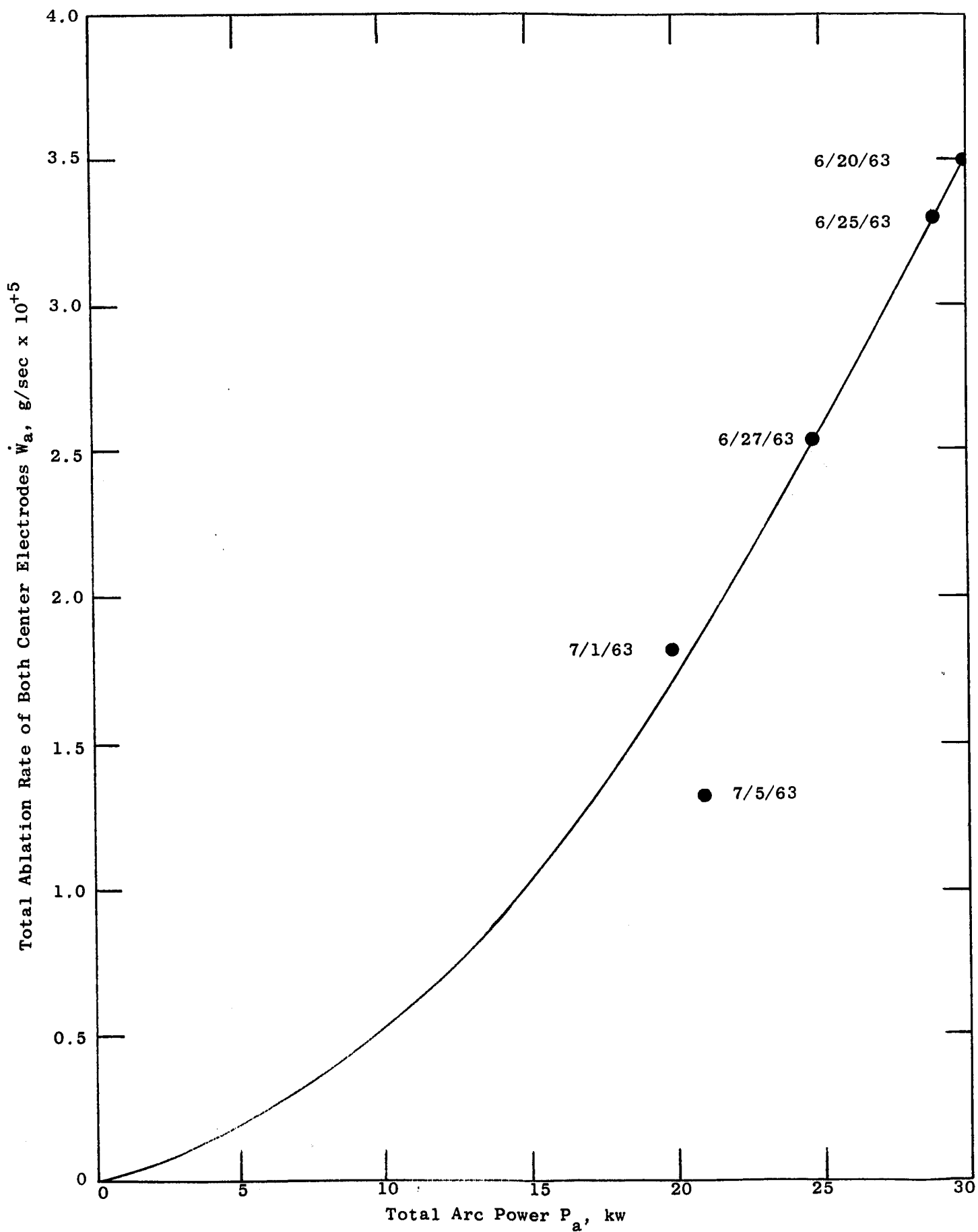


Fig. 2.28: Ablation Rate of Center Electrodes as a Function of Total Arc Power

consequence on the functional operation of the engine. However, the opening up of the cracks and the loss of material along the cracks appeared to be a sporadic process. The progress of such a process cannot be predicted. Only very extensive tests will produce enough data to determine whether and when the loss of material along the cracks will eventually result in a complete disintegration of the nozzle.

2.2.3.2 Indicated Modification of the Tested Engine

Electrodes - The center electrodes of Engine Y16-1 were manufactured by slicing a 0.5 inch diameter swaged pure tungsten rod along the axis, removing during the process a slice of .125 inch thickness. The total cross-sectional area of the remaining material was 0.13375 inch². By redesigning the engine to take center electrodes sliced from a 0.75 inch diameter rod, the cross-sectional area can be increased to 0.3477 inch², i.e., by a factor of 2.6. If the ablation rate remains constant, the increase of material per unit length of electrode can assure a continuous operation of 250 hours assuming a constant ablation rate, or about twice that much if the ablation rate decreases after running 10-20 hours. The increase in cross-sectional area will also increase the heat conduction from the electrode tip. This secondary effect of the larger electrodes can be expected to result in a change in the ablation rate with respect to power as was measured with the electrodes made from a 0.5 inch diameter tungsten rod.

Tungsten rod with 2% ThO₂ was also considered for testing. Center electrodes were made from this material and the results are discussed in another section of this report.

Nozzle - The tungsten nozzle in Engine Y16-1 was machined from a 1.5 inch diameter pure tungsten rod. The 1.5 inch diameter bar was swaged in the General Electric Research Laboratory in Schenectady from a 3.5 inch diameter hydropressed sintered tungsten billet with a density of 95.75%. Apparently the swaging process produced a great amount of unrelieved stresses and did not create the desired optimum density in the center of the bar. In order to investigate the effect of material a special extruded piece of 2% thoriated tungsten was manufactured by the Manufacturing Department of the Refractory Metals Plant in Cleveland. The piece was worked down to its final dimension from a 3 inch diameter sintered bar. After the extrusion process the piece was completely inspected for soundness. No defects were found. A nozzle was manufactured from this material and tested. The results are presented later in this report.

2.3 Investigation of the Effect of the Magnitude of the Reactive Impedance in the Electrical Circuit on Engine Operation

2.3.1 Test Procedure

The effect of the magnitude of the reactive impedance in the electrical circuit was investigated with Engine #4, before Engine Y16-1 became available for testing. The primary objective was to ascertain whether the arc voltage - arc current relation could be influenced by the external electrical circuit.

It was observed that the three-phase engine operated stably over a wide range of power with a minimum reactive impedance in the external circuit. The minimum requirement for Engine #4 was determined experimentally by lowering the arc power until instability was observed as indicated by the Sanborn recorder traces of the three line powers. To cover a power range of 17 to 22 kw in the planned tests, the minimum requirement was found to be 0.52 ohm in each primary line (24 inductor turns per line). With this inductance value, the line currents, arc voltages, and power were recorded for many operating points. The test was repeated with an inductance of 0.575 ohms per line (26 inductance turns per line). The results of these tests are shown in Figs. 2.29, 2.30, and 2.31.

2.3.2 Results

Apparently the inductance value has no influence on the power-current relationship of a three-phase arc. This can be deduced from Fig. 2.29. An increase in the inductance, however, causes the voltage as indicated on a voltmeter which is calibrated for a sinusoidal voltage signal to approach the effective voltage, where the effective voltage is defined as

$$V_{\text{eff}} = P / \sqrt{3} I_L$$

where P = power, watts

I_L = line current, amps

This observation indicates that only the voltage shape is affected by a change in the inductance and that by increasing the inductance the high voltage spikes can be decreased. Any possible advantage of a decrease in the voltage spikes was not evaluated in this phase of the testing.

2.4 Effect of Firing Order on Arc Operation

The most efficient operation of a three-phase ac plasma arc jet engine has been observed to occur when the powers in each arc are approximately equal. From experience with the 30 kw three-phase engine, it has been found that the currents tend to be self-regulating, i.e., the currents in each of the three arcs are about the same. However, the voltages across each arc sometimes differ by as much as perhaps a factor of two. Therefore, an investigation was made into the causes of this situation.

Using tungsten electrodes and a thoriated tungsten nozzle, the engine was run and voltages recorded across each pair of electrodes. Then the electrical leads to the electrodes were interchanged and the test repeated. It was found that the electrodes across which the minimum voltage had been previously measured now, no longer indicated the minimum voltage. It was first believed that this might be caused by a characteristic of the power supply rather than a characteristic of the engine. However, by systematically changing the arrangement of the leads, it was found that the relative magnitude of the electrode voltages were dependent upon the following factors:

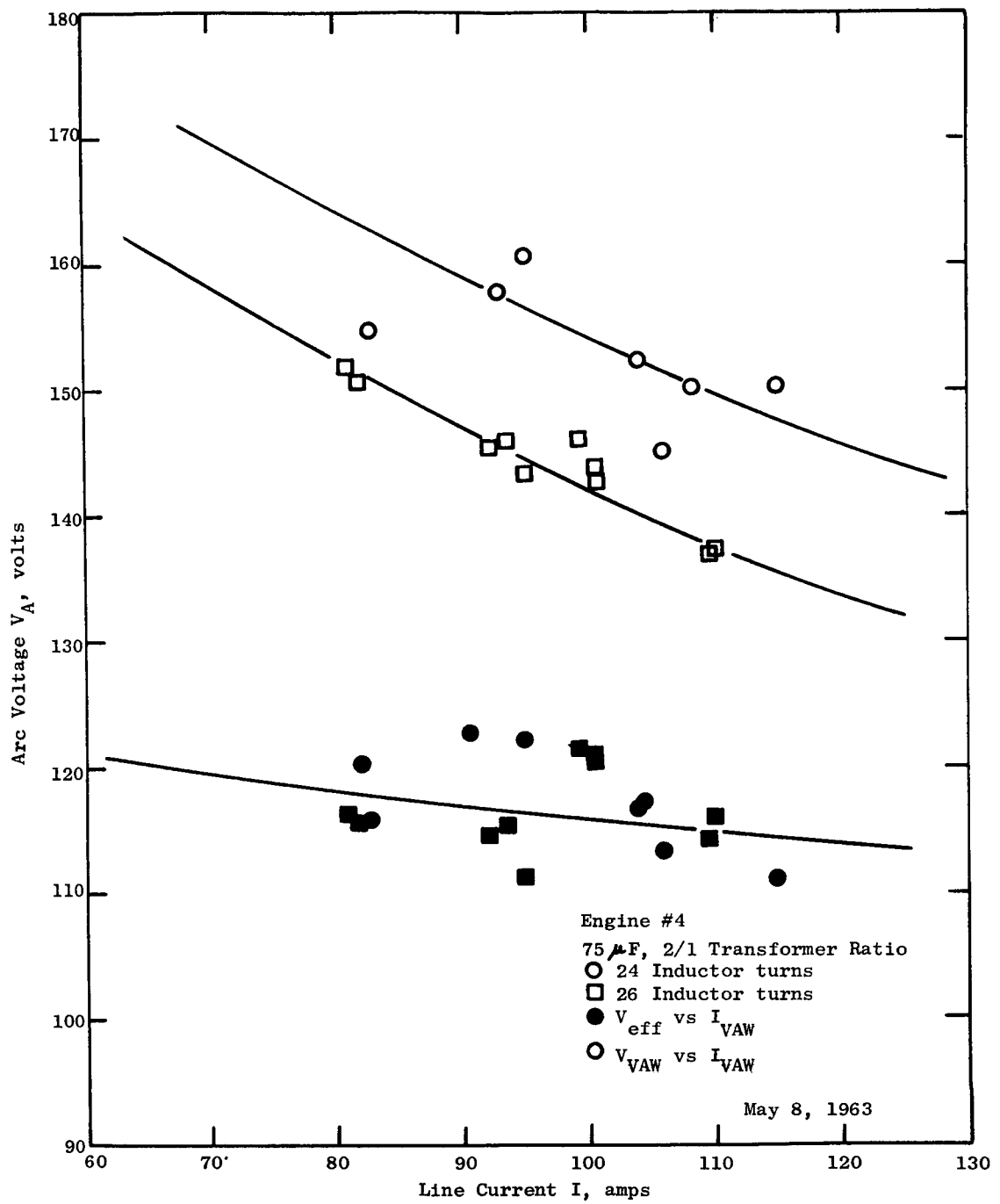


Fig. 2.30: Effect of Inductance on the Voltage-Current Relations of a Three-Phase Plasma Arc Jet Engine (Engine #4)

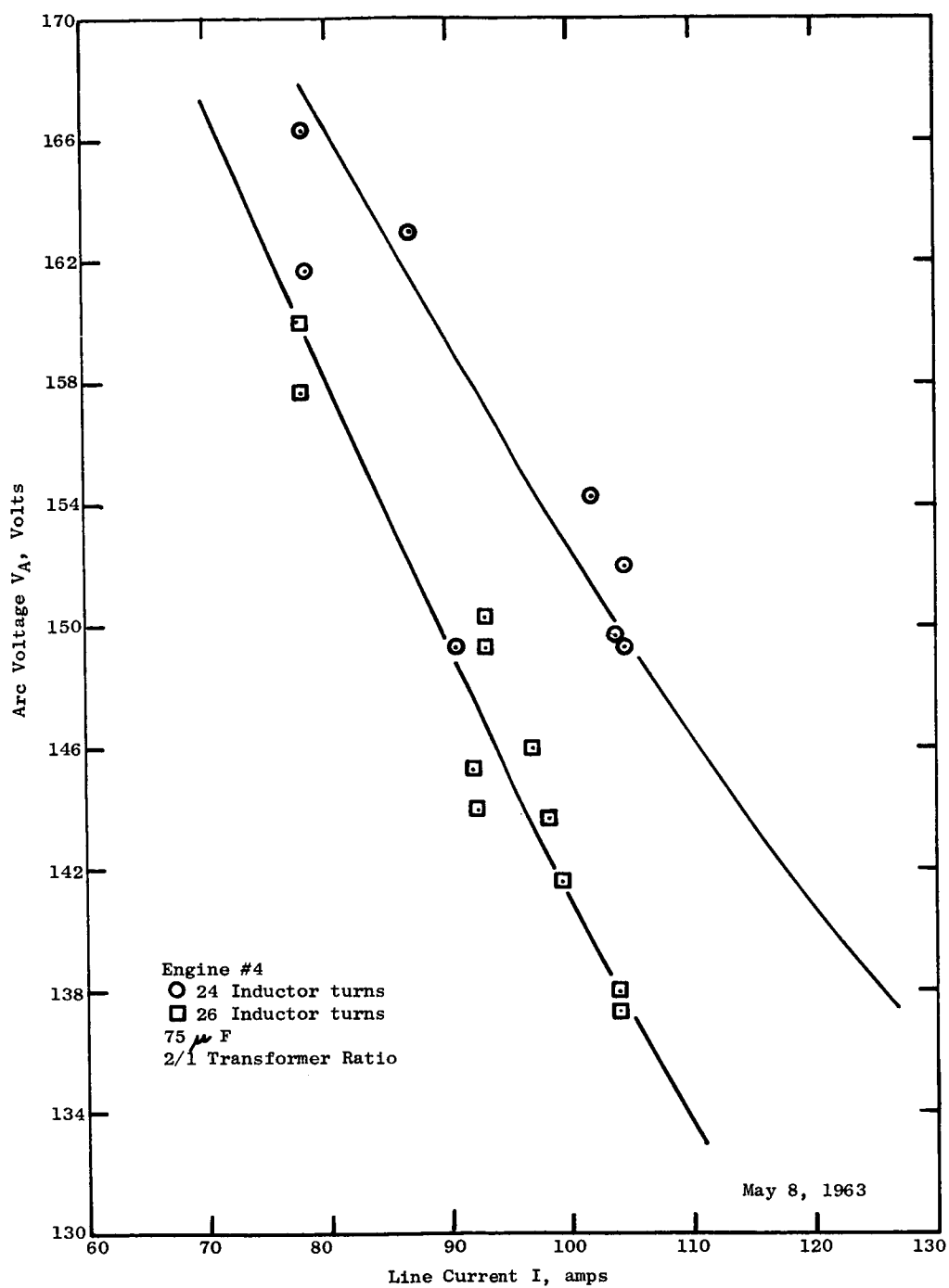


Fig. 2.31: Effect of Inductance on the Relation Between Indicated Voltage and Current (Electrodynamometer Readings, Engine #4)

1. The maximum voltage always occurs between the two center electrodes. Therefore, the arc current path between two center electrodes is electrically long, and in fact it visually appears to extend through the throat of the nozzle.
2. The minimum measured voltage occurs between the nozzle and one of the electrodes. Which one of the two electrodes is dependent solely upon the firing order of the three ac arcs in the engine. For example, Table 7 shows that when the firing order is clockwise the measured voltage between electrode A and the nozzle body B is the minimum of all three voltages. When the firing order in the engine is reversed by interchanging the power leads to the engine the voltage between electrode C and the body B is the minimum. This discovery of the dependency of the firing order on the measured voltage was of great interest, as previously it had always been assumed that the voltage difference between voltages V_{AB} and V_{CB} was due to a slight misalignment of the electrodes during assembly. This result again pointed out a very interesting fact about the three-phase engine design, that the electrical operating point of the engine was almost insensitive to electrode gap setting. This is in complete contrast to the electrical characteristic of a single phase arc jet engine.

ELECTRODE POSITION

A Center
B Body
C Center

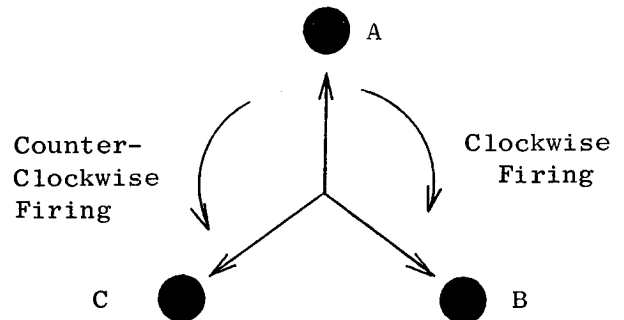


Fig. 2.32: Schematic of Electrode Firing

	Clockwise Firing		Counter-Clockwise Firing	
V_{AB} , Volts	140	110	250	110
V_{AC} , Volts	250	150	260	150
V_{BC} , Volts	250	130	180	100

Table 1: Voltage Measurements Between Electrodes

It must be pointed out that the quoted voltages are voltages measured with an electrodynamicometer voltmeter which has been calibrated for sinusoidal voltages. The differences in the measured voltage might not be due to a difference in the absolute RMS voltages but also due to a difference in the arc voltage shapes as can be seen in Fig. 2.33.

2.5 Performance Testing of the Three-Phase Plasma Arc Jet Engine (Y16-1)

Engine performance testing was initiated with the three-phase plasma arc jet engine, Y16-1, after the thrust measuring device had been completely checked out. By then the Y16-1 engine had been operated for over 50 hours reliably and had been started repeatedly without a single failure. During that time also, consistent ablation rate data had been obtained, which are reported in Section 6 of this report. These measured ablation rates had shown that erosion of the electrodes would introduce an error in the performance measurement of less than 1.55×10^{-4} percent. Also, the long duration runs had proven the design to be a realistic one, that is, it has incorporated design features which are favorable both for high performance and also for high reliability and extended operation at the 30 kw power level.

The test data obtained with this engine on September 18, 1963 are typical for several tests. They are tabulated in Table 2. As in all other test runs the thrust was measured keeping the flow rate constant and varying only the power. No attempt was made to obtain high specific impulse data by lowering the flow rate at the 30 kw level or by raising the power level above the 30 kw design point while keeping the flow rate constant. This was done after the other engines of the Y16-2 design were checked and all possible causes of failure were sufficiently well understood that there would be no delay in the results of the overall program.

The measured performances are not substantially above those quoted for dc arc jet engines of the same power level. It had been anticipated that the substantially lower arc currents would have a larger effect on the efficiency. The line currents of the three-phase ac engine are only 119 amps, while the line current with which the dc engine was operated at 30 kw is 205 amps. The analysis had actually predicted that with the regenerative cooling design a decrease in the engine heat loading would not lead to a substantial increase in the cooling efficiency as the cooling efficiency is already very high for the present engine design.

These performance tests had now proven the three-phase engine to fulfill the performance specifications and even exceed them slightly.

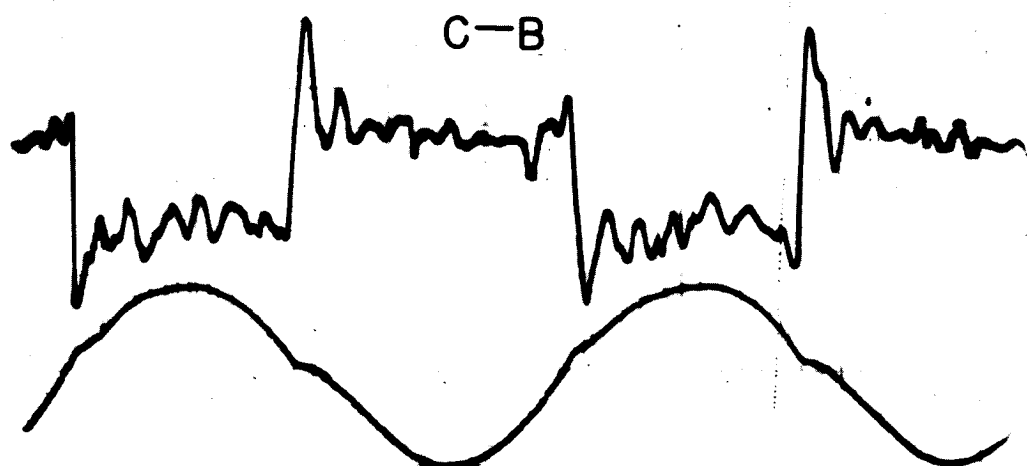
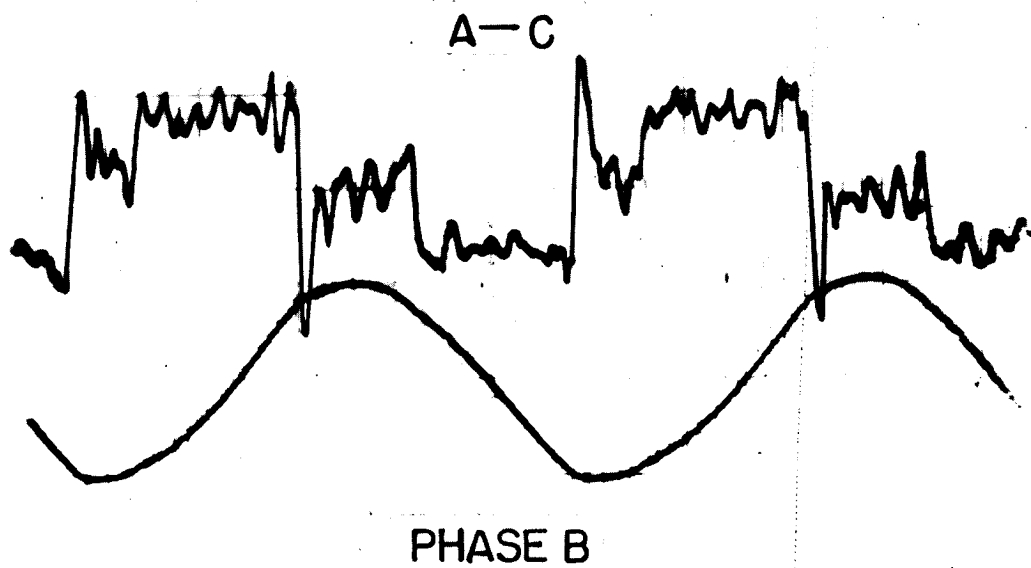
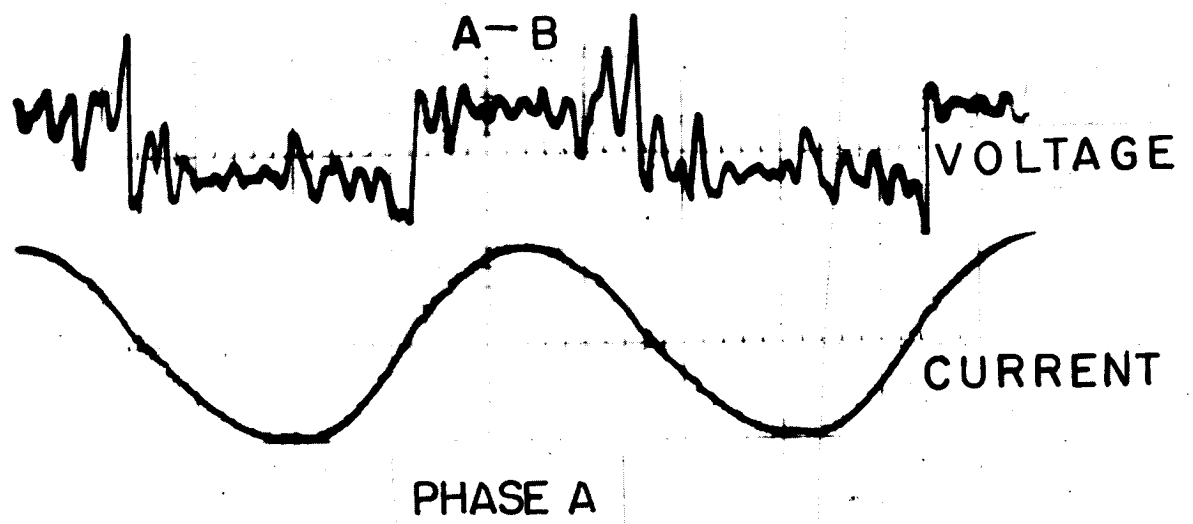


Fig. 2.33: Line Currents and Arc Voltages of a Stable Operating Three-Phase Arc Jet Engine

Time	Power, P kw	Flow Rate, w lb/sec	Displacement, d mils	Thrust, T g	Specific Impulse Isp, sec	Efficiency Percent	Current Amps
14:08							
14:45	27.0	5×10^{-4}	36.7	224	988	40.00	105
15:08	26.9	5×10^{-4}	36.7	224	988	40.15	110
15:31	29.5	5×10^{-4}	38.45	236	1040	40.57	116
15:50	30.0	5×10^{-4}	38.65	237	1046	40.35	119

Table 2: Test Data for Engine Y16-1 (September 18, 1963)

3. THE PLASMA ARC JET ENGINE Y16-2

3.1 Design of Engine Y16-2

The evaluation of the test results obtained with Engine Y16-1 suggested certain changes in the design of the engine. These indicated changes were essentially minor. Engine Y16-2 differs from Engine Y16-1 only in its front part, the insulator section and the guts of the engine. All radial O-ring seals which were originally designed into Engine Y16-1 were abandoned because of the required close tolerances which could not be held by the metal O-ring manufacturer. Modifications in that respect had already been carried out on Engine Y16-1 which resulted again in axial O-ring seals. The modifications proved successful and resulted in leak-tight sealing. Threading of fittings into the boron nitride insulator had proven impractical because of the repeated disassembly of the engine during the investigation of ablation rates. Swagelok fittings were modified in such a fashion that their threaded section extends 0.7 inch and could be threaded into a steel nut which lies flat in a counter bored recess. New O-ring seats were machined into the Swagelok fittings to take metal O-rings of special design. The new electrode holder has been designed to take electrodes made from a 0.75 inch diameter tungsten rod as shown in Fig. 3.1. The assembly of the new engine design is shown in Fig. 3.2. A photograph of the assembled engine is given in Fig. 3.3 while an exploded view appears in Fig. 3.4.

3.2 Testing of Engine Y16-2

After the most favorable engine configuration for the three-phase engine had been established with the design and testing of Engine Y16-1, Engine Y16-2 was built and tested. The Y16-2 engine design differs from the Y16-1 engine design in that it incorporates center electrodes made from a 0.75 inch diameter tungsten rod compared to center electrodes made from an 0.50 inch diameter tungsten rod in Engine Y16-1. By using the larger size electrodes in Engine Y16-2 the projected area of the electrodes had been increased 2.64 times. The ablation rate of the center electrodes in Engine Y16-2 was therefore expected to be considerably lower than in Engine Y16-1 as indicated by the ablation analysis described in Appendix III.

Testing of Engine Y16-2 was delayed due to an accidental fill-up of the test tank with water. The engine was apparently not damaged by the water and the silicone oil in which it was submerged for a substantial length of time. Heavy flaking off of boron nitride occurred during the following test run. Dislocation of a boron nitride piece in the throat section finally caused stagnation of the arc forcing a shut down of the engine. Upon disassembly, the internal surfaces of the boron nitride insulator and the electrode holder were found coated heavily with silica. Spalling and disintegration of the boron nitride was evident, but no damage had been done to the engine nozzle nor the electrodes. Unfortunately, both center electrodes were fractured when an attempt was made to remove them from the electrode holder which could not be removed from the insulator.

New parts were ordered and received. The engine was assembled again with the same electrode setting that had proven to be optimum for Engine Y16-1. The

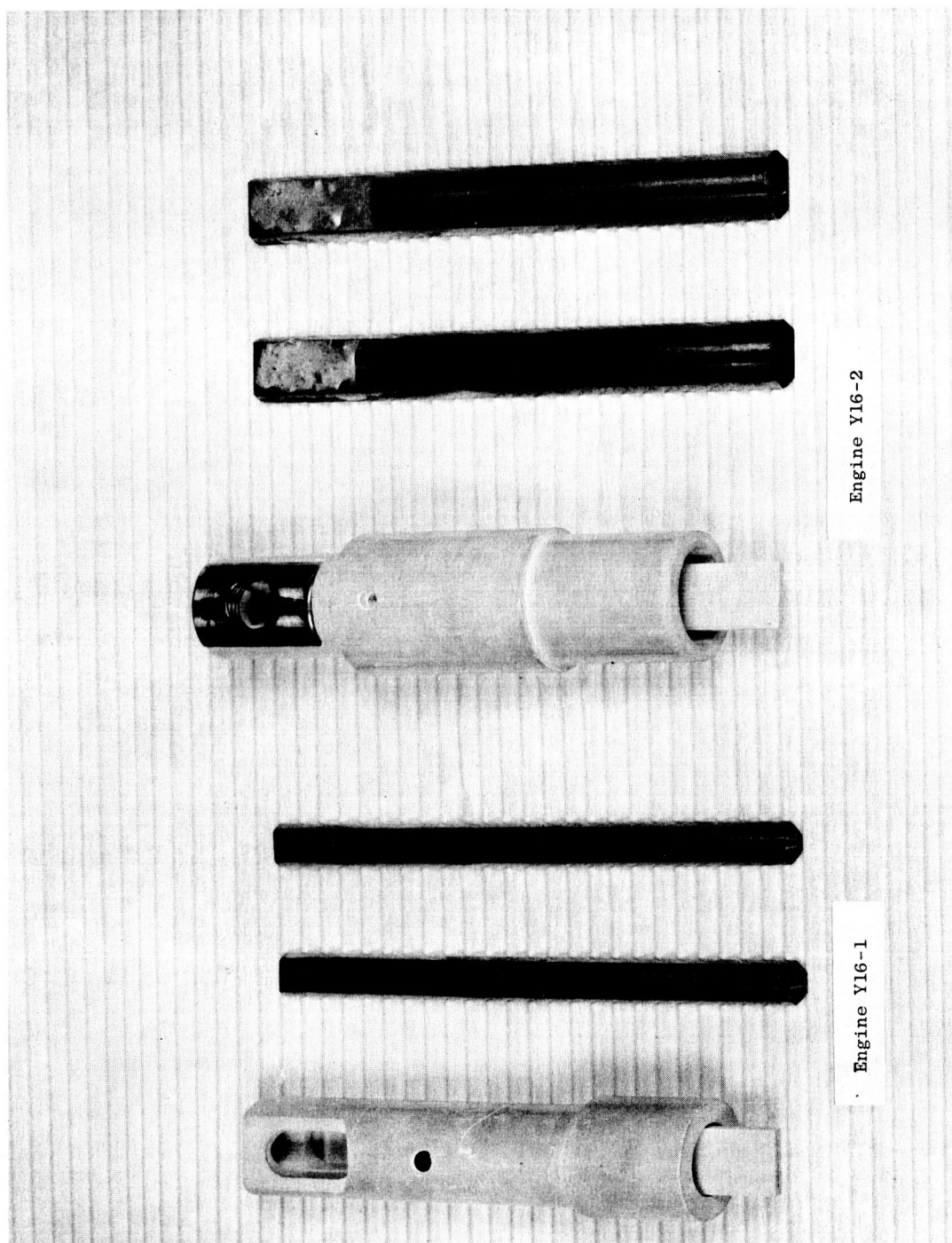


Fig. 3.1: Electrodes and Electrode Holder Assemblies of Engines Y16-1 and Y16-2

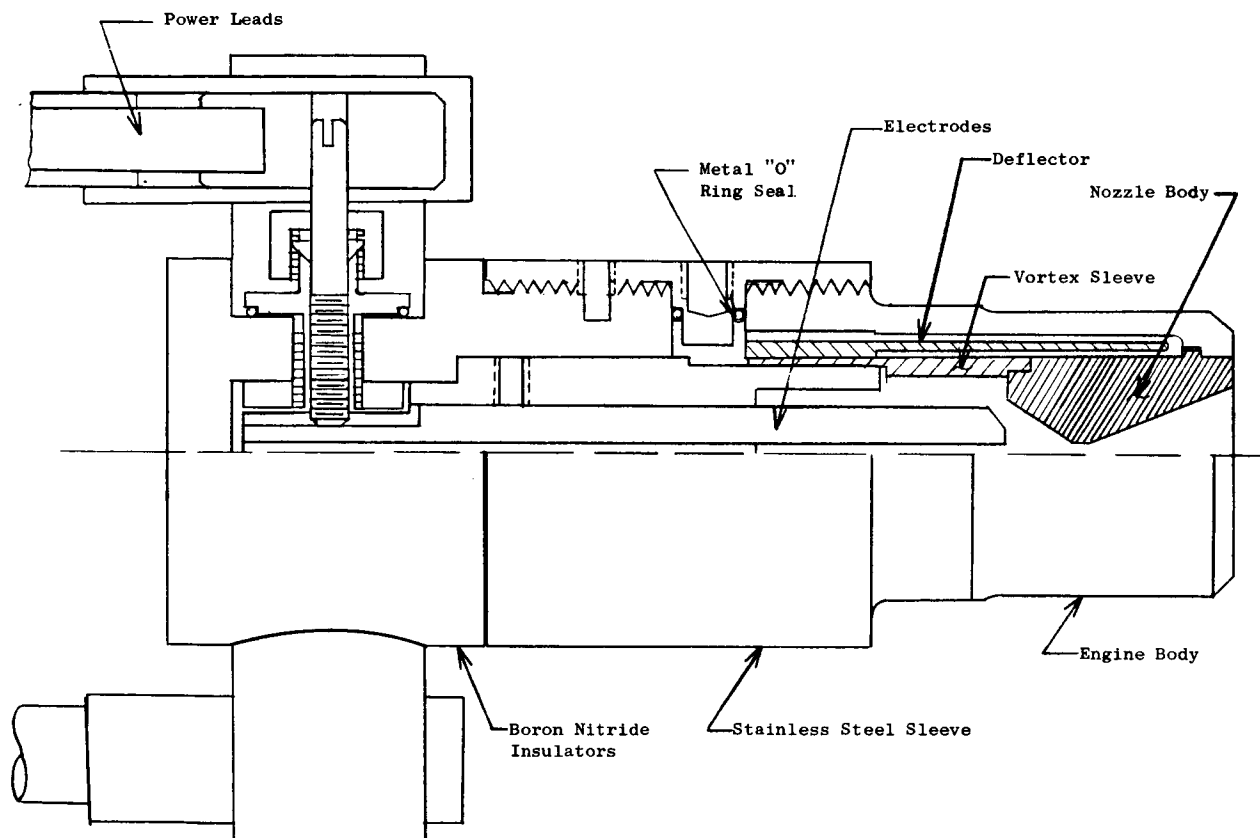


Fig. 3.2: Advanced 30 KW Three-Phase Plasma Arc Jet Engine (Y16-2)

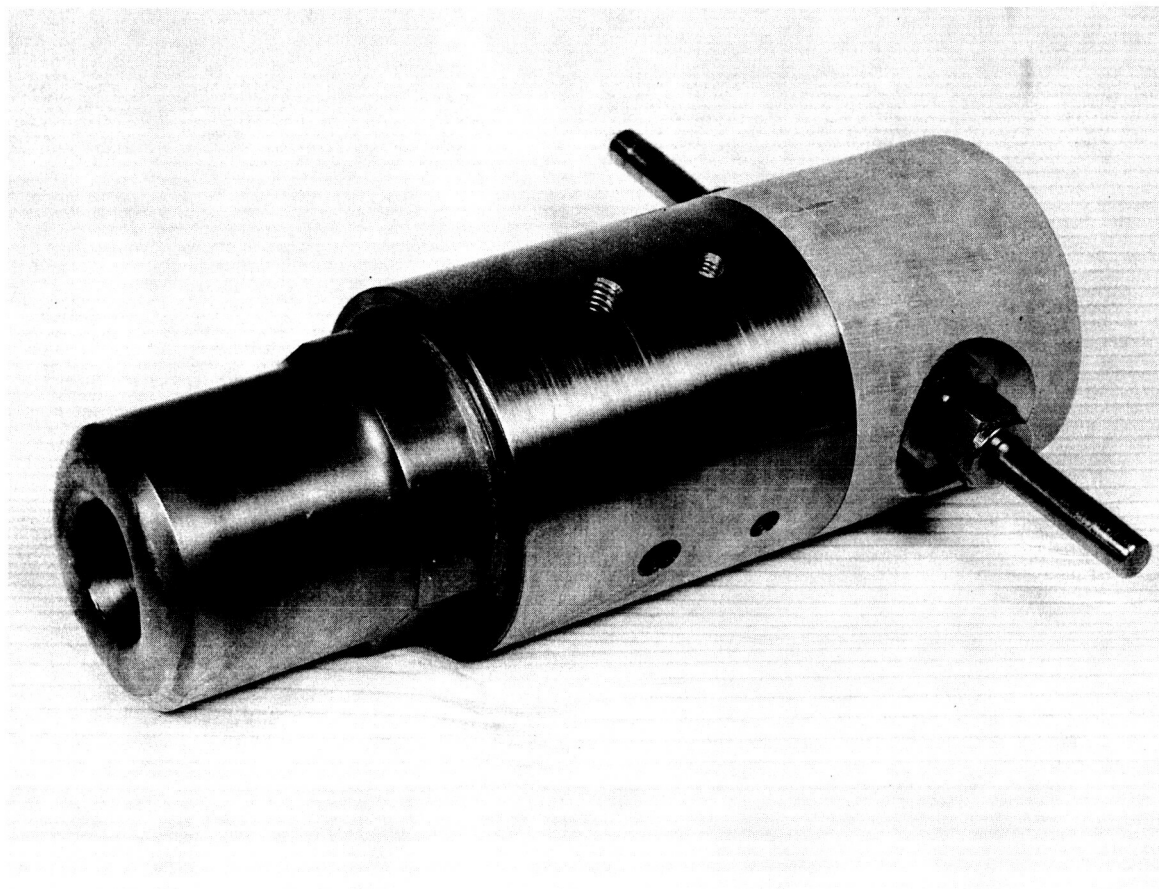


Fig. 3.3: 30 KW Three-Phase Plasma Arc Jet Engine (Y16-2) Assembled

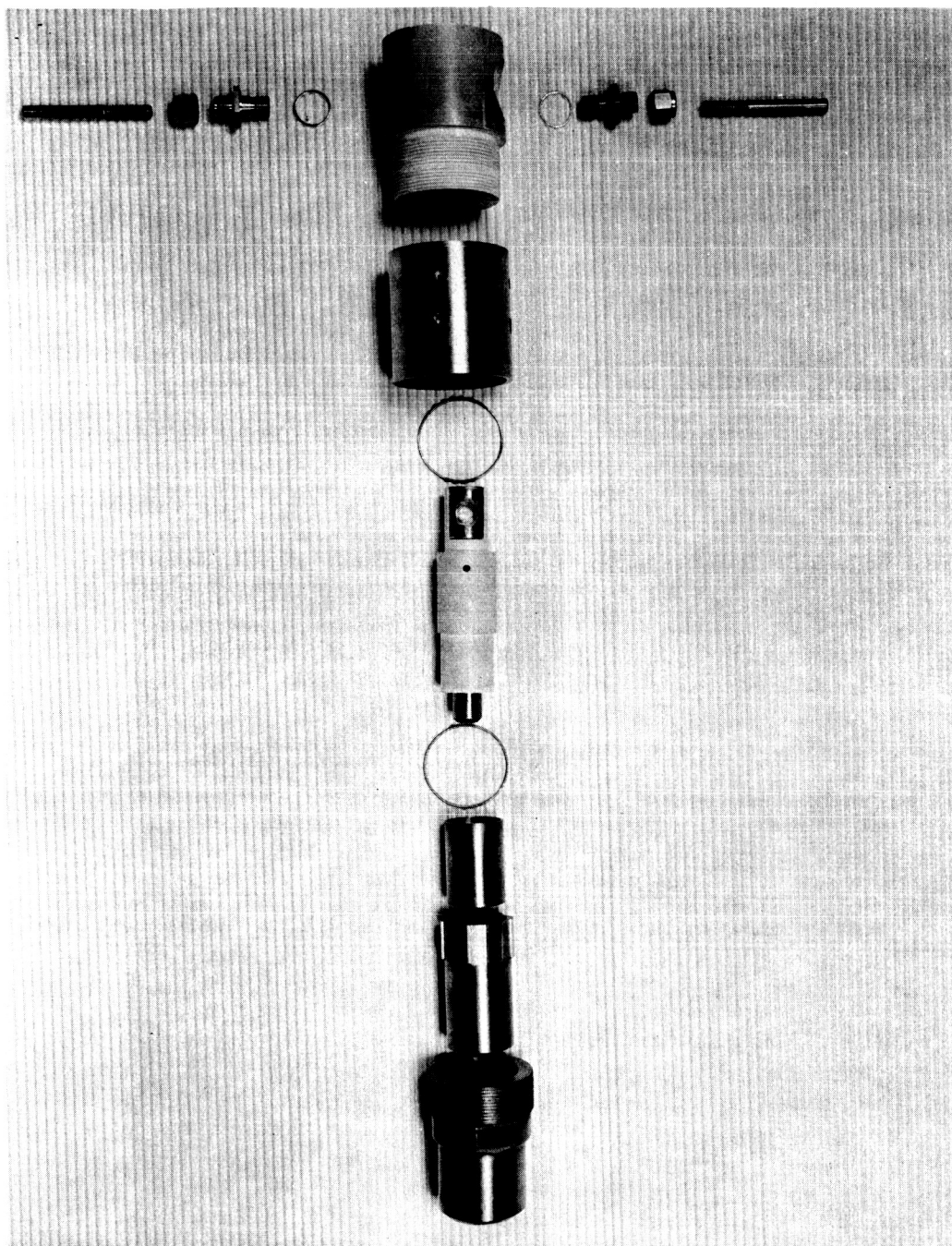


Fig. 3.4: 30 KW Three-Phase Plasma Arc Jet Engine (Y16-2) Exploded View

first test results indicated that the three line currents were slightly higher for this engine at the 30 kw power level than for Engine Y16-1. This variation in the voltage-current characteristic of the engine can be explained by the difference in the arc chamber size. Due to the larger electrodes the internal diameter of the vortex sleeve had to be enlarged to prevent arcing to the sleeve. The increase in the arc chamber size caused the vortex strength which is available with the fixed propellant flow rate to decrease. This, in turn, results in a less diffused arc and higher currents. Several modifications of the vortex sleeve have proven this explanation of the observed difference in arc current to be correct.

During an extended run of Engine Y16-2 with currents of 145 amps at 30 kw, no adverse effect on the engine was observed. The run had to be terminated only because of an overloading of the stabilizing inductors which were set for the electrical conditions prevailing with Engine Y16-1. It was observed that the power remained absolutely constant over the entire run. No voltage adjustments had to be made. The current traces on the oscilloscopes appeared as perfect sine waves. This indicated an extremely stable arc operation.

3.2.1 Experimental Investigation of Engine Y16-2 Operation

3.2.1.1 Testing for Abnormal Operating Phenomena

After several test runs of Engine Y16-2 it was realized that it was very difficult to repeat the results of previous test runs with this engine. This was quite contrary to the experience gained with Engine Y16-1 where operation could be duplicated consistently.

Several phenomena were observed that had to be individually tracked down and explained:

- a) Sudden drop in arc power
- b) Sudden rise in arc power about 30 seconds after startup
- c) Periodicity in arc power

Sudden Drop in Arc Power - The sudden drop in arc power was mostly observed after approximately six minutes of continuous stable arc operation. The time of drop in power was also found to depend on whether or not a new electrode holder was used in the test. This difference in time of sudden drop in power which was associated with a rise in the arc current had to be attributed to the electrode holder. When the electrode holder which is machined from boron nitride was finally tested for conductivity it was found that the holder had become surface conductive.

Two reasons for surface conduction could be found, diffusion of tantalum into the boron nitride or coating of the boron nitride by the filler of a durabola washer which was used in the engine to improve the distribution of the incoming propellant gas for cooling. Both possible causes for the surface conduction of the boron nitride were eliminated and from then on no further drop in power combined with a current rise was observed.

Periodicity in Arc Power - Periodicity in arc power has been observed only twice. Yet that it occurred indicated that there exists a resonating system in the plasma arc jet engine that can be tuned in by some possible combination of power, propellant flow rate, and electrode setting. The periodicity is actually a kind of instability. The arc power would jump instantaneously to a higher value and remain constant at that level for about 15 seconds, and then return instantaneously to the lower power level and remain at that level for about 10 seconds. As this phenomenon was observed only twice and could not be duplicated, it was impossible to pin down the interaction to either the volume in the propellant feed system or the thermal storage capacity of the engine.

Sudden Rise in Arc Power - It was observed that the engine operation would be most stable and at the desired voltage-current relation when a sudden jump in arc power occurs after approximately 20 seconds. This increase in arc power was found to be due exclusively to a jump in power which is measured in the power line going to the engine body, that is, the nozzle electrode. When observing closely the operation of the engine and the three indicated line powers on the Sanborn chart a close correspondence between the appearance of the exhaust and the power of the nozzle line can be found. Whenever the brilliance of the exhaust suddenly increases, as if the arc is drawn into the divergent section of the nozzle, the sudden increase in the power occurs. This increase in power is accompanied by a drop of all three line currents to a value of about 105 amps while the total power is 30 kw. If the electrode setting and the vortex sleeve position is correct the arc will jump to the higher power with the low currents and remain there.

3.2.1.2 Testing for the Effect of Gap Setting on the Power-Current Relationship

Testing the Engine Y16-2 for the effect of gap setting was a major task as the result of these tests would indicate whether Engine Y16-2 would be able to operate over long durations. From the ablation rate data obtained with Engine Y16-1 it could be expected that the electrodes would lose approximately 0.150 inch length. This decrease in length would result in a change of gap setting which had to be considered in the initial setting of the electrodes. The test results are tabulated in Table 3. The gap setting as given in Table 3 is explained by Fig. 3.5 which is drawn to a scale of 2/1. The present result indicate that the engine will operate over a wide range of gap settings but adjustment in the electrical system will be required to take care of the change in the voltage-current relation.

When studying the data it should be observed that the voltages tabulated are not actually the true voltages. These voltages were read from an electro-dynamometer which has been calibrated for sinusoidal voltages. The indicated voltages are about 40% above the effective voltages due to their shapes. Yet it is interesting to observe the apparent differences in the three arc voltages which can be explained by the configuration of the tested engine. But it should be made clear that these indicated voltage differences are not reflected back to the output voltages of the generator. These voltages remain perfectly sinusoidal and

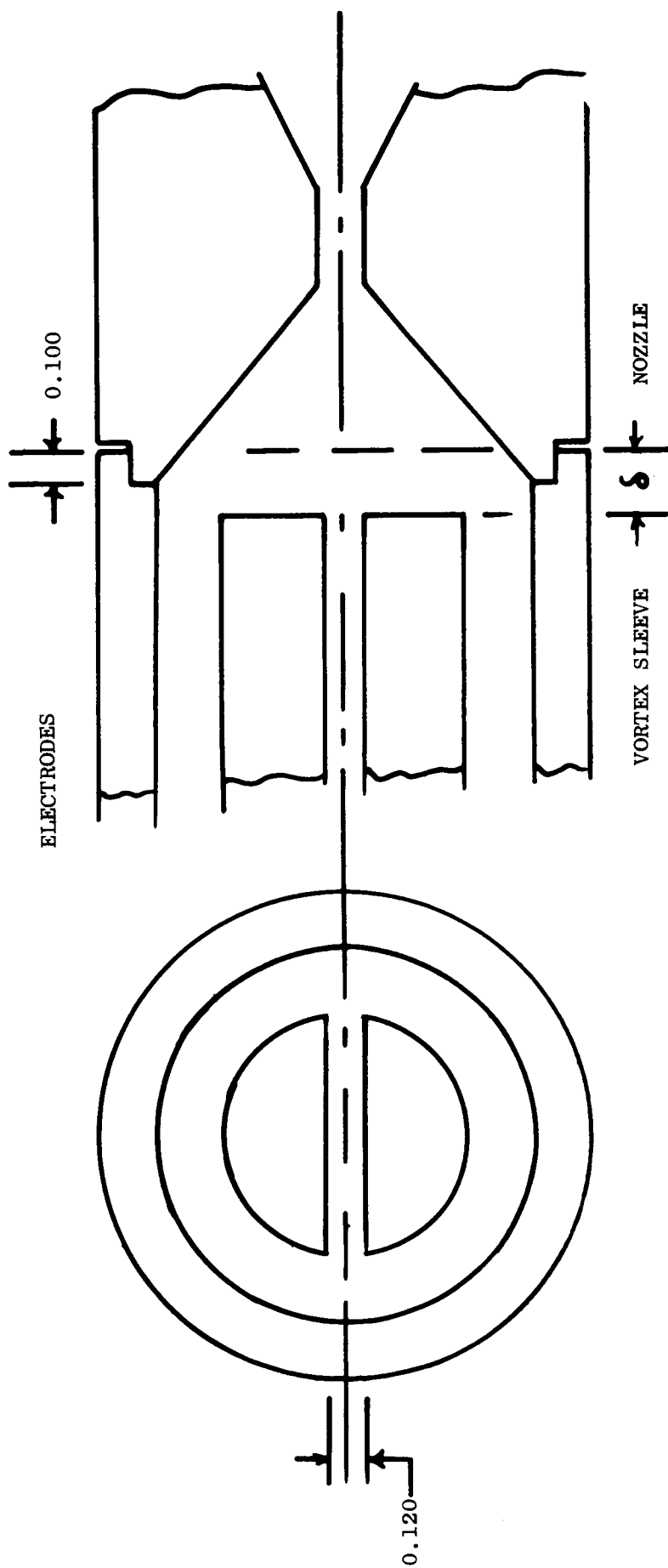


Fig.3.5: Y16-2 Electrode Setting (Double Scale)

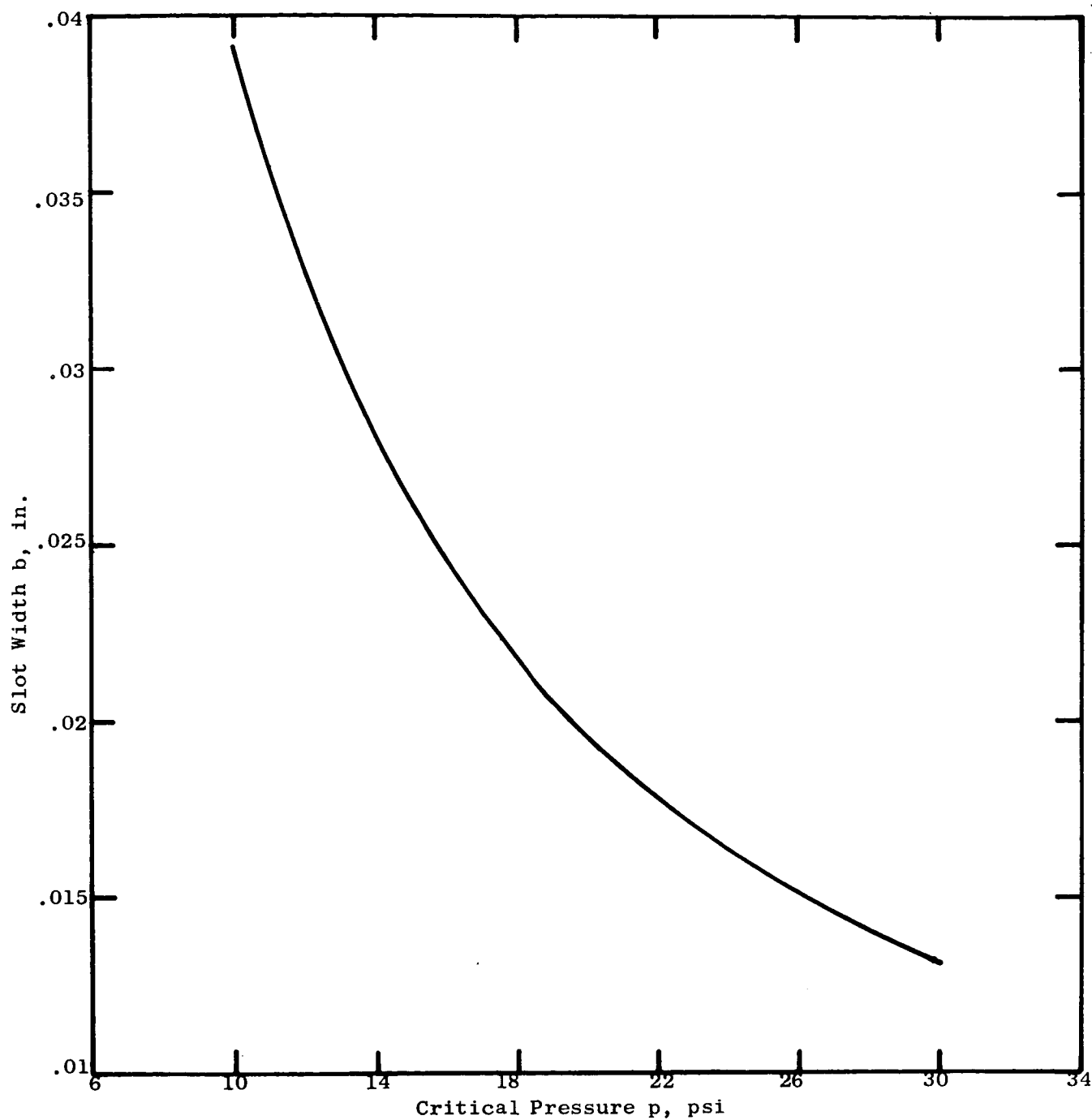


Fig. 3.7: Vortex Slot Width as a Function of Upstream Critical Pressure for a Flow Rate of 5×10^{-4} lb/sec

Date	Gap Setting δ , mils	Power P, kw	Voltages V, Volts			Current I, amps			Nozzle Material	I_{AV}	V_{AV}	$\sqrt{3} IV$
			V_{AB}	V_{AC}	V_{CA}	I_A	I_B	I_C				
10-31-63	0.062	29.9	145	245	245	125	120	118	.02 Th O ₂ -W	120	212	43.6
10-30-63	0	29.8	145	220	230	120	120	123	.02 Th O ₂ -W	121	198	41.5
10-28-63	0.140	30.0	195	270	285	109	111	112	.02 Th O ₂ -W	110	250	47.6
10-31-63	0.062	31.1	170	240	240	130	122	120	W	124	217	46.4

Table 3: Effect of Electrode Setting on the Power-Current Relation of Engine Y16-2

of equal magnitude. The power supply sees only sinusoidal voltages and currents. The power factor seen by the power supply is determined only by the amount of stabilizing inductance and the size of the capacitors.

3.2.1.3 Two Modes of Operation

An interesting phenomena was discovered during the initial operation of Engine Y16-2. The symptoms of this mode of operation of the engine were a sudden drop in power associated with an increase in currents and a drop in the indicated arc voltages.

After several runs it became apparent that the transition from the normal operation to the high current operation was affected by the temperature of the engine. Whenever the engine was started from cold conditions the transition would occur in about 230 seconds. After a shutdown the operation would be normal for a given length of time, the time being a function of the length of shutdown and the amount of cooling with hydrogen flow during the down time.

This behavior indicated a dependence of the arc operation on the engine temperature. Calculations were made of all possible thermal expansion effects that could affect the operation of the arc. None of the results could explain the observed arc behavior. It was then realized that this sudden change could be associated with a flow change.

The Engine Y16-2 has been designed such that the propellant flow in the engine follows a path that will assure the optimum heat transfer from the engine to the propellant. The propellant enters the engine through the insulator and flows into a plenum chamber which is formed by the insulator inner surface, the metal "O" ring and the upper rim of the engine body. From this chamber the propellant flows into the outer path along the body which is formed by the body and the deflector. The flow returns toward the front in the path formed by the deflector and the nozzle body. At the level where the nozzle body and the vortex sleeve come together, two slots which are machined tangentially to the inner diameter of the vortex sleeve permit the propellant to enter the arc chamber. The propellant tangential velocity causes a vortex flow that moves the arc and prevents it from permanently attaching itself to one spot of the converging section of the nozzle.

In the Y16-1 engine there has never been the problem of the arc remaining stagnant. In Engine Y16-2 stagnation occurred several times for no easily explained reason, when apparently all components had remained the same and the engine was assembled as required.

A close analysis of the engine design indicated that there actually exist two flow paths, the one that was designed into the engine and the other a leakage path around the electrodes. By adding up the tolerances it became clear that a larger part of the propellant flow could enter the arc chamber along the electrodes. By having this axial flow the arc is actually forced to the wall opposing the effect of the vortex.

In Fig. 3.6 the flow passages in the engine are shown schematically.

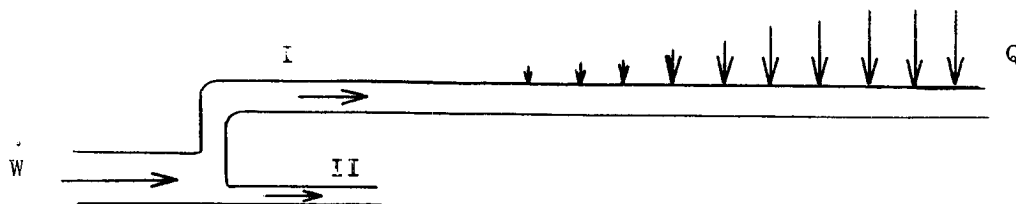


Fig. 3.6: Flow Passages in the Y16-2 Engine

The upper pass I is the pass with which the engine was designed to operate. The propellant enters the pass and is heated to increasing temperatures. The final temperature before entering the arc chamber is approximately 3000°R. The lower pass II is the leakage pass around the electrodes. The gas flowing through this pass remains relatively cool before being discharged into the arc chamber. Analyzing the flow with the heating of the propellant in pass II, it can be seen that on starting the main flow of the propellant will enter the arc chamber through pass I. On heating up of the engine the temperature of the gas flowing in pass I increases. This causes a choking of the flow in this pass and a redistribution of the total flow to pass II, the leakage around the electrodes. With this analysis of the flow pattern as a function of the relative magnitudes of the flow passes and the temperature of the engine body, the observed dependency of the engine operation on the flow and the length of the operation could be explained. From Fig. 5.7 it can be seen how closely the tangent vortex slots were designed for optimum flow velocity into the arc chamber. Any redistribution of the flow had to be detrimental. That this problem was not encountered in the Engine Y16-1 is due to the much smaller leakage passes possible with the smaller electrodes and the apparently less critical flow in the smaller arc chamber.

New separators that separate the two center electrodes were made to very close tolerances. This almost eliminated the visible pass. As an added precaution the electrodes were sealed into the electrode holder. After this change in the assembly procedure had been taken, sudden drops in power associated with a drop in the voltage and a steep increase in the current were no longer observed.

3.3 Performance Testing of Engine Y16-2

After engine Y16-2 had been shown to operate reliably it was tested for performance. The engine has been designed for a propellant weight flow rate of 5×10^{-4} lb/sec and a power of 30 kw. In the performance tests these two parameters were therefore kept as constant as possible. The results of this test are tabulated in Table 4. They indicate that there is no appreciable difference between the performances of Engine Y16-1 and Engine Y16-2 as was to be expected. The engine performs above the specified minimum requirement of 1000 sec. specific impulse and 0.5 lb of thrust at 30 kw.

Time	Power, P kw	Flow Rate, \dot{W} lb/sec	Displacement, d mils	Thrust, T lb	Specific Impulse Isp, sec	Efficiency Percent	Current Amps
14:36							
14:45	30.7	4.936×10^{-4}	35.0	0.5054	1024	36.8	113
14:51	30.5	5.0×10^{-4}	36.0	0.520	1040	38.7	122
15:00	29.5	5.0×10^{-4}	35.8	0.517	1042.5	39.9	121
15:00	30.1	5.0×10^{-4}	36.0	0.520	1040	39.2	121
15:08	28.3	5.0×10^{-4}	34.6	0.4996	999	38.5	113

Table 4: Test Data for Engine Y16-2 (October 18, 1963)

3.4 Long Duration Operation of Engine Y16-2

After receipt of the go-ahead by the Project Manager of NASA, long duration operation of Engine Y16-2 was initiated. The engine was started December 8, 1963. It operated satisfactorily for 15 hours when the arc operation dropped into the low power mode and remained in this mode for over 1/2 hour. Attempts to dislodge it from this operating mode failed. The currents were lowered until a jump into the high power mode occurred. But when the currents were raised again to bring the engine up to full power the arc jumped back to the lower mode at about 27 kw. There were apparently no adverse effects to the electrodes or the nozzle as no visible ablation was observed. The run was terminated after 15 hours. Upon inspection of the engine the nozzle was found in good condition. The electrodes had deep craters in the center and the entire area over which arc attachment had occurred was rugged. A picture of the electrodes after this run is shown in Fig. 3.8.

It is of interest to note that the arc apparently never moved to the outer edges of the electrodes as no signs of arc attachment could be found in this area. The arc must, therefore, have remained attached to the center of the electrodes despite the fact that the arc would have been shorter by striking from the outer edges to the nozzle.

The long duration run revealed a condition that was not apparent from the short duration runs on which the decision to start the long duration run was based. During the 6 hour and shorter runs all material lost came from the center of the electrodes. The loss during these runs, however, was never large enough to lead to the instability that was observed after 15 hours.

After the 15 hour run the electrodes were dressed and the engine was assembled with a gap of .200 in. Upon starting, the engine operated in the low power mode and remained in that mode. All attempts to bring the engine into the high power mode at a power level of 30 kw failed. Whenever it was attempted to raise the power above 27 kw the arc jumped back into the low power mode. After 20 minutes the arc suddenly jumped into the high power mode on its own. From that point on the engine performed well at above 30 kw for over 4 hours when the tests were discontinued.

The results of this test are not conclusive. They actually have raised some more questions about the conditions which determine the mode of operation of the Y16-2 engine.

The power-current relation of Engine Y16-2 when operating unstably is shown in Fig. 3.9. It can be seen that the power-current relation has two branches. The lower branch is considered the low power mode relation, while the upper branch is called the upper mode operation. In the low power mode there exists effectively no control over the arc power. In the upper mode the arc power is responsive to increased applied voltage. The breaking point, that is the point at which the arc will jump to the low power mode, is apparently a function of the electrode tip configuration. The arc will not remain in the

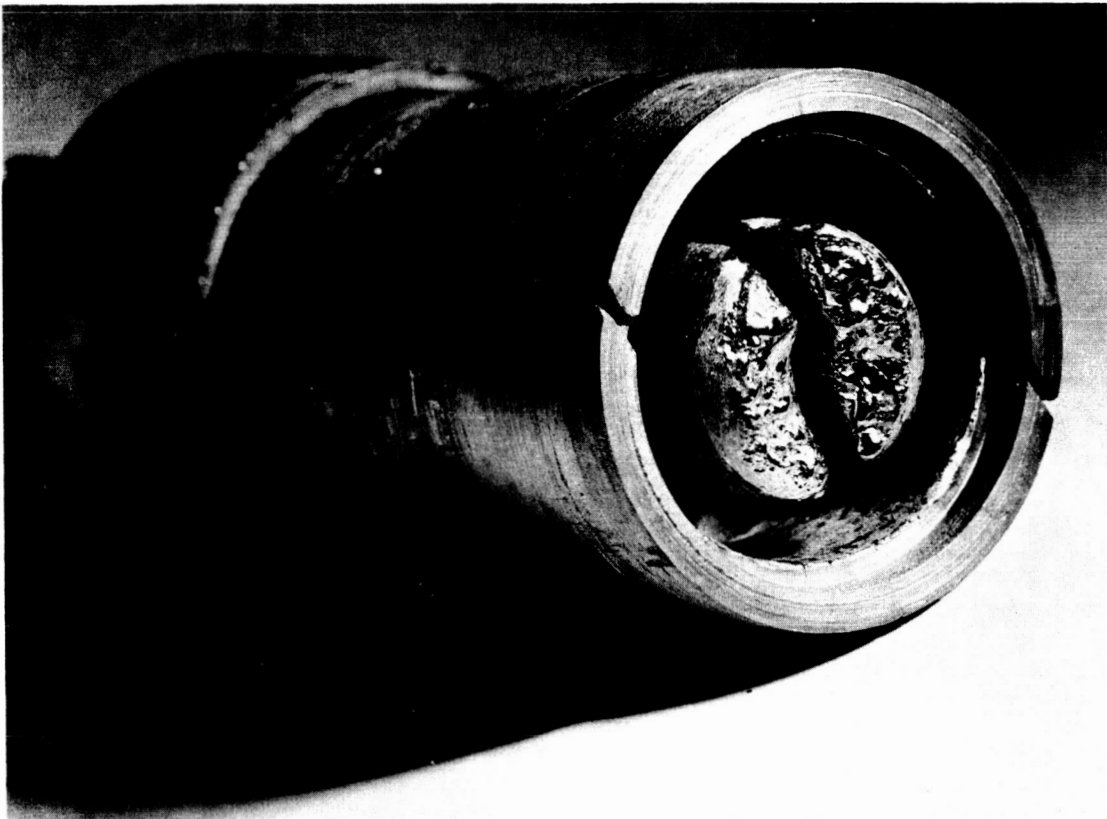


Fig. 3,8 : Electrodes of Engine Y16-2 After 15 Hours Continuous Operation

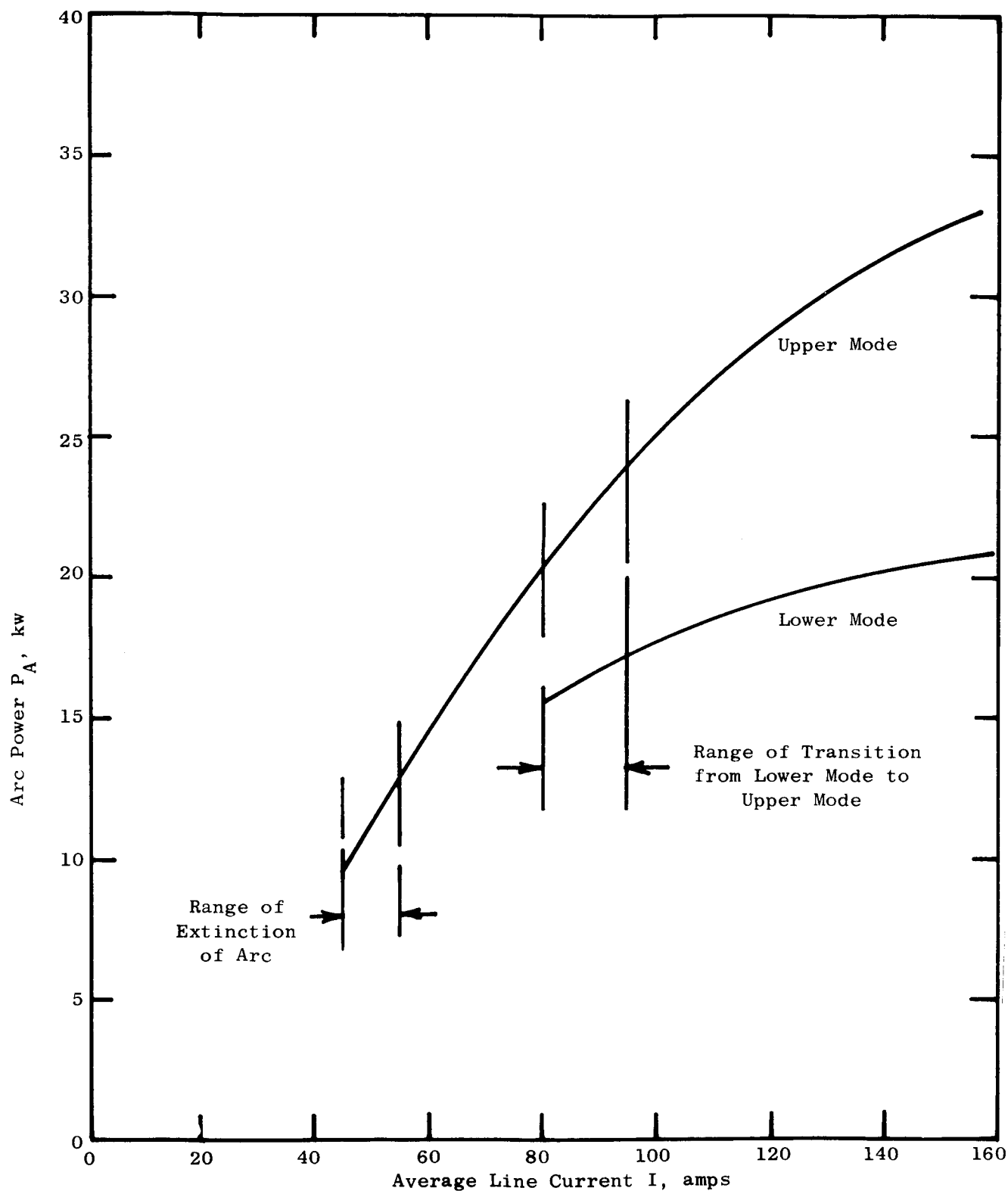


Fig. 3.9: The Instability of Arc Operation in the Y16-2 Three-Phase Plasma Arc Jet Engine Design

lower mode necessarily but will sometimes return on its own to the upper mode. Return to the upper mode can also be accomplished by decreasing the current until the arc jumps into the upper mode. The arc power can then be increased by raising the applied voltage. Apparently, the arc is always more stable in the upper mode at the low current. The stability of the arc at currents of about 120 amps, however, depends on the electrode tip configuration.

4. LONG DURATION OPERATION OF ENGINE Y16-1

4.1 Initial Long Duration Test

The difficulties experienced with the Y16-2 engine seemed to require long duration runs for their solution. It was decided to operate Engine Y16-1 for an extensive length of time to determine if a decrease in the ablation rate can be expected after a considerably longer time of operation. This decision was based on the experiences of other investigators with respect to ablation rates of the center electrodes of dc engines as was communicated to us by Mr. Harold Ferguson, Project Manager of this contract. According to the data submitted to NASA by the other contractors the ablation rate decreased markedly with time of operation. The longest time Engine Y16-1 had previously been operated was 6 hours. For this time the ablation rate was equal to the ablation rate of several shorter runs, lasting from 1/2 hour to 4 hours and 40 minutes.

Engine Y16-1 was operated for 24 hours at a power level of 30 kw. The run had to be terminated at that time because of a delay in the delivery of additional hydrogen supply. The ablation rates for this entire run were 1.2×10^{-5} and 0.8×10^{-5} g/sec respectively for the two electrodes. These rates were about half as large as those which would have been predicted from the ablation rate data plotted in Fig. 4.1. The ablation rates measured for the 24 hour run indicate that Engine Y16-1 is not limited to 100 hours operation as was predicted when considering the ablation rate data obtained from 1/2 to 6 hour duration runs. The engine should therefore have a lifetime of at least 200 hours based on the overall ablation rate data measured for the 24 hour test run.

4.2 250 Hour Duration Run With Repeated Restarts

4.2.1 Continuous Operation

The 24 hour run had indicated that the ablation rate of the center electrodes of the three-phase arc jet engine is also affected by the length of time of operation and that with increasing operating time the rate decreases. The measured ablation rates of the 24 hour run proved that Engine Y16-1 would be capable of operating for at least 200 hours with respect to electrode life. Based on this result it was, therefore, decided to carry out the 250 hour duration run with Engine Y16-1.

The run was initiated December 27, 1963 at 23:58 with the thrust measuring device having been calibrated prior to the start. During the first days of operation the power varied between 29.0 and 31.2 kw. At the 30 kw power level and a flow rate of 5×10^{-4} lb/sec the average performance of the engine was

Thrust, T	0.511 lb
Specific Impulse, I_{sp}	1022 seconds
Efficiency, η	38.0 percent

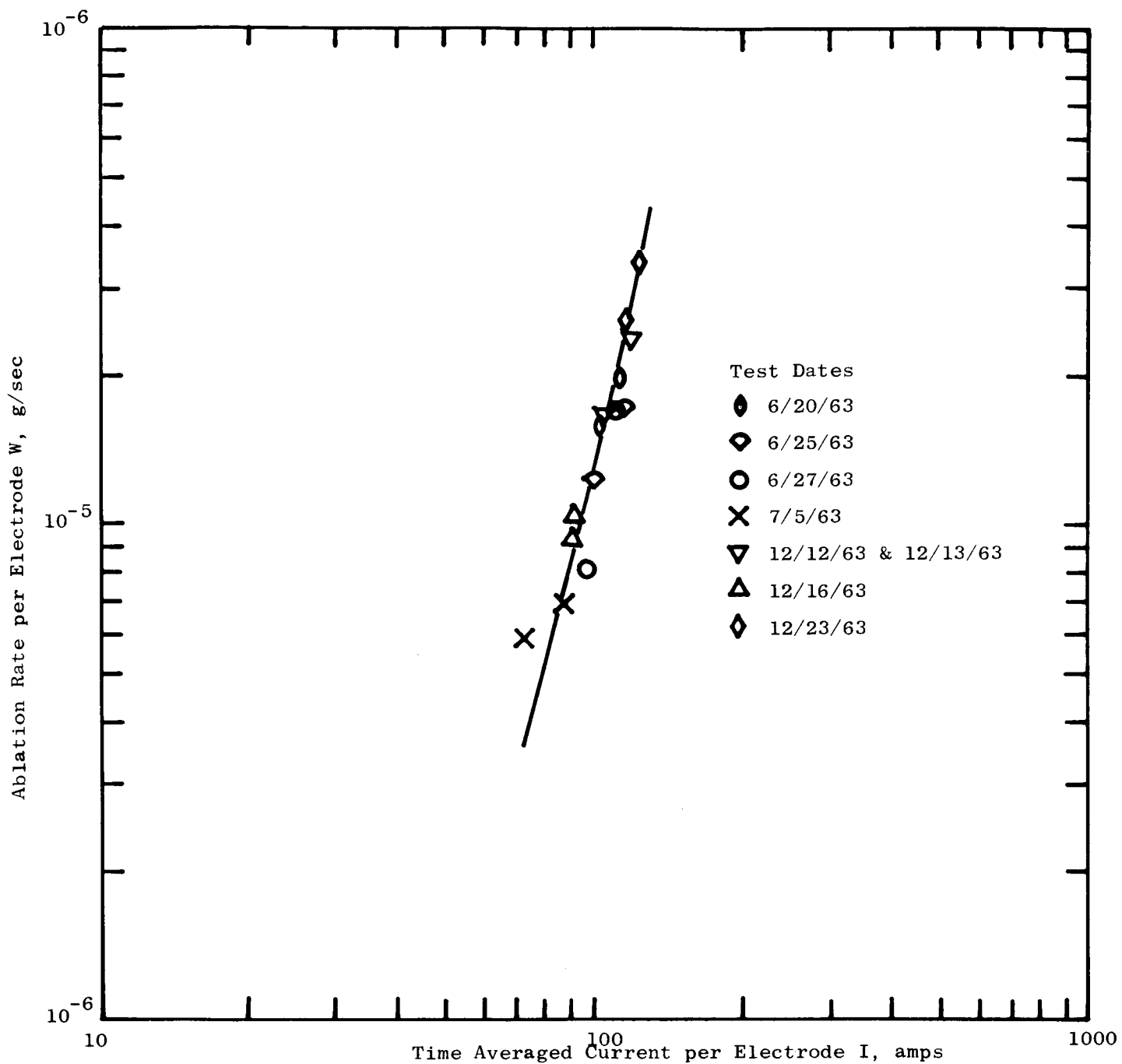


Fig. 4.1: Ablation Rate as Affected by Currents

The pressure in the test tank as indicated by the vacuum gage varied between 0.4 mm Hg and 2 mm Hg due to pressure variations in the steam supply for the ejector system.

During the 250 hours four engine restarts were performed. They were necessitated for different reasons. After 88 hours and 57 minutes an external arc was observed originating from the electrical lead C on top of the thrust rig and striking to the tank. Upon inspection it was found that the ceramic insert in the Conax fitting had fractured and permitted an arc to form from the copper lead through to the external part of the fitting which is mounted in the bottom plate of the thrust rig. The ceramic insert was replaced. While the test tank was open for the repair the opportunity was taken to recalibrate the thrust rig.

After only 13 hours and 3 minutes another arc was observed on top of the thrust rig. Upon shutdown an electrical breakthrough in the RTV insulation was found. The insulation was repaired. After 148 hours and 22 minutes of accumulated operating time a shutdown occurred which was initiated by the automatic protection device. During the changeover from the depleted hydrogen supply to a fresh hydrogen supply the supply pressure increased to such a degree that the pressure in the engine exceeded the upper pressure limit on the protection device. After 217 hours and 53 minutes the fourth shutdown of the engine was necessitated by another small external arc. It should be noted that all these restarts were occasioned by problems in the equipment outside of the engine and that there was no malfunction in the engine itself.

The run was terminated after 250 hours and 10 minutes.

4.2.2 Restarting of Engine Y16-1

During the long duration operation four restarts had taken place which were necessitated by external equipment difficulties. These restarts were all preceded by a complete cool down of the engine. The time at which these restarts occurred during the long duration run are summarized in Table 19.

Restart	Total Elapsed Operating Time
1	88 hrs. 57 min.
2	102 hrs. 0 min.
3	148 hrs. 22 min.
4	217 hrs. 53 min.

Table 5 : Restarts During the 250 Hour Duration Run

After the official completion of the 250 hour run the engine was restarted with a total down time of 18 minutes. The start was perfect in every respect.

The power and pressure returned to the values at which the engine had operated before the last shutdown. This behavior indicated that no discernible changes had occurred in the engine due to the transient heating and cooling associated with starting and shutdown of the engine operation.

4.2.3 Inspection of Engine Y16-1 After The Long Duration Run

After 250 hours and 10 minutes of operation and a total of five restarts, Engine Y16-1 was taken apart for inspection. It could immediately be observed that the electrodes had ablated such that a pronounced change of the setting of the ends of the electrodes had occurred over the run. This change in the length of the electrodes was not the same for the two electrodes. Electrode A, i.e., the electrode connected to phase A of the electrical system was shorter by a visible amount than electrode C.

The electrodes were weighed. The electrode material loss was such that the effective ablation rates for the two electrodes were 0.786×10^{-5} g/sec and 0.544×10^{-5} g/sec respectively. The combined ablation rate was, therefore, 1.330×10^{-5} g/sec. When the rate is compared with the ablation rate determined for test runs lasting up to six hours this rate is found to be lower by a factor of 2.63 and only slightly less than the ablation rate determined for the 24 hour run.

The electrodes as they appeared after the run are shown in Figs. 4.2 and 4.3. The initial tip configuration of the electrodes is shown in Fig. 4.4.

The nozzle showed some signs of wear. The nozzle throat diameter had increased by 16 mils, i.e. the initial nozzle diameter was 0.168 in. while after the run the diameter had increased to 0.184 in. Four radial cracks were visible, when looking into the convergent section of the nozzle, which were almost 90° apart. The nozzle as it appeared after the run is shown in Fig. 4.5 while for comparison a new nozzle of the very same design is shown in Fig. 4.6.

4.2.4 Performance Testing of Engine Y16-1 After Long Duration Run

During the 250 hours of continuous operation, gelling of the silicone oil in the thrust measuring device had taken place. When the engine was shut down the thrust indication did not return to its original zero because the restoring force of the displacement transducer spring could not overcome the viscosity of the gel. However, the displacement of the thrust rig under an applied force of the order of 0.4 lbs or greater was not affected by the change of viscosity.

The thrust measuring device was drained completely and disassembled. The jelly-like substance was taken out of the displacement transducer which was then thoroughly cleaned. After reassembly of the thrust measuring device the tank was filled with a new fluid. The device was recalibrated and checked out for extraneous effects on the thrust indications. It was found that after the rework of the device, it had been restored to its original performance.

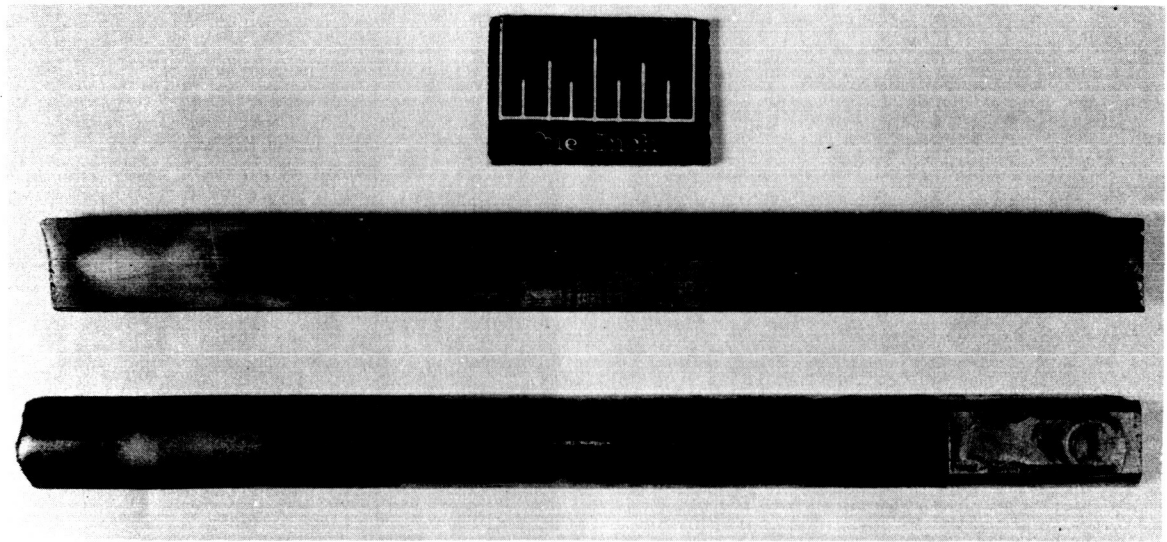


Fig. 4.2: Center Electrodes of 30 KW Three-Phase Engine After 250 Hours Operation (Y16-1)

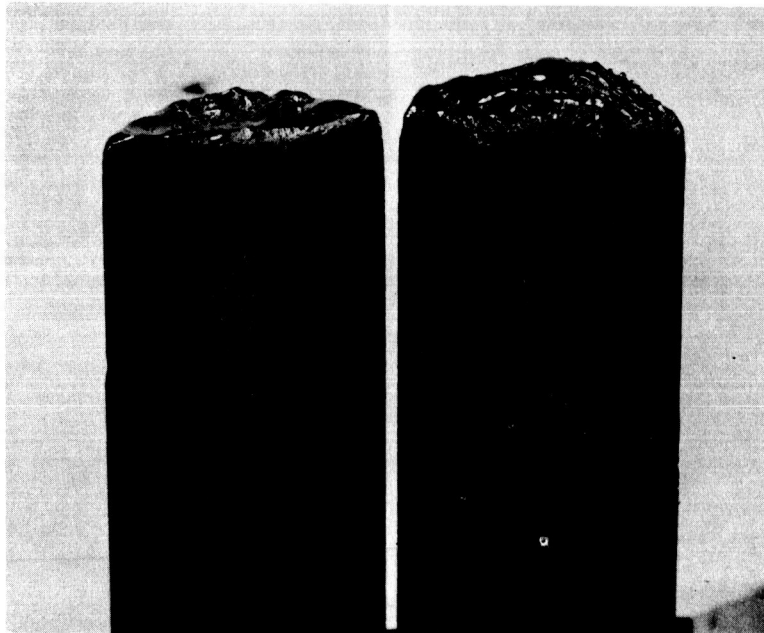


Fig. 4.3: Electrode Tips of 30 KW Three-Phase Engine After 250 Hours Operation (Y16-1)



Fig. 4.4: Center Electrodes of 30 KW Three-Phase Engine Before Operation (Y16-1)

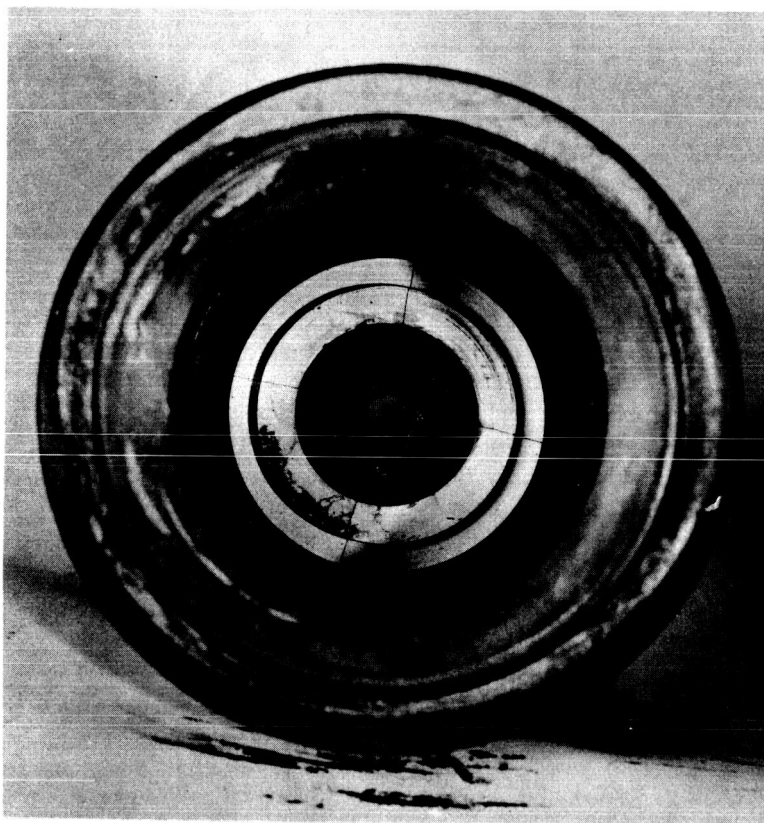


Fig. 4 .5: Nozzle of 30 KW Three-Phase Engine After
250 Hours Operation (Y16-1)

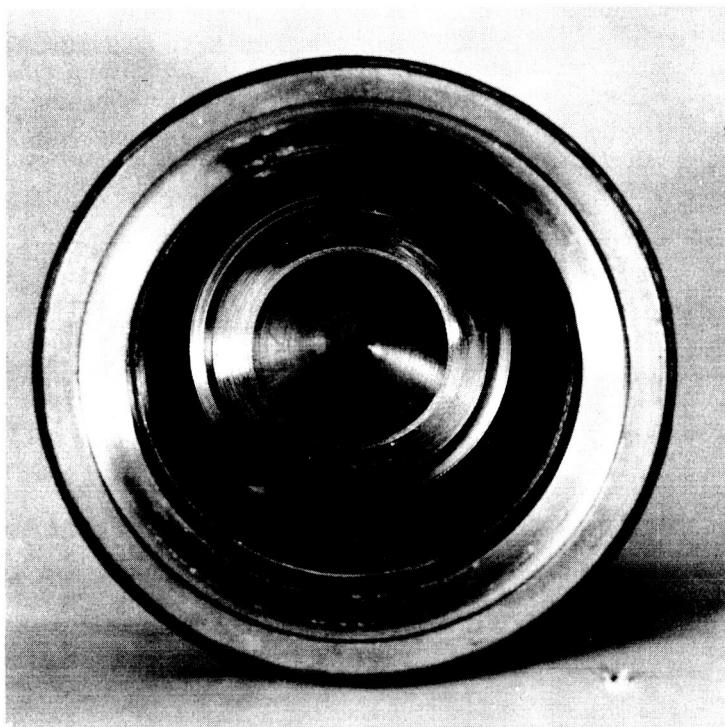


Fig. 4.6: Nozzle of 30 KW Three-Phase Engine Before Operation (Y16-1)

Engine Y16-1 was retested for its performance after 250 hours of operation, and 5 additional restarts were successfully performed to satisfy contractual requirements. The results of this test are shown in Fig. 4.7. In Fig. 4.8 the performance data of the engine at the start of the 250 hour test run are shown. It has to be pointed out again, as is being explained in Appendix VII, that the variations in the measured performance are to a great extent due to changes in the ambient pressure in the test tank, i.e. the performance data of the engine as it is determined in the described tests are relative with respect to the vacuum conditions obtained with the steam ejector system. The data presented have therefore to be evaluated with a clear understanding of the discussion in Appendix VII of this report.

For comparison the analytically determined performance of Engine Y16-1 is shown in Fig. 4.9. The upper curve is the performance of the engine when operating with a throat diameter of 0.168 in. The lower curve is the expected performance of the engine when operating with a throat diameter of 0.184 in. diameter. Both performance curves assume an ambient pressure of 1 mm Hg. It can be seen that only a slight deterioration of the performance can be expected with the opening up of the nozzle throat by 16 mils. This analytical prediction was borne out by the test as described above.

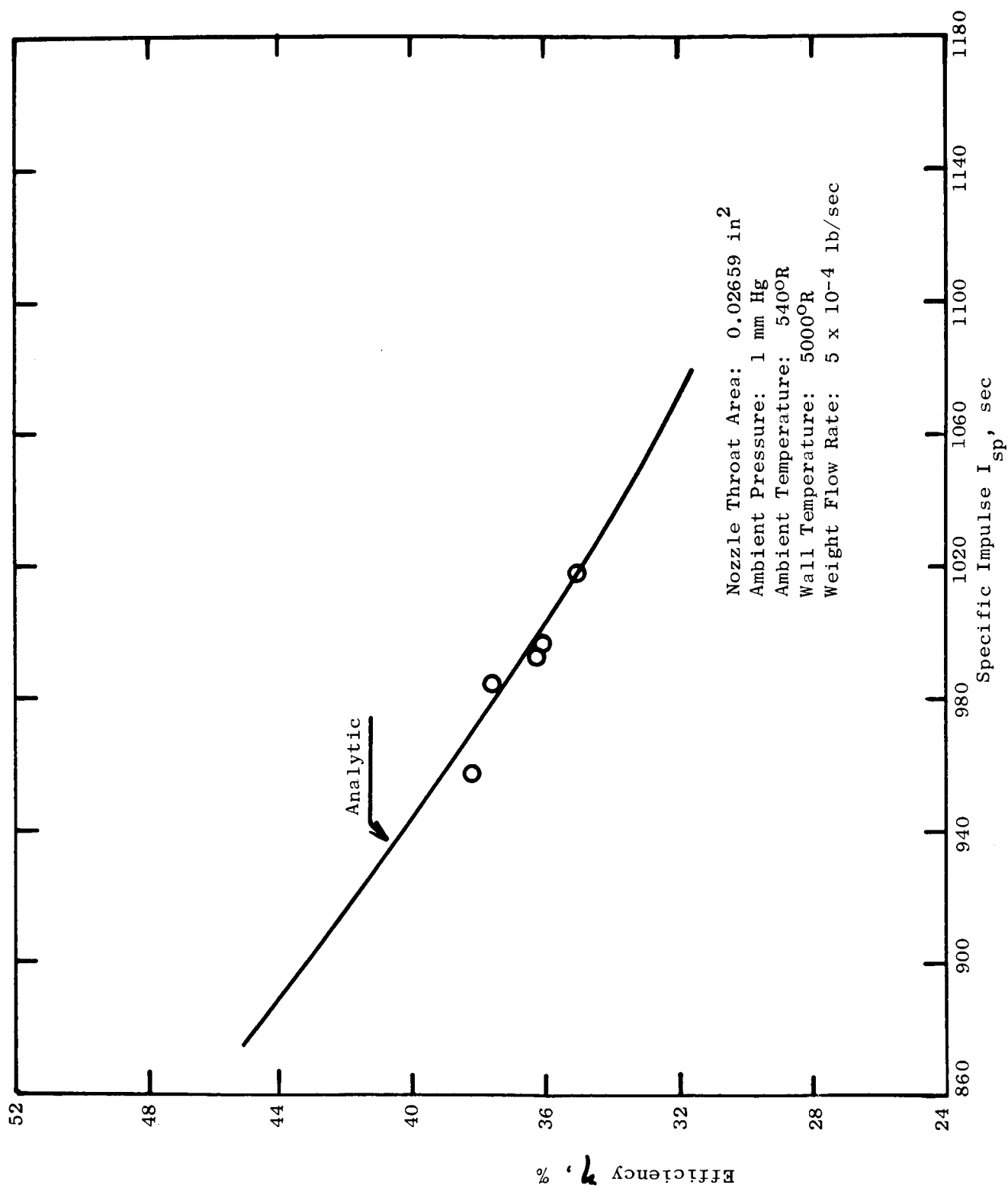


Fig. 4.7: Performance of Engine Y16-1 After 250 Hour Test

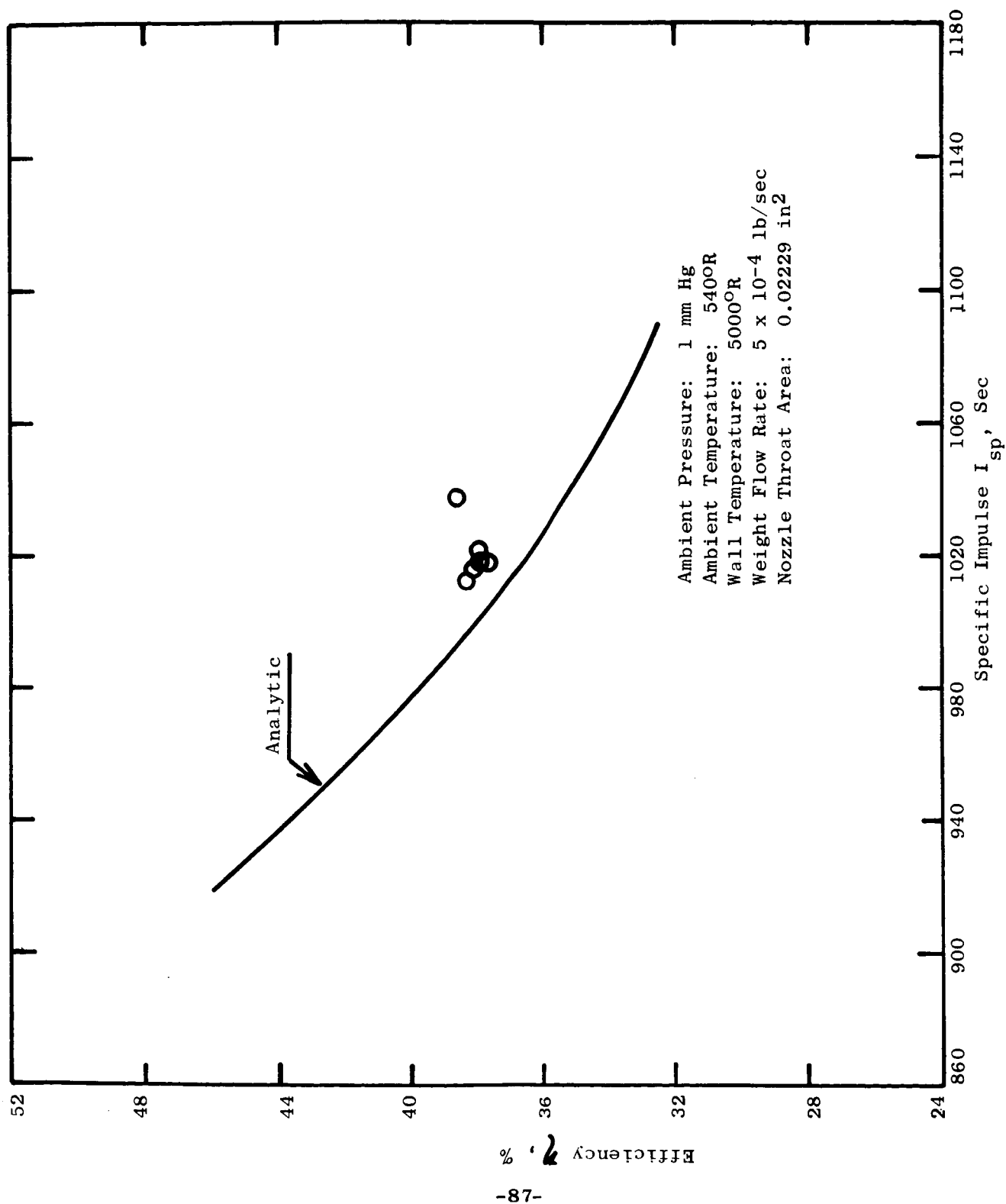


Fig. 4.8: Operating Points of Y16-1 Engine At Start of 250 Hour Test Run

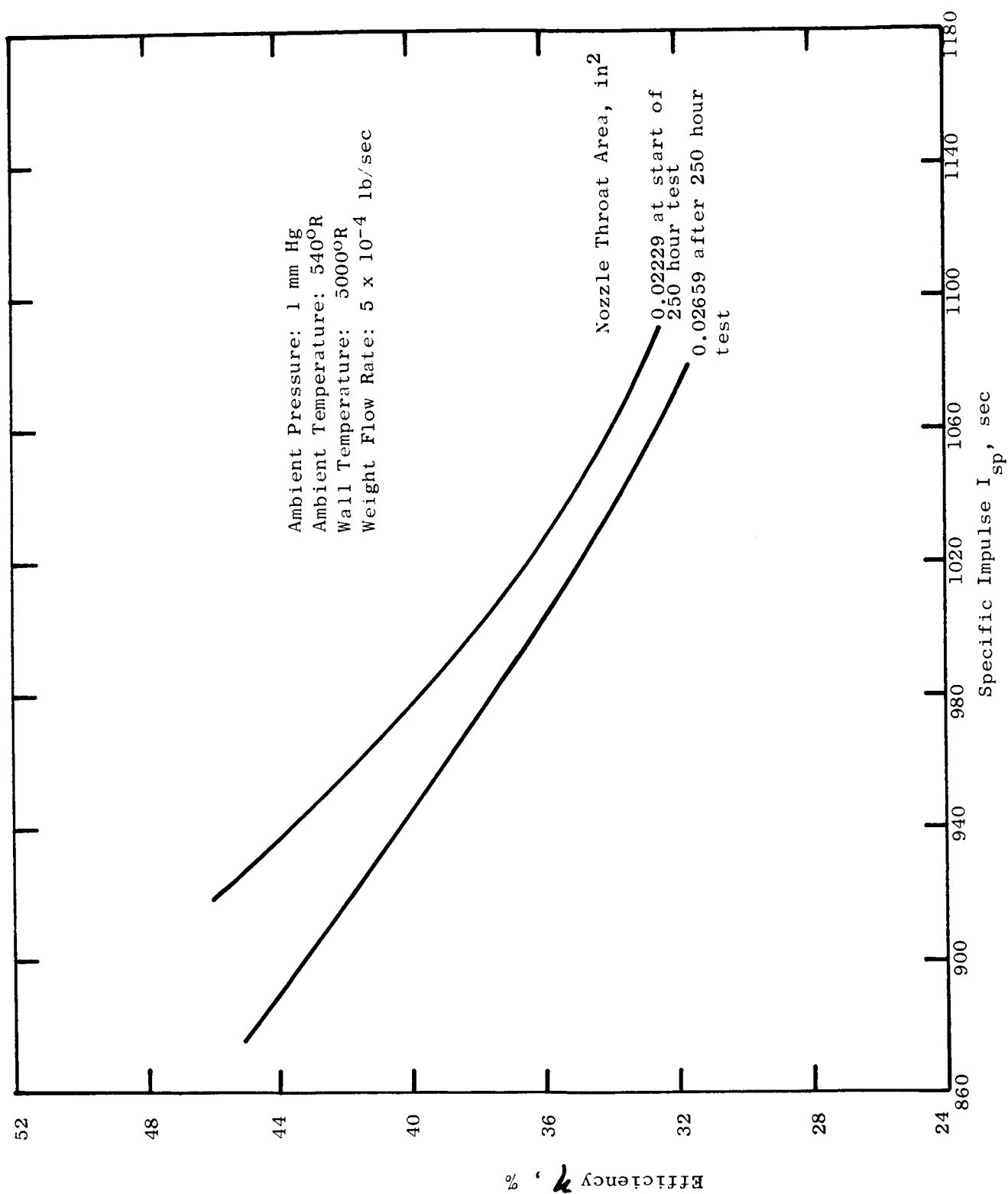


Fig. 4.9: Analytical Predicted Effect of Nozzle Deterioration on the Performance of the Engine Y16-1

5. SINGLE PHASE ENGINE TESTING

5.1 Modification of the Single Phase Plasma Arc Jet Engine Facility

Until the receipt of this contract the test facility in Building 200 had been used primarily for the testing of small attitude control engines and for a MHD program. The propellant flow rates and the power levels employed in those tests were substantially below the levels contemplated for the single phase tests of this program.

The test facility was, therefore, modified to permit operation at power levels up to 12 kw and propellant flow rates up to 2.3×10^{-4} lb/sec of hydrogen. In addition, instrumentation and equipment were added to simulate closely the operation in the three-phase plasma arc jet engine facility.

The electrical power source for this test facility is a Behlman power supply. This power supply is capable of delivering up to 220 volts at frequencies of 300 to 3000 cycles/sec which are continuously adjustable. The supply is rated at 14 kva. A single phase transformer is used to simulate supply voltage conditions over a wide range. The arc stabilizing impedance is provided by an inductor coil. The air reactor has an adjustable movable ferrite core to provide a continuous fine adjustment of this impedance during operation. The core is lowered into the reactor by a reduction gear motor which is operated from the control console. The position of the ferrite core is indicated by the voltage drop measured across a rheostat. The complete electrical system and instrumentation is shown schematically in Fig. 5.1.

The instrumentation is mounted in a control and instrumentation console from which the operator can continuously monitor the operation of the arc. The supply voltage, the arc current, and the arc voltage are displayed on three Tektronix scopes. The approximate arc voltage, arc current, and total voltage are measured by standard volt and current meters which have been calibrated for sinusoidal currents and voltages. The power into the arc is measured by an electronic wattmeter and an electrodynamicometer.

The propellant supply system is shown schematically in Fig. 5.2. The propellant is stored in two commercially supplied bottles. Only one bottle is used during arc operation. As soon as the pressure drops below 200 psia, a pressure switch actuates a relay which closes the solenoid valve of the spent hydrogen supply bottle and opens the solenoid of the unused supply bottle. The reservoir minimizes the pressure fluctuation during the bottle changeover. The propellant flow rate is regulated by an Annin valve which has a nominal flow coefficient of $C_v = 0.02$. The valve is remotely regulated by a panel loader which operates on shop air. The propellant flow rate is measured by the pressure upstream of a sonic orifice. The orifice is part of a flow measuring system which is similar to the flow measuring system for the three-phase engine facility discussed elsewhere in this report.

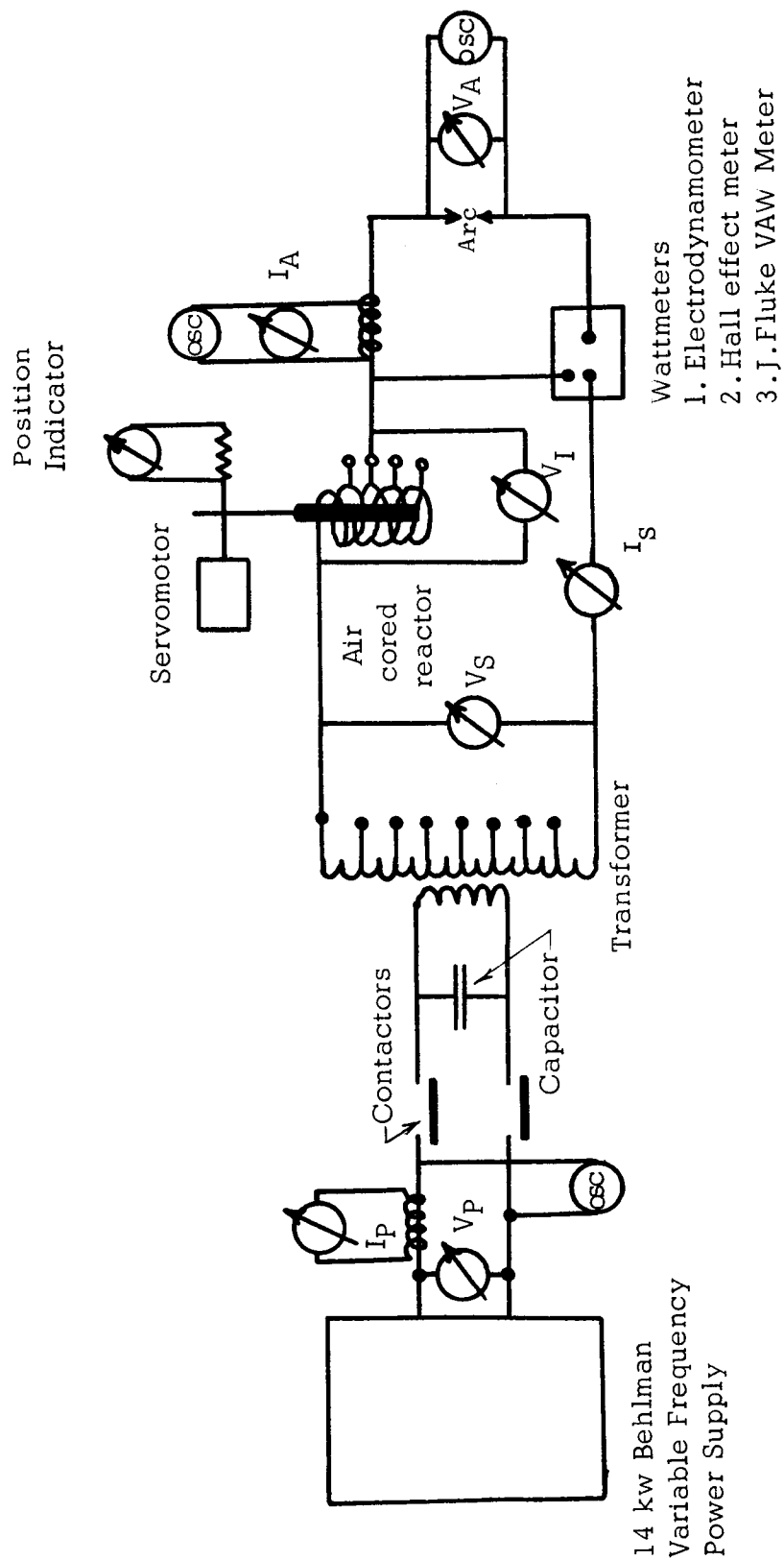


FIG. 5.1: ELECTRICAL SYSTEM FOR SINGLE PHASE AC PLASMA ARC JET ENGINE TEST FACILITY

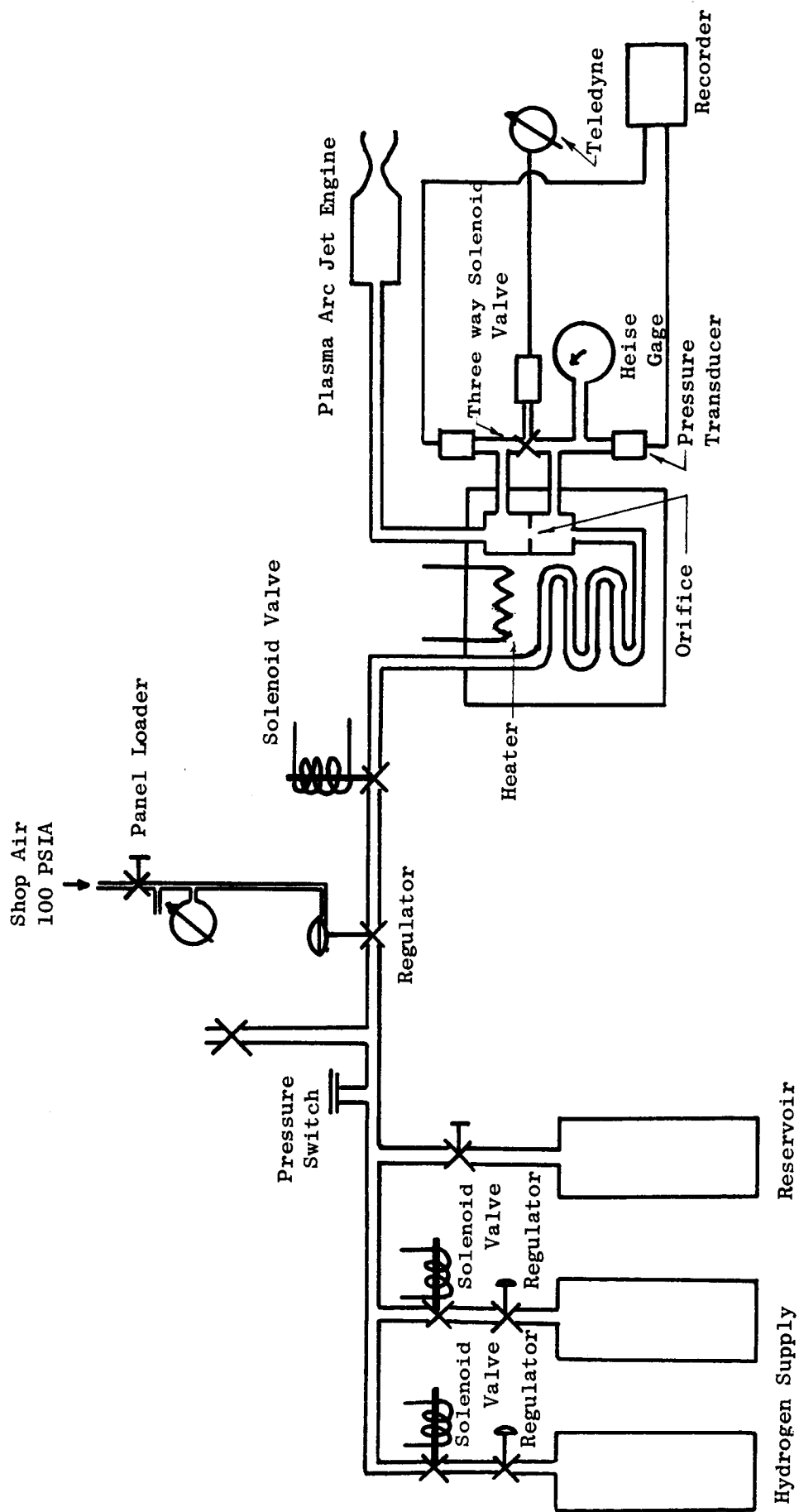


FIG. 5.2 Propellant Supply System for Single-Phase AC Plasma Arc Jet Engine Test Facility

The orifice pressure is measured by a Wallace and Tiernan precision Bourdon Tube gauge, type FA 233161, for high accuracy. For continuous reading the output of a pressure transducer is recorded on a Sanborn recorder. The propellant flow rate is set by adjusting the Annin valve for an orifice pressure read off the precision pressure gage which has scale divisions of 0.20 psi. A three-way valve permits a second pressure transducer to be connected either to the pressure upstream or downstream of the orifice. Its output is indicated on a Teledyne readout meter.

5.2 Checkout Testing of Single Phase Plasma Arc Jet Engine

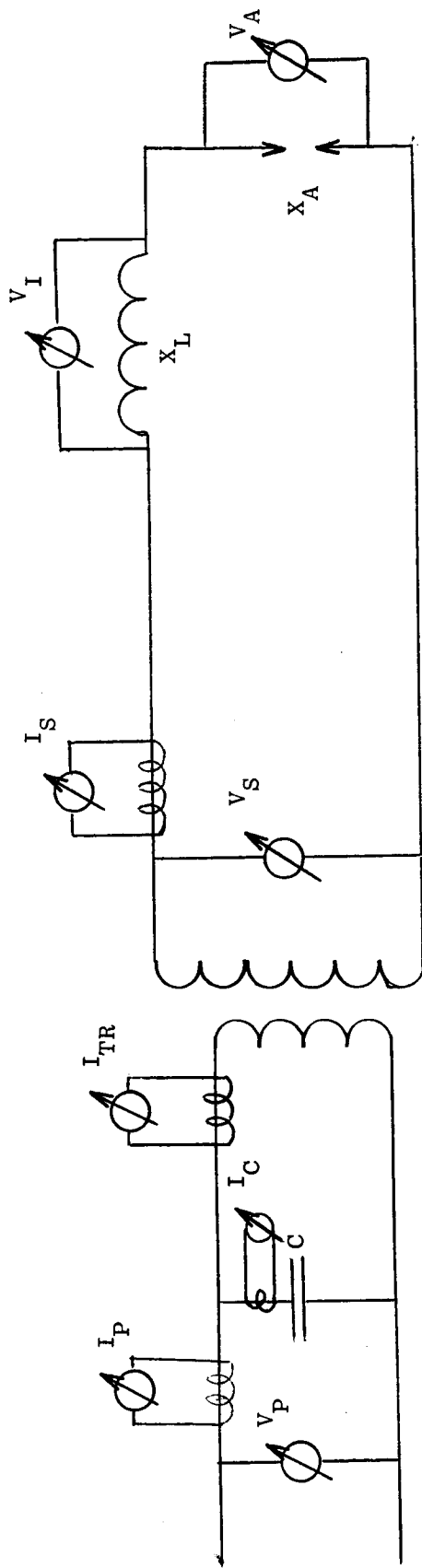
Checking out of the facility was initiated by substituting a resistor of approximately 3 ohms for the arc. Indications were that the current transformer measuring the arc current was damaged and had to be replaced. Otherwise, all instruments checked out indicating the electrical values within the expected accuracy of the standard commercial panel meters.

After completion of the initial checkout, testing of the single phase engine was started. The first tests lasted only a few seconds after which the fuses in the power supply blew. The overloading of the power supply was due to a steep rise of the current in the primary line immediately after starting of the arc which caused the 0-200 amp meter on the control panel to peg. The maximum current in the primary, under any circumstances, should not have exceeded 150 amps. These calculations were verified by substituting resistance values ranging from 0 to 4 ohms for the arc in the circuit.

When finally the arc was operated well below the design power it was found that the current transformation across the transformer was about twice the value of the voltage transformation at a power of 2 kw, i.e., the KVA loading of the primary circuit was twice the KVA loading of the secondary circuit. This phenomenon of a changing current transformation occurred also with the current transformer used to measure the current in the secondary line, I_s . The data for all these tests is shown in Table 6.

In the second test the capacitance, which was originally hooked up across the two primary lines, was placed across the lines in the secondary circuit. This was done to correct the power factor directly in the secondary circuit and thereby minimize the current flow through the power transformer. With this circuit the current ratio becomes about three times the voltage ratio, indicating that the capacitor location also had an effect on the KVA loss. The data of this test is shown in Table 7. The reason for the low power factor was found to be a characteristic phenomenon for transformers which always occurs when the secondary current is rectified.

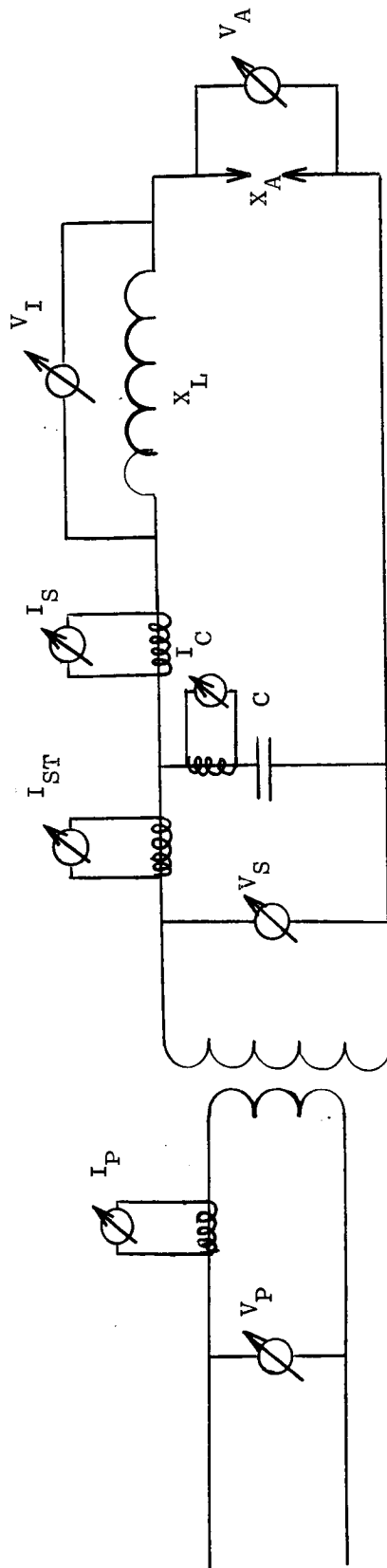
When the transformer was completely by-passed and the engine was operated directly from the Behlman power supply, the engine was started and operated as expected, and no unpredicted currents were measured. The test data of this run is shown in Table 8.



July 29, 1963

f cps	V _P volt	I _P amp	I _C amp	I _{TR} amp	V _S volt	I _S amp	V _I volt	V _A volt	L μH	X _{LC} ohm	X _{LM} ohm	C μF	X _{CC} ohm	X _{CM} ohm	r _V	r _I	X _A ohm	r _I /r _V	V _A X _I kva
1000	71	122.5	58	178	126	41	113	45	480	3.014	2.78	110	1.445	1.225	1.775	4.34	1.0976	2.445	1.845
1000	71	109	58	161	128	37	117	43	560	3.516	3.16	110	1.445	1.225	1.8	4.35	1.1622	2.42	1.59
1000	68	139	57	192	121	45	109	41	410	2.57	2.42	110	1.445	1.192	1.779	4.27	0.911	2.40	1.85
900	72	139	52	188	130	44	113	53	480	2.71	2.57	110	1.605	1.38	1.80	4.27	1.205	2.37	2.33
1100	71	97	64	155	127	38	111	52	480	3.32	2.92	110	1.31	1.11	1.788	4.08	1.368	2.28	1.976
1250	70	70	75	140	123	35	109	54	480	3.77	3.51	110	1.55	.933	1.757	4.0	1.543	2.276	1.89

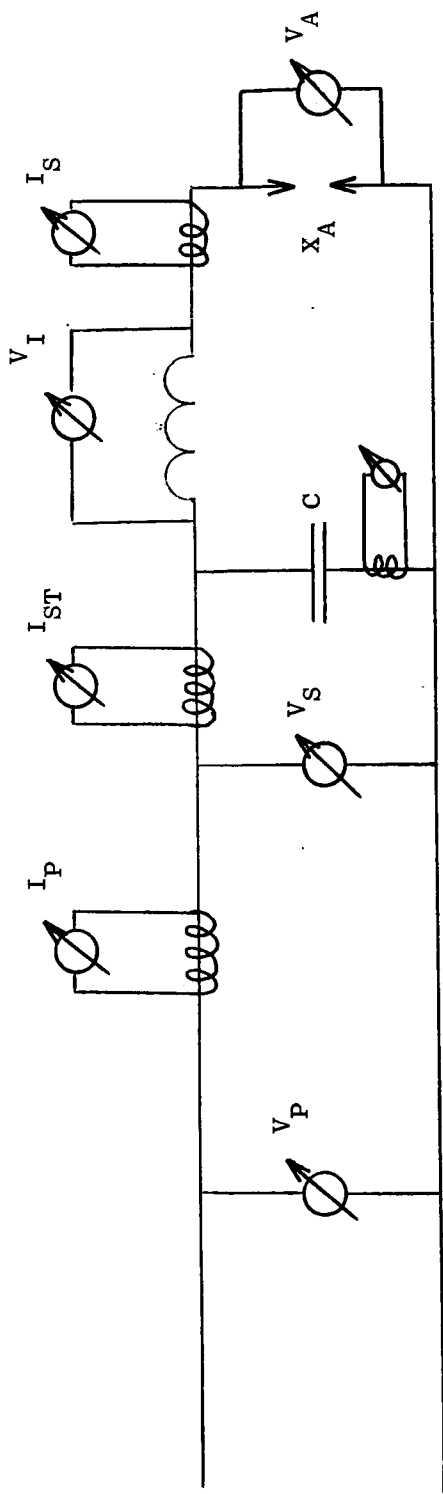
Table 16: Test Data of Single Phase Plasma Arc Jet Engine



Date: July 30, 1963

cps	V _P volt	I _P amp	I _C amp	I _{ST} amp	V _S volt	I _S amp	V _I volt	V _A volt	L μH	X _{LC} ohm	X _{LM} ohm	C μF	X _{CC} ohm	X _{CM} ohm	r _V	r _I	X _A ohm	r _L /r _V	V _S volt	V _A ^{xI} kva
RES	75	58.5	41.5	30.5	151	32	83	129	480	3.01	2.56	31.5	5.16	3.64	2.01	1.92	4.03	.96	153.8	4.13
	75	48	28	24	150	31	81	125	480	3.01	2.61	21	7.58	5.36	2.00	2.0	4.03	1.0	149.0	3.88
	90	58	34	30	178	37	98	151	480	3.01	2.65	21	7.58	5.23	1.98	1.93	4.09	0.97	180.0	5.58
ARC	66	120	25.5	22	125	38	108	54	480	3.01	2.84	21	7.58	4.9	1.89	5.45	1.42	2.88	120.7	2.05
	75	145	29	26	139	44	124	52	480	3.01	2.82	21	7.58	4.79	1.85	5.6	1.18	3.03	134.4	2.29
	75	145	28.2	25	138	44	124	52	480	3.01	2.82	21	7.58	4.89	1.84	5.8	1.18	3.15	134.4	2.29

Table 7: Test Data of Single Phase Plasma Arc Jet Engine



July 31, 1963

V_P	I_P	I_C	V_S	I_S	V_I	V_A	L	X_{L_C}	X_{L_M}	C	X_{C_C}	X_{C_M}	X_A	V_S	P_A
volt	amp	amp	volt	amp	volt	volt	μH	ohm	ohm	μF	ohm	ohm	ohm	volt	kw
188	36	35	175	57	162	62	480	3.01	2.84	21	7.58	5.00	1.09	173.4	3.5
154	27	30	144	44	123	65	480	3.01	2.80	21	7.58	4.80	1.48	139.0	2.86
166	27	30	155	48	138	63	480	3.01	2.87	21	7.58	5.17	1.31	151.7	3.02
166	27	30	154	49	138	61	480	3.01	2.82	21	7.58	5.13	1.24	150.8	2.989
188	35	36	174	57	161	62	480	3.01	2.82	21	7.58	4.83	1.09	172.5	3.534

Table 8: Test Data of Single Phase Arc Jet Engine

5.3 Design of the Single-Phase AC Plasma Arc Jet Engine

The single phase plasma arc jet engine was designed so that it can be operated over a wide range of powers, flow rates, and stagnation pressures, without modification to the engine. Since the main objective of the single phase tests was to gain an understanding of the interrelation of thermodynamic and electrical parameters, no special effort was made to optimize the divergent section of the nozzle of this engine.

The operating design point for this engine was selected to coincide closely with the operating design point of the three-phase 30 kw plasma arc jet engine. In order to obtain an effective specific impulse of 1000 seconds the three-phase engine had to be designed for a theoretical specific impulse of at least 1100 seconds. The higher theoretical performance, which is based only on the thermodynamic cycle efficiency, is required to make up for the fluid dynamic losses in the divergent section of the nozzle. From a parametric study, a nominal design stagnation temperature of 6500°R was selected. At a stagnation pressure P_o of 1 atm and a total available power P_t of 7.5 kw, the following additional design data were obtained.

Energy addition per pound of hydrogen ΔH $5.7621 \times 10^{+4}$ B/lb

Weight flow rate per unit throat area \dot{W}/A^* 2.2032×10^{-2} lb/sec-in²

When a cooling efficiency η_c of 90% is assumed, 10% of the electrical energy is radiated, then the following values can be calculated.

Energy requirement per pound of hydrogen $6.40233 \times 10^{+4}$ B/lb

Total propellant flow rate \dot{W} 1.10681×10^{-4} lb/sec

Throat Area A 0.080 in.

To obtain a stagnation pressure of 2 atm with the same nozzle design at a stagnation temperature of $T_o = 6500^\circ\text{R}$.

Energy addition per pound of hydrogen ΔH $4.8964 \times 10^{+4}$ B/lb

Weight Flow rate per unit throat area \dot{W}/A^* 4.5307×10^{-2} lb/sec-in²

Assuming again a cooling efficiency $\eta_c = 90\%$

The energy requirement per pound of hydrogen $5.44 \times 10^{+4}$ B/lb

Total propellant flow rate \dot{W} 2.276×10^{-4} lb/sec

Total power P_t required 11.795 kw

Therefore, it can be seen that the design facilitates investigations over a wide variety of operating conditions with a single nozzle. The complete operating range of this nozzle design is shown in Fig. 5.3.

For the expansion process, an area ratio of $A/A^* = 30$ has been chosen. The thermodynamic and fluid dynamic data for the two extreme conditions to be investigated with this design are given in Table 9.

Stagnation Pressure P_o , atm	1	2
Expansion Ratio P_o/P_{ex}	926.77	824.85
Static exit temperature T_{ex} , $^{\circ}R$	747.15	864.2
Specific impulse (ideal) I_{sp} , sec	1120	1101
Exit Mach Number (ideal) M_{ex}	5.77	5.51
Thermodynamic Efficiency $\eta_{Ther.}$, %	43.3	49

Table 9: Thermodynamic and Fluid Dynamic Data of Single Phase Plasma Arc Jet Engine

The mechanical design of the single phase arc jet engine is shown in an assembly drawing in Fig. 5.4. In many respects this design closely follows the 30 kw three-phase plasma arc jet engine design. The main metal "O" ring seal, the double regenerative propellant flow path, the encapsulation of the boron nitride insulator into a stainless steel shell, and the ample provision for the possible installation of nozzles with various constrictor lengths are all similar to the design details of the three-phase engine. The main deviation from the three-phase design is the positioning of the center electrode. The design of the seal and easy adjustment of the center electrode could only be applied to the single phase engine because of the different design used for the three-phase engine.

The center electrode and the nozzle body are made out of tungsten. The engine body is machined from molybdenum whose specifications are given in Table 10. The gland nut, the insert, and the shell are made of stainless steel. Both insulators are made of boron nitride. The metal "O" ring material is Inconel X. Stainless steel has been used wherever the temperatures permit its application. An effective barrier against heat flow to the boron nitride insulator is obtained when the cold propellant enters the engine near the scaling area. This information, gained from experience with previous engines, was obvious from the large temperature gradients observed on the outside surface of the engine.

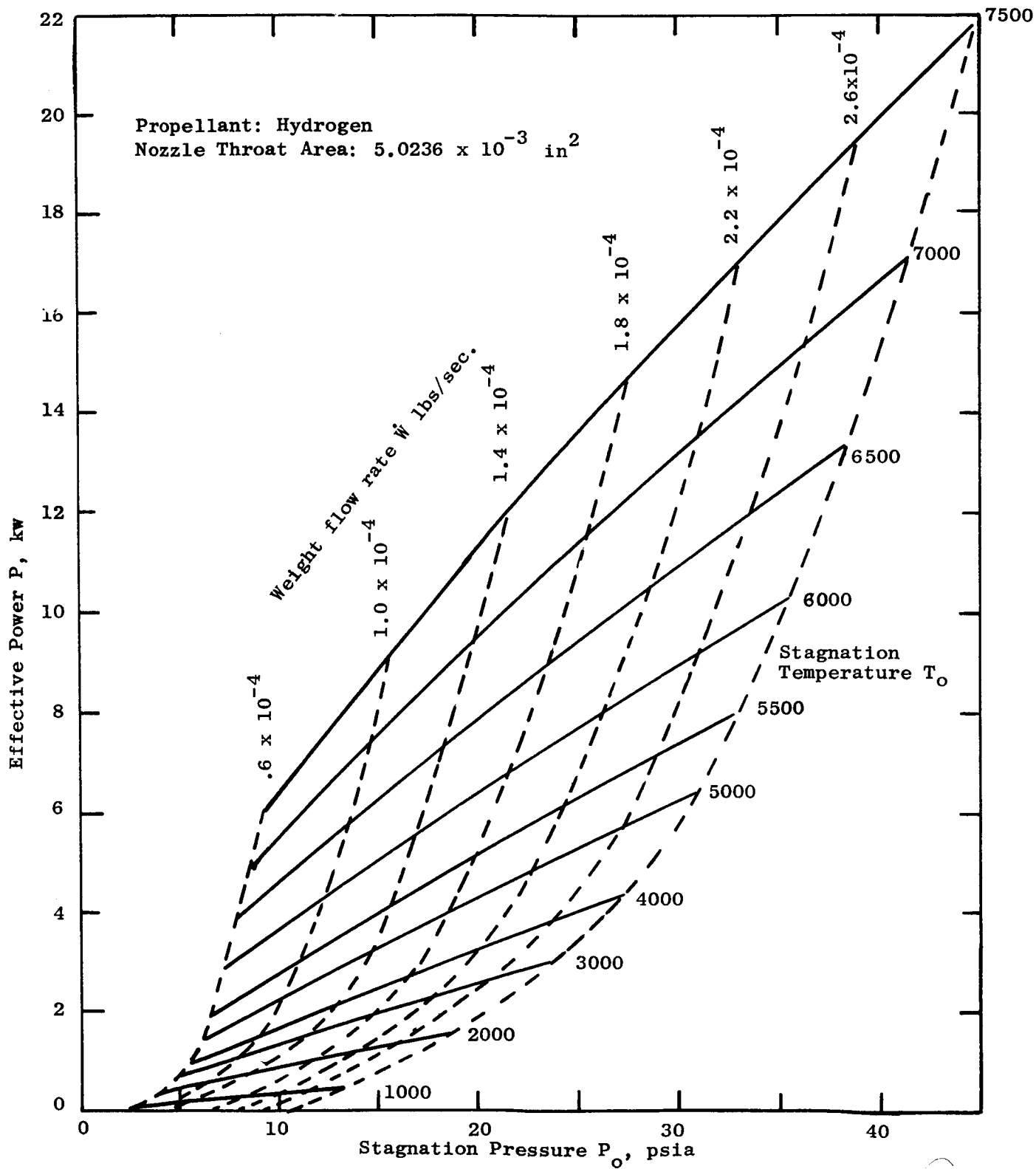


Fig. 5.3: Design Operating Curve for Single Phase Plasma Arc Jet Engine

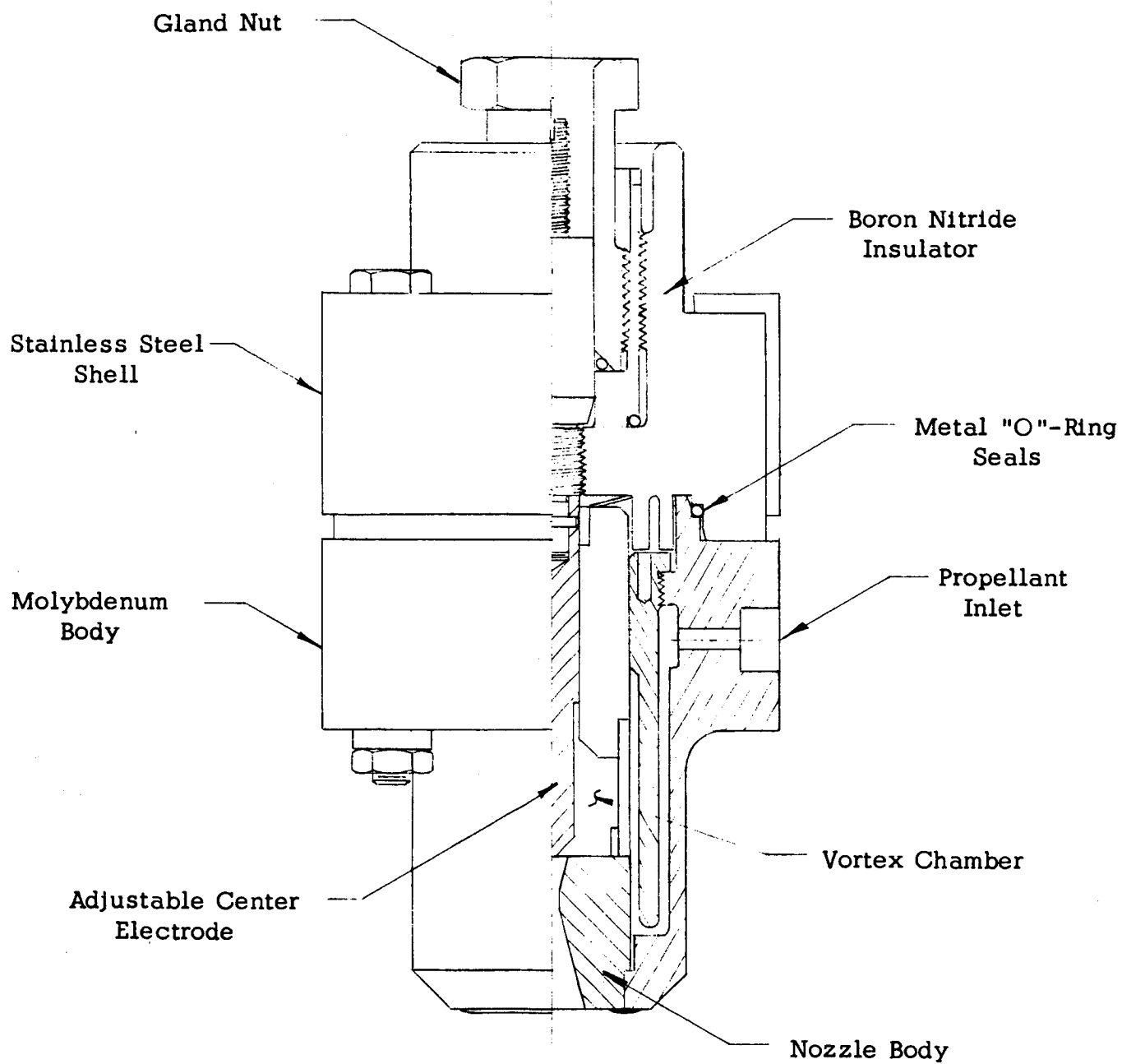


Fig. 5.4: Single Phase AC Plasma Arc Jet Engine

CHEMICAL COMPOSITION			Minimum Percent	
Carbon	0.04		0.01	
Titanium	0.55		0.40	
Zirconium	0.12		0.06	
Gaseous Elements	0.005		-	
Trace Elements	0.020		-	
Molybdenum	-		99.25	
MECHANICAL PROPERTIES				
Diameter of Bar in Inches	Minimum Tensile Strength, PSI	Minimum Yield Strength, PSI (0.2% Offset)	DPH Hardness (10 kg)	
			Minimum	Maximum
Over 13/32 to 7/8	115,000	100,000	260	320
Over 7/8 to 1-1/8	110,000	95,000	250	310
Over 1-1/8 to 1-7/8	100,000	85,000	245	300
Over 1-7/8 to 2-7/8	90,000	80,000	240	290
Over 2-7/8 to 3-1/2	85,000	75,000	235	285
Over 3-1/2 to 4-1/2	80,000	70,000	230	280
Maximum grain size of recrystallized bars ASTM No. 3 (ASTM E 112)				

Table 10: Chemical Composition of Climelt Molybdenum Metal (TZM Molybdenum)

The main metal "O" ring seal is designed so that the sealing surfaces are activated by a radial interference fit. Therefore, longitudinal thermal expansions cannot open up the seal. The bolts are used only to hold the two sections of the body together. Though an expansion of these bolts would not cause an opening of the main "O" ring seal, precautions have been used to keep the bolts at a temperature well below the body temperature of the engine. The bolts are insulated from the molybdenum body by alumina washers to decrease the possibility of arcing.

All parts of the engine are shown in an exploded view in Fig. 5.5. The completely assembled engine is shown in Fig. 5.6. The nozzle weld which is made using a rhenium-tungsten wire as filler material can clearly be seen.

5.4 Power Control for an AC Plasma Arc Jet Engine

Electric arcs are, in general, controlled by adjustment of the arc gap and the applied voltage. The arc operation is sensed by monitoring the arc current. All arc jet engines, however, are being designed with fixed electrode spacing based on the requirements that the electrodes are made of a low-consuming material, such as tungsten. This requirement is necessary to make a plasma arc jet engine applicable for space operation. In addition, the plasma arc jet propulsion system has to operate from a fixed regulated voltage source.

In general, it is assumed that electrodes are non-consuming in plasma arc jet engines although ablation does occur over a period of time. The gradual loss of electrode material leads to an increase of the arc gap setting, which in turn results in a change in the arc operating point with respect to arc voltage and arc current at a desired power. This interdependence of electrode spacing and arc characteristic is shown in Fig. 5.7 for a dc arc engine. It can be seen that the engine is perfectly capable of functioning well within a wide range of gap settings which are much larger than can be expected during normal life time operation. Such small variations, however, require continuous adjustments of the power conditioning components.

A typical electrical system for a single phase ac plasma arc jet engine is shown in Fig. 5.8. This system is actually not contemplated for space application. It is only being used to investigate system operation features for a three-phase plasma arc jet engine system as it requires fewer components and simplifies the amount of adjustments and changes by one-third. The major components of such a system are the transformer, the stabilizing ballast, the capacitor, and the contactors. The important realistic assumption is made that the arc jet propulsion system is only one of many systems operated from a common space power source whose voltage output is fixed.

The power in the arc can be regulated by adjusting the transformer ratio or by varying the effective ballast impedance. It is extremely difficult to make continuous changes in the transformer ratio. Therefore, adjustment of the impedance has been the most commonly applied technique.

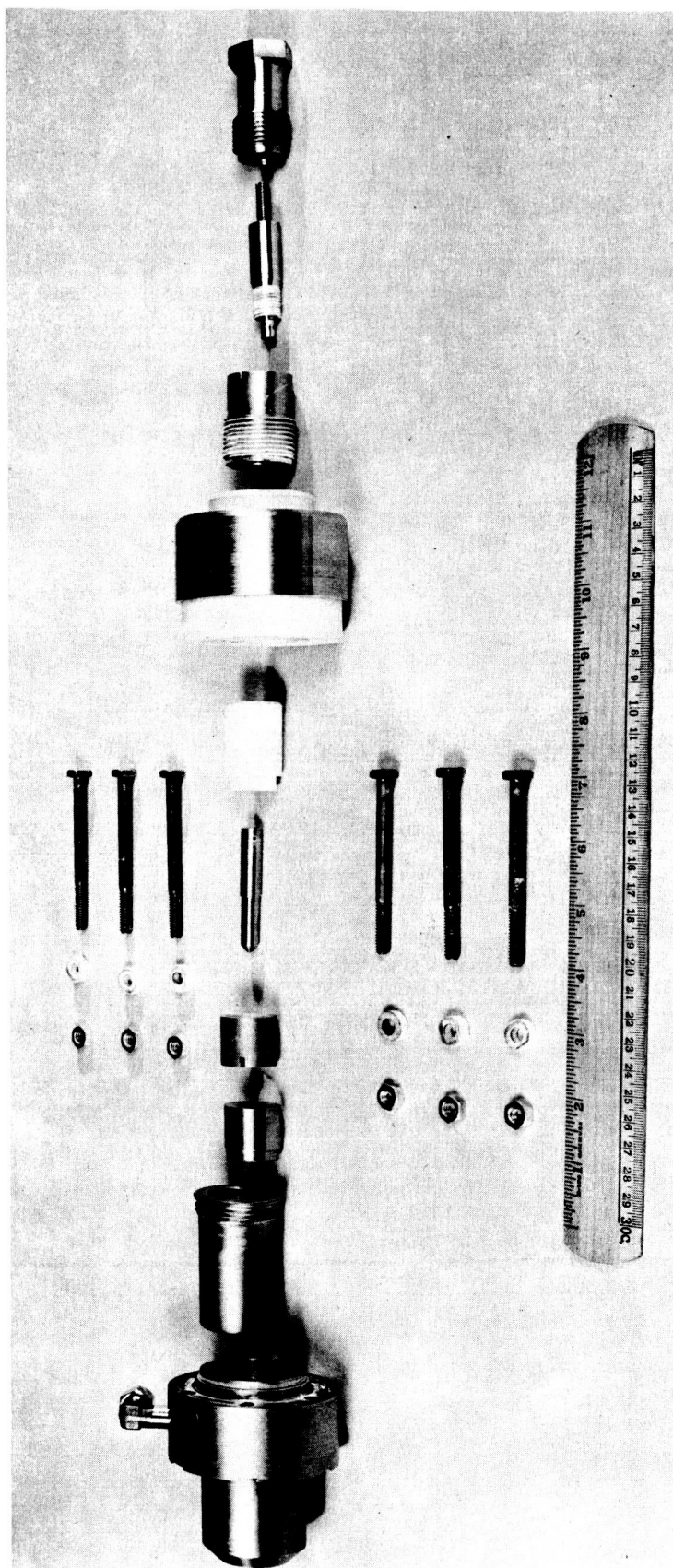


Fig. 5.5: Exploded View of Single Phase Plasma Arc Jet Engine

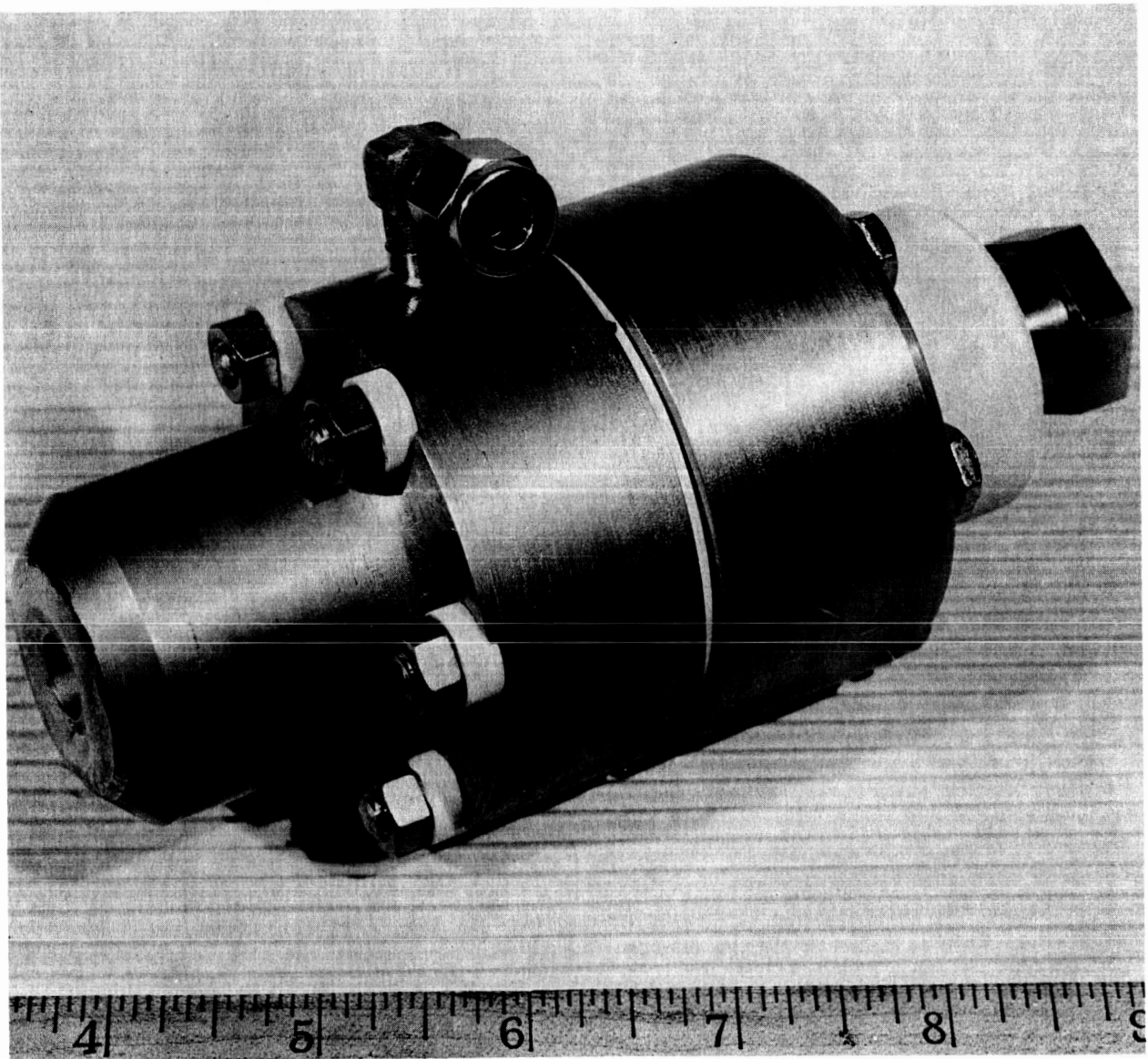


Fig. 5.6: Single Phase Plasma Arc Jet Engine

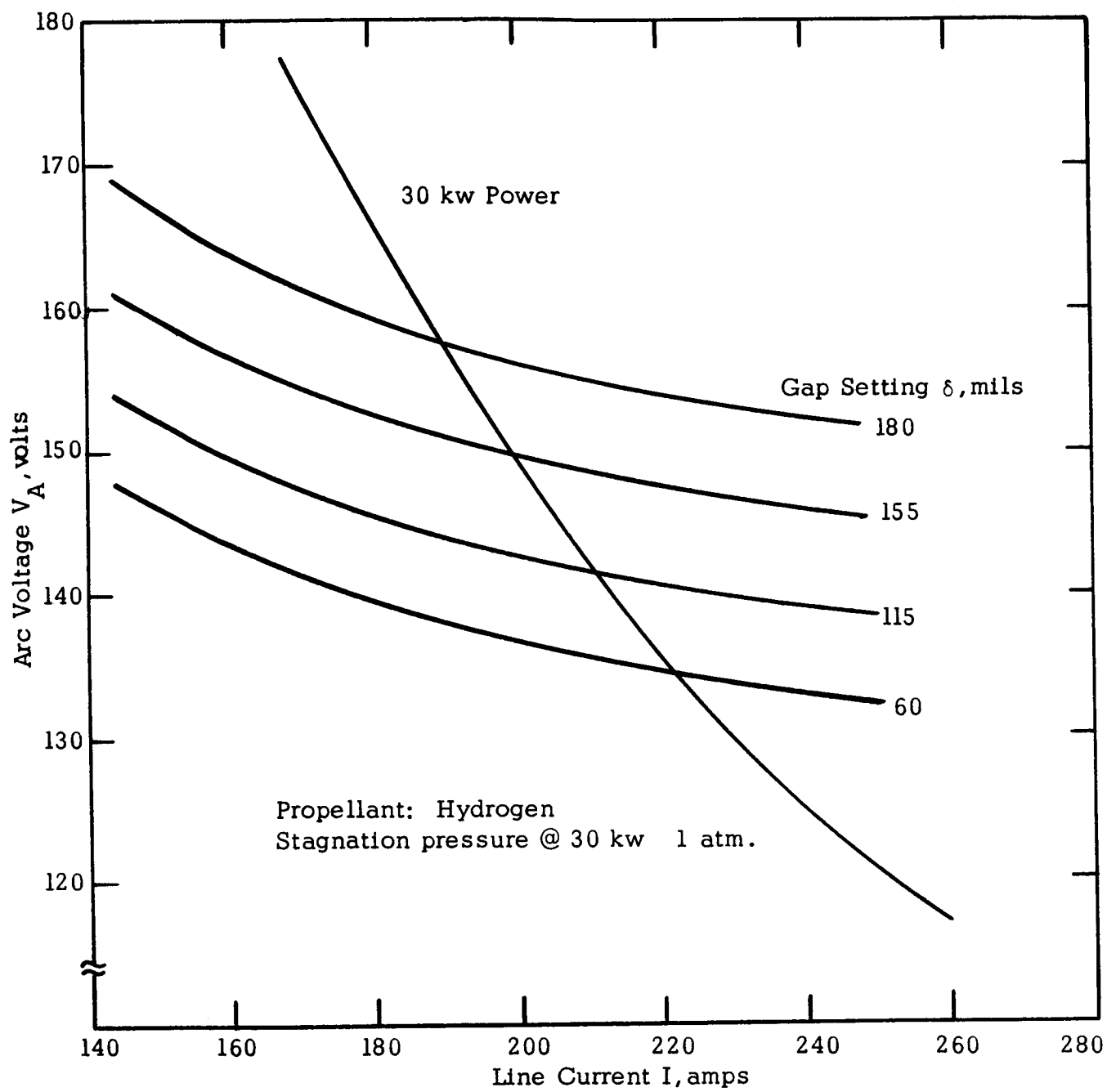


Fig. 5.7: Arc Characteristic of a DC Plasma Arc Jet Engine

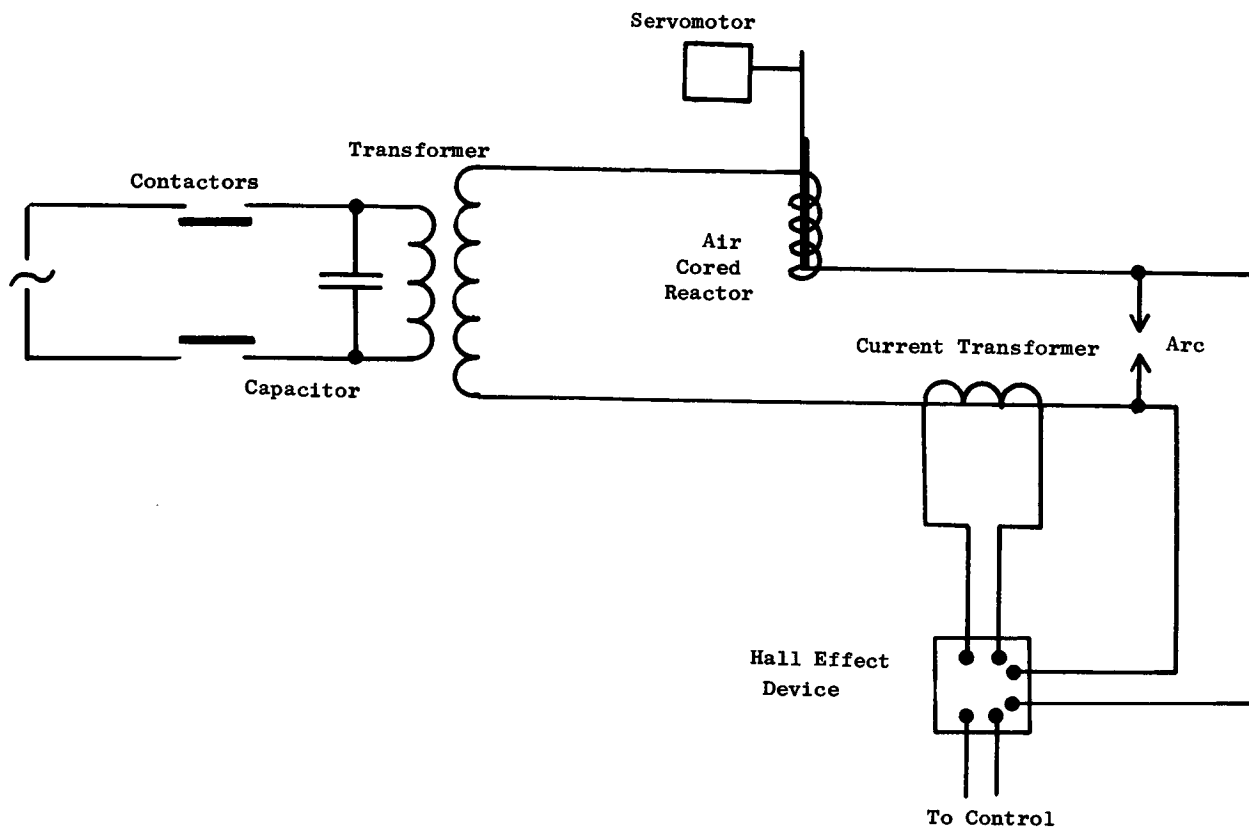


Fig. 5.8: Electrical System for Single Phase AC Plasma Arc Jet Engine

The ballast impedance can either be an air cored reactor with a ferrite core or a saturable reactor. In the case of an air cored reactor, the impedance can be varied by moving a ferrite core, thereby changing the magnetic flux and the reactance. The impedance of a saturable reactor is controlled by varying a dc current in the secondary winding.

Since the plasma arc jet engine will not operate with constant power at a constant current over long periods, the arc power cannot be controlled by making adjustments with respect to the arc current. It is necessary to monitor the arc power itself for its control. The device presently considered for this application is a Hall effect device which generates a signal voltage proportional to the product of arc current and arc voltage. Such a device has been checked out for power measurements in the three-phase plasma arc jet engine installation. It is shown in Fig. 5.9.

The Hall effect device can be applied for the control of a single phase engine. In the present system the stabilization of the arc is achieved with an air cored reactor whose impedance can be adjusted by a movable ferrite core. Fig. 5.10 gives the schematic of the control system.

The output of the Hall effect power transducer consists of a dc component and an ac component having a frequency twice that of the supply. A low pass filter is applied to remove this component. The small balanced signal from the transducer is then converted by a differential amplifier to a larger unbalanced output.

A summing amplifier compares a reference voltage with the amplified signal voltage. The difference of these two voltages is amplified and is used to operate either a "core-in" or a "core-out" actuator which operates until the difference has been reduced to within a specified deadband. The width of the deadband is controlled by the gain of the summing amplifier. It is mainly determined by stability considerations.

The system, as it is described, is essentially a relay servomechanism. Because of its simplicity, it can provide the desired information on the usefulness of Hall effect devices for power control at low cost.

The "core-in" and "core-out" control for the actuator motor is achieved simply with silicon-controlled rectifiers. The summing amplifier and the differential amplifiers are very simple in their design and are built in the laboratory as a special purpose package. All of the electronics have been mounted on a 10 inch by 17 inch chassis.

An alternative method of controlling the actuator motor, in order to achieve a proportional, type one servo, is to arrange the silicon-controlled rectifier circuit so that the power proportional to the error is applied to the motor. The circuitry for this is quite conventional. Alternatively, a pair of saturable reactors may be used in a very straight-forward manner to do the same job. Of the two methods, the SCR circuit is simpler and cheaper.

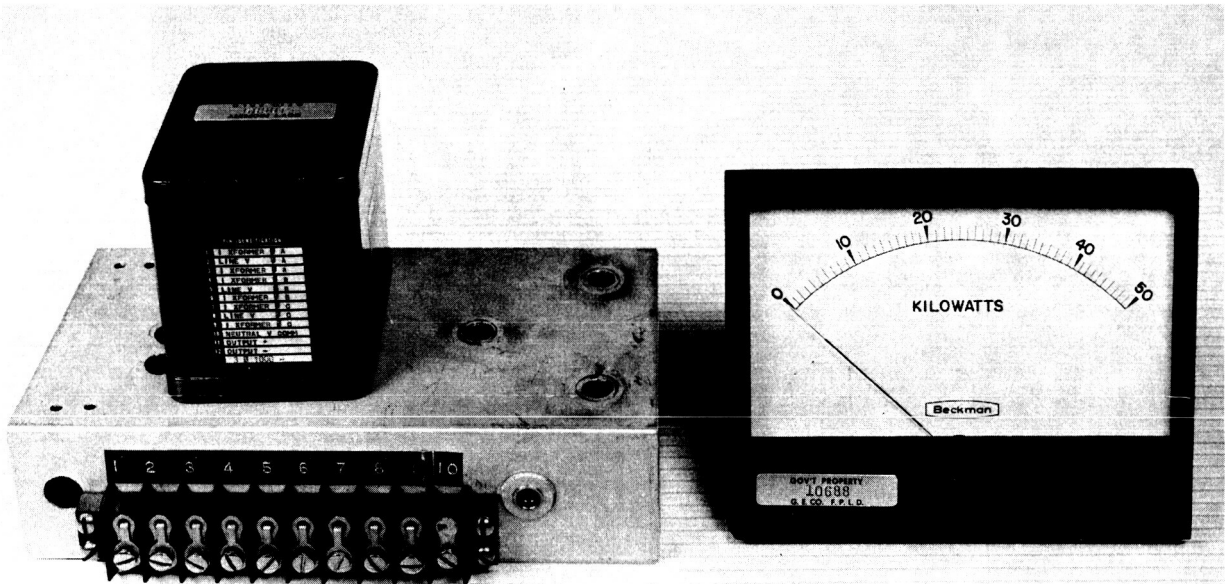


Fig. 5.9: Hall Effect Device with Meter

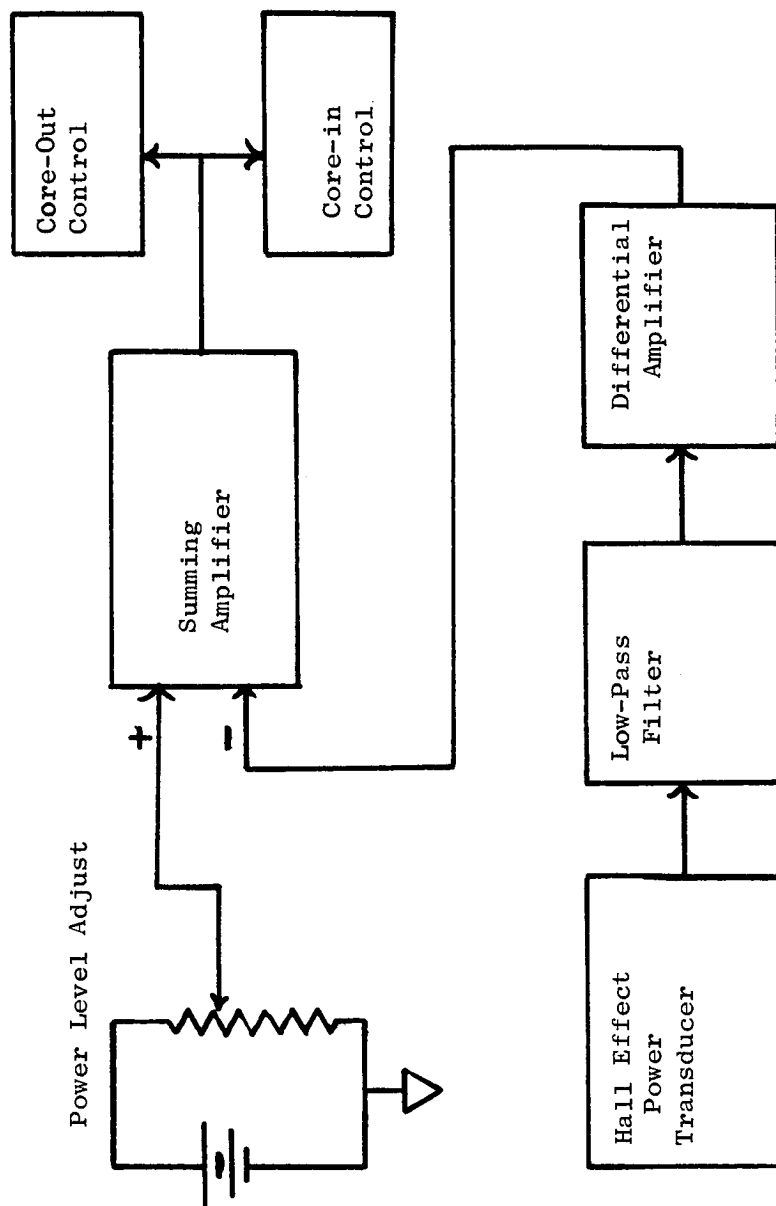


Fig.5.10: Automatic Power Level Control for a Single Phase Arc Jet Engine (Step Control Method)
Air Cored Reactor System

In Fig. 5.11 the schematic of the control system for a single phase ac plasma arc jet engine which is stabilized with a saturable reactor is shown. The electrical system for this case is shown in Fig. 5.12, while in Fig. 5.13 the electrical system for a three-phase plasma arc jet engine is shown. The components of this control system vary only slightly from the components of the system described earlier. This system will be evaluated as soon as the needed range of the stabilizing impedance for the single phase engine has been established.

The control power for the saturable reactor is approximately 3% of the arc power, while the power consumed by the power amplifier is negligible. The magnitude of the control power appears, therefore, to be the major difference between the use of air cored reactors and a saturable reactor at the present time when considering overall system efficiency. On the other hand, the difference of the two kinds of stabilizing ballast has not been evaluated yet. These are due to the difference in the electrical characteristic of the load voltage and load current when employing either one of the two devices in the circuit. This can be seen from Fig. 5.14.

5.5 Testing of the Single Phase Arc Jet Engine

The purpose of operating and testing the single phase engine was to be able quickly to explore various possibilities for improvements in the more complex three-phase engine. Accordingly, the single phase engine was designed to operate at the same temperatures and pressures as the large 30 kw arc jet engine. The engine has proved its value, since a number of tests were conducted which show the effects of different parameters on engine performance. For example, electrode ablation rates were measured in this engine and were found to fall on the same curve as the ablation rates measured with the large engine.

The tests which were performed on the small engine were as follows:

1. Correlation with the engine design curve
2. Operation with ac, dc, and rectified ac
3. Stable operation over a range of power levels.
4. Operation at unity power factors
5. Arc electrical characteristics
6. Measurement of ac electrode ablation rates
7. Measurement of dc electrode ablation rates
8. Measurement of electrode and nozzle body temperatures
9. Measurement of nozzle erosion
10. Operation at off-design pressure levels
11. Use of tungsten and thoriated tungsten electrodes
12. Effects of frequency on engine operation

5.5.1 Correlation With the Design Curve

The design curve for the single phase engine was given in Fig. 5.11. In addition, the calibration curve for the propellant flow meter is shown in Fig. 5.15.

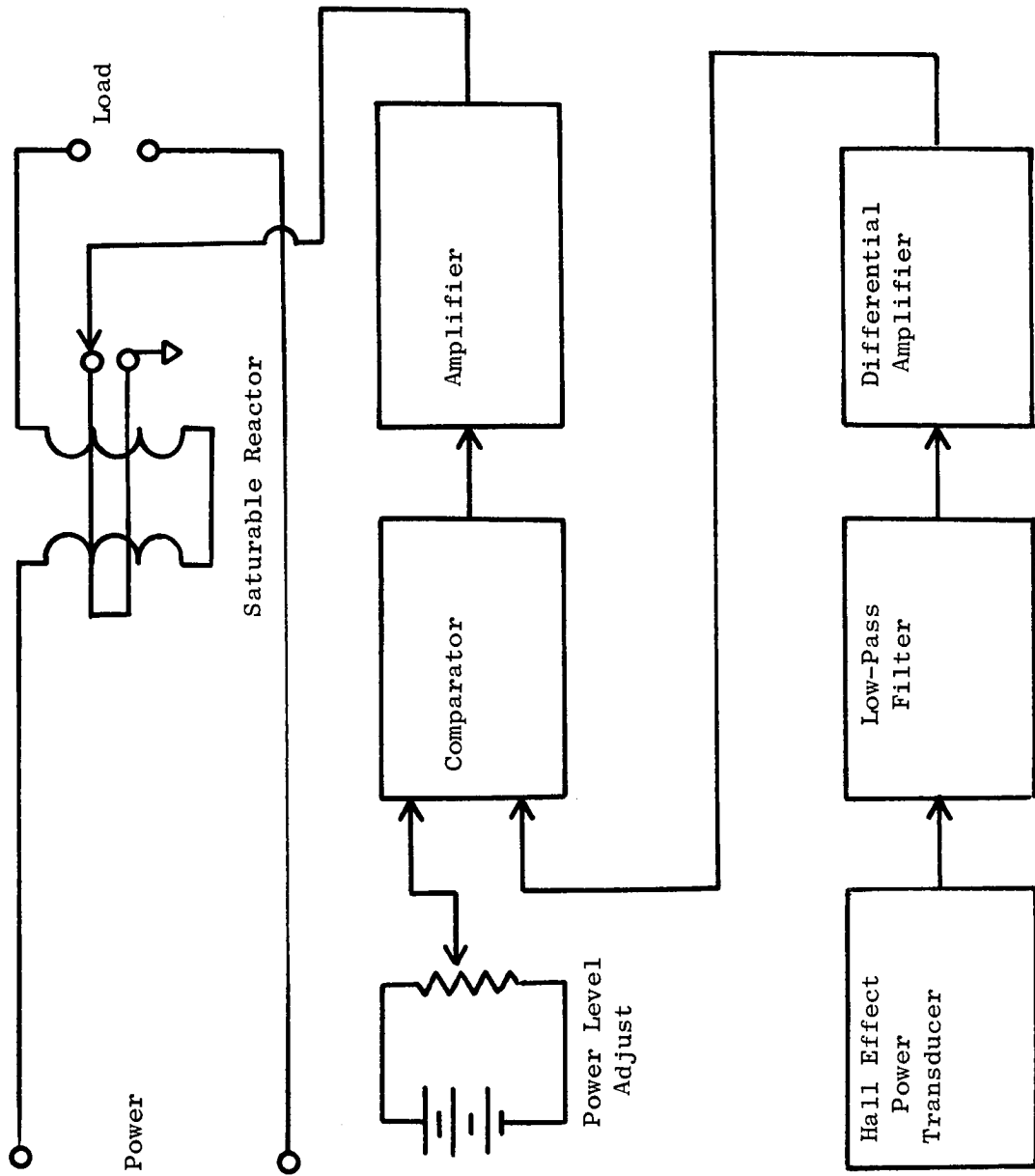


Fig. 5.11: Automatic Power Level Control for a Single Phase Arc Jet Engine (Step Control Method)
Saturable Reactor System

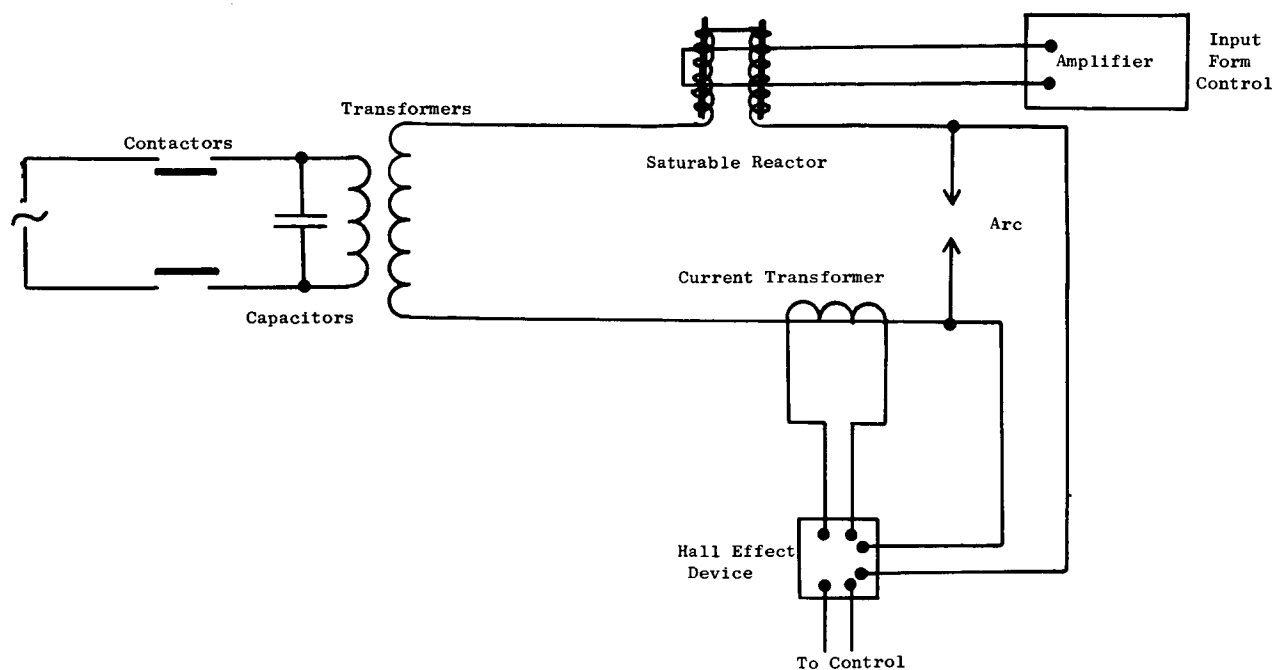


Fig. 5.12: Electrical System for Single Phase AC Plasma Arc Jet Engine (Saturable Reactor)

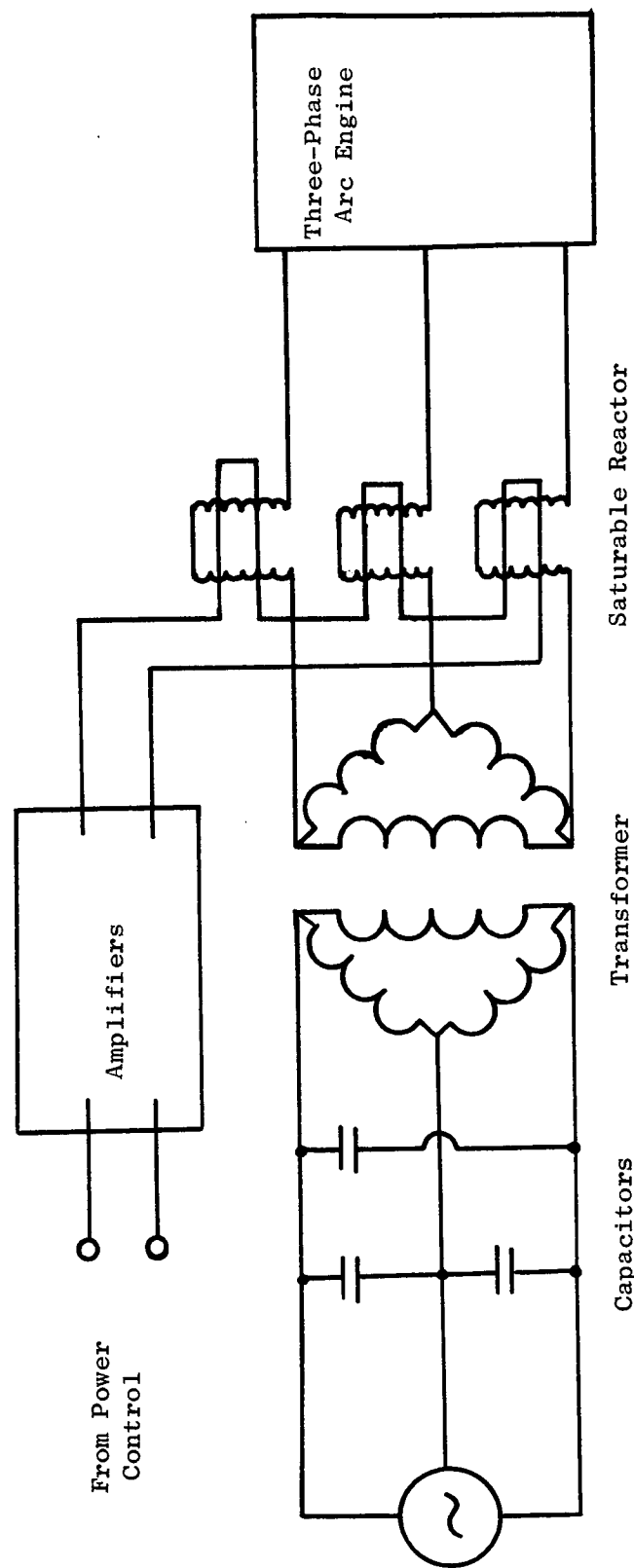
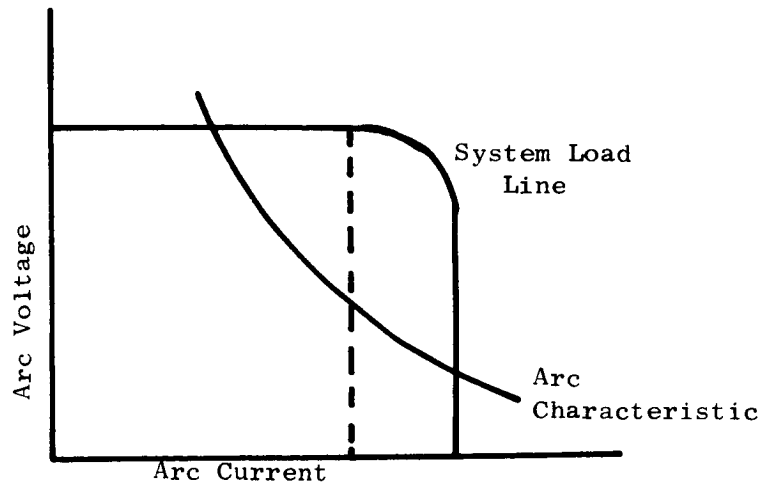
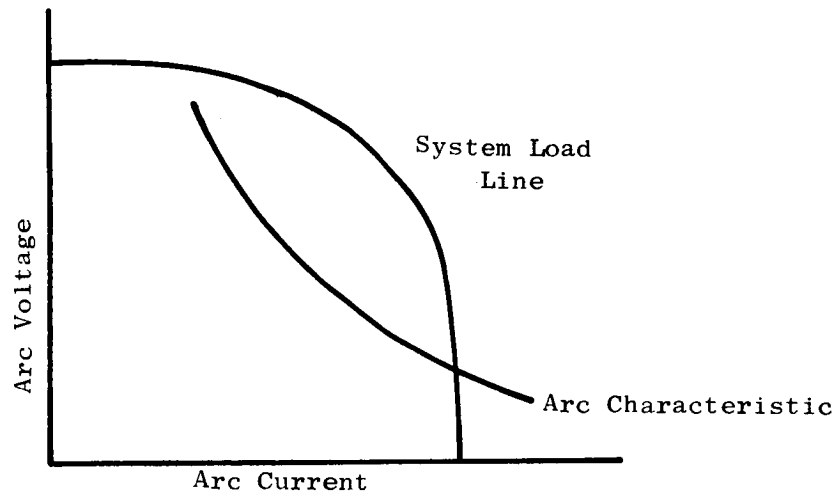


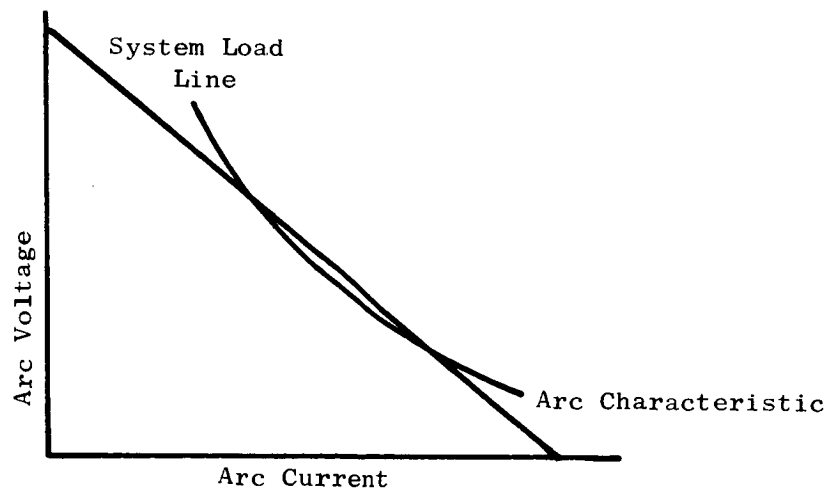
Fig. 5.13: Electrical System for a Three-Phase Plasma Arc Jet Engine



A. Saturable Reactor Controlled



B. Cored Reactor Controlled



C. Resistance Controlled

Fig. 5.14: Electrical Characteristics of External Impedance Stabilized Arcs

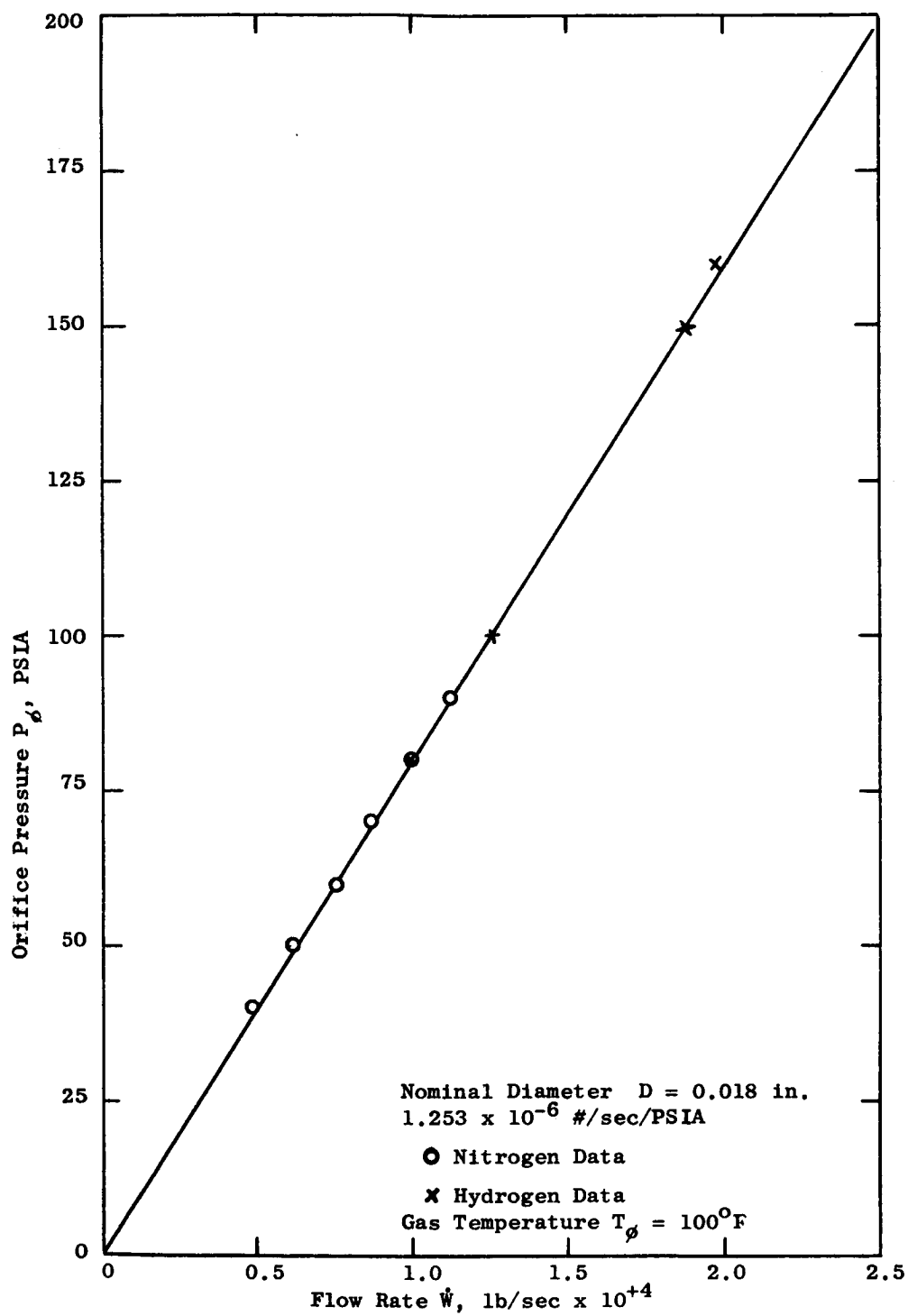


Fig. 5.15: Orifice Calibration for Hydrogen (18 mils)

The engine was usually operated at an orifice pressure of 80 psia which can be seen to correspond to a flow rate of 1.0×10^{-4} lb/sec. This flow rate gave a measured stagnation pressure of 14.7 psia at a power level of 7.5 kw, which is in agreement with the design curve. Therefore, it may be concluded that the thermodynamic analysis which led to the construction of the design curve has been experimentally validated by the actual engine operation.

5.5.2 Operation With Different Current Forms

The engine was designed primarily to operate with alternating current. It has also proved useful in tests with rectified alternating current and with direct current. The rectified ac tests were conducted by using the Behlman ac power supply, but operating with an increase in the stagnation pressure. The increased flow rate and stagnation pressure decreased the ionization sufficiently that the engine was able to conduct current in only one direction, that is from the center electrode to the nozzle. Operation in this manner reduces the power factor considerably but it permits investigation of the effects of fluctuating direct current. For the steady direct-current tests a General Electric DC Motor-Generator set capable of supplying up to 25 kilowatts was used.

With this power supply the engine was tested with dc at the same power level as the ac tests so that a direct comparison between ac and dc operation became readily available. Results of the dc tests indicated that the stability of the arc is not greatly different from the ac operation, but that dc operation produces a reduced electrode ablation at the tested power levels. This is in full agreement with the ablation analysis which is discussed elsewhere in this report. However, the analysis also indicates that the nozzle of a dc engine will, under some conditions, ablate more than the nozzle of an ac engine. The primary effect of nozzle ablation is a reduction in engine performance, whereas the effect of electrode ablation is a reduction in engine operating life. For laboratory purposes and for many practical engines, the problem of nozzle ablation is even more important than the problem of electrode ablation, because it is much more difficult to replace the nozzle than to move the electrode or insert a new one. Consequently, the operation of an ac plasma arc jet engine may prove to be preferable to dc operation.

5.5.3 Stable Operation Over Range of Power Levels

The engine was operated with good stability over a wide range of power levels. For instance, at one particular setting of the capacitor, the power level was varied continuously from 4.0 to 8.0 kilowatts, simply by adjustment of the supply voltage and the stabilizing inductance during operation. The engine was therefore operated with both ac and dc in this wide range of power for comparison. Using stabilizing resistances the power level could be continuously varied from 2.5 kw to 10 kw with ac or dc power supply.

5.5.4 Operation at Unity Power Factors

The arc jet engine system was operated at various power factors to ascertain the effect of the electrical system on the engine stability. From

considerations of system efficiency it is preferable to operate at unity power factor. The values of inductance and capacitance required for this condition at any desired operating point are shown in Fig. 5.16,

5.5.5 Arc Electrical Characteristics

The electrical characteristics of the arc jet engine were obtained experimentally for both ac and dc operation. It is important to obtain these data to determine the effects of engine modifications on the operating properties of the system.

The electrical characteristics can be conveniently expressed as a power-current relationship. In Fig. 5.17, the relationship is given for dc operation of the engine and the relationship for ac operation is shown in Fig. 5.18. The same engine was used for both of these tests. If the two curves were superimposed, the data points would tend to form one continuous curve. Therefore, the power-current characteristics for this engine are not greatly different for ac or dc operation, under the same conditions.

5.5.6 Measurement of AC Electrode Ablation Rates

A series of tests was run with the single phase engine to determine electrode ablation rates for ac arc operation. The procedure used was to measure the electrode weight before and after a measured time of testing. The test times as well as the power levels were varied at a constant electrode gap setting. It was found that the measured ablation rate was not affected by the duration of the test for test times up to about three hours. This is in agreement with the results of the three-phase engine ablation tests as discussed elsewhere in this report. It means that ablation is not affected by starting, and that loss of material from the electrodes is a continuous process. This is true at least for electrodes that are properly designed. If, however, the electrode is improperly designed, the loss of material may be rather large during initial operation until the electrode contour assumes a more efficient geometry.

The data obtained with these tests are plotted in the form of ablation rates as a function of power in Fig. 5.19. These data confirm experimentally what had been indicated theoretically, that the ablation rate increases monotonically with the power. However, this is not to imply that power is the only independent variable affecting the ablation rate; rather a number of other important parameters contribute to the loss of material. These include the electrode geometry, electrode material, stagnation temperature, gap setting, arc current, and the voltage-current relationship of the arc. Most of these variables were maintained in these tests as nearly constant as possible, in order to determine the variation of ablation rate with power level only. The comparison between experimental and analytical ablation results is discussed later in this report.

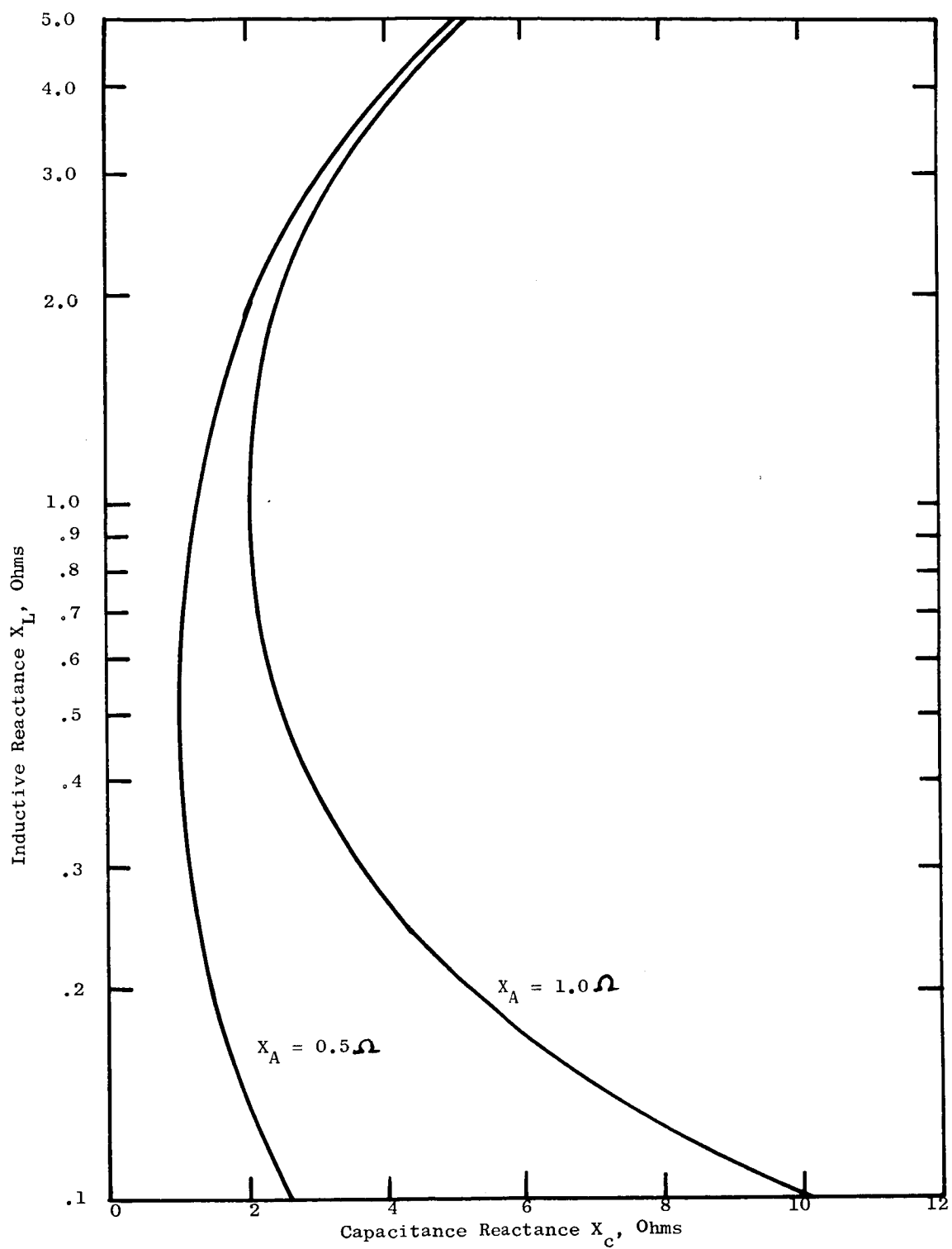


Fig. 5.16: Inductance - Capacitance Graph for Unity Power Factor

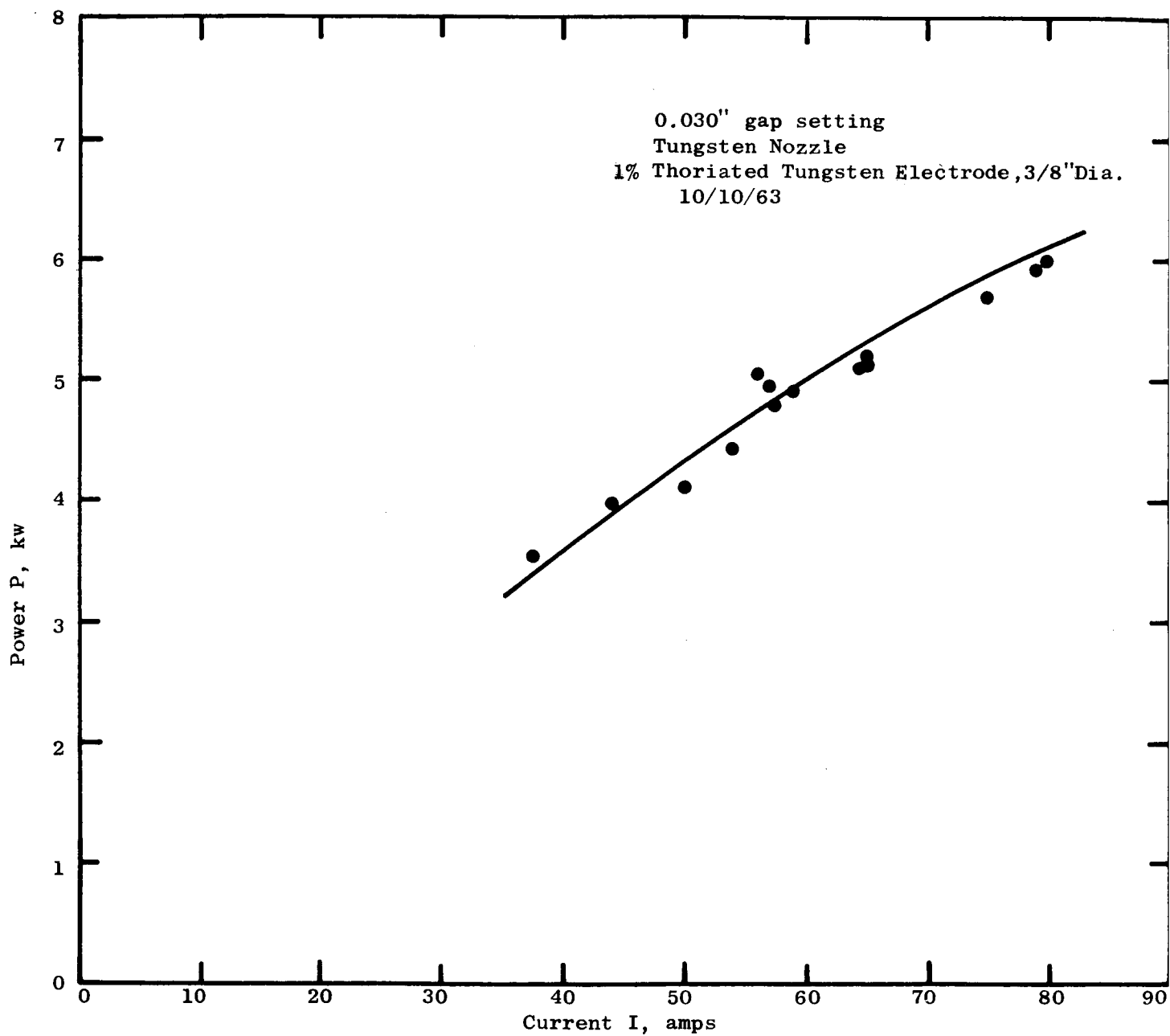


Fig. 5.17: Power-Current Characteristic of a DC Arc Engine

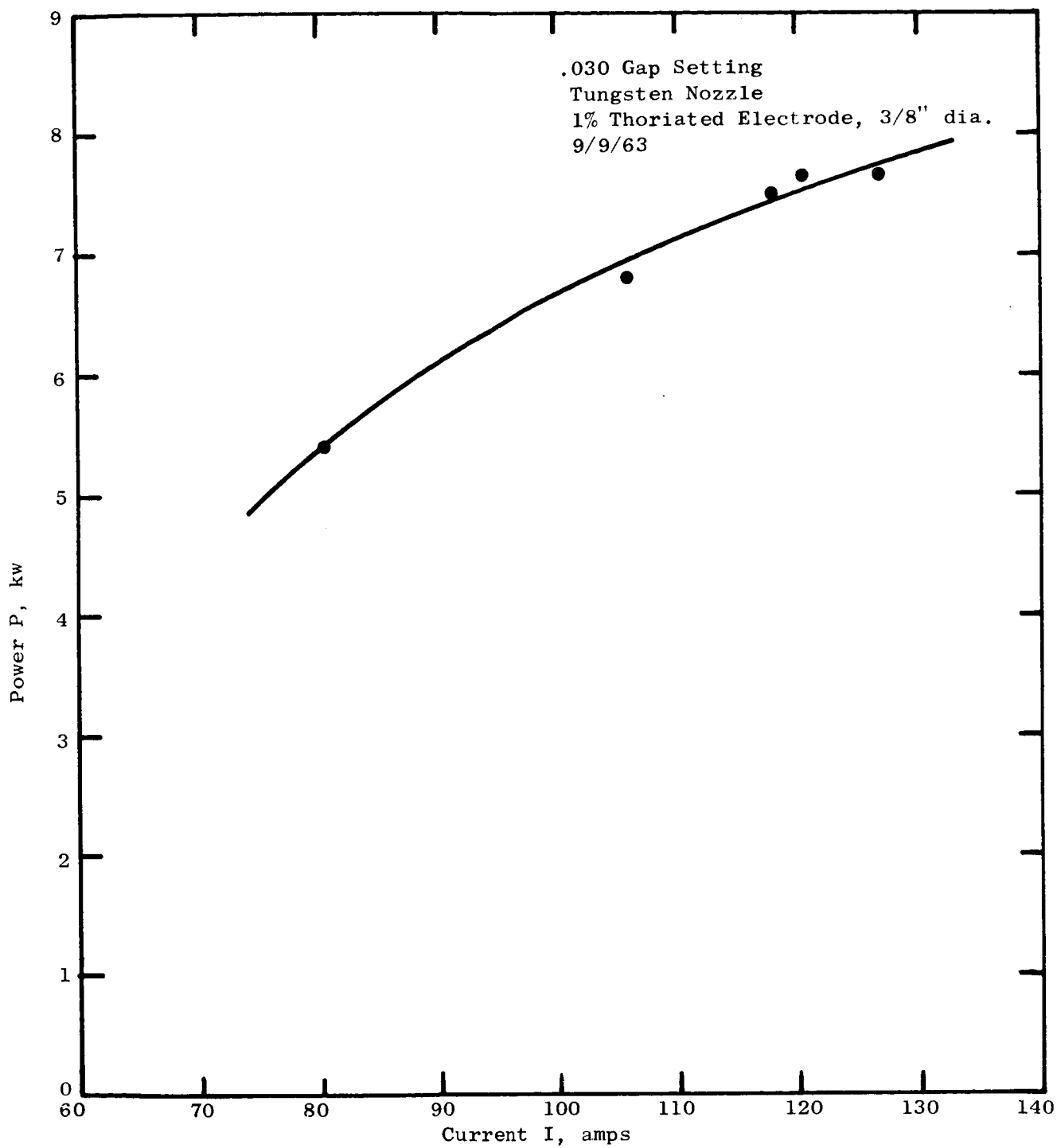


Fig. 5.18: Power-Current Characteristic for an AC Arc Engine

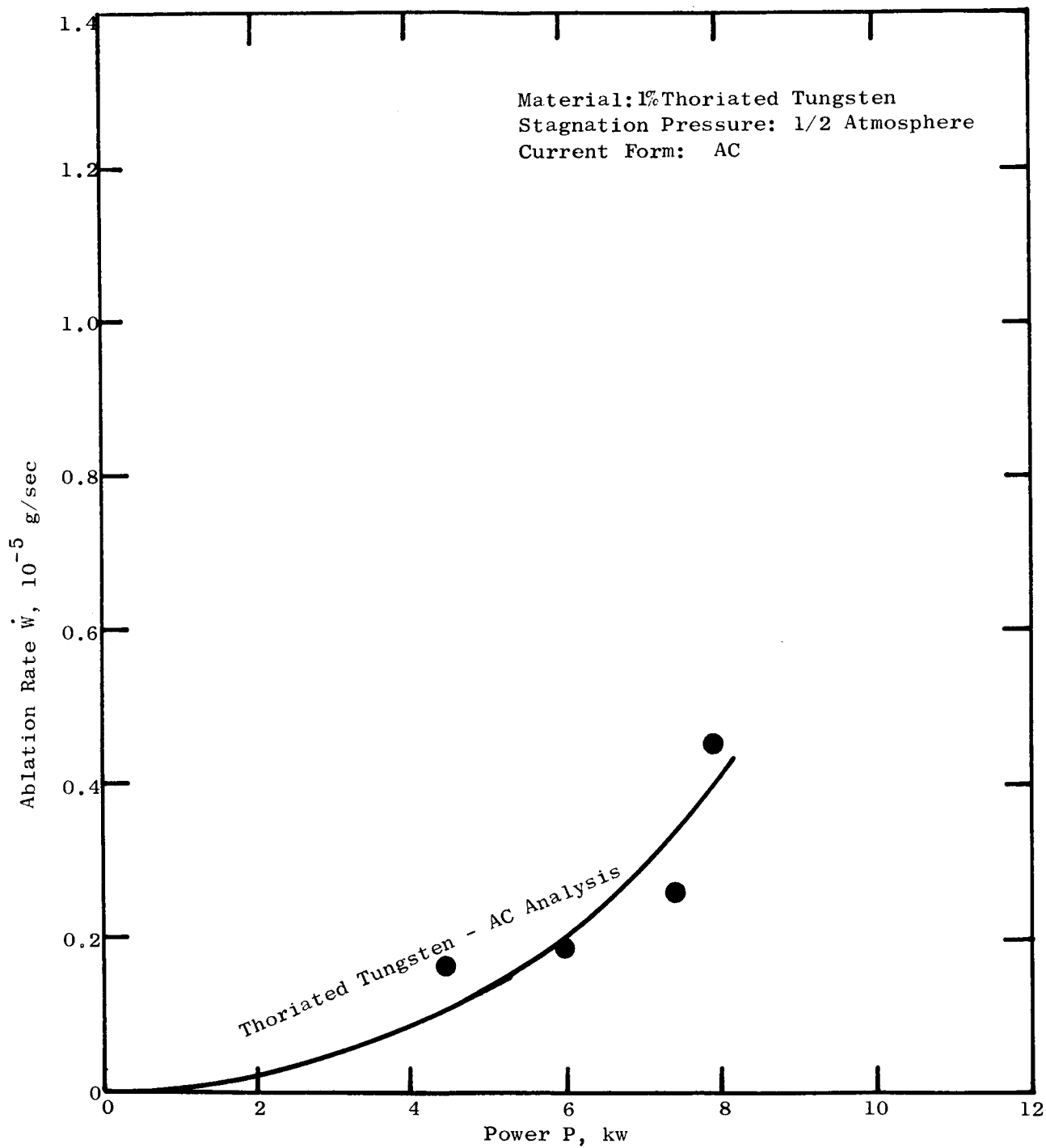


Fig. 5.19: Ablation Rate of Electrode - Single Phase Engine (AC Data)

5.5.7 Ablation Rates for DC Engines

The 7.5 kw arc jet engine can be operated with ac or dc power without any change in the engine configuration. Therefore, the engine was operated with dc in the power level range of 4.0 to 8.0 kilowatts in order to measure the electrode ablation rates at various power settings. The purpose was to compare the dc electrode ablation with the ac electrode ablation previously discussed. It was furthermore desired to compare the dc engine electrode ablation with the dc ablation analysis which will be presented later in this report.

The graph of Fig. 5.20 shows the measured values of electrode ablation as a function of power level for a thoriated tungsten electrode. It is significant to observe that the experimental results show agreement with the analysis for dc engine operation, although the analysis slightly overestimates the measured ablation rates.

The ablation rates for a dc engine operating with a tungsten electrode have also been measured over the power range of 4.0 to 8.0 kw. These ablation rates were in the range of 0.4×10^{-5} to 0.7×10^{-5} g/sec which are on the order of ten times as large as those for the one-percent thoriated tungsten electrode. This result was to be expected and it is indicated by the analysis of dc ablation. Therefore thoriated tungsten electrodes are to be preferred over tungsten electrodes when their operating temperature is below the melting point. It should be noted that the melting point of thoriated tungsten is 100 to 300°K lower than that of tungsten.

An interesting phenomenon was observed for the dc engine with tungsten electrode at very low power levels. When the power to the engine was decreased below about 4 kw before the nozzle had an opportunity to come to a steady-state temperature, the arc showed an unusual instability. The arc itself moved in and out of the nozzle with a frequency of about one excursion per second and the arc voltage and current values fluctuated widely at the same frequency. By increasing the power supplied to about 4.5 kw the instability was eliminated. However, the engine could have been operated at below 4 kw if the nozzle had been allowed to heat up for a few minutes at a higher power level. This same engine has been operated stably at power levels below 3 kw with ac power.

The results of this dc instability seemed to be rather severe. The measured ablation rate was higher than expected, the electrode had a sandblasted effect over its entire surface, and the nozzle showed evidence of temporary arcs striking all over its inside surface. This type of dc arc instability should obviously be eliminated or avoided during engine operation because of its deleterious effects.

5.5.8 Measurement of Electrode and Nozzle Body Temperatures

The temperature of the electrode in the arc jet engine was measured with an optical pyrometer. It was a Leeds and Northrup model with a temperature range of 1075°C to 4200°C. This instrument is capable of measuring a temperature to within about 10-20°C when used by an experienced operator. The temperatures

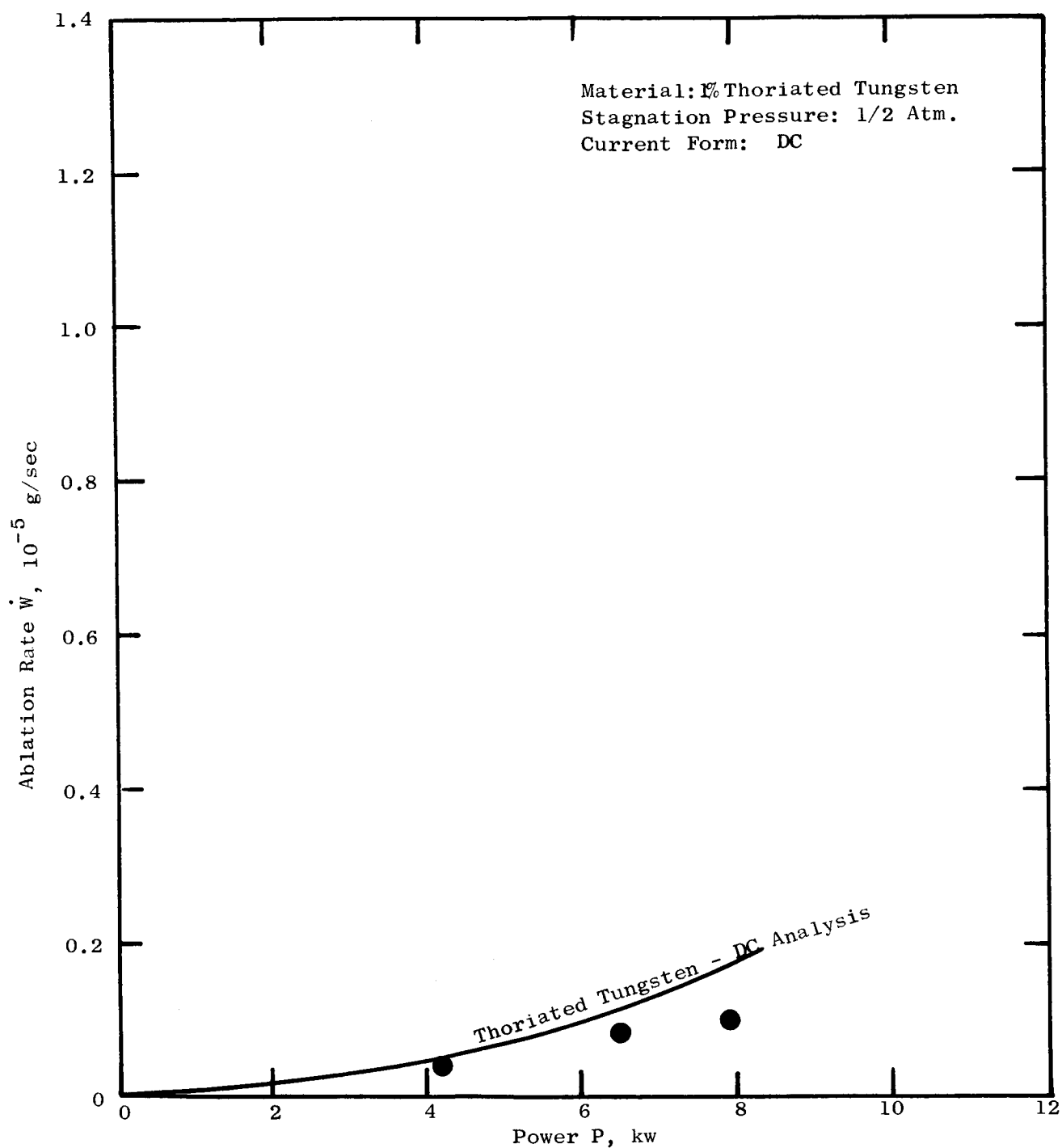


Fig 5.20: Ablation Rate of Electrode - Single Phase Engine (DC Data)

were measured by sighting the hottest spot viewed through the nozzle throat and determining its temperature. In addition, the temperature of a selected spot on the nozzle was recorded. The spot chosen was on the outside surface of the nozzle body, adjacent to the rim of the nozzle. This spot was selected to give only a comparative indication of the nozzle temperature for the various tests, since the hottest part of the nozzle cannot be viewed directly by this apparatus.

The data given in Fig. 5.21 show the variation of electrode and nozzle body temperatures as functions of power. The electrode temperatures show a good agreement with the analytically predicted values found from the ablation analysis. It should be emphasized that the maximum nozzle temperature will be much higher than the measured temperature of the selected spot. The measured temperatures have been corrected for the effects of sighting through a window and a mirror. These corrections were approximated by assuming a black body condition for the electrode; and they indicated that the measured temperatures must be increased by about 150°C to obtain the correct values. The nozzle body temperatures should be increased by a lesser amount, but this is not particularly important as there is presently no analysis with which to compare them. Therefore, the nozzle body temperatures were not corrected and they are included only to show the general trend of the body temperatures.

In further tests on measurement of electrode temperatures, an interesting phenomenon was discovered. There is a difference of about 300°C to 400°C between the temperatures at the center of the electrode and at the outside of the electrode. Such a situation is in agreement with the model used for ablation analysis. This effect was shown to be reproducible for a number of tests, and the graph of Fig. 5.22 demonstrates the presence of the two temperature zones. The data on this graph have not been corrected for the effects of sighting through a window and mirror. Such correction would raise both curves by about 150°C.

It is very important to be able to determine, both experimentally and analytically, the electrode and nozzle temperatures for various operating conditions. This is because the ablation rates of the electrode and nozzle material can be directly related to the surface temperatures. These ablation rates are crucial information for the design of engines expected to operate for long durations.

5.5.9 Measurement of Nozzle Erosion

It is known that the nozzle of an arc jet engine undergoes a certain amount of erosion during operation. This loss of material is due to several combined processes; erosion, evaporation, melting, and sputtering. Apparently the problem has not hitherto been attacked analytically, or even experimentally. Little mention has been made of it even in the most recent literature on the subject of plasma arc jet engines.

In the series of investigations on the single phase arc jet engine, some measurements were made of the increase in nozzle throat area due to erosion. For instance it was found that the nozzle throat diameter became enlarged some 40% over its original size of about 0.040 inches during a total running time with both

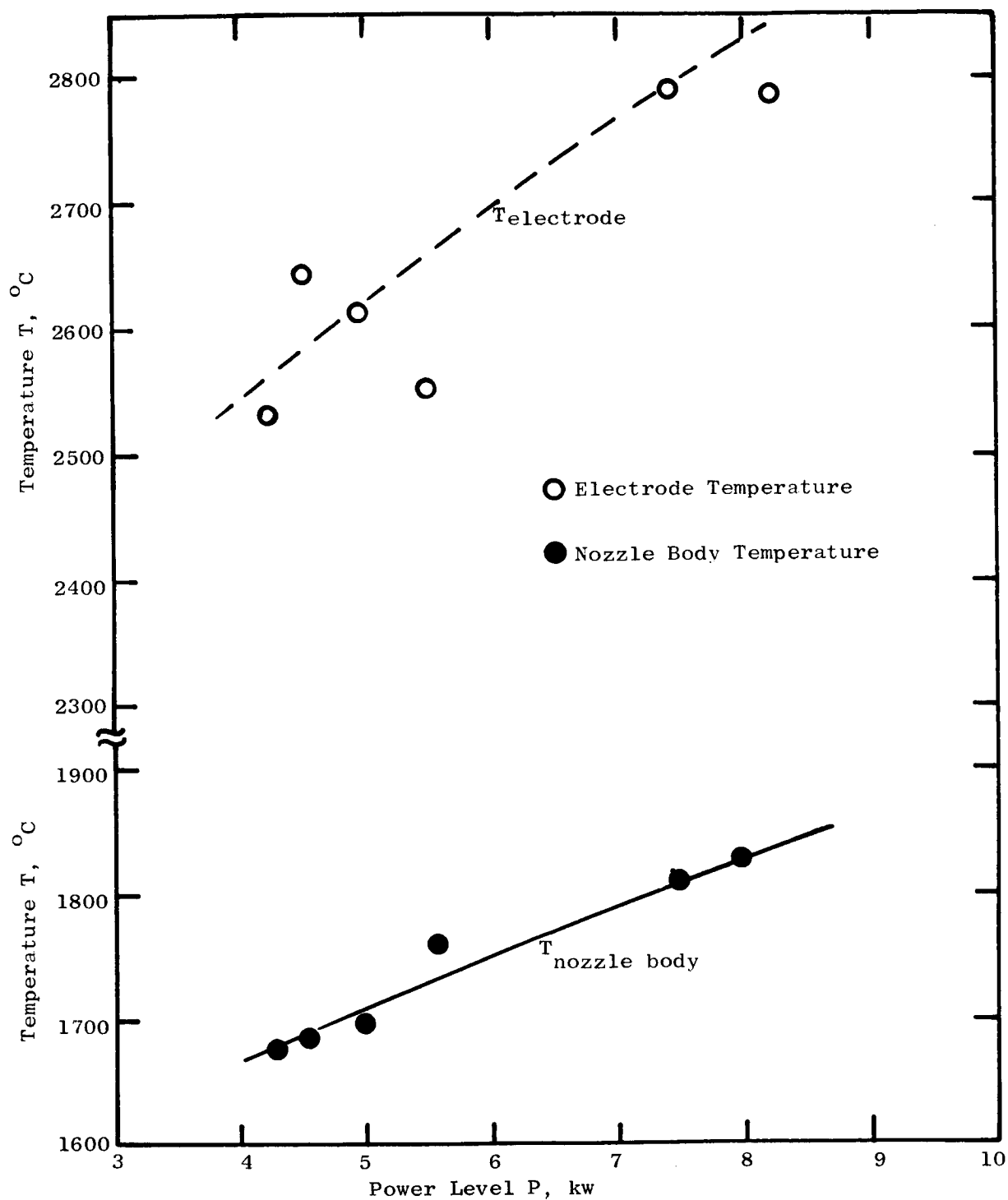


Fig. 5.21: Temperature of Electrode and Nozzle Body
 30 mil gap, single phase engine (AC)
 (Uncorrected Pyrometer Readings)

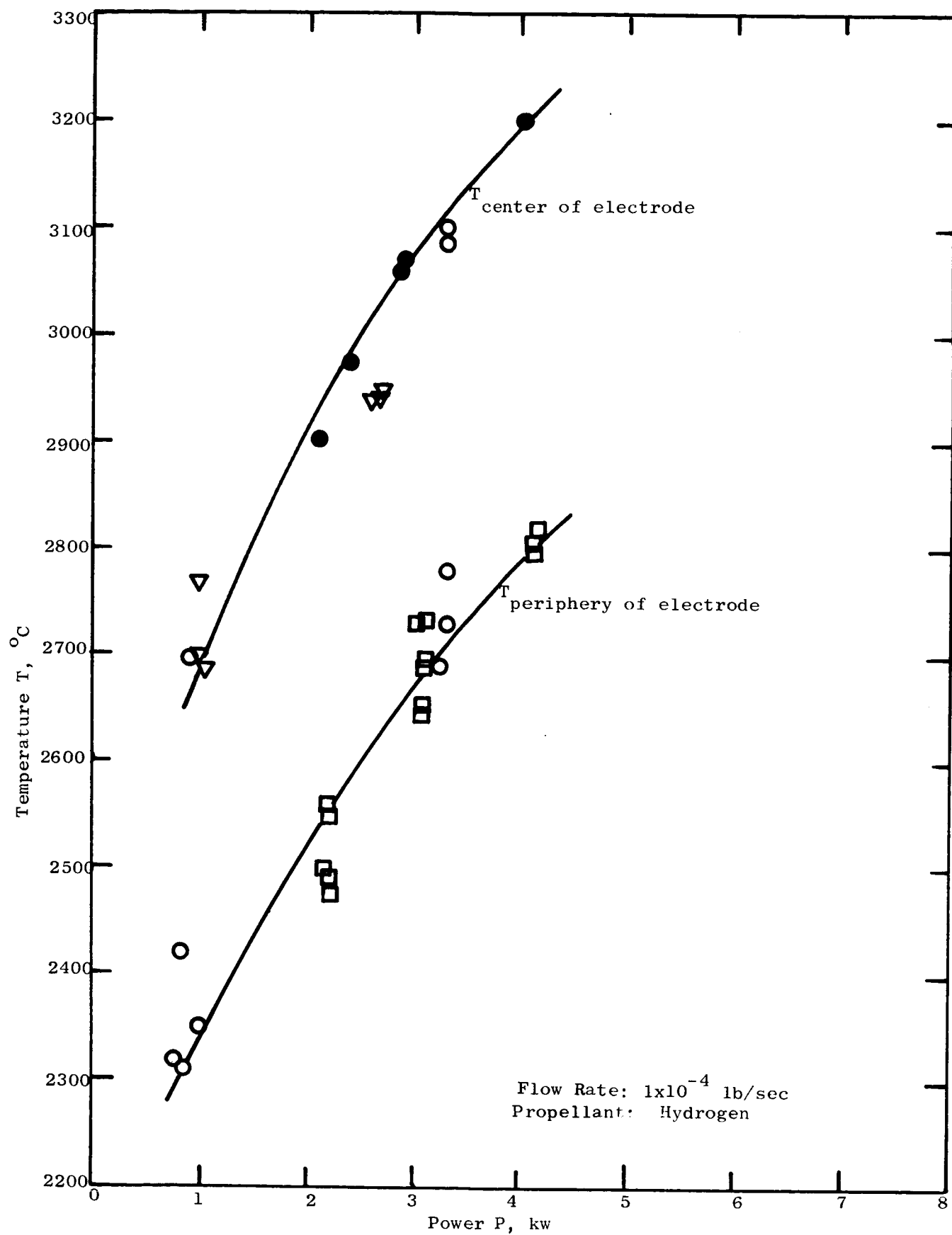


Fig. 5.22: Measured Temperatures of DC Arc Cathode (Uncorrected Pyrometer Readings)

ac and dc power on the order of 15 hours. It is very important, in the design of an engine, to be able to estimate the nozzle erosion rate in order to minimize the loss in engine performance accompanying the nozzle enlargement.

5.5.10 Operation at Lower Pressure Levels

The single phase arc jet engine was operated at stagnation pressures below the design pressure. The primary purpose was to determine if the predicted and measured rates of ablation were in agreement at these levels. The pressures were in the range of one-third to one-half atmosphere. As can be seen from Fig. 5.19, the predicted and measured ablation rates were only in fair absolute agreement, but they were definitely in good relative agreement with regard to their tendency to increase with power level and decrease with stagnation pressure.

It was gratifying to note that the ablation analysis predicted correctly the effect of stagnation pressures. The results are particularly important for the design of engines operating at higher pressures with which higher engine efficiencies can be attained. By applying the ablation analysis, an optimum design with respect to efficiency and lifetime can be obtained.

5.5.11 Use of Tungsten and Thoriated Tungsten Electrodes

The single phase engine was tested using both tungsten and thoriated tungsten electrodes. It was visually observed that the thoriated tungsten electrode operated at lower temperature. The data shown in Figs. 5.19, 5.20, and 5.22 were obtained with the thoriated tungsten electrode.

It is particularly of interest to determine the optimum amount of thorium for the electrode. The reason that high-percentage mixtures of thoriated tungsten are being considered is because of an investigation performed a few years ago at the General Electric Research Laboratory (Ref. 1). This investigation studied electrodes of tungsten with additions of thorium and other oxides as coatings, cores or sintered materials. It was determined that an optimum concentration of about 13 percent thorium gave superior performance not only in terms of ablation rate but also in several other aspects of arc operation.

5.5.12 Effects of Frequency on Arc Engine Operation

The single phase plasma arc jet engine was operated over the range of frequencies from 300 to 1400 cycles per second. The purpose was to discover the effects of frequency on electrical characteristics, rectification, starting and stability of the arc engine.

The system that was used to investigate these effects is shown in Fig. 5.23. It employed an auxiliary starter that was shorted out after the engine began running. Stability was obtained by use of a ballast resistor in the arc engine circuit. Although this resistor caused a power loss it was preferable to an inductance-stabilized system. The reason is that the values of inductance and capacitance which are required to give a power factor near unity change greatly over the frequency range of interest. Therefore it would be necessary to change

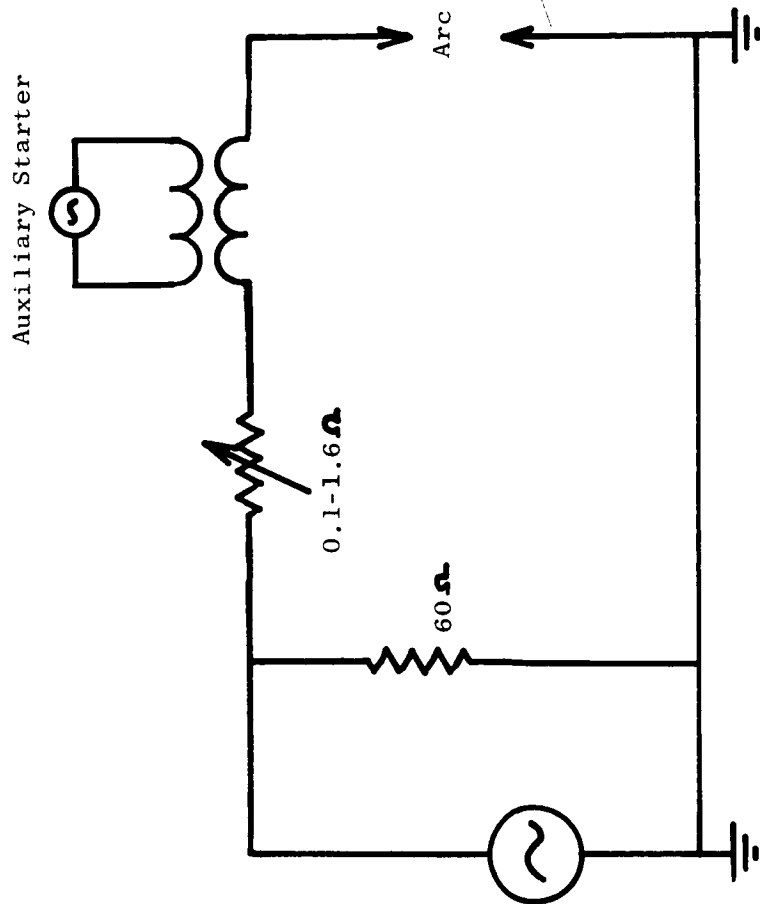


Fig. 5.23: Schematic Diagram of Circuit Used for Frequency Testing

capacitors and inductors frequently during the testing in order to obtain the required range of impedance variation. Since that would require starting and stopping the engine several times during the tests, it was decided to use resistance-stabilization instead.

5.5.12.1 Electrical Characteristics

The procedure used in this testing was to vary the power supply frequency while maintaining the power level and flow rate constant. In the graph of Fig. 5.24 the variations of arc current and voltage are shown for a power level of 4.2 kw over the range of frequencies 400-1000 cps. Notice that the voltage and current are both essentially constant. This leads to the conclusion that there is no significant effect of frequency on the arc impedance. Therefore the arc may be considered as a pure resistance with no elements of inductance or capacitance. In Fig. 5.25 a similar test was run at higher power over the wider frequency range from 300-1400 cps. Again the arc current was found to be constant over the range of frequency. At a frequency of 350 cps the current became rectified.

Pictures were taken of the current and voltage traces on an oscilloscope over the range of frequencies tested. These pictures are shown in Fig. 5.26. It can be seen that there is no significant change in the shape or size of the voltage or current curves as the frequency is varied. The current trace is always a slightly distorted sinusoid and the voltage is essentially a square wave with reignition spikes. As the frequency is decreased the traces are naturally spread out until, at 400 cps, the sweep rate was changed so as to keep at least one complete cycle on the screen. These pictures again demonstrate that there is no significant effect of frequency on the electrical characteristics of the arc engine.

Arc Rectification - It was previously shown, with regard to Fig. 5.25, that when the frequency is decreased at a constant power level, a point is reached where the arc current becomes rectified. This is an expected result because, as the frequency decreases, the time between successive arcs striking between the electrodes increases. Therefore the electrodes have more time to cool off between current surges. Since the current is carried by thermionically emitted electrons, a high temperature is required for the arc to strike. Now the inside electrode is relatively small and is partly shielded by the body from radiation loss. Therefore it stays hot enough to emit enough electrons to carry the current. However the nozzle is rather large and is regeneratively cooled by propellant flow, conduction and by radiation. Therefore it becomes sufficiently cool at low frequencies that it cannot emit enough electrons to carry the current flow. Therefore, at low frequencies, the electrons will flow only from the center electrode to the nozzle and the current will be rectified. In order to obtain a non-rectified arc at low frequency, it is necessary either to increase the power level or decrease the propellant flow rate, so that the nozzle will attain a higher temperature.

Starting - The starting of the arc was accomplished readily at all

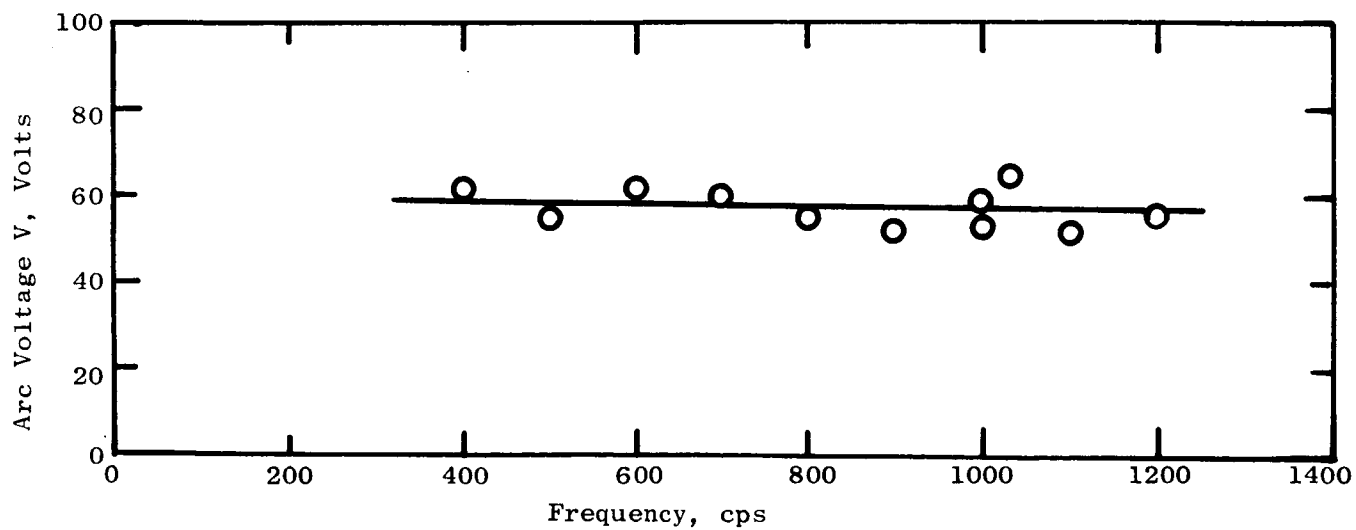
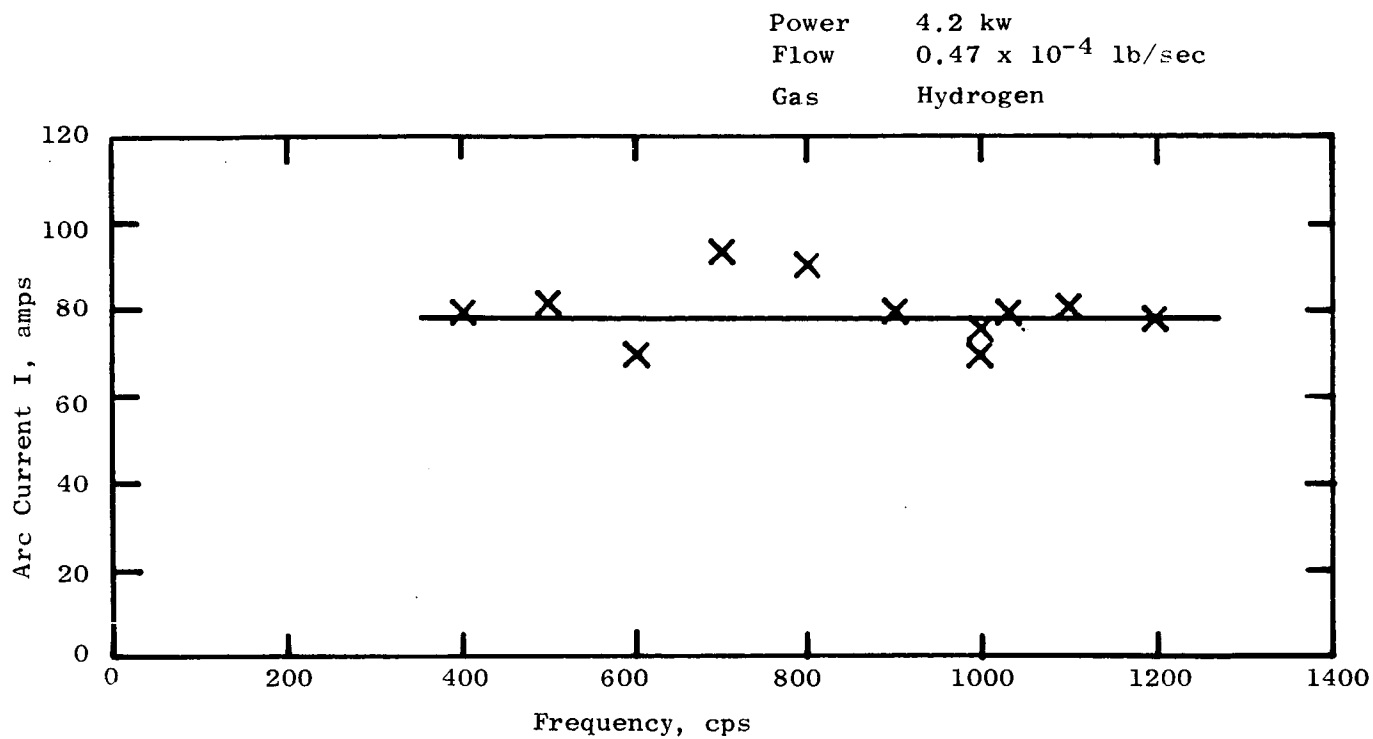


Fig. 5.24: Effects of Frequency on Electrical Characteristics of an Arc Jet Engine

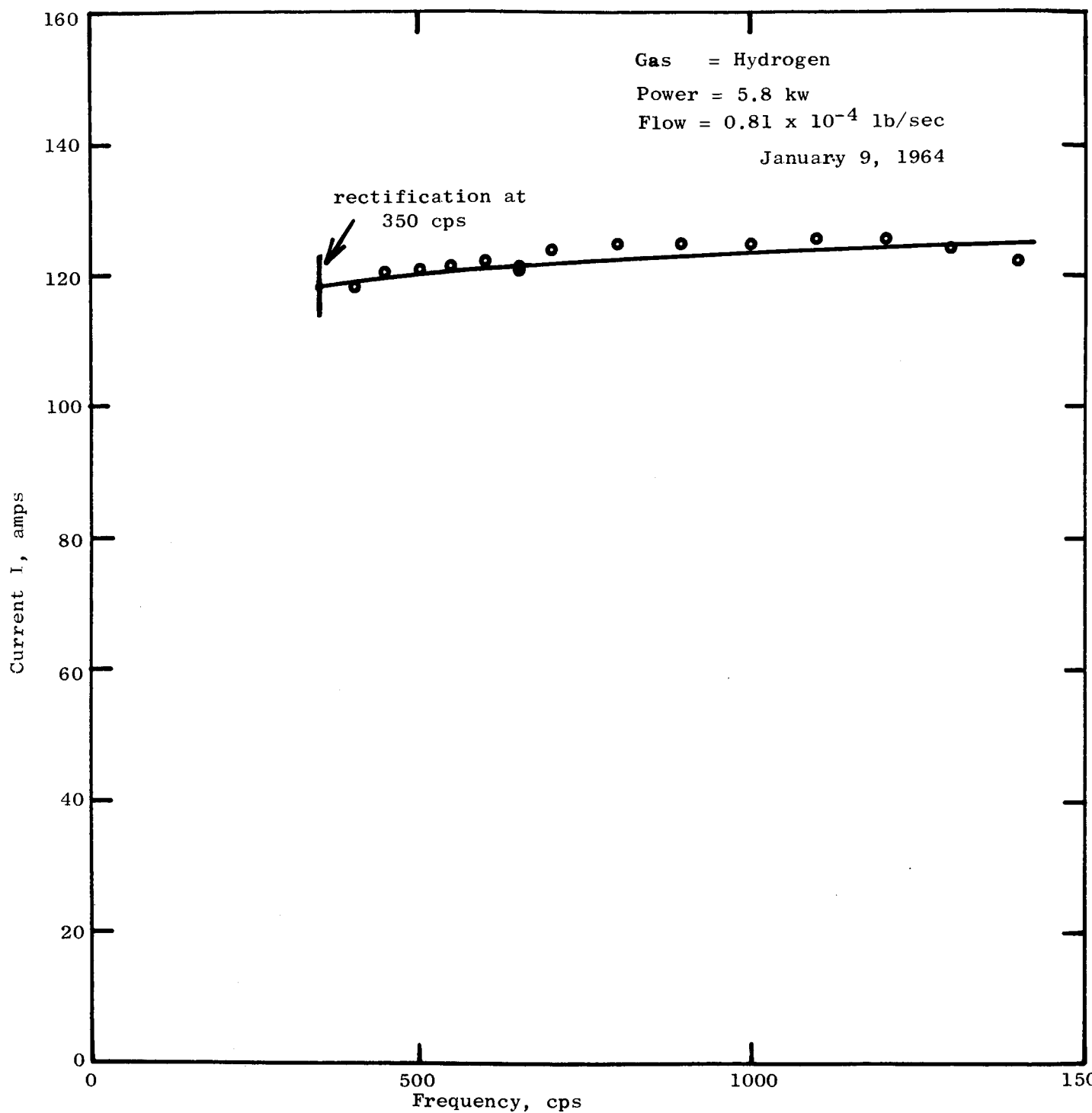
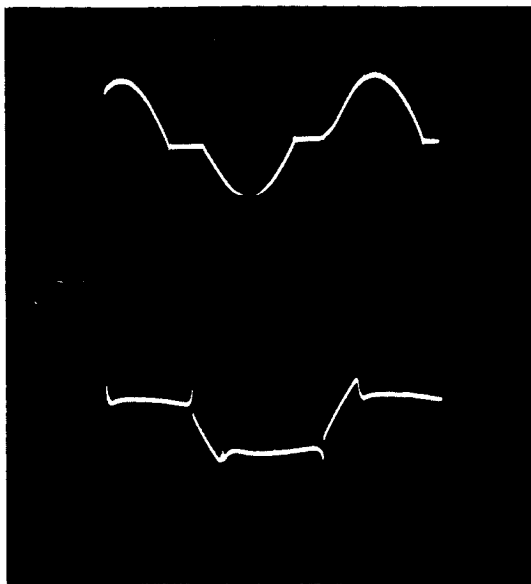
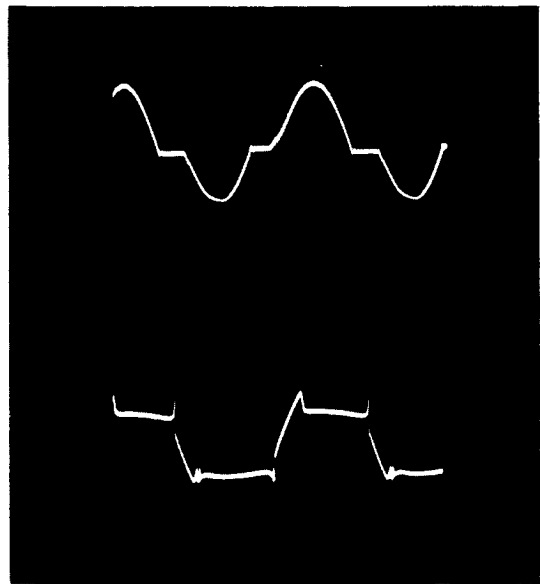


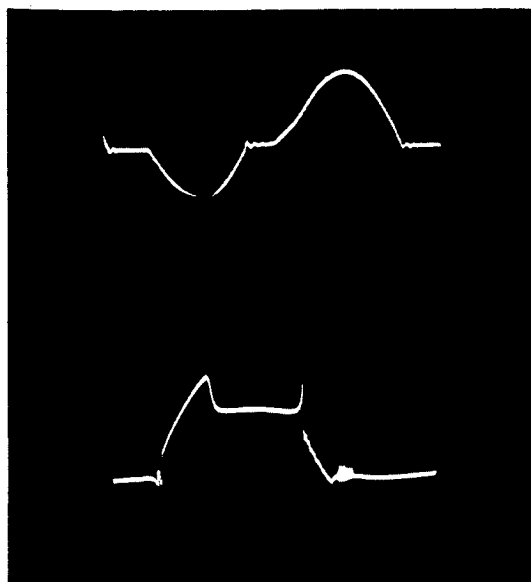
Fig. 5.25: Effect of Frequency on AC Arc Current



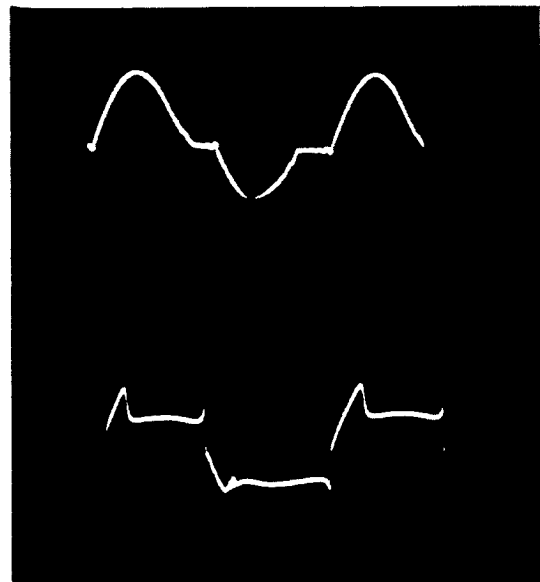
300 cps



400 cps

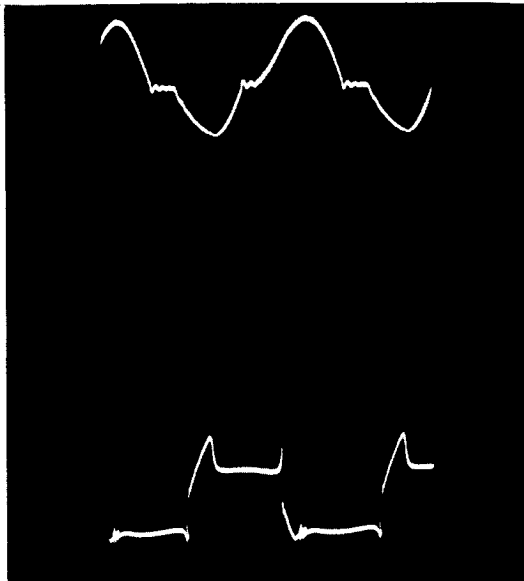


520 cps

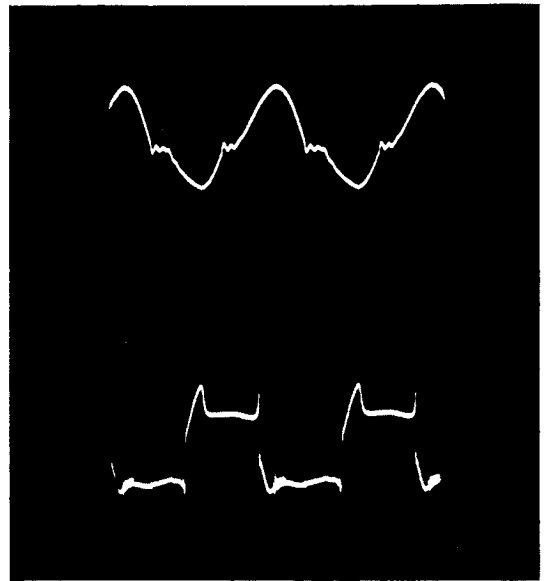


650 cps

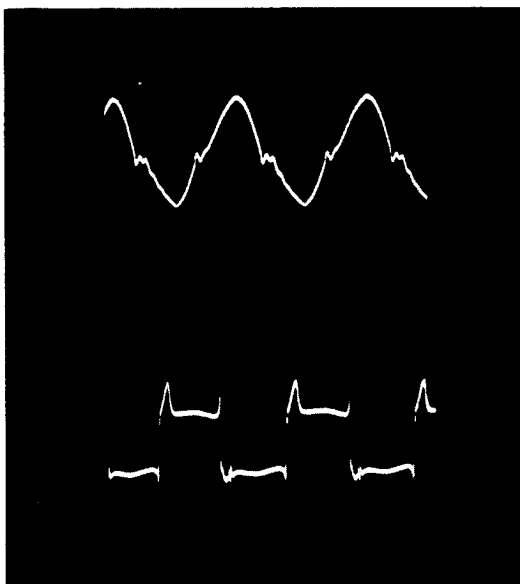
Fig. 5.26a: Current and Voltage Traces of an AC Arc at Different Frequencies



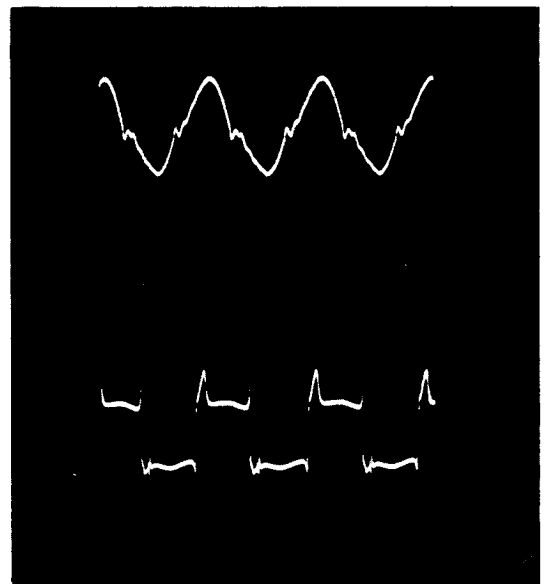
800 cps



1000 cps



1200 cps



1400 cps

Fig. 5.26b: Current and Voltage Traces of an AC Arc at Different Frequencies

frequencies tested in this program. It was done by using a high-voltage auxiliary starting supply in combination with a low chamber pressure and an auxiliary starting gas (argon). The arc started easily in all cases although it normally began with a rectified current. As the argon flow was turned off and the power increased the current would attain a non-rectified form provided the frequency and power level were sufficiently high.

5.6 Conclusions

The following observations and conclusions can be made about the single phase engine tests:

1. The single phase arc jet engine has been operated over a range of powers with ac, dc and rectified ac. The engine performance is in agreement with the theoretical design curve, thereby validating the thermodynamic analysis on which the design was based.
2. Electrode ablation rates have been measured for tungsten and thoriated tungsten electrodes with ac and dc power. Good agreement with the analytically predicted values has been obtained.
3. Electrode temperatures have been measured and have been shown to be predictable by analysis.
4. Starting, stability and electrical characteristics of an arc engine are not affected by frequency, over the range of 300-1400 cps. However, rectification is more difficult to prevent at the lower end of this range of frequencies.

6. CONCLUSIONS AND RECOMMENDATIONS FOR FUTURE EFFORTS

6.1 Conclusions

There are a number of significant conclusions which have been determined as a result of this program. First, and most important, it has been shown that a three-phase ac plasma arc jet engine can be operated at performance figures exceeding 1000 seconds specific impulse and 0.5 lb thrust at 30 kw, for durations longer than 250 hours. This engine can be started easily as shown by the required ten restarts and by a number of subsequent restarts. Furthermore, the performance does not significantly change with time and in fact it changed less than five percent during the 250 hour test.

In order to design and operate three-phase engines and to achieve the specified performance levels, there were a number of other supporting efforts which yielded interesting and important discoveries during the course of this program. These are summarized below:

- 1) Accuracy of instrumentation for performance measurements of a plasma arc jet engine is crucial to the successful completion of a test program. The thrust measuring device, propellant flow metering system and wattmeters must be painstakingly calibrated against all extraneous effects. In addition, the ambient pressure in the test tank must be properly monitored because of its pronounced effect on the measured engine thrust. All of these precautions were carefully observed in this test program.
- 2) A power control system was devised and operated which automatically maintained a constant engine power level.
- 3) The firing order of the electrodes in a three-phase ac engine has a significant effect on the relative distribution of power in the three arcs. Judicious selection of a firing-order sequence tends to maximize the output of the engine.
- 4) The three-phase ac plasma arc jet engine was operated over its performance envelope, and it was found throughout to show good experimental agreement with the analytically predicted performance. Therefore, it has been shown that the computer analysis which predicts engine performance has been completely validated.
- 5) A single phase plasma arc jet engine was designed and operated with both ac and dc power. Its operation again gave verification of the computer-predicted analysis. Moreover, the engine yielded information on electrode temperature, ablation, power control and frequency effects which was utilized in the development of the three-phase engine.
- 6) There was found to be no effect of frequency on electrical characteristics, stability or starting of the single phase ac

engine over the range of 300-1400 cps. However, rectification was more difficult to eliminate at the lower end of this frequency range.

- 7) An ablation analysis has been derived which has been shown successful in determining the rate of electrode erosion in ac and dc engines. This analysis shows the effects of parameters such as power, current, stagnation pressure, materials, and electrode geometry.
- 8) Satisfactory electrode materials for a 30 kw three-phase plasma arc jet engine have been found to be high density thoriated tungsten for the nozzle and high density tungsten for the electrodes.
- 9) The long duration run of Engine Y16-1 for 250 hours at design performance has proven that three-phase plasma arc jet engines can be operated efficiently and reliably for long missions, and that they can be repeatedly started without loss in performance.

6.2 Recommendations

The results of this investigation have shown that a three-phase plasma arc jet engine is practical, efficient, reliable, and long-lived. A three-phase engine is naturally considered to be the ultimate type of engine to be operated from a three-phase power system. Therefore, since such engines have now been shown to be practical, the next logical step is to bring about improvements in three-phase engines. These improvements are generally considered to fall into the following three categories:

- 1) High specific impulse - Plasma arc jet engines should be capable of extended operation at specific impulse values in the range 1500-2000 seconds. Improvements in engine materials, design, and operating conditions are required to achieve this goal.
- 2) High efficiency - Use of revised designs, based on recently developed analyses, show promise of bringing about significant increases in engine efficiency. For example, operation at a stagnation pressure of 10 atmospheres can increase engine efficiency by at least 15 to 20 percent.
- 3) Basic understanding of arc jet technology - These efforts should include further investigations into electrode ablation and the interaction of electrical parameters in a three-phase plasma arc jet engine.

APPENDIX I

I. INSTRUMENTATION OF THREE-PHASE PLASMA ARC JET ENGINE FACILITY

I.1 Thrust Measuring System Design

I.1.1 Basic Considerations in the Design of Thrust Measuring Devices for Plasma Arc Jet Engines

One of the most critical items in the evaluation of the performance of a plasma arc jet engine is the determination of the thrust. Experience has shown that most of the difficulties encountered in the measurement of the thrust are due to the relatively low thrust level, and to thermal expansion of the arc jet engine as well as the supporting structure, power leads, and propellant supply leads. A thrust measuring device has therefore to be designed such that thermal expansions will not influence the mechanism with which the thrust is correlated. This can be explained best by the example of a cantilever beam type thrust measuring device. In such a device the strain on the surface of the beam as measured by strain gages is correlated with the thrust. The strain on the beam, however, is actually proportional to the moment around the point of the strain gage. Any change of moment can, however, not only be due to thrust, but also to an increase in the length of the beam, shift of the c.g. of the engine and unrelieved thermal stresses in the leads.

A thrust measuring system, therefore, has to be designed to measure only the change of thrust and be completely unaffected by any one of the other changes which coincide by necessity with any change of thrust of a plasma arc jet engine.

Two points were emphasized in the design of the thrust measuring device for the 30 kw three-phase plasma arc jet engine. The first objective was to eliminate the effects of possible thermal expansions in the power leads on the thrust measuring mechanism. The thrust measuring system measures only horizontal forces which cause a horizontal displacement, while the unrelieved thermal expansion forces in the power leads operate perpendicular to the thrust force and cannot result in a horizontal displacement. The second objective of the design was to minimize all changes due to heat radiation or to changes in power, and propellant flow rate. This is achieved by controlling the component temperature by an oil bath whose temperature is controlled by cooling coils and a heater.

Provisions were also to be made that the plasma arc jet engine could be installed into a calorimeter jacket which can be added to the basic thrust measuring device when desired. This jacket which is suspended under the base plate performs two functions: it decreases the radiation from the engine body to the thrust measuring structure and it measures the radiation heat transfer losses from the engine body surface. The basic design of the thrust measuring device is shown in a cut away drawing in Fig. I.1. The functional design is better realized from Fig. I.2.

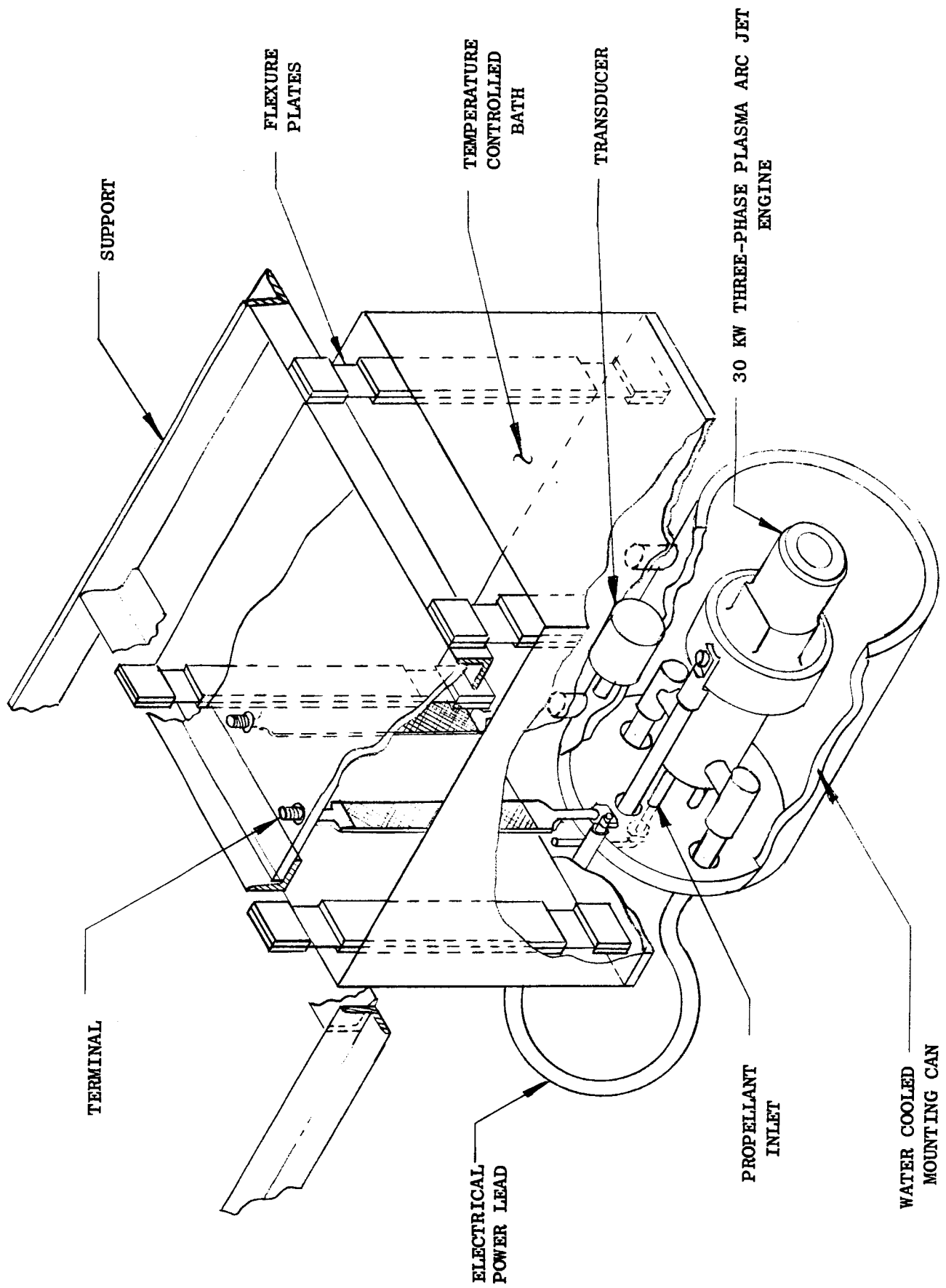


Fig. I.1: Thrust Measuring System

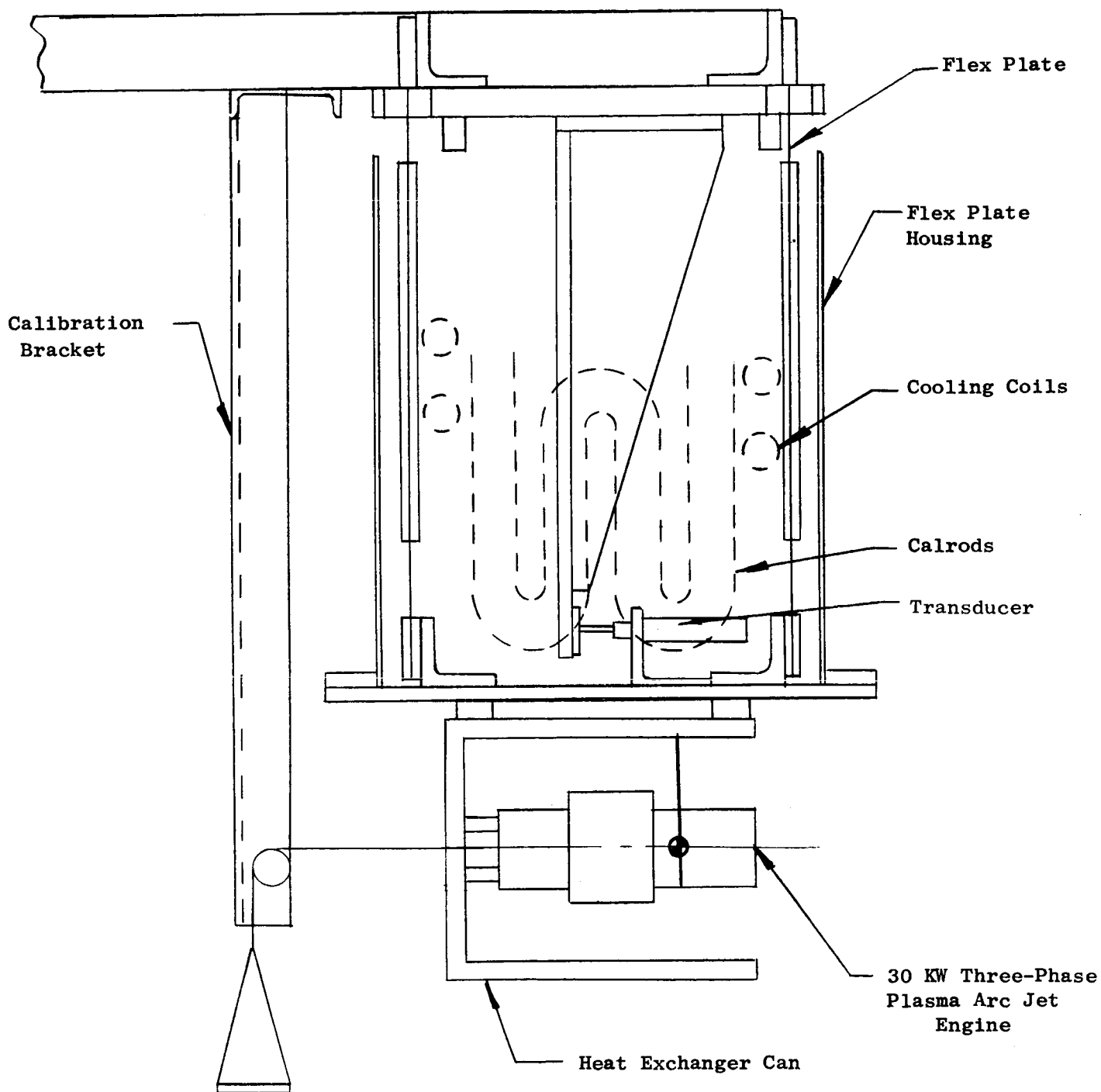


Fig. I.2:: Thrust Measuring Device (Side View)

I.1.2 Design of Thrust Measuring Device

The basic thrust measuring device consists of a container suspended on four flex plates from a support plate. The four flex plates which are attached to the floor of the container are highly flexible over only a short length at their ends. They are stiffened in the center portion to obtain the hinge effect at their ends. In this design, only horizontal forces on the container can effect a movement of the container bottom. The hinges were calculated so that a thrust of 0.5 lb will displace the bottom plate by 36 mils against the top plate. This displacement was made as large as possible in order to minimize any possible displacement due to thermal expansion as compared to the displacement due to the thrust. The displacement is measured by a linear displacement transducer (Daytronic differential transformer, Model 103C-200) which was modified to operate in oil. The displacement is measured by a linear displacement transducer (Daytronic differential transformer, Model 103C-200) which was modified to operate in oil. The displacement is indicated on a transducer amplifier-indicator (Daytronic transducer amplifier indicator, series 300C) which is equipped with a differential transformer plug-in unit, Type 60. In the present design, the transducer is mounted on the bottom of the container which is filled with a silicon oil (F50 Versilube, chlorophenyl silicone). The spring activated transducer follower bears against an angle iron which is attached to the top plate. The angle iron can be positioned accurately by a fine threaded screw so that the relative position of the displacement transducers can be adjusted to the optimum position.

All leads to the plasma arc jet engine are brought through the container. The engine can either be suspended under the container on a bracket or in a water jacket partly enclosing the engine. The temperature of all leads can vary only over a very narrow range during power and propellant flow rate changes by filling the container with the silicon oil which is kept at a constant elevated temperature of 212°F. The temperature of the oil bath is controlled by a 6 kw heater element. The heater is actuated by a Sim-Ply-Trol temperature controller which anticipates a temperature drop below the operating temperature of the oil bath. The power output of the heater is made adjustable by changing the potential on the heater with a Variac. This makes it possible to rapidly raise the temperature of the oil bath to the design operating temperature previous to engine operation. The bath can be cooled by a water cooling coil. After startup of the engine, the power can be cooled by a water cooling coil. After startup of the engine, the power to the heater is lowered to a point at which intermittent heater operation can hold the temperature variation of the bath within a small range. Provisions have been made to instrument the flex plates with strain gages to obtain a check on the behavior of the displacement transducer.

When the plasma arc jet engine is suspended in the water jacket, water can be circulated in a closed system through the jacket and an external heat exchanger which is part of a water cooler. The power radiated to the water jacket by the engine can be evaluated by measuring the temperature rise of the water flowing through the jacket. This temperature rise is then compared with

the temperature rise in an external heat exchanger with a measured power input.

The schematic of the complete thrust measuring system is shown in Fig. I.3. The system can be operated without the water jacket even though on this schematic the water jacket is shown as an integral part of the system.

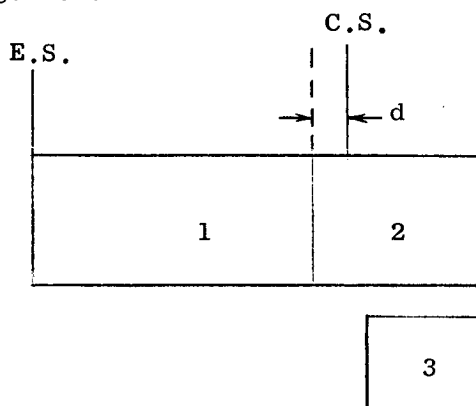
The complete thrust measuring device is shown in Figs. I.4 and I.5.

I.1.3 Analytical Evaluation of the Thrust Measuring Design

I.1.3.1 Effect of Thermal Expansion of the Plasma Arc Jet Engine on Thrust Indication

All thrust measuring devices have to be calibrated not only when the plasma arc jet engine does not produce any thrust, but also when the temperature distributions in the device and in the engine are far different from the temperature distributions during engine operation. The effect of differential thermal expansion, however, is so intimately connected with the operation of the plasma arc jet engine that it cannot be separated from the thrust indication during engine operation. Recalibration of a thrust measuring device during engine operation cannot confirm that the indicated displacement is due to the thrust of the engine only. It can only re-establish that the device continues to exhibit the same relation between the increment of force to the increment of displacement.

A simplified model of the present design of the 30 kw three-phase plasma arc jet engine is shown in Fig. I.6.



C.S. - Critical Suspension

E.S. - End Suspension

1 - Insulator

2 - Molybdenum engine body

3 - Tungsten nozzle

4 - Distance of point of suspension from joint between 1 and 2

Fig. I.6: 30 KW Three-Phase Plasma Arc Jet Engine Model

I.7. For comparison, the model of a radiation cooled engine is shown in Fig.

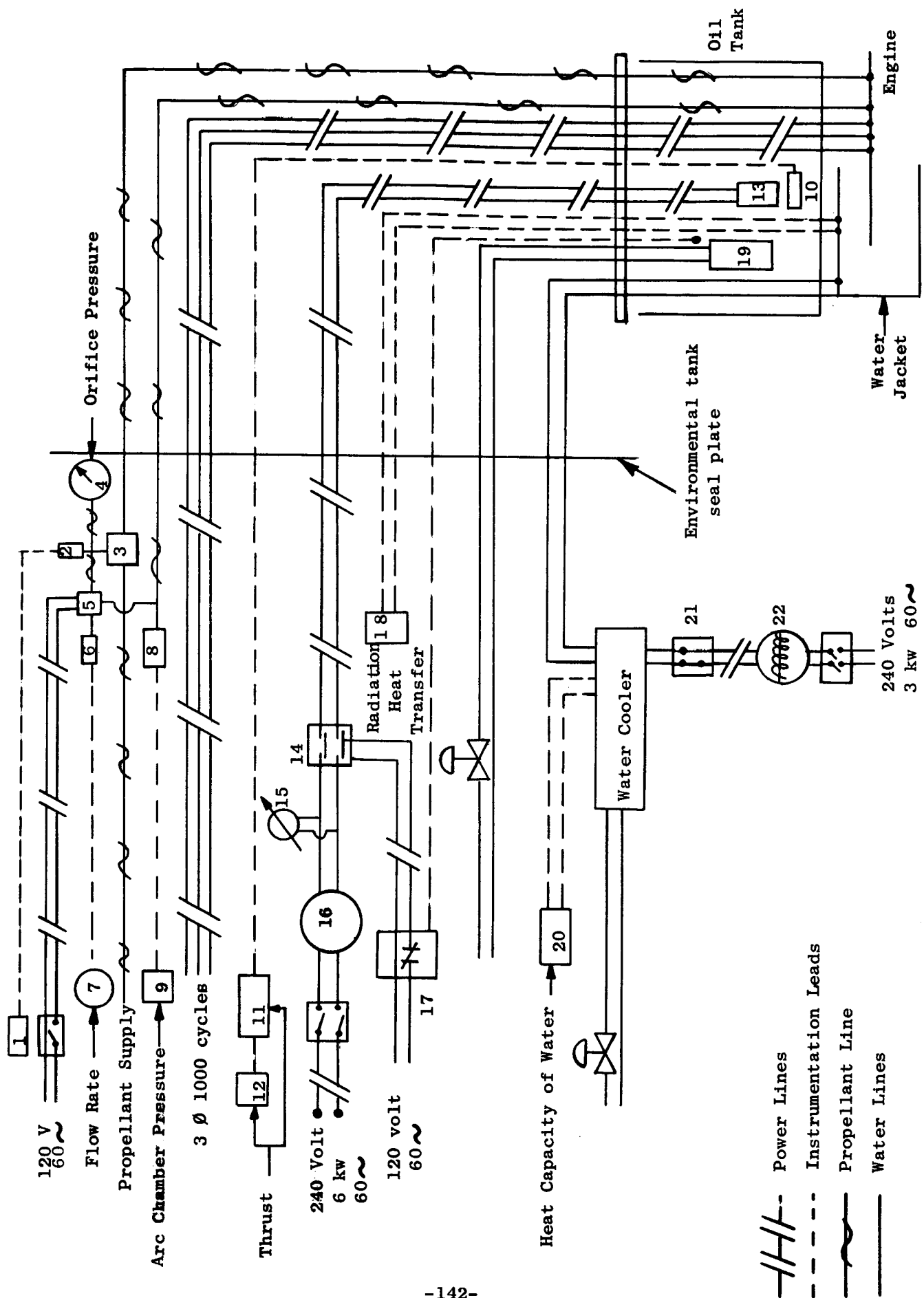


Fig. 1.3: Schematic of Thrust Measuring System

LEGEND FOR FIGURE I.3

- 1 Sanborn Recorder
- 2 Pressure Transducer
- 3 Propellant Flow Measuring System with Sonic Orifice
- 4 Precision Pressure Gage (Wallace and Tiernan FA 233161)
- 5 Three-way Solenoid Valve
- 6 Pressure Transducer
- 7 Taber Pressure Read-Out
- 8 Pressure Transducer
- 9 Sanborn Recorder
- 10 Linear Displacement Transducer (Model 103C-200)
- 11 Differential Transformer Indicator (300C with Type 60 Plug-in Unit)
- 12 Sanborn Recorder
- 13 Heater
- 14 Contact (G.E. #CR 1055002 AEA)
- 15 Voltmeter
- 16 Powerstat (Superior 1256C 240 Volt, 28 amp)
- 17 Sim-Ply-Trol Meter Relay Series 200
- 18 Sanborn Recorder
- 19 Water Cooling Coil
- 20 Sanborn Recorder
- 21 Wattmeter
- 22 Powerstat (Superior 117-U2 240 volt, 10 amp)

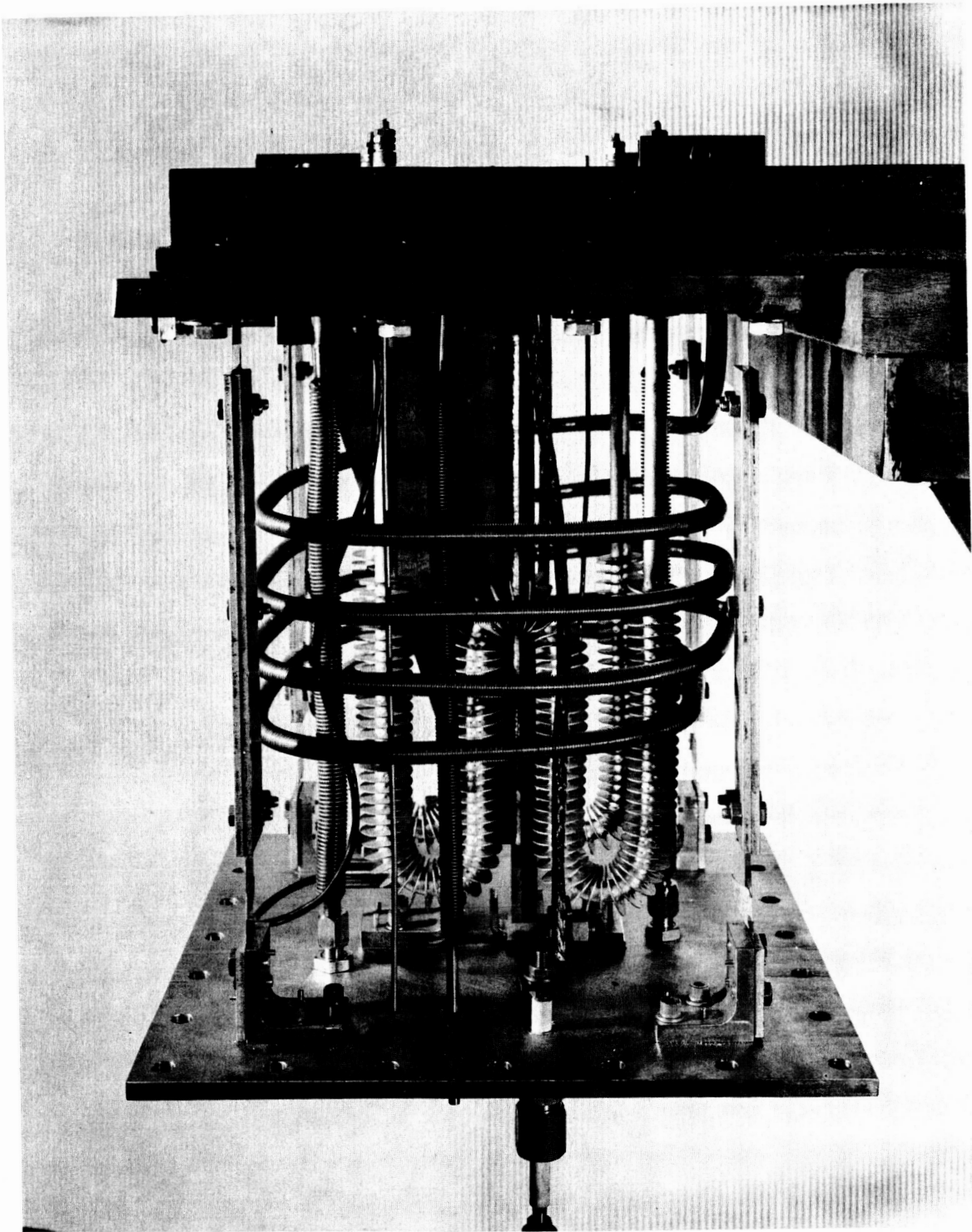


Fig. I.4: Thrust Measuring Device with Tank Removed (Side View)

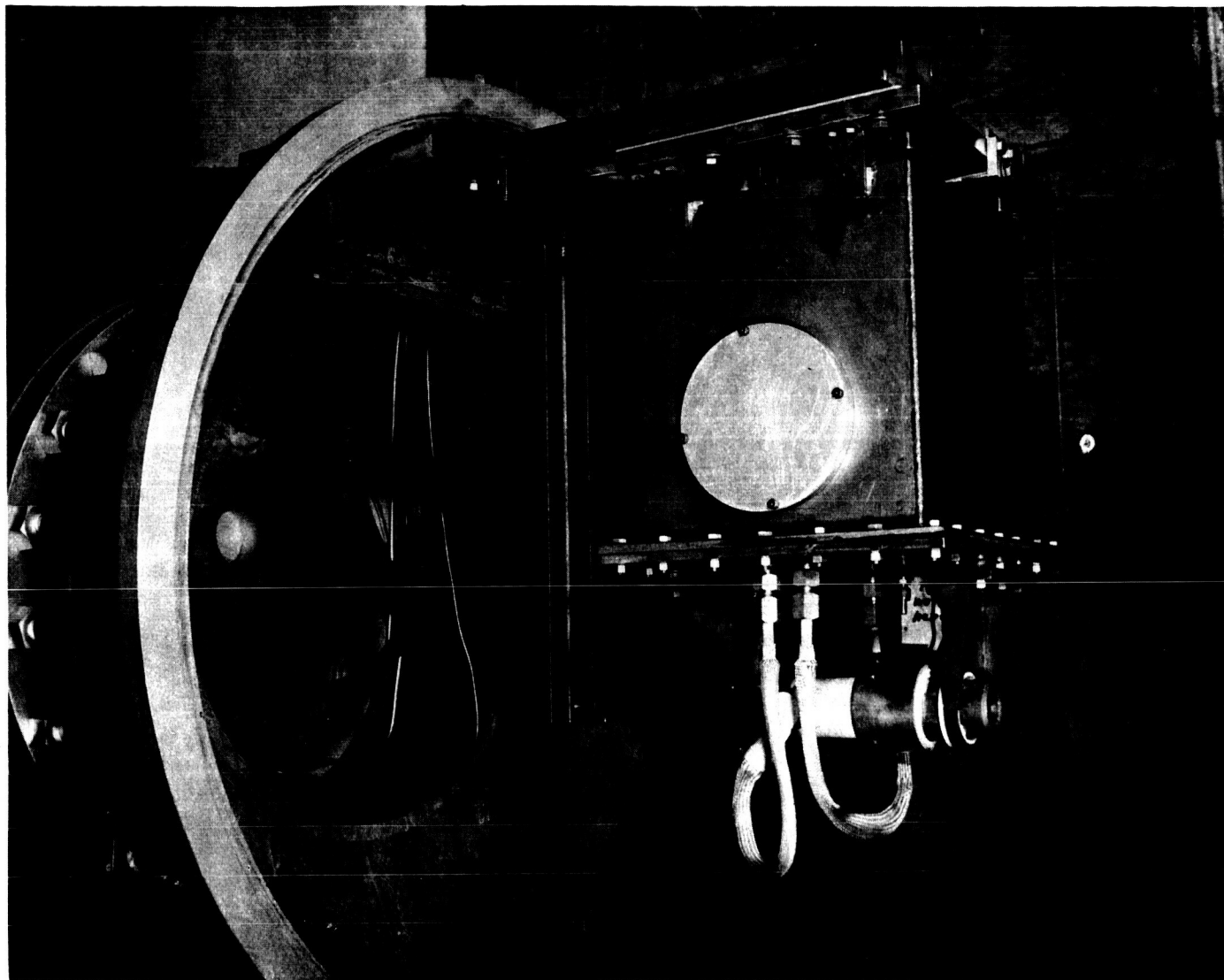


Fig. I.5: Thrust Measuring Device Installed in Test Tank with Engine

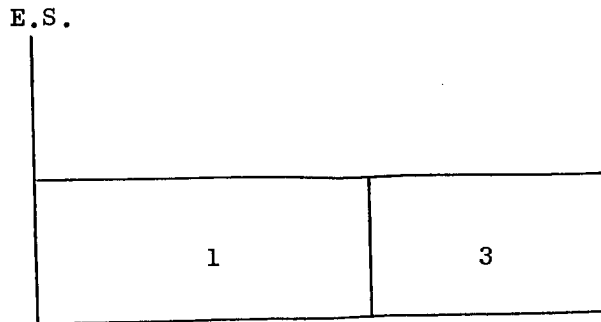


Fig. I.7:: Radiation Cooled Engine Design Model

In the case of the regeneratively cooled engine, the design is very similar to a temperature compensating system. The shortest component, the nozzle, is the hottest part and it expands in the opposite direction from the expansion of the longer cooler parts, the insulator and the engine body. In the case of a radiation cooled engine all parts expand in the same direction. Yet using temperature values observed on the regeneratively cooled engine during operation, a shift of the center of gravity of 38.5 mils is found for the case that the engine is suspended at E.S. The shift of the center of gravity can be reduced to 13.8 mils by suspending the engine at the junction of the insulator and the body. A point of suspension can actually be found such that no shift of the center of gravity will occur for a very specific temperature distribution in the engine. This point is not the location of the center of gravity of the cold engine! The point of suspension is determined from the requirement that the shift of the center of gravity relative to the junction of part 1 and 2 of the regeneratively cooled engine is equal to the increase in the length d . This critical point exists at 1.25 inch from the joint for the present 30 kw three-phase engine design. This point of suspension can, however, never be determined with the desired accuracy as the temperature distribution in the engine is not known well enough. It is, therefore, of interest to establish the possible error in the thrust measurement due to thermal expansion. It is important to note that in case the engine is suspended at E.S. the error due to thermal expansion will lead to a higher thrust reading.

The applicable model of the thrust measuring device with the engine is shown in Fig. I.8.

The displacement of the device due to thrust T is

$$s = \frac{T}{P} \left[b + \frac{2}{k \sinh bk} - 2 \frac{\coth bk}{k} + L \left[1 - \frac{1}{\cosh \frac{bk}{2}} \right] \right]$$

where

s = displacement, in.

T = thrust, lb

P = total weight of device including the engine, lb

b = total length of flex plates, in.

L = length of stiff section, in.

$$k = \sqrt{P/4EI}$$

E = modulus of elasticity of flex plates, lb/in²

I = moment of inertia of flex plates, in⁴

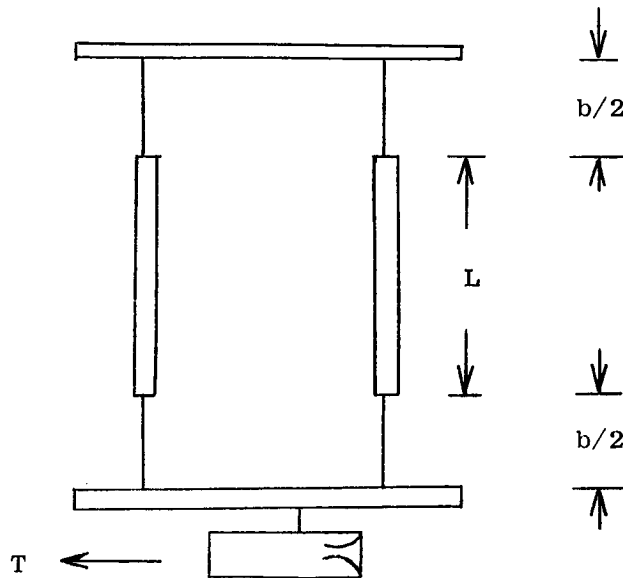


Fig. I.8.: Model of Thrust Measuring Device

For the present thrust measuring device, $bk = 17.64$

so that

$$\coth bk \approx 1$$

$$\frac{1}{\sinh bk} \approx 0$$

The equation for the displacements can, therefore, be simplified

$$s \approx \frac{T}{P} \left[b + L - 2\sqrt{\frac{4EI}{P}} \right]$$

This relation is easily recognized as the slightly modified pendulum equation for small displacements with the additional term: $2\sqrt{4EI/P}$

In case of a pendulum, the center of gravity is always beneath the point of suspension. Any shift in the center of gravity is therefore equivalent to a displacement. The model of the thrust measuring device can therefore be simplified as shown in Fig. I.9..

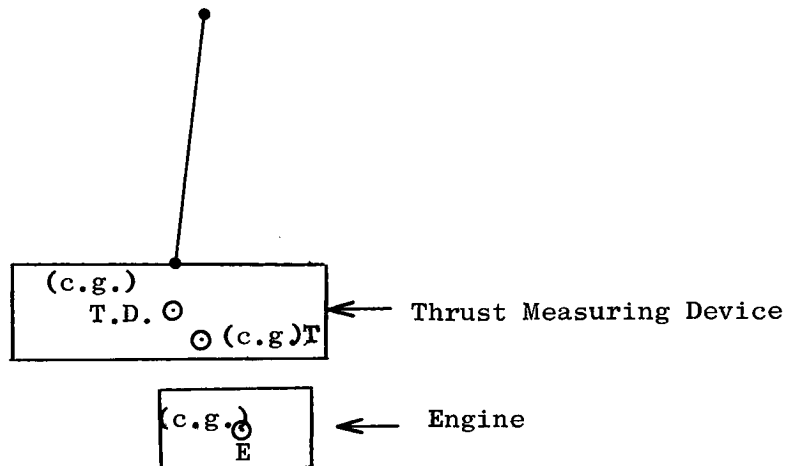


Fig. I.9: Simplified Model of Thrust Measuring Device

The displacement due to the shift of the centers of gravity of any of the components of a system is given by

$$\Delta X_{cg} = \frac{\sum (W \Delta X)_n}{\sum W_n}$$

where W_n is the weight of the components.

Assuming that there occurred only a shift of the center of gravity of the engine

$$\Delta_s = \frac{W_E \Delta X_{cg E}}{W_d + W_E}$$

The error in the thrust measurement due to thermal expansion is then

$$e\% = \frac{W_E}{T} \times \frac{\Delta X_{cg E}}{\left[b + L - 2\sqrt{\frac{4EI}{P}} \right]} \times 100$$

For the representative values of

$$W_E = 10 \text{ lb}$$

$$T = 0.5 \text{ lb}$$

$$b + L = 13.5 \text{ in.}$$

$$\Delta X_{cg E} = .0385 \text{ in.}$$

the maximum error in the thrust reading due to thermal expansion is $e = 5.7\%$, that is when the engine is suspended at E.S. Only by suspending the engine at the critical point can this error be eliminated completely.

I.1.3.2 Forces Between Electrical Leads in the Oil Tank of the Thrust Measuring Device

The forces between two electrical leads which are the conductors for the three-phase alternating current device can be found from

$$\bar{F} = \frac{L \times I_{\max}^2}{2r}$$

where \bar{F} = effective continuous force, dynes
 L = lead length, cm
 I_{\max} = peak current, e.m.u.

For an effective current of 150 amps the mutual force exerted upon two conductors in the thrust measuring device is 1.182 g. It actually varies periodically as shown in Fig. I.10. It can, however, be assumed that the vibration of the leads are damped out by the oil in which they are suspended.

Based on the same analysis and a current of 200 amps the force between the two leads carrying a direct current would be 4.19g.

The effect of this force on the thrust indication is not easily assessed. It can be evaluated experimentally by shortening the leads electrically and applying voltage to the primary circuit with an inductance as load. Currents will then flow without delivering any power, yet generating the same effect on the electrical leads as under normal operating conditions.

I.1.3.4 Thermal Expansion of Electrical Leads

In order to assess the effect of thermal expansion of the electrical leads in the tank on the thrust measuring device the temperature increase in the leads had to be evaluated. The temperature difference between the leads and the oil bath can be expressed by

$$\Delta T = \frac{3}{8} \frac{c \delta}{k_o c} \frac{I^2 R}{j L^{3/4}}$$

where T = temperature difference, $^{\circ}R$
 I = current, amps
 R = lead resistance, ohms
 j = conversion factor, $1.05839 \times 10^{+3}$ watt/B
 L = length of leads, in.
 k_o = thermal conductivity of oil, B/ $^{\circ}R$ -sec-ft
 c = lead width, in.

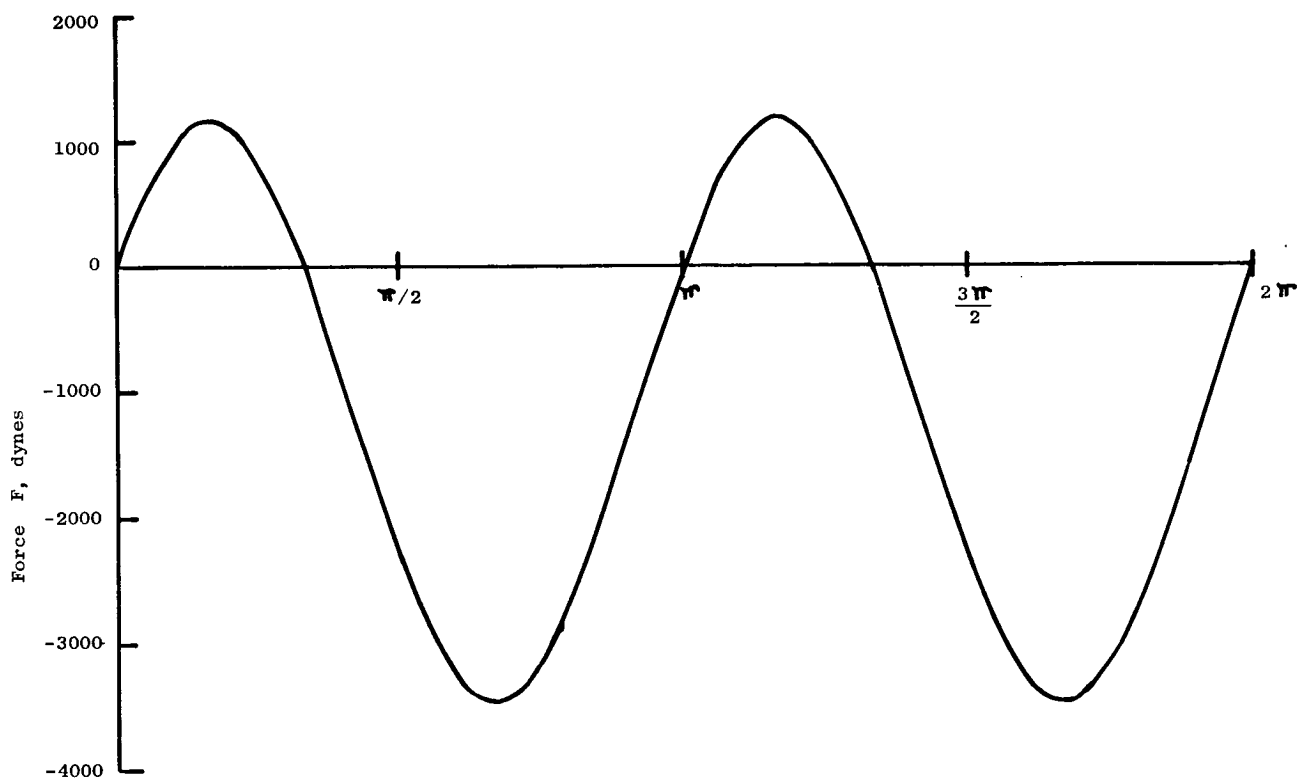


Fig. I.10: Relation of Forces Between Electrical Leads for a Current of 150 Amps

$$c_{\delta} = 3.93 \left[\frac{20}{21} + \frac{\nu_o}{\alpha} \right]^{\frac{1}{4}} \left[\frac{g \beta_o \Delta T}{\nu_o} \right]^{-\frac{1}{4}} \left[\frac{\nu_o}{\alpha} \right]^{\frac{1}{2}}$$

ν_o = kinematic viscosity of oil, ft^2/sec

β_o = thermal expansion coefficient of oil, $^{\circ}\text{R}^{-1}$

$\alpha = k / \rho c_p$

c_p = specific heat, $\text{B}/\text{lb-}^{\circ}\text{R}$

g = gravitational constant, $32.2 \text{ ft}/\text{sec}^2$

The temperature difference was found by a trial and error solution to be 3.3°R . This very low temperature increase from the temperature at which the thrust measuring device will be calibrated should have no effect on the thrust indication.

I.1.4 Checkout Testing of Thrust Measuring Device

Prior to operation of the thrust measuring device, several problems peculiar to the combination of the steam ejector system and the thrust measuring device were investigated, in addition to the verification of the insensitivity of the thrust indication to various operating conditions.

I.1.4.1 Elimination of Mechanical Problems

The principle of the thrust measuring device requires that all electrical lines, propellant lines and suspension members are maintained at a uniform temperature. This temperature is equal to the temperature at which the device has been calibrated. To effect this condition, all members are submerged in an oil bath which can be kept at a constant temperature. The oil selected for the bath is a silicone oil, Versilube F-50, manufactured by the General Electric Company. It was selected for the thrust measuring device because of its low vapor pressure and its stability at elevated temperatures.

As the vacuum in the test tank is obtained by a steam ejector system the possibility of water settling on and in the oil exists. The oil has a specific gravity equal to water so any dissolved water can cause electrical shorts between the uninsulated electrical lines which pass through the oil bath. In order, therefore, to avoid condensation of water vapor on the oil the temperature of the oil has to be kept above the boiling temperatures of water at all possible vapor pressures, i.e., above 212°F , at all times.

The elevated temperature of the oil bath proved to have an adverse effect on the displacement transducer which is used for the correlation of the engine thrust with the displacement of the thrust device. This transducer is located on the bottom of the oil container of the thrust device. After approximately one day in the hot oil, the weak brass spring in the transducer was found to have taken on a permanent set. Without the action of the spring the follower was

prevented from returning to its outmost position. This unexpected defect was remedied by installing a steel spring external to the transducer. This modification of the transducer has been proven to function satisfactorily. The transducer has thereafter remained unaffected by the temperature of the oil bath. The steel spring has, however, a slightly higher spring constant than the original brass spring. The modification therefore slightly affected the total deflection of the thrust measuring device for a given thrust. The thrust device was recalibrated after the modification was completed.

The calibration of the thrust device was performed several times. The results remained constant and were repeatable. The maximum deviation of the displacement readings never exceeded the reading accuracy of the indicator meter. The calibration curve obtained for the first test run is shown in Fig. 1.11. The results of the calibration indicate that the thrust measuring device is displaced linearly over the entire thrust range which is contemplated to be measured with the device.

A major problem which was anticipated was the movement of the thrust device upon closure of the test tank. As can be seen in Fig. 1.5 the thrust device is mounted on the bulkhead which travels on two rails during opening and closing of the test tank. Great pains were taken to assure that the bulkhead keeps its relative position at all points on the rail. A slight shift of its position still occurs during the tightening up of the flange of the stationary part of the test tank and the flange of the bulkhead. The tilting of the bulkhead results in a relative movement of the thrust device by 63.4 mils. The zero shift exceeds by 13.4 mils the maximum deflection that can be read off the scale intended for the high accuracy readings of the displacement. This problem could not be eliminated completely by realigning the bulkhead. The present shift is due to a tilt of only 0.27 degree from the horizontal alignment of the test tank with the bulkhead. Any greater accuracy in the alignment can hardly be expected. On the other hand the drift of the initial zero position is such that it is opposite to the displacement of the thrust device due to thrust, that is, the effect of thrust is such as to displace the thrust device to its initial zero. All measurements of displacement are, therefore, within the range of calibration which was shown to be absolutely linear. By giving the thrust measuring device an initial relative displacement, all readings can still be made on the 0 to 50 mil scale.

I.1.4.2 Testing for Extraneous Effects on Thrust Indication

In the analysis of the thrust measuring device, the four operating effects that could influence the thrust readings were discussed. These effects are: a) Bourdon tube deflection of the propellant feed line and the pressure pickup line, b) magnetic field interaction of the power leads, c) thermal expansion of the electrical power leads, and d) shift of center of gravity of the plasma arc jet engine.

Bourdon Tube Effect - It was shown in the earlier discussion that the thrust device was designed and built to be unaffected by Bourdon tube type forces and that, therefore, no indication of displacement of the thrust measuring device

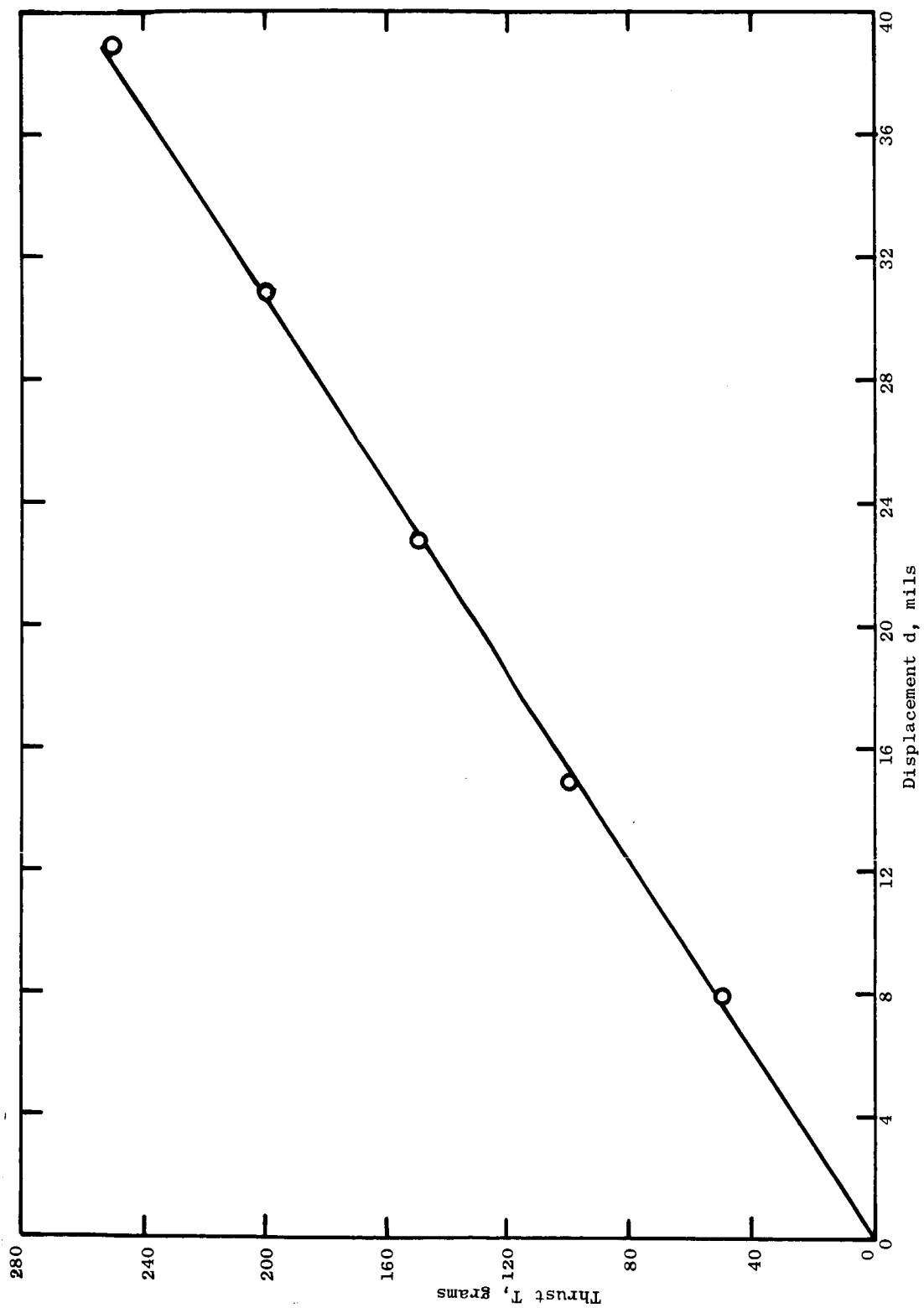


Fig. I.11: Calibration of Displacement Transducer of Thrust Measuring Device (August 30, 1963)

should occur with pressurization of the propellant feed line or the pressure pickup line. To verify this prediction the feed line and the pressure pickup line were capped off and pressurized. The pressure in the line was varied over a range of 30 psi. Absolutely no movement of the thrust measuring device was indicated by the displacement transducer. This test was repeated while simulating various thrust levels. Again the displacement of the device remained unaffected by the pressure in the lines.

Effect of Magnetic Field Interaction and Thermal Expansion of the Electrical Power Leads - Though the effect of magnetic field interaction and thermal expansion of the electrical power leads can be analyzed separately, the two effects can be separated experimentally only with great difficulty when testing for their individual contributions to the indicated displacement of the thrust measuring device. Both effects are due to current flow in the power leads. It was felt that only if an influence on the displacement of the thrust measuring device could be detected due to current flow in the power lines would an attempt be made to determine whether and to what degree this influence was due to magnetic field interaction or due to thermal expansion of the leads.

The analysis of the magnetic field interaction had shown that the two power leads closest together would exert a periodically varying force upon each other, the root-mean-square value of this force being 1.182 g. This force, however, should not result in any displacement of the thrust measuring device because of the symmetry of the position of the leads with respect to the thrust measuring suspension.

The heat transfer analysis pertaining to the temperature in the electrical power leads had predicted a temperature rise of 3.3°R above the ambient oil temperature in which the leads are submerged. The minute thermal expansion of the flexible leads should result in a force which is perpendicular to the thrust and should therefore also have no effect on the displacement. In order to test the thrust measuring device for these two effects, the three power leads emerging from the thrust device oil tank were shortened electrically. This test setup is shown in Fig. I.12. Power was applied to the leads and the current was varied between 0 and 150 amps. The power was left on for several minutes to allow the power leads to come to a steady-state temperature.

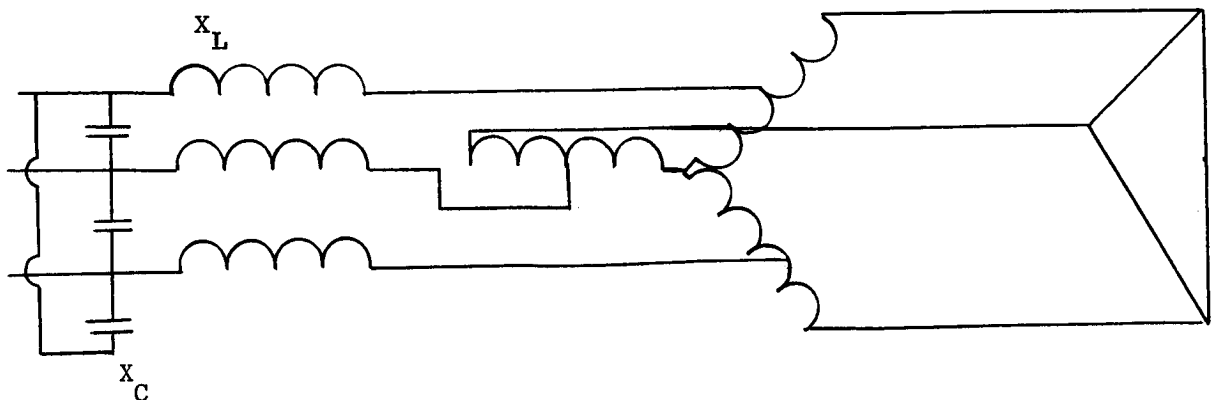


Fig. I.12: Test Setup for Checking of Currents Effect on the Indicated Displacement of Thrust Measuring Device

Again, no movement of the thrust device either from the null position or from an initial deflection due to a simulated thrust could be detected.

Effect of Shift of Center of Gravity - In the analysis of the behavior of the thrust device it was shown that the displacement of the device due to forces is similar to that of a pendulum. The shift of the center of gravity of the plasma arc jet engine when suspended under the thrust measuring device should, therefore, have a similar effect as the shift of the center of gravity of a component suspended from a pendulum. In the worst possible case, that is when the engine is fastened to the thrust device by its front end, the contribution in the displacement of the thrust device due to the shift in the center of gravity of the engine relative to the thrust measuring device is 5.7% of the total displacement at a thrust of 0.5 lb. This error can be completely eliminated by suspending the engine at its critical point, that is, the point whose distance from the center of gravity remains constant despite non-uniform thermal expansion of the engine.

To establish the correctness of the analytical predictions, an 18 lb weight was suspended from the thrust measuring device at various locations. This test setup is explained by Fig. I.13. The data obtained in this test are presented in Table 1 and Fig. I.14.

Thrust, T_1 grams	Position x, inches	Indicated Displacement, mils	Deflection mils
0	5	- 7.8	-2.1
0	0	- 9.9	0
250	0	+27.	0
250	0.5	+27.2	+0.2
250	1.0	+28.2	+1.2
250	1.5	+27.9	+0.7
250	2	+28.0	+1.8
250	4	+29.9	+2.7
250	4.5	+30.9	+2.9
250	5	+30.5	+3.3

Table 1: Effect of a Shift of Center of Gravity of an 18 lb Weight on the Indicated Displacement of the Thrust Measuring Device

From these experimental data the maximum possible error due to a shift of the center of gravity of the engine can be evaluated. The data show that the thrust measuring device will indicate a displacement of 0.75 mils per inch of shift of the center of gravity. The largest possible shift of the center of gravity of the present engine design due to thermal expansion was calculated to be 0.032 in. From the calibration of the thrust measuring device it was found that with 250 g thrust the indicated displacement is 37.7 mils. The shift in

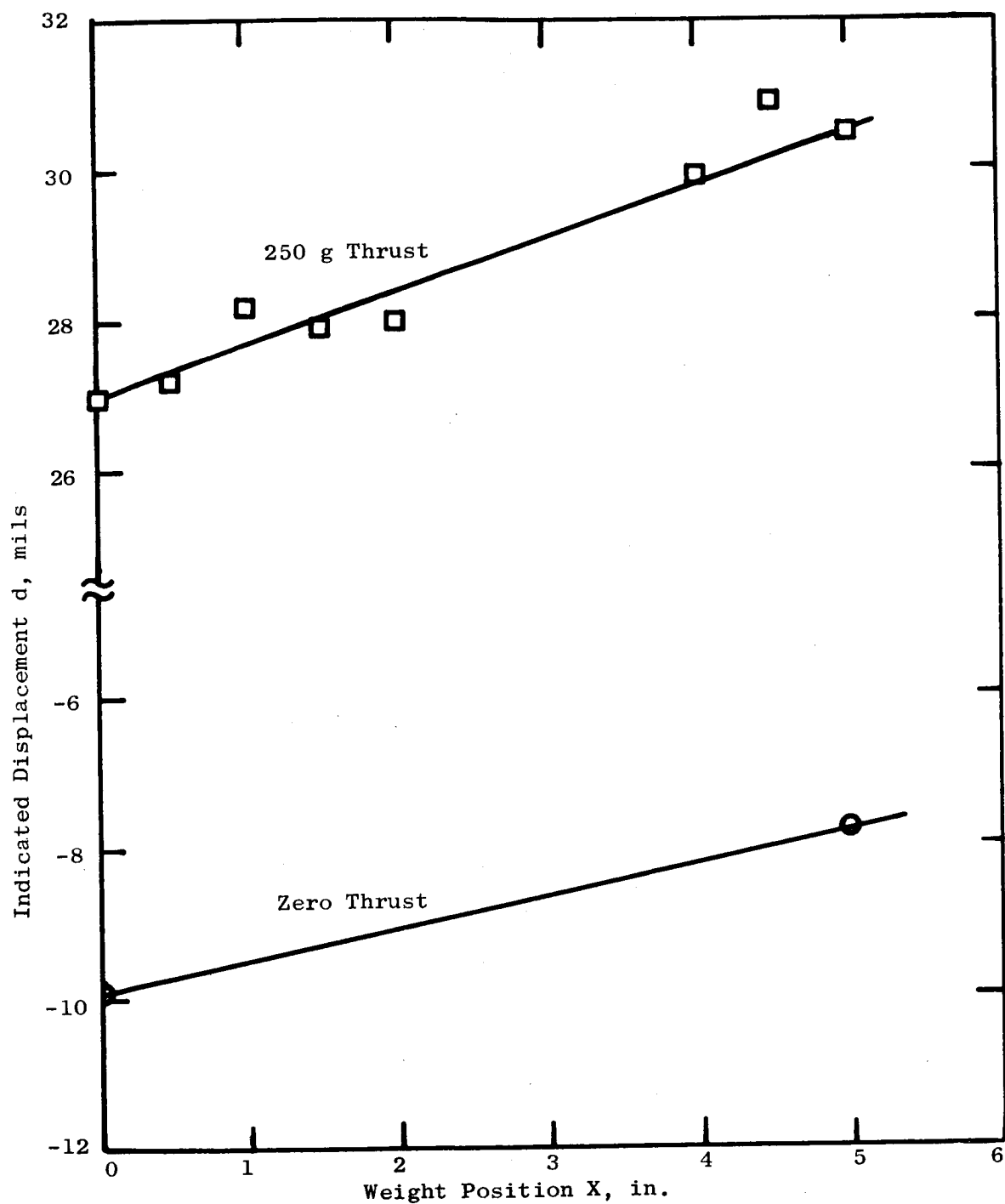


Fig. I.14: Effect of Shift of Center of Gravity on the Indicated Thrust Meter Displacement ($W = 18$ lb)

the center of gravity could therefore result in an error of the indicated displacement due to thrust of

$$e = \frac{0.032 \times 0.75 \times 100}{3.77} = 0.064\%$$

The error due to the maximum possible shift in the center of gravity of the engine is therefore far below the overall accuracy of the thrust measuring system.

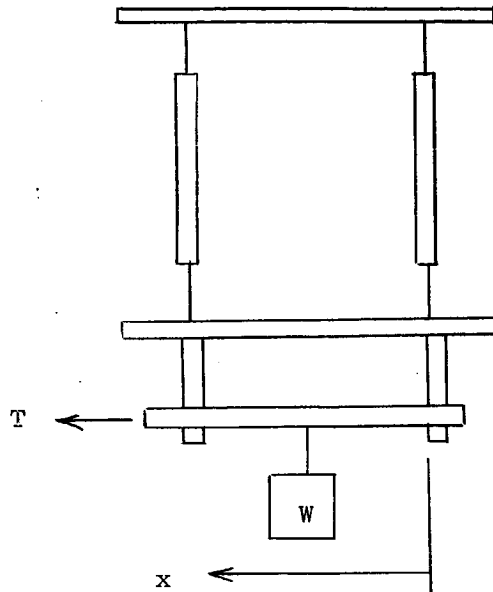


Fig. I.13: Test Setup for Determination of the Effect of a Shift of the Center of Gravity of a Plasma Arc Jet Engine on the Thrust Indicator of the Thrust Measuring Device

I.1.5 Effects on Thrust Indication Under Operating Conditions

After the thrust measuring device had been checked out for all extraneous effects and the difficulties with the displacement transducer had been eliminated, testing of the device under operating conditions was initiated. The testing was mainly accomplished by operating Engine Y16-1 for long durations.

During the first operational test of the thrust measuring device it was found that the heat losses from the thrust device were almost equal to the heat input due to radiation from the engine and the heat generated in the electrical power leads. Only a very small quantity of cooling water was required. This favorable condition could be attributed to the heat shields which were added to the bottom and the front panels of the oil tank.

During the first few minutes of the first run a steady increase in the thrust indication occurred. The thrust apparently increased beyond the time when

the arc chamber pressure had reached steady-state value. The only explanation for this phenomenon was a drift in the displacement zero of the thrust device. This drift could only be attributed to a tilting of the bulkhead to which the thrust measuring device is attached. Such tilting could be traced to thermal expansions occurring in the test tank and the exhaust pipe. This explanation of the observed drift pointed to the need for an absolute zero indicator, that is, a device that would record the change of the thrust measuring device position due to tilting of its support. The zero indicator was built with a cantilever from which a 65 lb weight was suspended. The cantilever beam was instrumented with two strain gages near its solid point of suspension at the tank support structure. The weight was submerged in a high viscosity oil to dampen out the vibration of such highly sensitive position indicator. The signal of the strain gage bridge was then calibrated in such a fashion that upon moving the bulkhead to which the thrust device is attached, the recorded shift of the thrust device is equal to the indicated shift of the position indicator. On opening and closing of the test tank it was ascertained that in all positions the thrust device and the position indicator recorded exactly the same drift. With the absolute zero position indicator any drift of the zero of the thrust device due to tilting of the test tank can now be corrected. Application of the corrections which were indicated by the zero indicator to the displacement indicator was shown to produce very consistent performance data over long duration operation of the engine.

After it had been established that tilting of the test tank did occur due to thermal expansion, attempts were made to reduce the effect as much as possible. At the present time drifting has been eliminated almost completely. This is indicated by the very small drift recorded in the position indicator. The maximum drift has lately never exceeded 2 mils which is equal to 13.1 g of thrust or 5.8% of the measured thrust for which corrections were made in the final performance evaluation, i.e., the indicated drift is subtracted from the indicated displacement due to thrust.

The serious influence of very small tilting of the support on the thrust reading can be recognized when realizing that tilting of the tank by an angle of only 0.162° can cause an error of 250 g in the thrust measurement.

I.1.6 Accuracy of Thrust Measurements

The accuracy of the measurement of the thrust with the new thrust measuring device has proven to be only a function of the reading accuracy of the displacement transducer indicator. The repeated calibration of the thrust measuring device has shown the movable part to be displaced absolutely linearly against the fixed section of the device and with a hysteresis effect less than the reading accuracy. The displacement is read from a scale that permits readings with an accuracy of ± 0.3 units. The thrust to be measured causes an indication of 38 units. The possible error in the measurement is therefore

$$e_{\text{thrust}} = \frac{0.3 \times 100}{38} = 0.79\%$$

The thrust measuring device is calibrated before and after each test run. This is a precaution indicated by the possibility of changing the weight of the thrust measuring device due to loss of oil. The total weight of oil in the tank is about 65 lb. The loss of about 1 inch of oil level reduces the weight of the thrust measuring device by about 5 lb. The total suspended weight is about 180 lb. From the relation of the displacement of the thrust measuring device

$$s = \frac{T}{P} \left[b + \frac{2}{k \sinh bk} - 2 \frac{\coth bk}{k} + L \left[1 - \frac{1}{\cosh bk/2} \right] \right]$$

it can be seen that because

$$\frac{\Delta S}{S} = - \frac{\Delta P}{P}$$

an error of 2.8% per inch of difference in oil level can be made in the thrust determination if loss of oil due to evaporation, spillage, or overflow is neglected. The possible error is much larger actually than the error due to the reading inaccuracy.

From the relation between indicated change in displacement and thrust it can also be seen that loss of oil leads to large changes in displacement. If oil is lost during a test run, the thrust measurements of the run, if used at all, should be based on the calibration after the test run to assure that conservative results are reported.

I.2 Design and Calibration of Propellant Flow Measuring Systems

I.2.1 Propellant Flow Rate Determination

One of the three important items of data for the determination of the performance of a plasma arc jet engine is the propellant flow rate. It has been recognized that the most accurate and reliable procedure for gas metering is to correlate the pressure upstream of a sonic orifice with the weight flow rate of the propellant at a given temperature. Such a correlation has to be obtained by a calibration procedure.

It can be seen from the sonic orifice relation

$$\dot{W} = \left[\frac{\gamma g}{R} \left[\frac{2}{\gamma + 1} \right]^{\frac{\gamma + 1}{\gamma - 1}} \right]^{\frac{1}{2}} \frac{A}{\sqrt{T_o}} P_o$$

that when an orifice has been calibrated by correlating the propellant flow rate with the orifice pressure such a correlation remains only valid as long as the coefficient

$$\left\{ \left[\frac{\gamma g}{R} \frac{2}{\gamma + 1} \right]^{\frac{\gamma + 1}{\gamma - 1}} \right\}^{\frac{1}{2}} \frac{A}{\sqrt{T_o}}$$

remains constant. For any gas, the ratio of the specific heat, γ , and the gas constant R , are constant at room temperature. The orifice area, A , might change by corrosion over a long time depending on the material used in the manufacturing of the orifice disc. The temperature, T_o , has either to be kept constant by a temperature control or a correction has to be applied to each measurement to account for the variation of the temperature during calibration and measurement.

Previously, the tacit assumption was made that the gas remained constant and was always equal to the temperature of the day of calibration of the orifice. This assumption is valid only as long as the required accuracy of the propellant flow rate is less than 4%. In order, therefore, to improve on the accuracy of performance measurements, the accuracy with which the propellant flow rate is determined has to be substantially increased.

I.2.2 Propellant Flow Measuring System Design

To obtain the required accuracy in the propellant flow measurement a system was designed which can be calibrated and operated at a preset constant temperature. The flow rate has therefore become completely independent of the ambient temperature. This system is shown in a cutaway drawing in Fig. I.15.

The propellant is heated from the ambient temperature to a constant temperature in a heat exchanger coil which is submerged in a constant temperature bath. The temperature of the bath is kept regulated by a thermostatically controlled heater. The gas temperature at the orifice can be monitored by a thermocouple. The orifice pressure is measured by a high precision Wallace & Tiernan Precision Bourdon Tube gauge and is also remotely monitored by a pressure transducer.

During operation, the largest temperature variation in the propellant supply system was less than 2°R. Such a variation in temperature results in a propellant flow rate uncertainty of less than 0.2%. Since, however, with each orifice pressure reading the gas temperature is recorded a correction for any variation from the calibration temperature can be applied. This makes the uncertainty in the flow rate due to temperature negligible.

The orifice of the system was designed to obtain a flow rate of 5×10^{-4} lb/sec with an orifice pressure of 200 psia. The smallest sub-division on the precision pressure gage is 0.2 psia. The accuracy of the pressure reading, therefore, can be better than 0.1%. Since the repeatability of the determination of the propellant flow rate has proven to be very high, the accuracy of the flow measurement is mainly a function of the accuracy with which the system can be calibrated.

I.2.3 Propellant Flow Measuring System Calibration

Many procedures have been suggested for the calibration of sonic orifices. All procedures have to solve the problem of determining the mass flow rate by

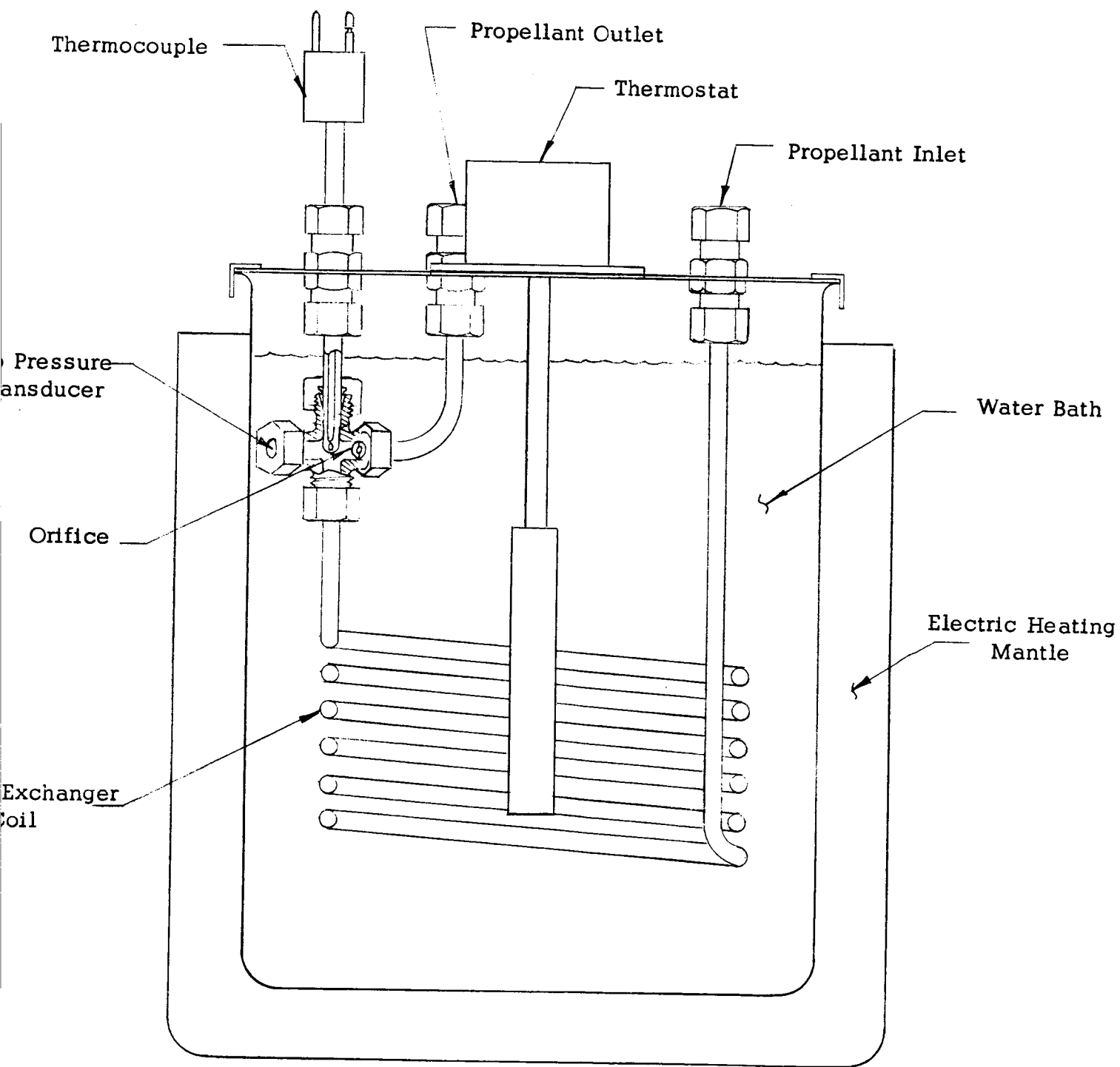


Fig. I.15: Propellant Flow Measuring System

direct or indirect means. Claims have been made for greater accuracy of some procedures, but none is completely satisfactory. In each case the weight flow rate has to be determined by applying thermodynamic gas relations to reduce measured values. In most cases the gas temperature and pressure and a displaced volume are measured. The equation of state is then applied to calculate the mass flow rate. The basic principle was used in the calibration of the two flow measuring systems in our test facility.

Two "Precision" wet test meters, manufactured by the Precision Scientific Company, Chicago, Illinois, were available to measure the volumetric flow rate. One of the meters is designed for 1 cu ft/Rev. while the other one is rated at 0.1 cu ft/Rev. According to the manufacturer, the wet test meters have an accuracy of better than 0.5% as long as the flow rate is such that the speed of the meter does not exceed two revolutions per minute. At 2.5 revolutions per minute, the accuracy of a wet test meter drops to 1% and deteriorates rapidly with increasing flow rate. Both wet test meters were calibrated by the manufacturer with a standard bottle supplied by the Bureau of Standards. Since the volumetric flow rate of hydrogen at the maximum design orifice pressure is above the capacity even of the large wet test meter for both orifices, nitrogen was also employed in the calibration. By employing nitrogen as the test gas, the volumetric flow rate could be reduced by a factor of 3.7278 making it possible to calibrate the two orifices up to their maximum design orifice pressure, which is 200 psia at a temperature of 100°F.

The calibration setup employed is shown in Fig. I.16. The orifice pressure was set by a Heise gage (H 10342) which has a pressure range from 0 to 360 psia. The smallest sub-division of the gage is 0.5 psia, though the pointer blade width is less than 1/10 of the space between the scale markings. The gage was calibrated prior to its use in the Calibration and Standards Laboratory of the Flight Propulsion Division with dead weight testing equipment. Before entering the wet test meter, the test gas was bubbled through a saturator to insure complete saturation of the gas with water vapor. The time elapsed between a given number of revolutions of the wet test meter was measured with an electric timer with a smallest time division of 1/10 second. The volume flow rate, as measured by the wet test meter, was reduced to the mass flow rate of hydrogen at a gas temperature of 100°F by the following two equations:

$$\dot{W}_{H_2} \left(\frac{\#}{\text{sec}} \right) \Big|_{@100^\circ\text{F}} = 14.061 \times 10^{-3} \frac{k V_{N_2} (\text{ft}^3) P_{WTM} (\text{in } H_2O)}{t(\text{sec}) \times T_{WTM} (^{\circ}\text{K})}$$

$$\dot{W}_{H_2} \left(\frac{\#}{\text{sec}} \right) \Big|_{@100^\circ\text{F}} = 3.77189 \times 10^{-3} \frac{k V_{H_2} (\text{ft}^3) P_{WTM} (\text{in } H_2O)}{t(\text{sec}) \times T_{WTM} (^{\circ}\text{K})}$$

where

$$k = \left[\frac{T_{\phi} + 459}{559} \right]^{\frac{1}{4}}$$

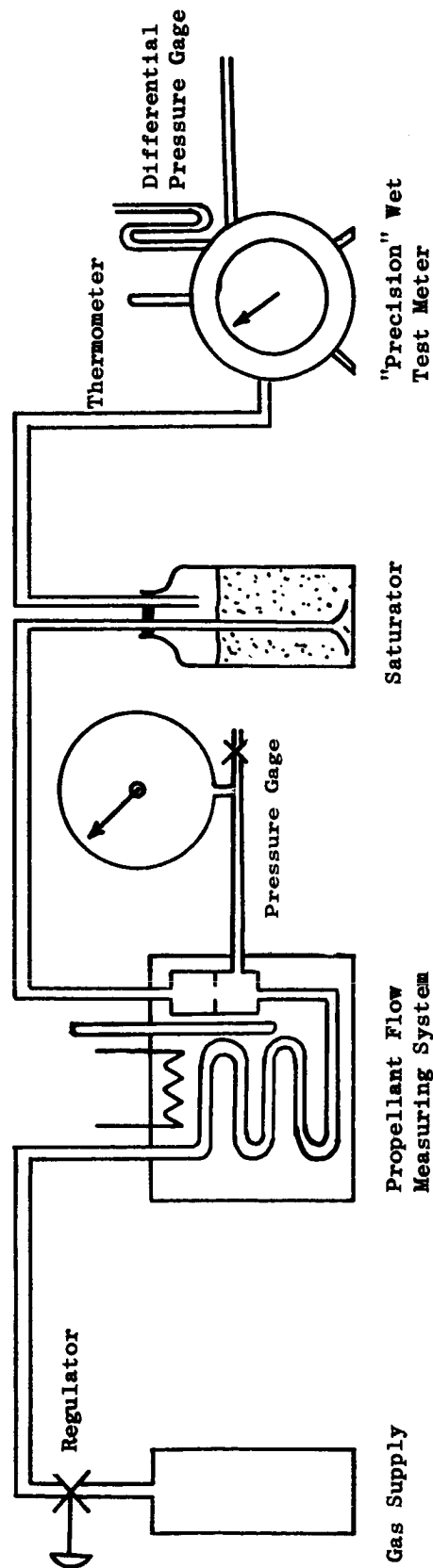


Fig. I.16: Calibration Test Setup of Propellant Flow Measuring System

which is the temperature correction factor taking into account any deviation of the temperature of the gas from the nominal gas temperature of 100°F. The correction which had to be applied to the measured wet test meter pressure was taken from the Handbook of Chemistry and Physics.

Slight variations in the gas temperature of the orifice occurred. They were mainly due to the continuous change in the gas flow rate through the heat exchanger during calibration. The factor k was used for correcting the flow rate to the standard calibration temperature of 100°F. The deviation of any point was never larger than 0.25% from the line of the least square sum. Since the wet test meters are accurate within 0.5%, the largest deviation of the mass flow rate from the measured flow rate is well below 1%.

I.3 Calibration of Instrumentation

The third factor that enters into the determination of the performance of a plasma arc jet engine is the input power measurement. Three electronic wattmeters are employed to achieve the highest possible accuracy in the measurement of the power input to the three-phase plasma arc jet engine. A rigid calibration procedure for these three meters was initiated. The calibration circuit used for the calibration of each meter is shown in Fig. I.17. The applied load consists of a pure resistance which can be adjusted over a wide range.

The voltage across the load and the current is measured with two Sensitive Research Instrument Corporation thermocouple meters (Model USPEW-5A, Serial No. 941243 B&C) which have an accuracy of better than .75% at all frequencies under consideration. The ac power is supplied by an electronic power supply (Behlman Model 14002/L/IBET, Serial No. 201312) whose frequency can be varied from 300 to 3000 cycles/sec. Both the current and the voltage across the resistor are displayed on a two channel Tektronix oscilloscope and checked for their shape and relative displacement to each other. No phase shift between voltage and current was observed.

First the voltage of the VAW meter is calibrated against the thermocouple voltmeter varying the voltage as well as the frequency. For the calibration of the current, the very same procedure is followed as used for the voltage calibration. The calibration of the meter is concluded with the adjustment of the power indication of the VAW meter. The calibration has confirmed that the effect of frequency on the power measurement is negligible in the range from 300 to 3000 cycles/sec. This can be seen in Table 12.

The output of the VAW meter is a dc signal voltage which is applied to a millivoltmeter. This signal voltage can also be fed into a high impedance preamplifier of a Sanborn recorder and can be recorded continuously. In order to accomplish an easy calibration of the Sanborn recorder output, the voltage output of each VAW meter was obtained at an indicated power of 225 watts, which is equal to the full scale deflection of the millivolt meter. These measured output voltages are for each meter respectively 21.1 millivolt, 29.13 millivolt, and 20.5 millivolt.

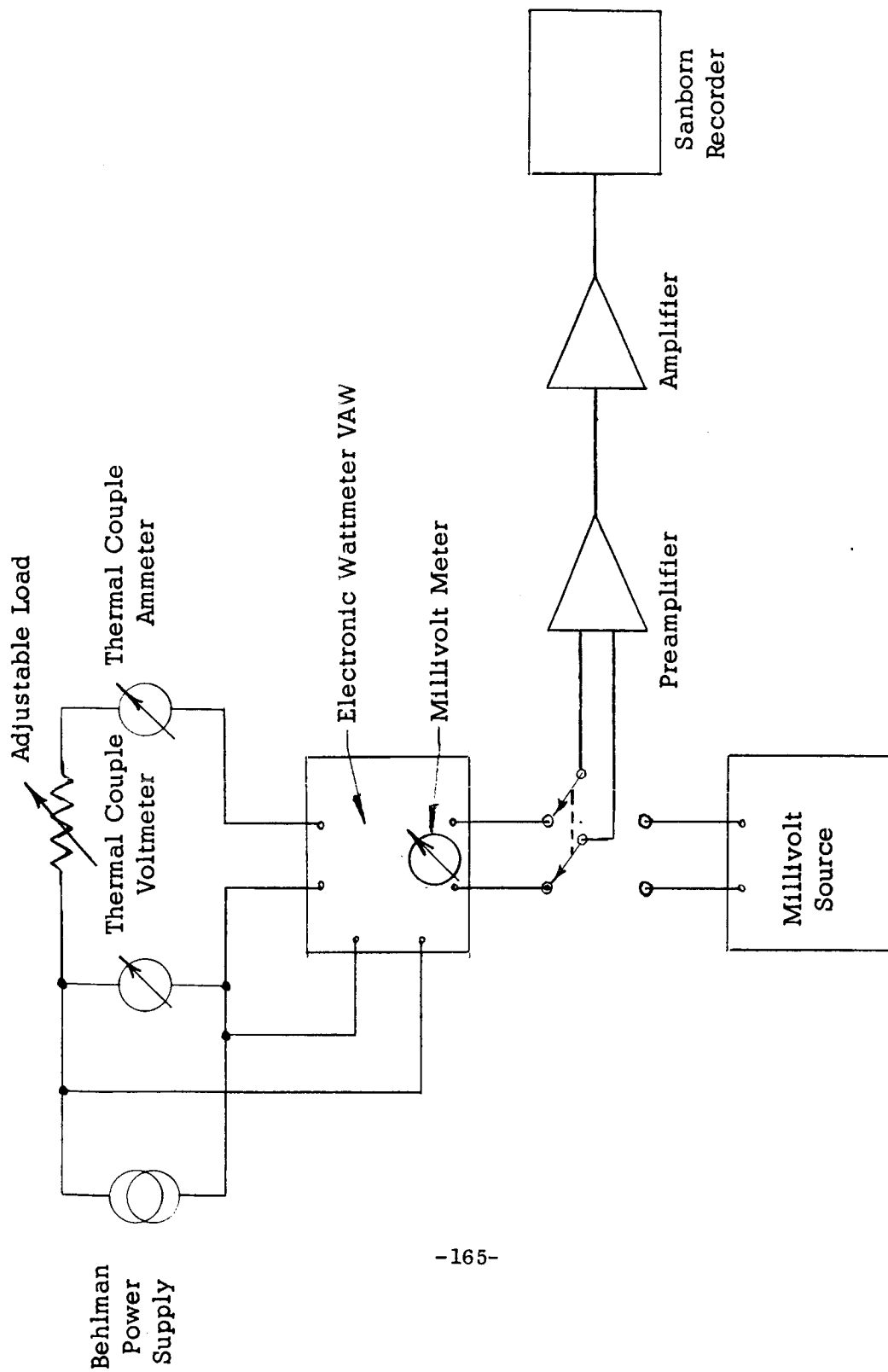


Fig. I.17: ELECTRONIC WATTMETER CALIBRATION CIRCUIT

Standards

Thermocouple Meter: Sensitive Research Instrument Corp.
Universal Polyrange Model USPEW-34

Voltage: Serial No. 941243 C

Current: Serial No. 941243 B

Frequency: 1000 cycles/second

Voltage (volts)		Current (Amperes)		Power (Watts)	
SRI (a)	VAW	SRI (b)	VAW	axb	VAW
20	19.7	.505	.502	10.1	10.1
39	38.5	.700	.70	27.3	27.0
60	59.5	.872	.87	52.3	52.0
80	79.5	1.02	1.02	81.6	81.5
100	99.0	1.148	1.15	114.8	115.0
119.5	118.5	1.26	1.27	150.6	150.8

Frequency (cps)	Voltage Volts		Current (Amperes)		Power (Watts)	
	SRI(a)	VAW	SRI(b)	VAW	axb	VAW
500	100	99.9	1.15	1.16	115.	115
1000	100	100	1.15	1.15	115	115
1500	100	99.9	1.148	1.16	114.8	115
2000	100	99.9	1.15	1.16	115	115
2500	100	100	1.15	1.16	115	116
3000	100	100	1.15	1.16	115	115

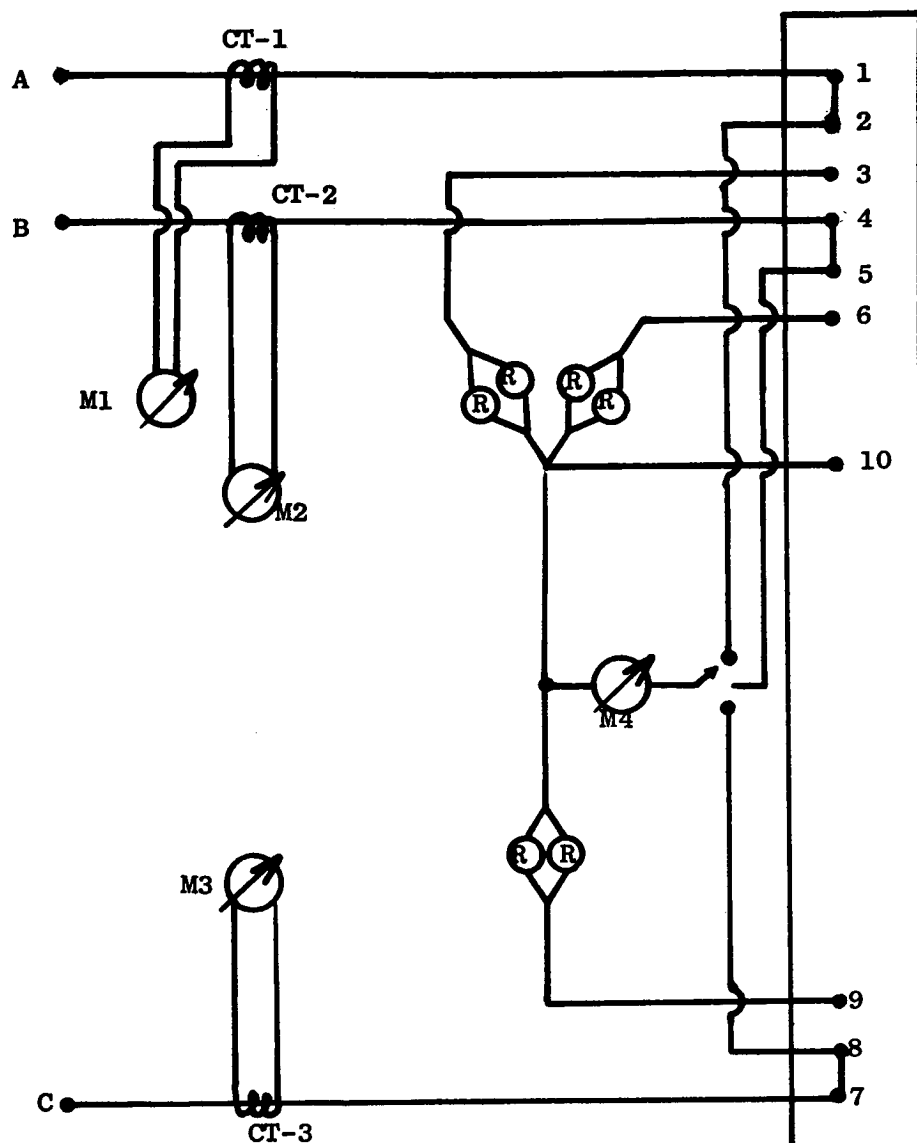
Table 12: Calibration of Electronic Wattmeter (John Fluke
Model 101, VAW Meter, No. 793)

I.3.1 Calibration of the Hall Effect Wattmeter

The Beckman Hall Effect Wattmeter which was used with the three-phase engine to give an extra check on the power was calibrated by duplicating the voltage and current levels expected during arc operation. The nominal arc jet engine power to be measured is 30 kw with a line current of approximately 150 amps and a line to line voltage of approximately 120 volts. Since the line currents are applied to the Hall effect wattmeter through current transformers with a transformer ratio of 200:5 the current seen by the Hall device is only 1/40 of 150 amps or 3.75 amps and the actual power measured is only 750 watts at an indicated power of 30 kw. To simulate the arc load the resistance in each leg of a Y connected load is approximately 18 ohms. By connecting two 300 watt lamps in parallel, a pure resistance of approximately 22 ohms can be obtained. The calibration circuit employed is shown in Fig. I.18.

The Hall effect meter was calibrated over a frequency range of 400 to 3000 cycles/sec and an indicated power of 5 to 32 kw. The test results confirmed that the meter calibration is unaffected by the frequency in the range of calibration. The indicated power is, however, 2.7% below the actual power at 30 kw. The calibration curve obtained for a balanced circuit is shown in Fig. I.19.

Under certain arc operations the power indicated by the Hall effect device is about 4 kw lower than the power measured by the VAW and the electro-dynamometer devices. In such cases power measurements on the power supply equipment always indicated that the power indications of the VAW and the electro-dynamometer device were consistent.



R :: 300 watt flood lamp
 M1 :: SRI #941242A Current \emptyset A
 M2 :: SRI #941242C Current \emptyset B
 M3 :: SRI #941242B Current \emptyset C
 M4 :: SRI #941243B Voltage \emptyset A, B, C

 CT-1 Weston Model 461 #21292 10:5 \emptyset A
 CT-2 Weston Model 461 #20656 10:5 \emptyset B
 CT-3 Weston Model 461 #20657 10:5 \emptyset C

 A, B, C as marked on Behlman Supply

Fig. I.18: Calibration Circuit for the Hall Effect Wattmeter

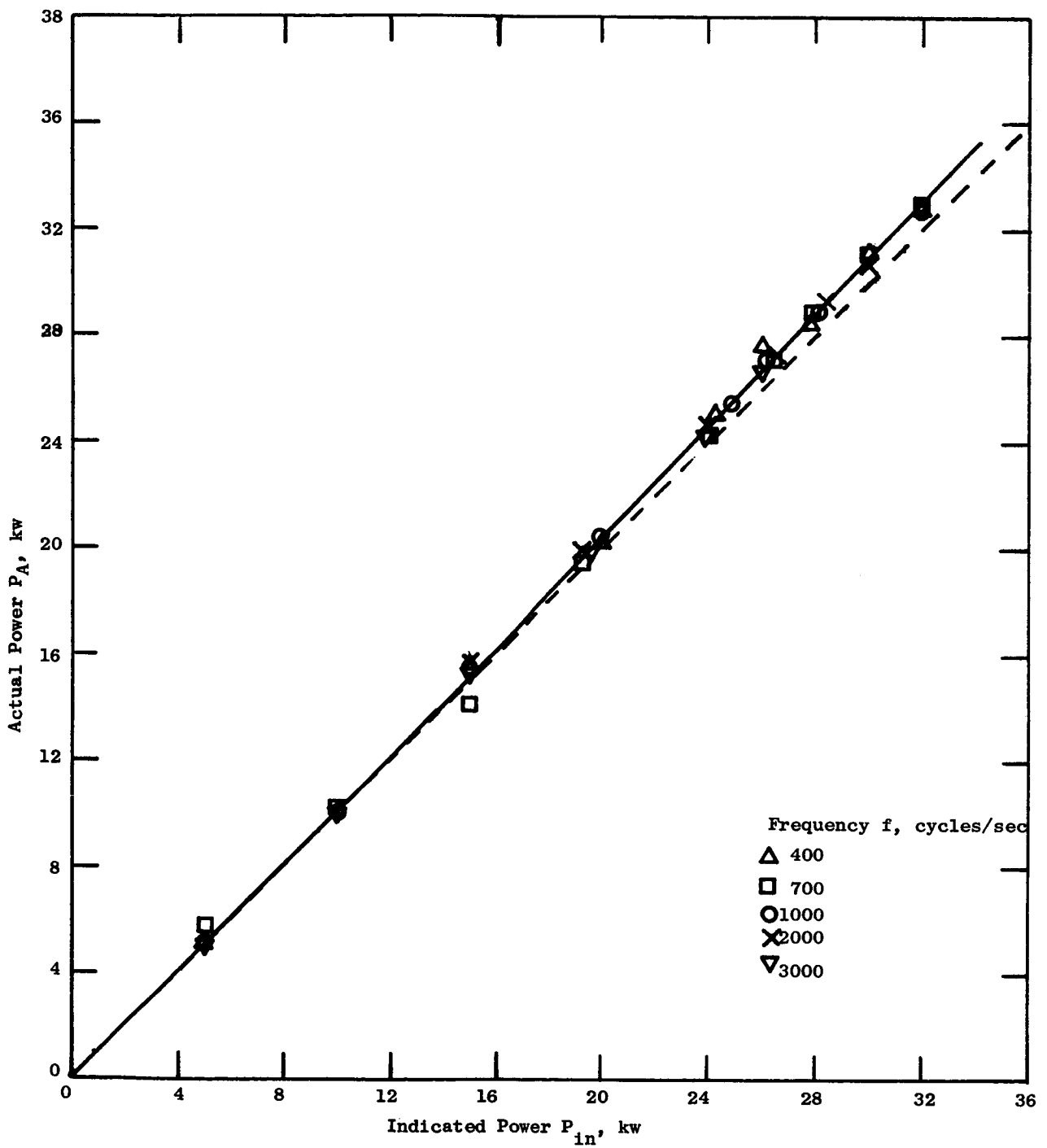


Fig. I.19: Calibration Curve for Three-Phase Hall Effect Watt-meter System (May 15, 1963)

APPENDIX II

II. EFFECT OF NON-UNIFORM ENERGY DISTRIBUTION IN THE PROPELLANT GAS

It has been repeatedly asserted by some sources in the literature that non-uniform energy distribution in the propellant can actually lead to a higher performance of a plasma arc jet engine. This is contrary to the commonly accepted position that non-uniform energy distribution can result only in a decrease in the performance. This latter conclusion has been based on accumulated experimental and theoretical experience of many other jet propulsion systems.

An analytical investigation was made to determine the effect of non-uniform energy distribution. To simplify the problem it was not assumed that the non-uniformity of the gas is continuous but that the propellant is divided into two distinct fractions, one of low-energy propellant and one of high-energy propellant. Also in this first attempt the fluid dynamic and heat transfer effects, which were shown in earlier reports to have a very strong influence on the overall efficiency of a plasma arc jet engine, were neglected. The analysis therefore is strictly based on ideal thermodynamic phenomena. The energy of the gas is expressed by its stagnation temperature assuming that complete thermodynamic equilibrium has been reached at that temperature. The fractions are defined to be weight fractions so that

$$n_1 = \frac{\dot{w}_1}{\dot{w}}$$
$$n_2 = \frac{\dot{w}_2}{\dot{w}}$$

where

n_2 is the weight fraction of the low energy propellant
 n_1 is the weight fraction of the high energy propellant

If the total propellant weight flow rate is \dot{w} and the total electrical power is P , then for each weight fraction n_1 and stagnation temperature T_1 there is a distinct weight fraction n_2 with a stagnation temperature T_2 which is required by conservation of energy. Since the pressure is assumed to be continuous, all conditions are determined for the same stagnation pressure.

The analysis has been carried out for two cases which differ only by the stagnation pressure; the propellant weight flow rate \dot{w} is 5×10^{-4} lb/sec of hydrogen and the total power is 30 kw. The results are plotted in Fig. II.1 to II.4. Though the curves of Figs. II.3 and II.4 could have been superimposed on Figs. II.1 and II.2 they have been shown separately for clarity. From Fig. II.1 it can be clearly seen that the theoretical specific impulse based only on thermodynamic consideration is 1107 sec. Only under very restricted circumstances of non-uniformity could the specific impulse approach 1146 sec., i.e., exceed by 3.53% the specific impulse of uniform energy distribution. While the analysis indicates a very restricted condition which gives a small improvement in performance, there seem to be an almost unlimited combination of conditions leading to a

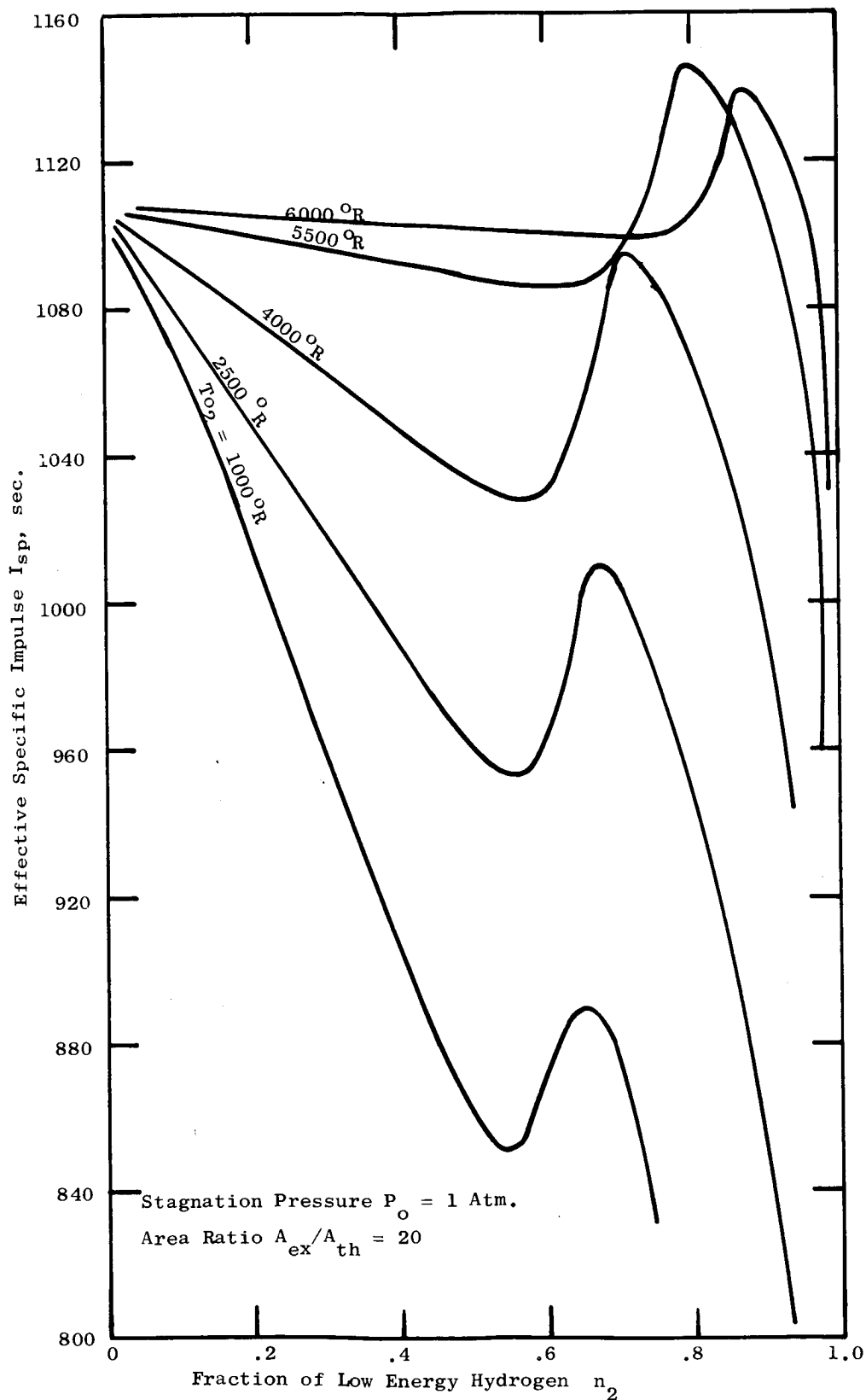


Fig. II.1: Effect of Non-Uniform Energy Distribution in the Exhaust of a Plasma Arc Jet Engine on the Effective Specific Impulse (Stagnation Temperature of Low Energy Hydrogen)

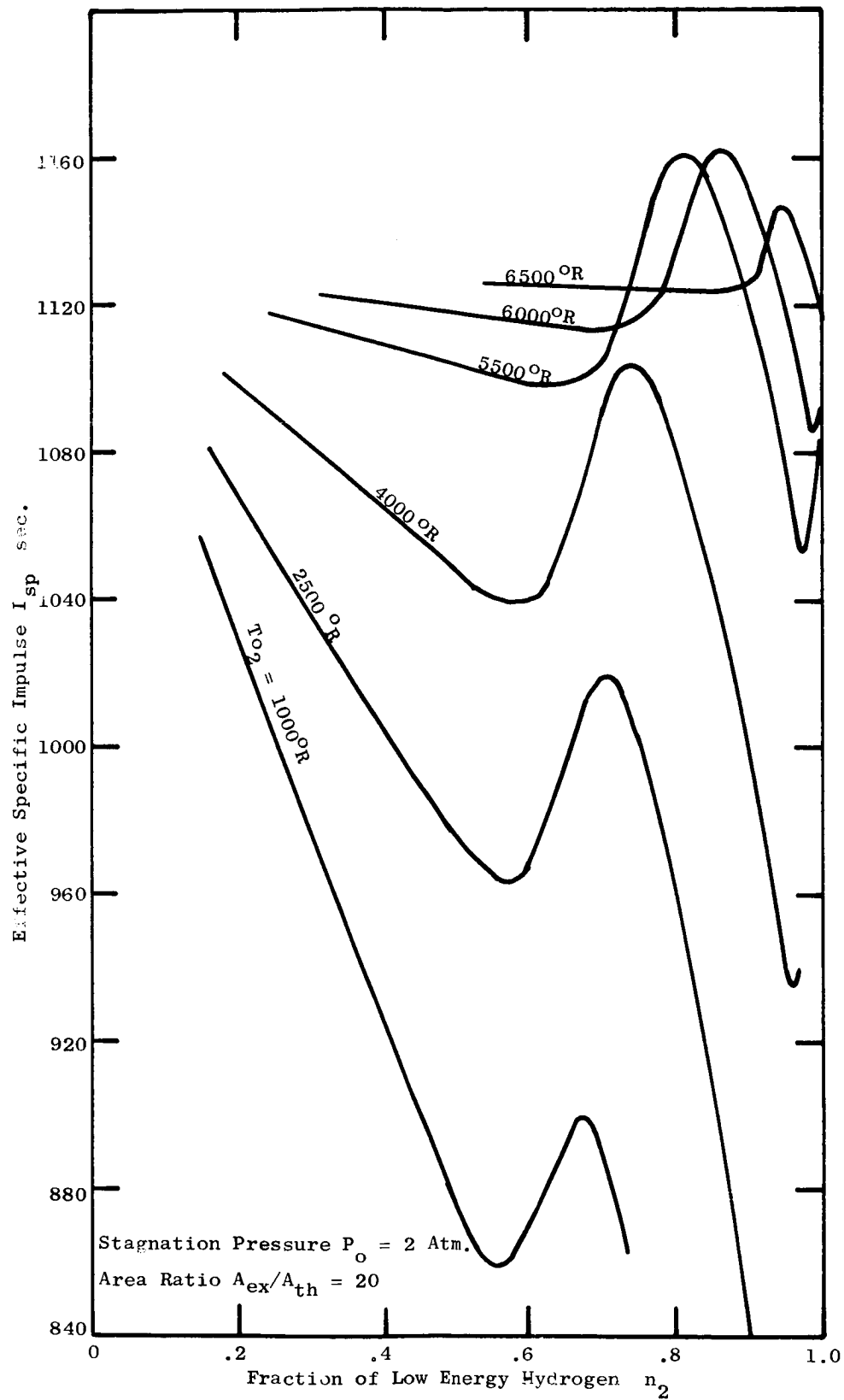


Fig. II.2: Effect of Non-Uniform Energy Distribution in the Exhaust of a Plasma Arc Jet Engine on the Effective Specific Impulse (Stagnation Temperature of Low Energy Hydrogen)

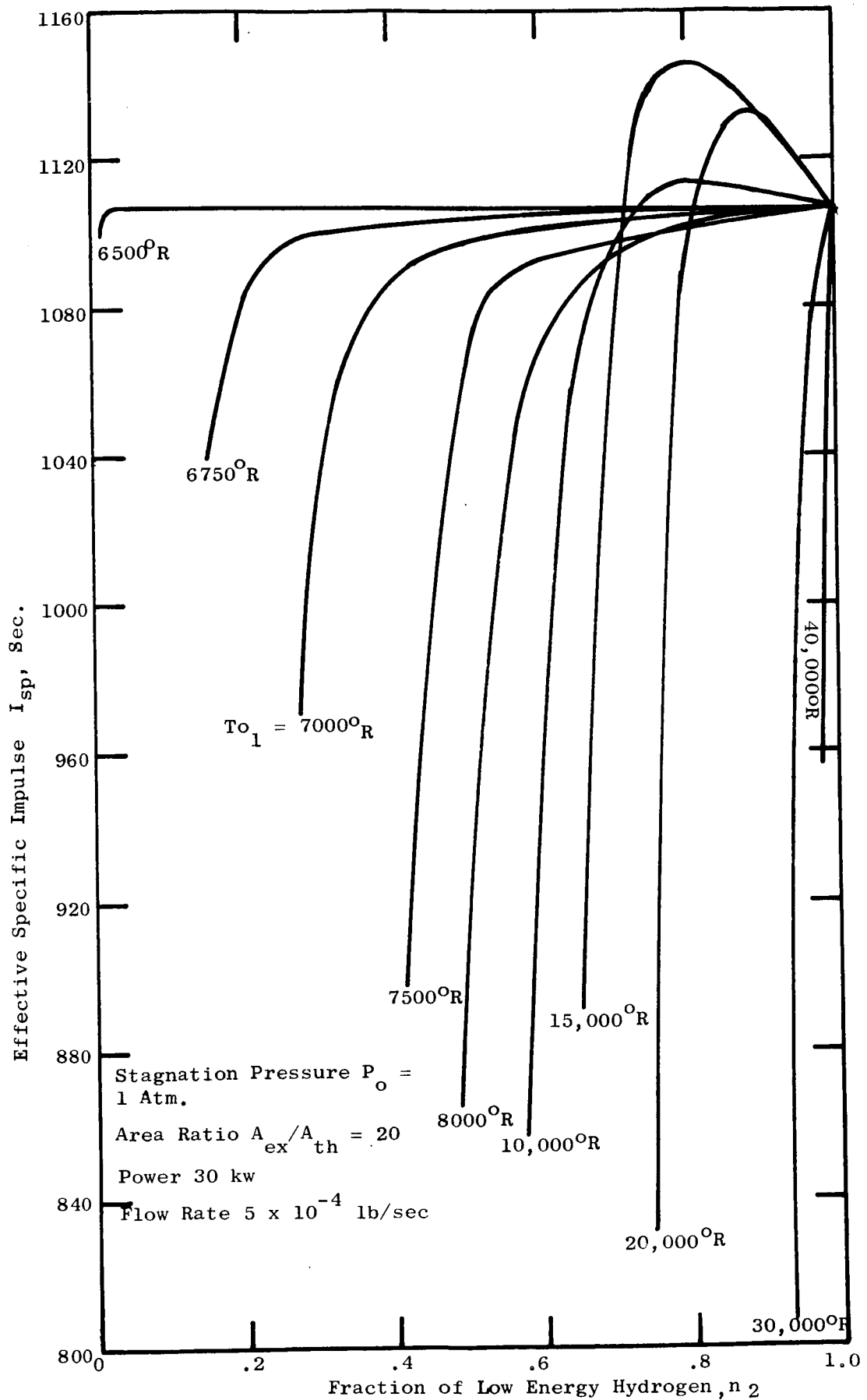


Fig.II:3: Effect of Non-Uniform Energy Distribution in the Exhaust of a Plasma Arc Jet Engine on the Effective Specific Impulse (Stagnation Temperature of High Energy Hydrogen)

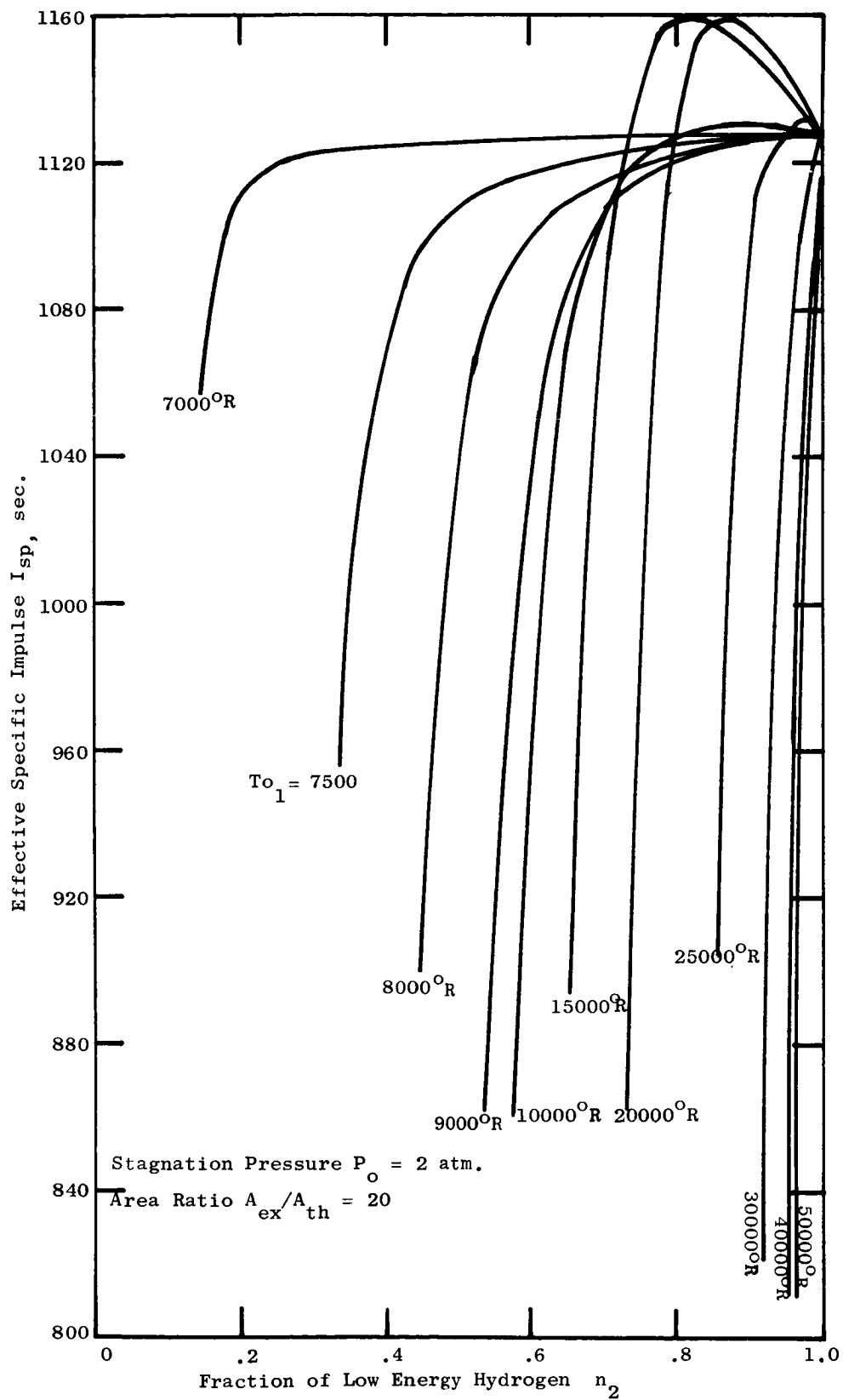


Fig. II.3: Effect of Non-Uniform Energy Distribution in the Exhaust of a Plasma Arc Jet Engine on the Effective Specific Impulse (Stagnation Temperature of High Energy Hydrogen)

drastic reduction of the performance. For instance, if a very small fraction of the gas is at a stagnation temperature of $40,000^{\circ}\text{R}$ the efficiency can drop to an extremely low value, as can be seen in Fig.II.4. The interesting result is that with some fraction of the gas at such a temperature the thermodynamic efficiency of an engine will always be below the efficiency based on a uniform energy distribution.

The analysis has indicated that in the design of a plasma arc jet engine all efforts should be made to obtain a uniform energy distribution in the propellant, as non-uniformity in the propellant can lead to a drastic reduction in the performance of such an engine.

APPENDIX III

III. ABLATION RATE OF THE ELECTRODES IN A PLASMA ARC JET ENGINE

An experimental investigation of the ablation rate of the center electrode in a three-phase plasma arc jet engine was carried out. It indicated that the ablation rate can be correlated with the electric power consumed in the arc. This is shown in Fig. III.1. The results of this investigation also made it appear that repeated starting of the arc had no effect on the ablation of the electrodes. From these observations it could also be deduced that ablation is a continuous process that could be subjected to an analysis.

With all probability, ablation of the electrode material is predominantly a process of evaporation. The rate of evaporation of the electrode material is a function of the material properties, the temperature of the material and the vapor pressure of the material. Contributing factors in the process of evaporation are the partial pressure of the surrounding gas, the velocity of the gas over the evaporating surface, and the temperature of the gas. In the first attempt to determine the influence of the most pronounced parameters on the evaporation rate of the electrode material, some of the contributing factors have to be neglected as they would make an analysis unwieldy at the present time.

III.1 Ablation Rate of a DC Engine Cathode

The simplest ablation analysis reduces to the setting up of an energy balance at the area of material loss of the electrode, where the ablation process is part of a cooling process. The energy exchange process at the negative electrode of a dc arc is shown in Fig. III.2. The energy input into the electrode is due to two processes.

1. Heat conduction to the cathode from the arc column
2. Energy released by ion bombardment

This energy is removed from the cathode by four processes

1. Latent heat of evaporation of electrons
2. Heat radiation
3. Heat conduction through the electrode
4. Latent heat of evaporation of electrode material

To be able to set up this energy balance, several assumptions have to be made which will later be shown to be valid by the results of the analysis.

- A. The current in the arc is predominantly carried by thermionically-emitted electrons
- B. The arc column temperature is equal to the stagnation temperature of the heated gas
- C. The voltage-current characteristic of the arc is as found experimentally and is shown in Fig. III.3

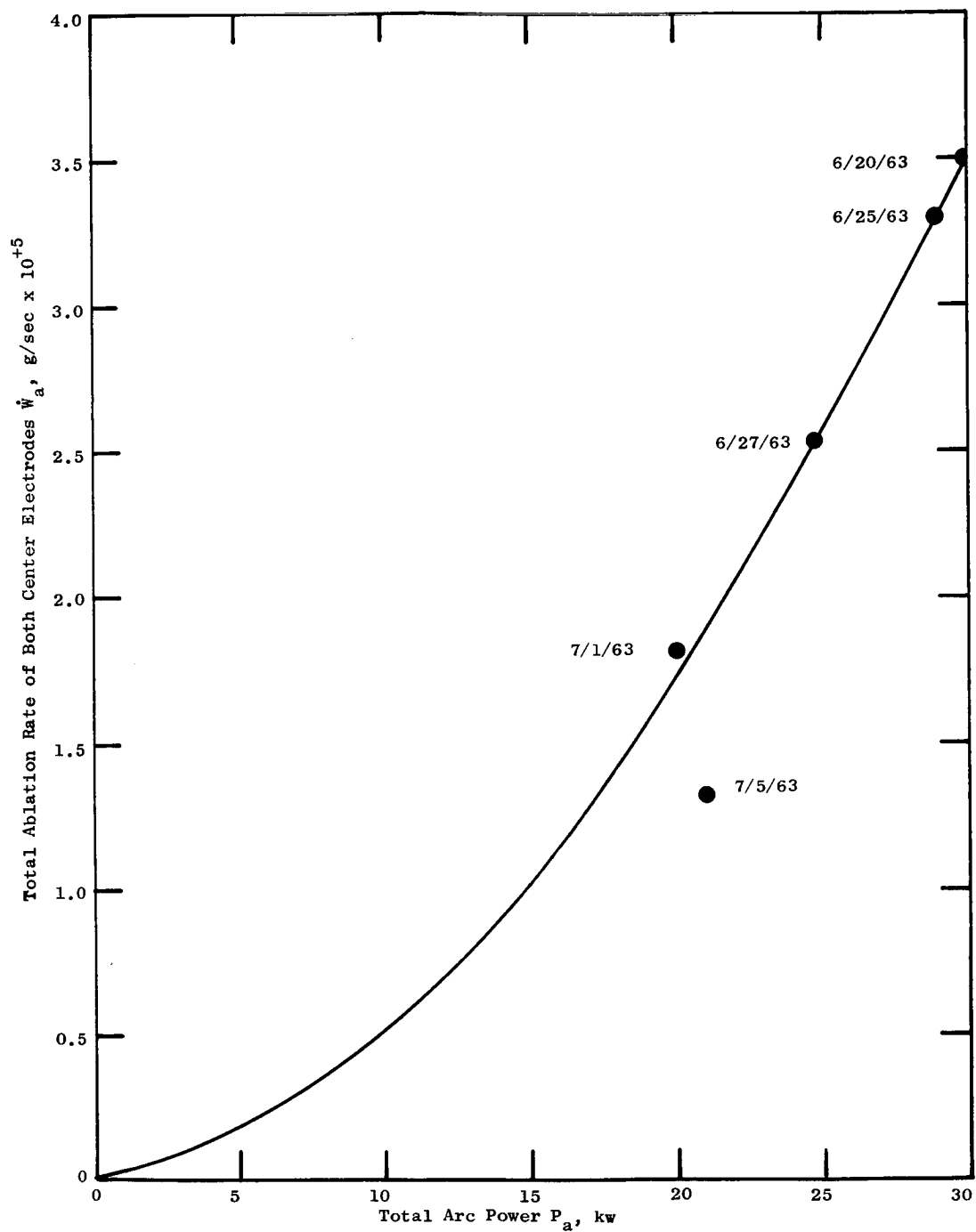


Fig. III.1: Ablation Rate of Center Electrodes as a Function of Total Arc Power

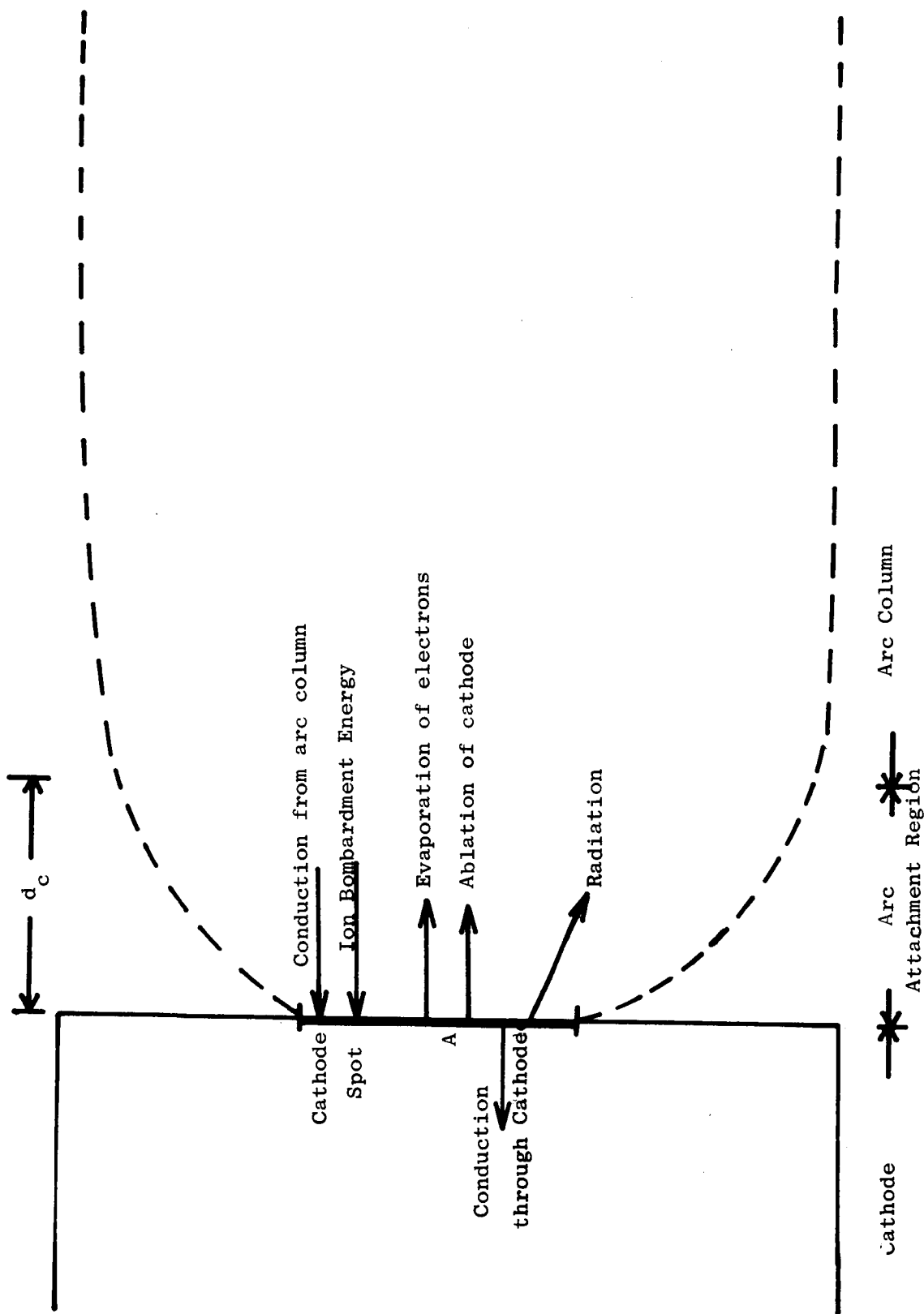


Fig. III.2: Energy Balance at the Cathode

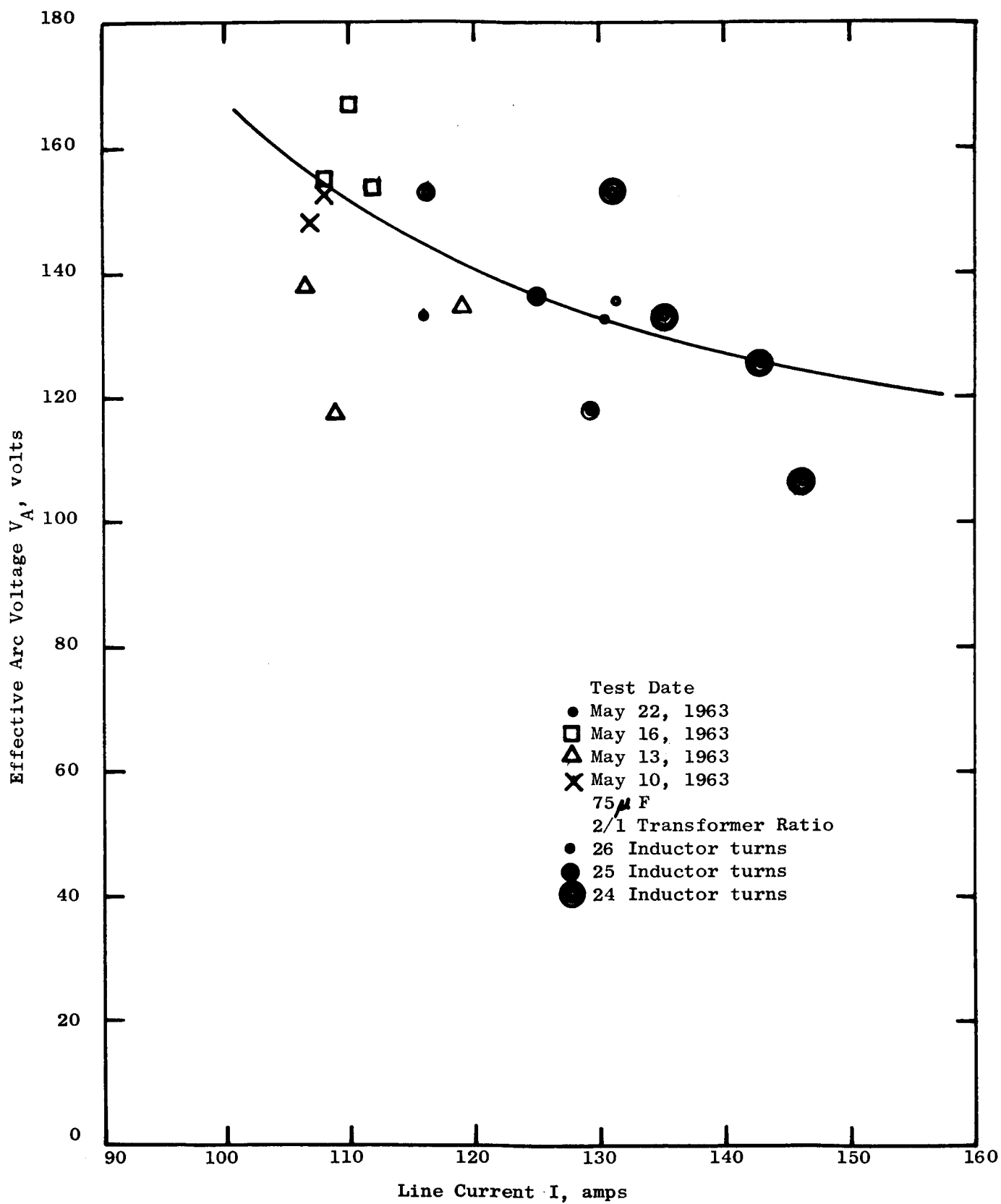


Fig. III-3:Electrical Test Data of Engine Y16-1 (Arc Voltage Vs Line Current)

- D. The arc attachment region depth, d_c , is equal to the electron mean-free path
- E. The colder end of the electrode has a constant temperature of 1000°R
- F. The cathode drop voltage is 10 volts

The energy balance equation for the cathode spot then becomes

$$j_i A (V_c + V_i - \phi_o) + \frac{k_g A (T_o - T)}{d_c} = \sigma \epsilon A T^4 + \frac{k_c A (T - T_1)}{L_c} \coth \frac{A \pi}{A_o} + j_e \phi_o A + \dot{w} L A$$

where

j_i = ion current density, $\frac{\text{amp}}{\text{cm}^2}$

A = area of cathode spot, cm^2

A_o = total area of cathode face, cm^2

V_c = cathode voltage drop, volts

V_i = ionization potential of gas, volts

ϕ_o = work function of cathode, volts

k_g = thermal conductivity of gas, $\text{watts/cm}^\circ\text{K}$

T_o = stagnation temperature of gas, $^\circ\text{K}$

T = temperature of cathode spot, $^\circ\text{K}$

d_c = depth of cathode attachment region, cm

ϵ = emissivity of cathode surface, dimensionless

σ = Stefan-Boltzmann constant, $5.67 \times 10^{-12} \text{ watts/cm}^2\text{-}^\circ\text{K}$

k_c = thermal conductivity of cathode, $\text{watts/cm}^\circ\text{K}$

T_1 = temperature at colder end of electrode, $^\circ\text{K}$

L_c = length of electrode, cm

j_e = electron current density, $\frac{\text{amp}}{\text{cm}^2}$

\dot{w} = evaporation rate of cathode, g/cm² - sec

L = latent heat of sublimation of the cathode material, watt-sec/g

In order to evaluate these terms, it is necessary to determine the current densities of electrons and ions. The electron current for a refractory material such as tungsten can be calculated from the Richardson-Dushman equation,

$$j_e = A_o T_o^2 \exp \left(- \frac{\phi_o \epsilon}{kT} \right)$$

where

A_o = constant for material, amps/cm² - °K²

ϵ = electron charge, 1.602 x 10⁻¹² erg/volts

k = Boltzmann's constant, 1.38 x 10⁻¹⁶ erg/°K

The use of this equation is discussed at length in references such as Cobine (Ref. 3), which also points out that the ion current is space-charge limited. Therefore, the Child's Law equation can be used for the ion current,

$$j_i = \frac{1}{9\pi} \sqrt{\frac{2\epsilon}{m}} \frac{(V_c)^{3/2}}{d_c^2} \quad (\text{electrostatic units})$$

where m is the mass of a positive ion.

It can be shown that the heat conduction in the cathode is affected less than 0.5% by the contribution of resistance heating in the cathode. Therefore, heat generation in the electrode can be neglected in the energy balance when making an initial attempt to correlate ablation rates with the power in the arc.

III.1.1 Tungsten Cathode

The energy balance equation can be solved by iteration to obtain the temperature of the cathode spot for a given arc power. Using the electrical characteristics of the engine such as given in Fig.III.3, the area of the cathode spot can be found. Then, since there exists a functional relation between the evaporation rate of tungsten and temperature, the results can then be expressed in terms of the electrode ablation rate as a function of arc power. The curve generated for conditions prevailing in the engine design Y16-1 is shown in Fig.III.4. The analytical curve is seen to show good agreement with the experimental data indicating that the most important parameters have been correlated by the energy balance.

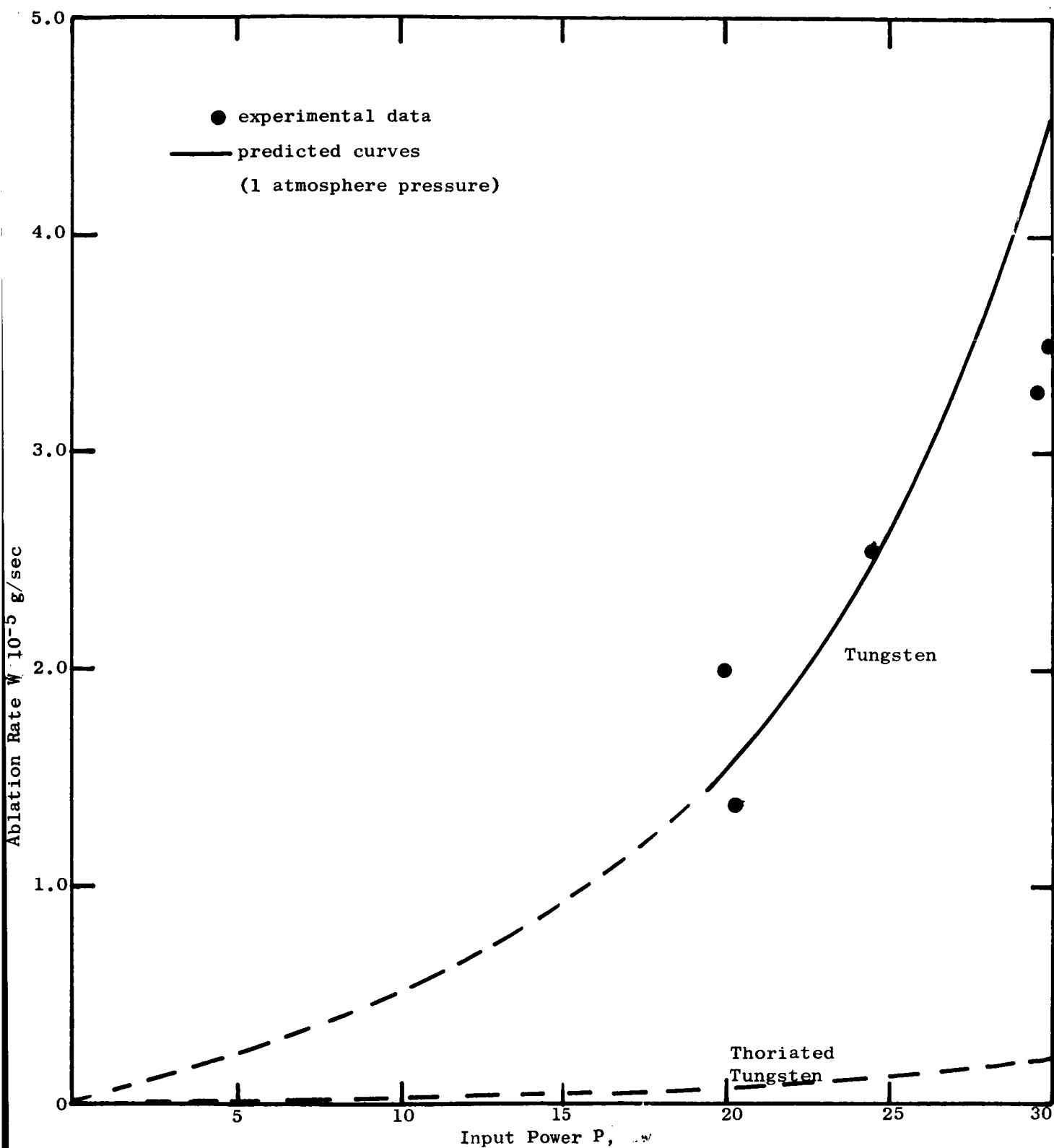


Fig. III.4: Ablation Rate of Tungsten Electrodes

It is instructive to inspect the relative magnitudes of the energy terms. For a 30 kw arc, these values are as follows:

$$\text{Inputs: Heat conducted to the cathode from the arc column} = 1780 \frac{\text{watts}}{\text{cm}^2}$$

$$\text{Energy released by ion bombardment} = 70 \frac{\text{watts}}{\text{cm}^2}$$

$$\text{Outputs: Latent heat of vaporization of electrons} = 1155 \frac{\text{watts}}{\text{cm}^2}$$

$$\text{Heat radiation from the cathode spot} = 307 \frac{\text{watts}}{\text{cm}^2}$$

$$\text{Heat conducted through the cathode} = 391 \frac{\text{watts}}{\text{cm}^2}$$

$$\text{Latent heat of ablation of cathode} = 0.4 \frac{\text{watts}}{\text{cm}^2}$$

At this power the electron current is

$$j_e = 255 \frac{\text{amp}}{\text{cm}^2}$$

and the ion current is

$$j_i = 1.1 \frac{\text{amp}}{\text{cm}^2}$$

It can readily be seen that the electron current density is much greater than the ion current density, in the region of the cathode. This is generally in agreement with references such as Cobine or Somerville (Refs.3 and 4).

It is also interesting to note that there are only four large energy terms. The energy input is mainly by conduction from the hot arc column; and the energy removal occurs primarily by electron evaporation, by conduction through the cathode and by radiation.

III.2 Ablation Rate of an AC Electrode

The preceding discussion has quantitatively predicted the ablation rate for the center electrode of a dc arc engine. This result can also be used for an ac electrode if the assumption is made that the cathode spot temperature is nearly equal to the anode spot temperature. This assumption is reasonably valid for cases when the anode is well cooled; however, in other situations the anode may be somewhat hotter than the cathode.

In this section, the results of a number of extensions to the analysis will be presented. The following general analytical procedures will be given which are applicable to both the three-phase engine and the single phase engine:

- . Ablation rate of an anode
- . Ablation for an ac electrode
- . Thoriated tungsten electrode ablation
- . Methods to decrease the electrode ablation

III.2.1 Ablation Rate for an Anode

The procedure to calculate the ablation rate for an anode follows much the same lines as that for a cathode, as was discussed in the previous section of this report. The model is similar to the model for the cathode, except that the energy inputs for the anode are

- energy of condensation of the electrons
- conduction from the arc column

Energy is released from the anode by

- heat radiation
- conduction through the anode
- evaporation of anode material

Therefore, the energy balance equation for the anode has the form

$$j_e (\phi_o + V_a) + \frac{k_g (T_o - T)}{d_a} = \frac{k_a (T - T_l)}{L_a} \coth \left(\frac{A \pi}{A_o} \right) + \epsilon \sigma T^4 + \dot{w}L$$

where

j_e = electron current density, amp/cm²

ϕ_o = work function of anode, volts

V_a = anode voltage drop, volts

k_g = thermal conductivity of propellant gas in the anode space,
watts/cm-°K

T_o = stagnation temperature, °K

T = temperature of anode spot, °K

d_a = depth of anode attachment region, cm

k_a = thermal conductivity of anode material, watts/cm-°K

A = area of anode spot, cm²

A_o = total area of anode face, cm²

ϵ = emissivity of anode surface, dimensionless

σ = Stefan-Boltzmann constant, 5.67×10^{-12} watts/cm²

\dot{w} = evaporation rate of anode, g/cm²-sec

L = latent heat of sublimation of the anode material, watt-sec/g

In order to evaluate the terms in the energy balance equation, it is necessary to determine the electron current density. At the anode, the electron current is space-charge limited due to the sheath of electrons which builds up around the anode surface. Therefore, the electron current density is given by the Child's law equation

$$j_e = \frac{2.33 \times 10^{-6} (V_a)^{3/2}}{\sqrt{1823.3 M} d_a^2}$$

where M is the weight of the particles, which in this case are electrons.

Several assumptions were employed in setting up the energy balance equation at the anode.

- A. The current at the anode is carried by the electrons, i.e., no positive ions are released at the anode
- B. The arc column temperature is taken equal to the stagnation temperature of the gas
- C. The voltage-current characteristic is known
- D. The arc attachment region depth, d_a , is considered equal to an electron mean-free path
- E. The cool end of the electrode is at a constant temperature of 1000°R
- F. The anode drop voltage is 10 volts

The energy term in the equation which accounts for conduction through the anode has a factor $\coth(A\pi/A_o)$. This is to account for the fact that the anode spot does not, in general, cover the entire anode surface and therefore the conduction is actually three-dimensional.

The evaporation rates of tungsten and thoriated tungsten are given in Figs. III.5 and III.6. These rates were obtained by utilizing data from several sources and a semi-empirical equation for evaporation rate. The electron emission rates of tungsten and thoriated tungsten are given in Figs. III.7 and III.8.

The results of this analysis indicate that the center electrode of a dc engine will be about 200°C hotter when it is an anode than when it is a cathode. This means the ablation rate is about 10 times greater at the 30 kw power level for the center electrode operating as an anode than when it operates as a cathode. From this the following conclusions can be drawn:

1. The nozzle of a dc engine, which is normally the anode, is expected to experience rather large ablation rates.
2. The ablation rate of a dc engine which operates with the center electrode as the anode is very large compared to the ablation rate of the cathode. Therefore, a dc engine should never be operated with the center electrode as the anode, as the resulting severe electrode ablation will cause engine failure in a very short time.

III.2.2 Ablation for an AC Arc

The ablation rates have been calculated for the electrode of an arc jet engine when the electrode is a cathode and when it is an anode. Now these analyses will be combined to obtain an analysis for ac operation. The model to be used for this purpose will postulate a quasi-steady state situation, as shown in Fig. III.9.

During the time that the electrode operates as a cathode, it will experience an energy input due to ion bombardment. The energy is given by

$$E_i = j_i (V_i + V_c - \phi_o)$$

where

j_i = ion current density, amp/cm²

V_i = ionization potential of propellant gas, volts

V_c = cathode voltage drop, volts

ϕ_o = electrode work function, volts

Therefore, on a time-averaged basis, the ion bombardment energy is

$$E_i = \frac{j_i}{2} (V_i + V_c - \phi_o)$$

since the electrode operates as a cathode only half the time.

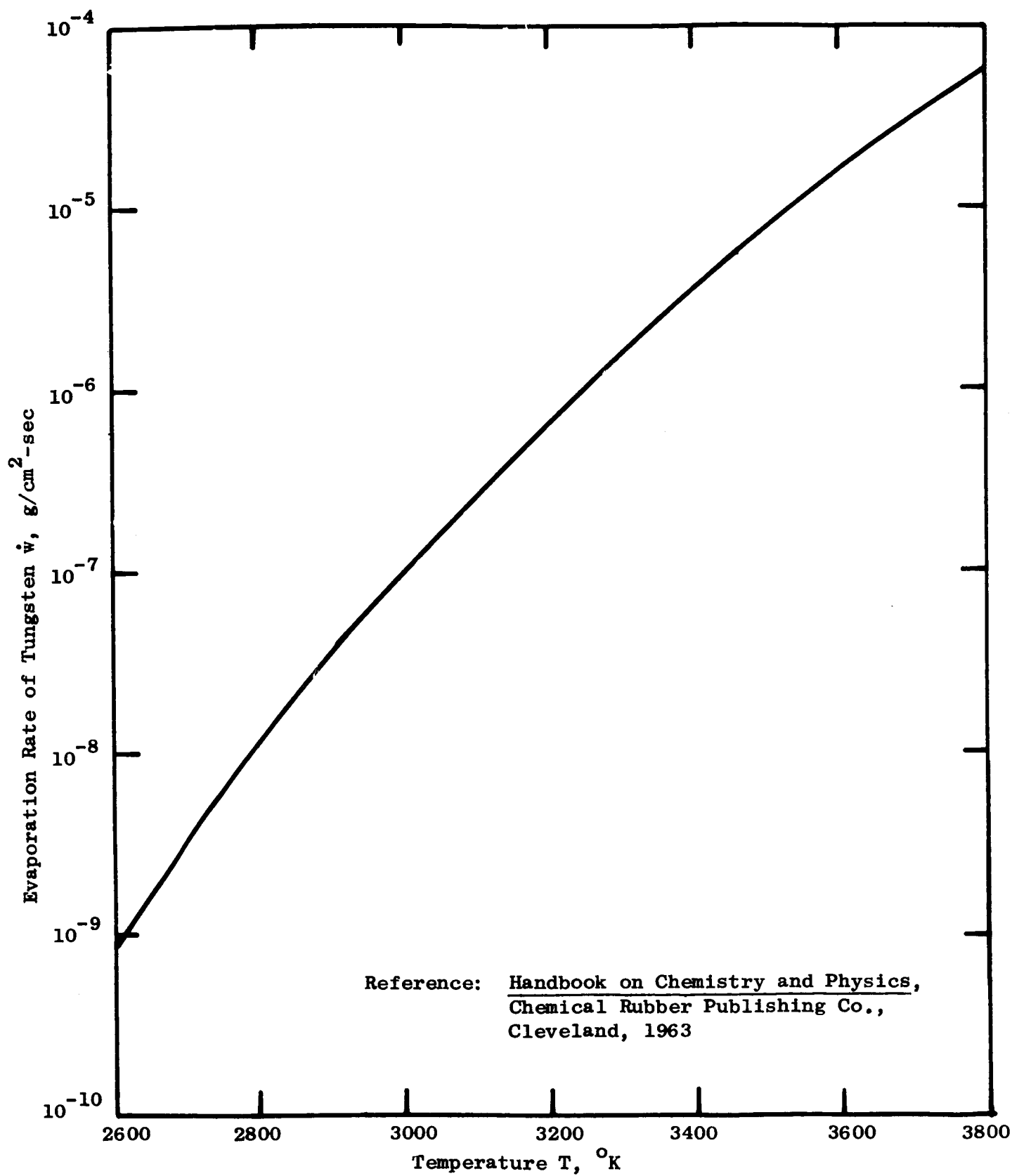


Fig. III.5: Evaporation Rate of Tungsten

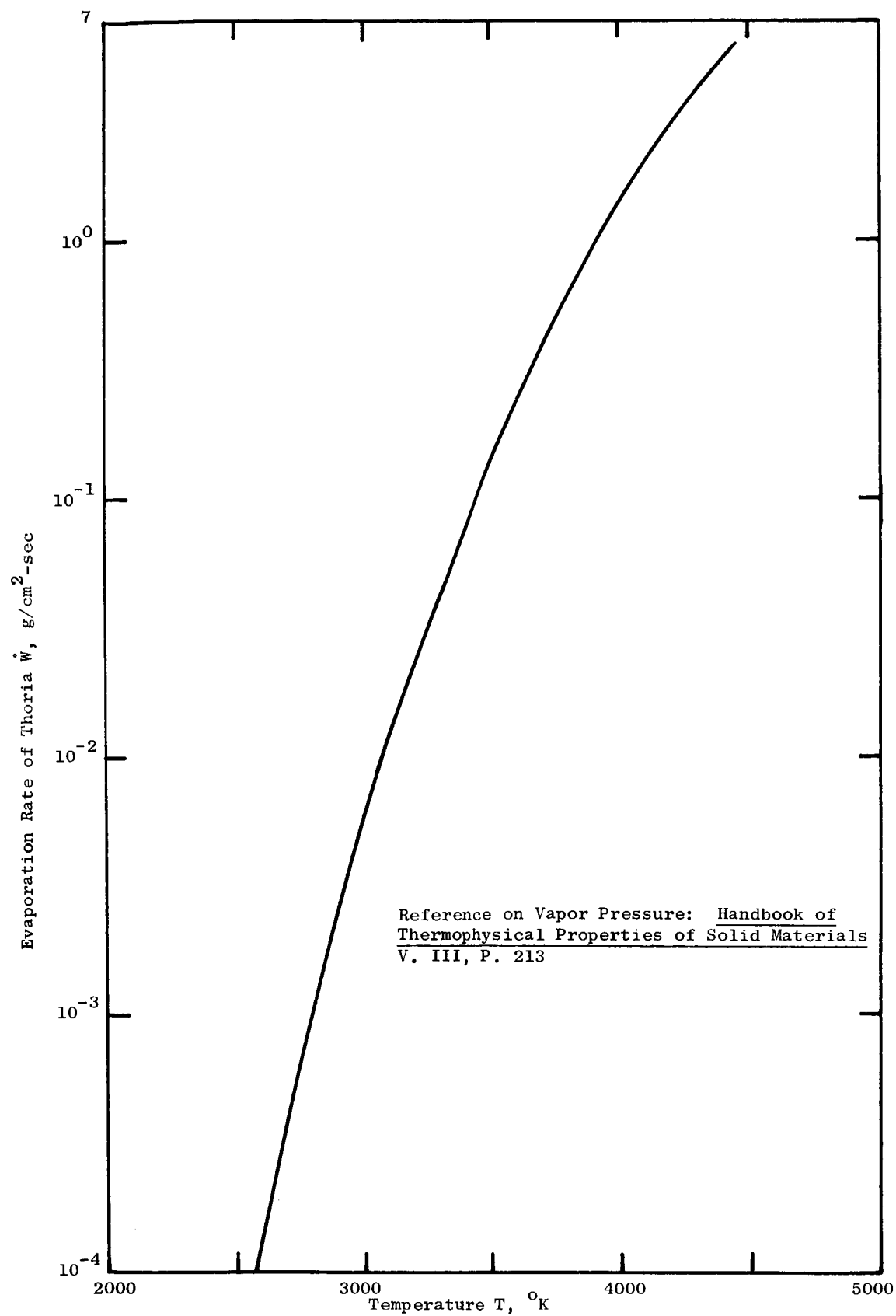


Fig. III.6: Evaporation Rate of Thoriated Tungsten

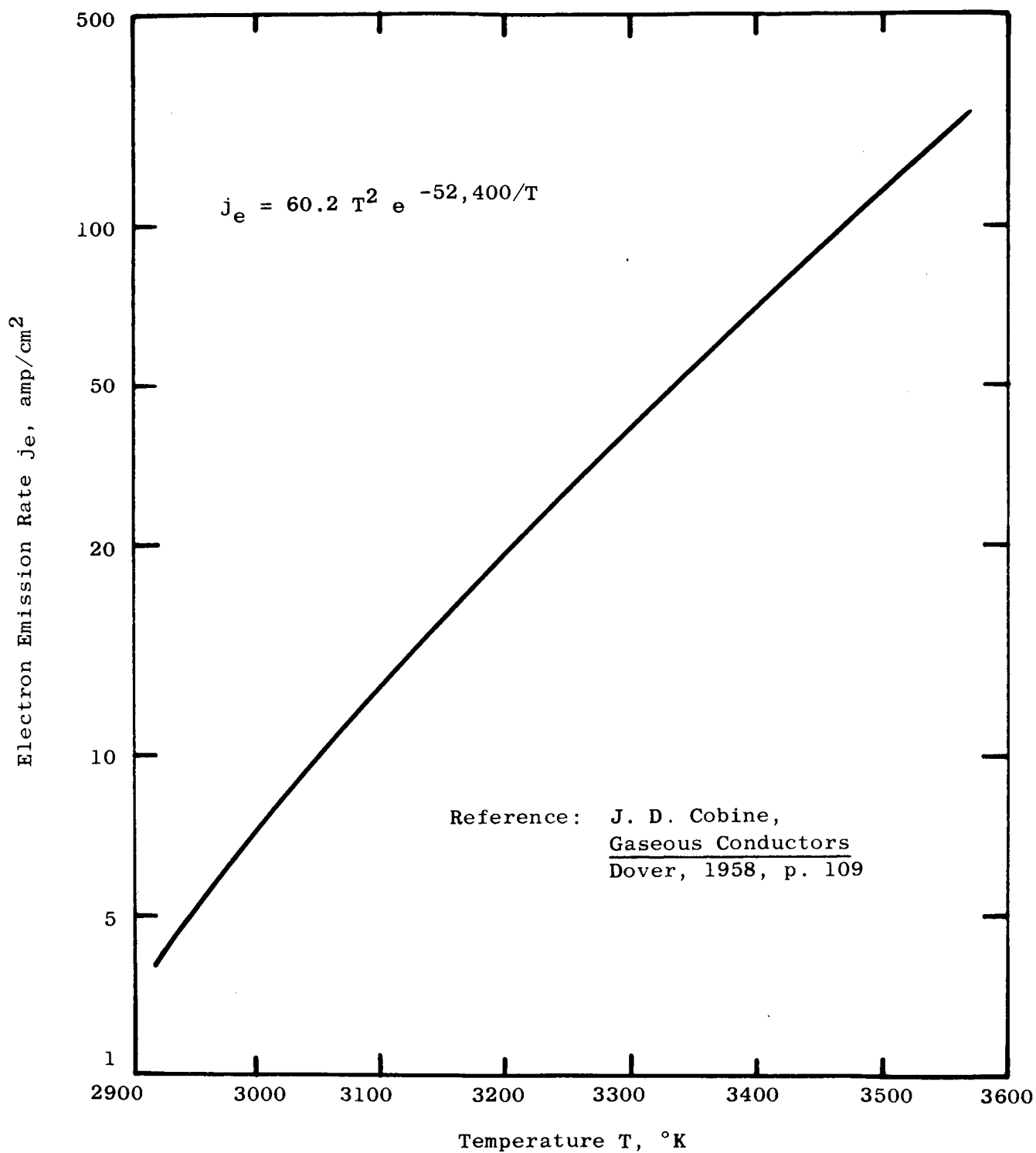


Fig. III.7: Electron Emission Rate for Tungsten

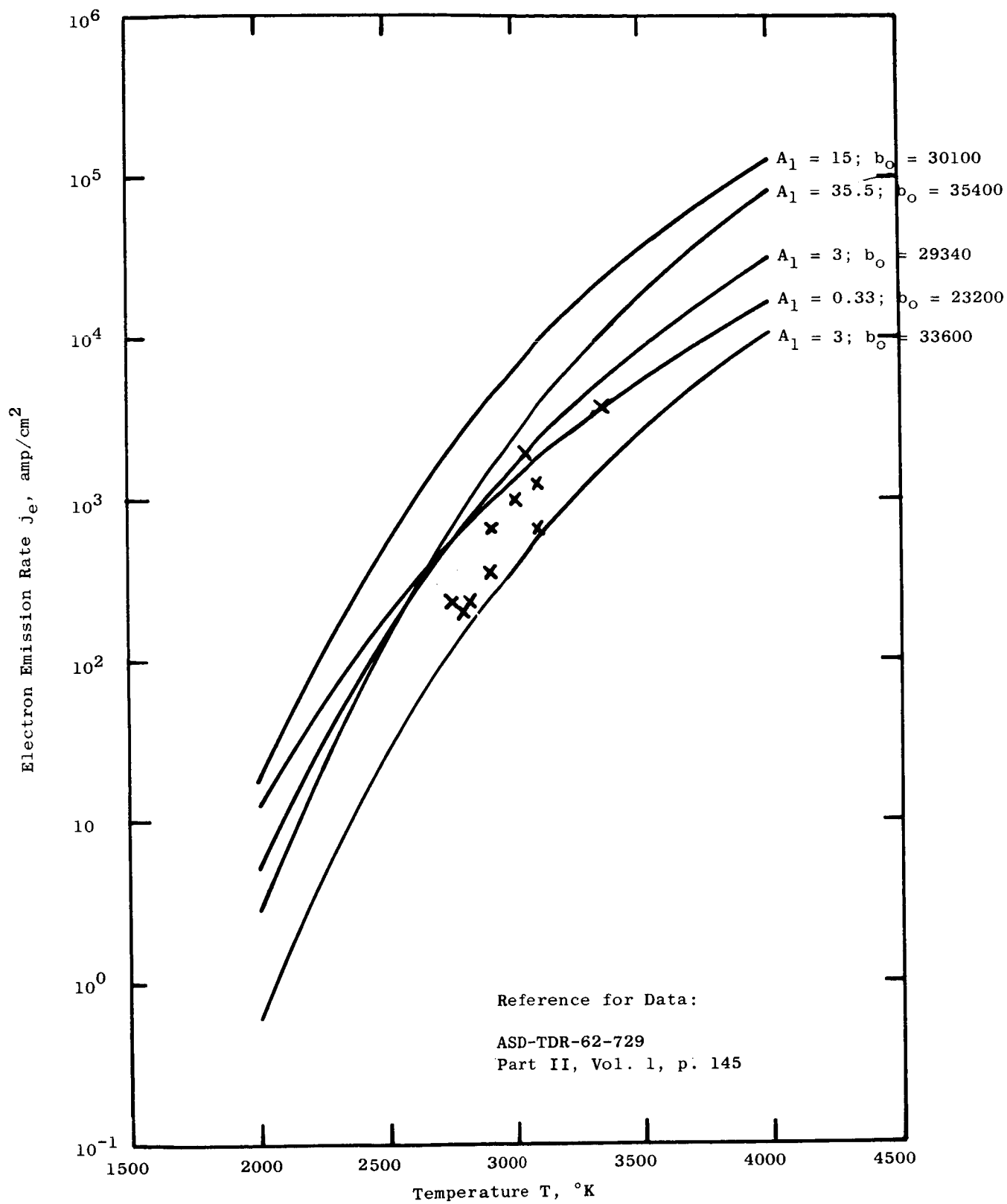


Fig. III.8: Electron Emission Rate for Thoriated Tungsten

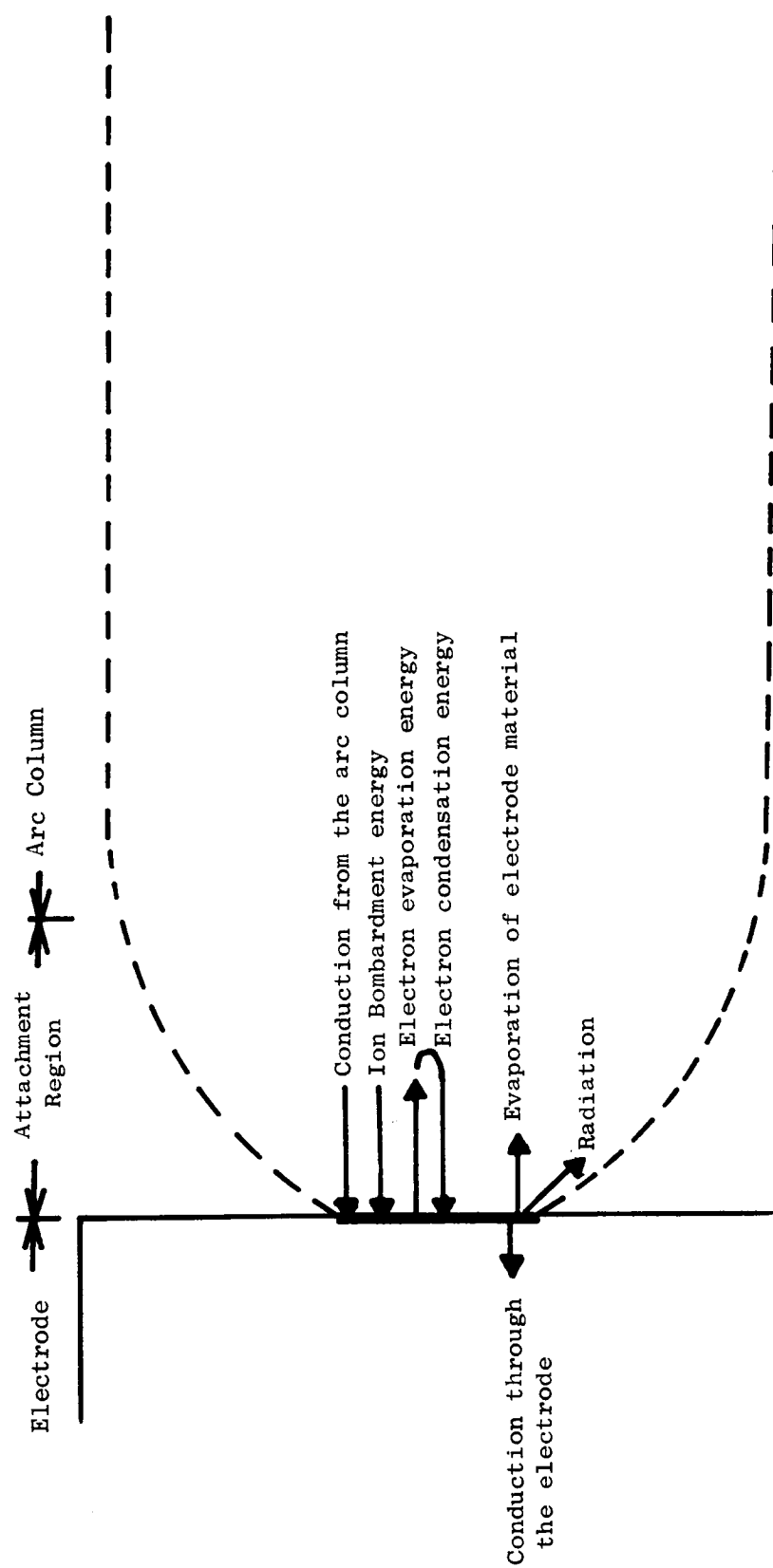


Fig. III.9: Energy Balance at the Electrode of an AC Arc

Consider now the energy terms associated with the electron movement. When the electrons leave the electrode, they remove the energy $E = j_e \phi_o$. When the electrode becomes an anode, the electrons return, bringing in energy given by $E = j_e(\phi_o + V_a)$. However, the electrons originate only from the hot spot on the electrode, whereas they presumably return to the entire electrode face. Therefore, the energy input to the hot spot must be multiplied by the factor (A/A_o) .

Therefore, the net energy input to the hot spot associated with the electron movement is given by

$$E_e = \frac{j_e}{2} \left[(V_a + \phi_o) \frac{A}{A_o} - \phi_o \right]$$

where the division by two is to account for the time averaged basis.

Therefore, the energy balance equation for the electrode in ac operation becomes

$$\frac{j_e}{2} \left[(V_a + \phi_o) \frac{A}{A_o} - \phi_o \right] + \frac{j_i}{2} (V_c + V_i - \phi_o) + \frac{k_g (T_o - T)}{d_c} =$$

$$\epsilon \sigma T^4 + \frac{k_c (T - T_1)}{L_c} \coth \left(\frac{A \sqrt{\pi}}{A_o} \right) + \dot{w}L$$

The results of this analysis are plotted in Fig. III.10. They show a good agreement with the experimental data obtained with the three-phase engine.

The ablation rate of the electrode of an ac engine can now be compared with the ablation rate of the center electrode in a dc engine. The analysis for a dc cathode was presented in a previous section of this report. In Fig. III.11 the comparison between these two ablation rates is made for 30 kw power engines. It can be seen that the ablation rate of an ac engine electrode is slightly larger than the ablation rate for the anode of a dc engine at the 30 kw power level. However, the ablation rate for the anode of a dc engine is expected to be slightly greater than for the ac anode. This is because an anode normally operates at a much higher temperature than does a cathode or an ac electrode unless it is provided with a large amount of internal cooling.

III.2.3 Thoriated Tungsten Electrode Ablation

The ac ablation analysis has been applied to a thoriated tungsten electrode in the three-phase engine. For this case most of the values are the same as those used for a tungsten electrode except that certain material values are changed. However, it is very difficult to establish some of the correct material values because of the scarcity of data in the literature. For example, the electron

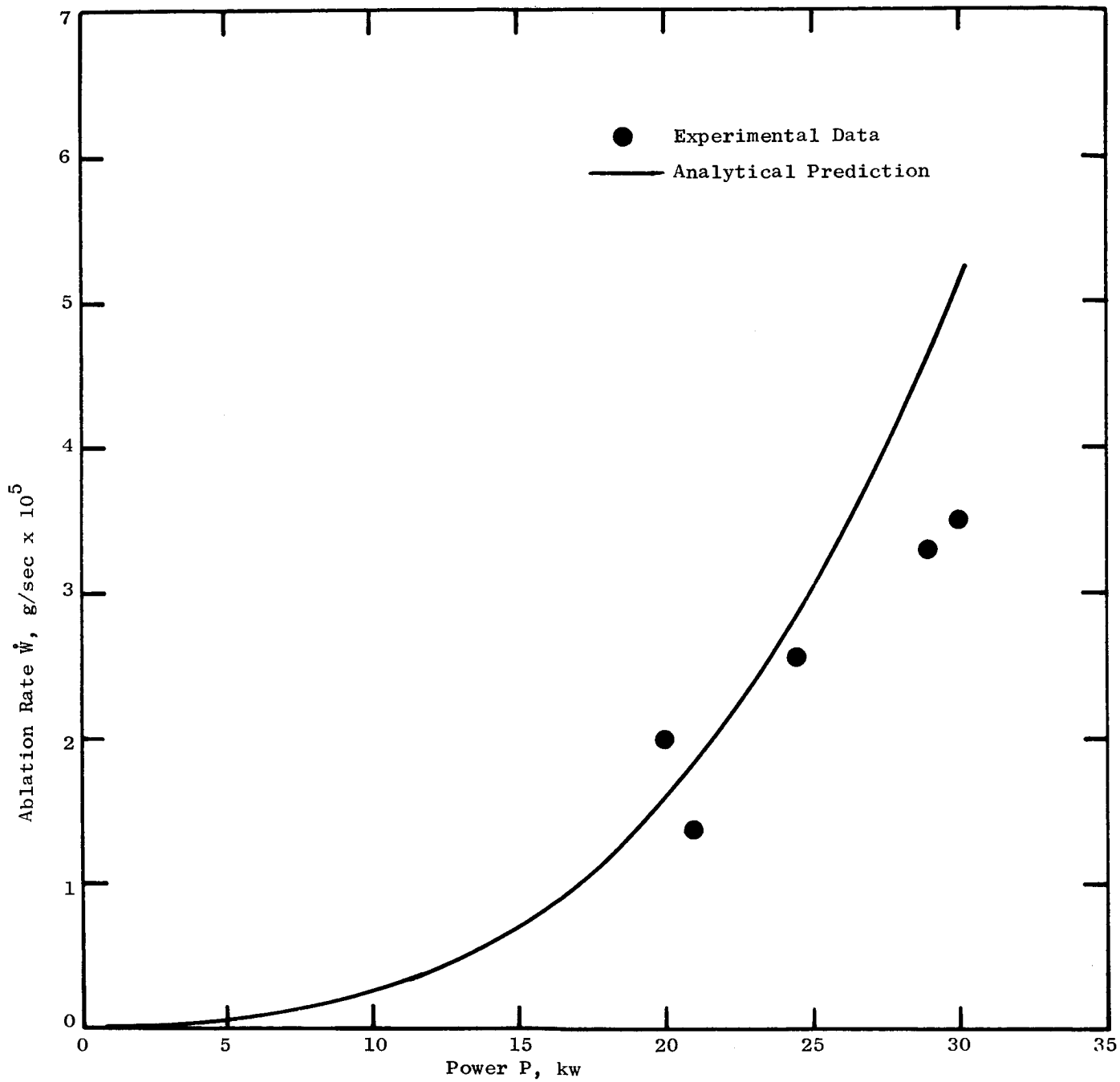


Fig. III.10: Ablation Rate of a Tungsten Electrode in an AC Arc at Stagnation Pressure One Atmosphere

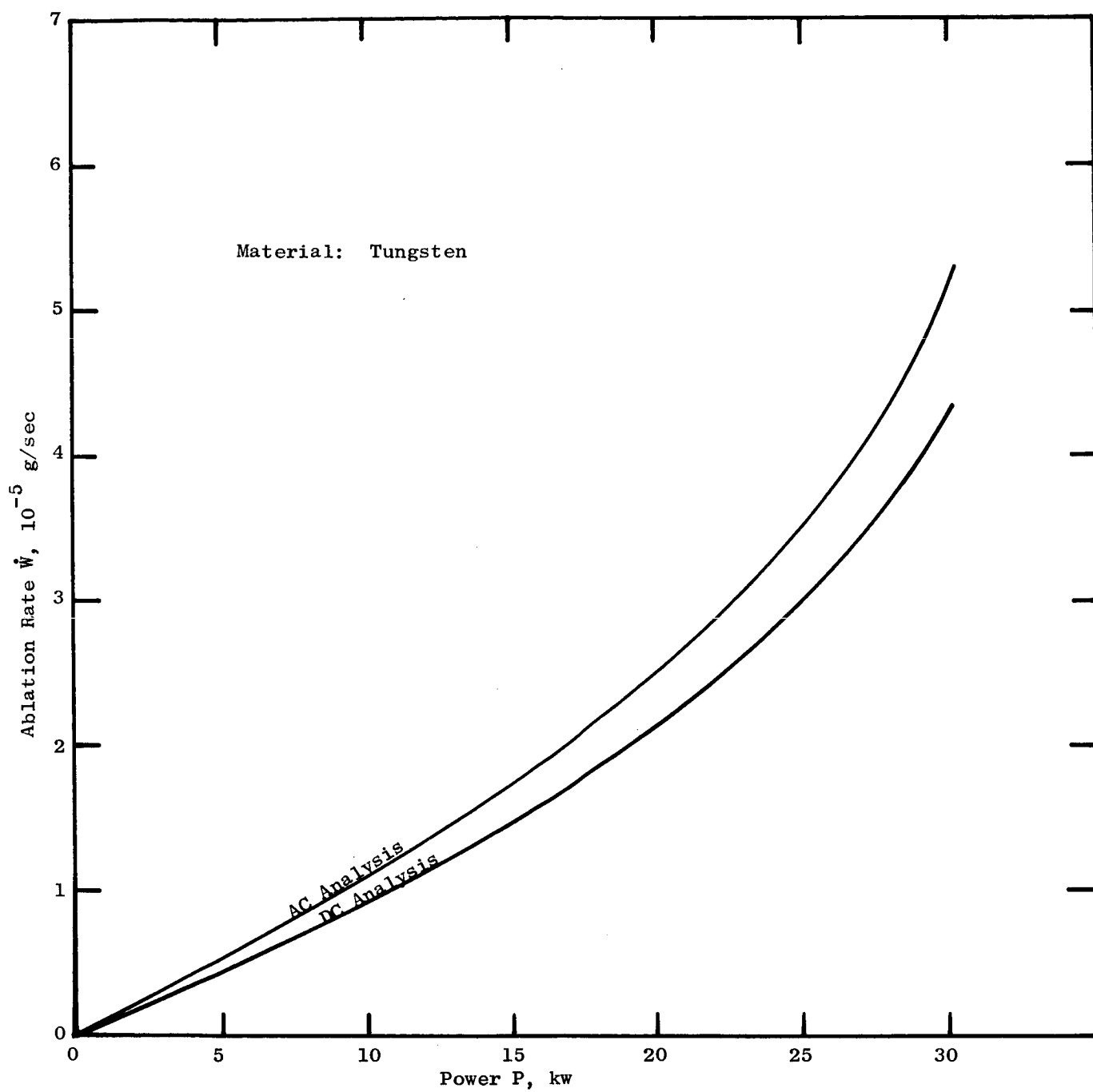


Fig. III.11: AC and DC Ablation Rates of the Center Electrodes
Three-Phase Engine, Atmospheric Stagnation Pressure

emission of thoriated tungsten is usually written in the form

$$j_e = A_1 T^2 \exp (-b_o/T)$$

where values of A_1 and b_o are reported by different sources (Ref. 5 and 6) as

$A_1 = 0.33$	$b_o = 23,200$
$A_1 = 3-15$	$b_o = 30,100-33,600$
$A_1 = 35.5$	$b_o = 35,400$
$A_1 = 3$	$b_o = 29,340$

The third set of constants were actually used in the calculations for the thoriated tungsten electrodes because they come from an actual experiment graph. However, this points up the uncertainties in the material values for thoriated tungsten.

Therefore, the analytical result for the ablation rate of thoriated tungsten electrodes is necessarily uncertain until the constants used in the energy balance equation are verified. The results of the ablation analysis for thoriated tungsten electrodes are shown in Fig. III.12. From these it can be concluded that thoriated tungsten should ablate somewhat less than tungsten. The difference between tungsten and thoriated tungsten will probably not be as large as indicated by this analysis which is based on rather uncertain material data.

Not enough experimental data have been obtained with the thoriated tungsten electrodes to enable a fair comparison with the analysis. However, the ablation rates thus far measured seem to show that the thoriated tungsten ablation curve actually lies very close to the tungsten curve at the 30 kw power level. The reason for this rather high ablation rate for thoriated tungsten is apparently the presence of melting on the surface of the electrode. Electrodes should never be used at temperatures above their melting point because the ablation rate can get very high. The melting point of thoriated tungsten is 100-300°K lower than for pure tungsten.

III.2.4 Operation at Higher Pressures

It has been shown elsewhere that greater thrust efficiency can be obtained if an arc jet engine can be designed to operate at higher than atmospheric pressure. However, there has been some question as to how great an effect this would have on the ablation rate.

The preceding analysis can be applied to the case of an arc jet designed to operate at a stagnation pressure of two atmospheres and at the same specific impulse as the one atmosphere engine. The results of the analysis are shown in

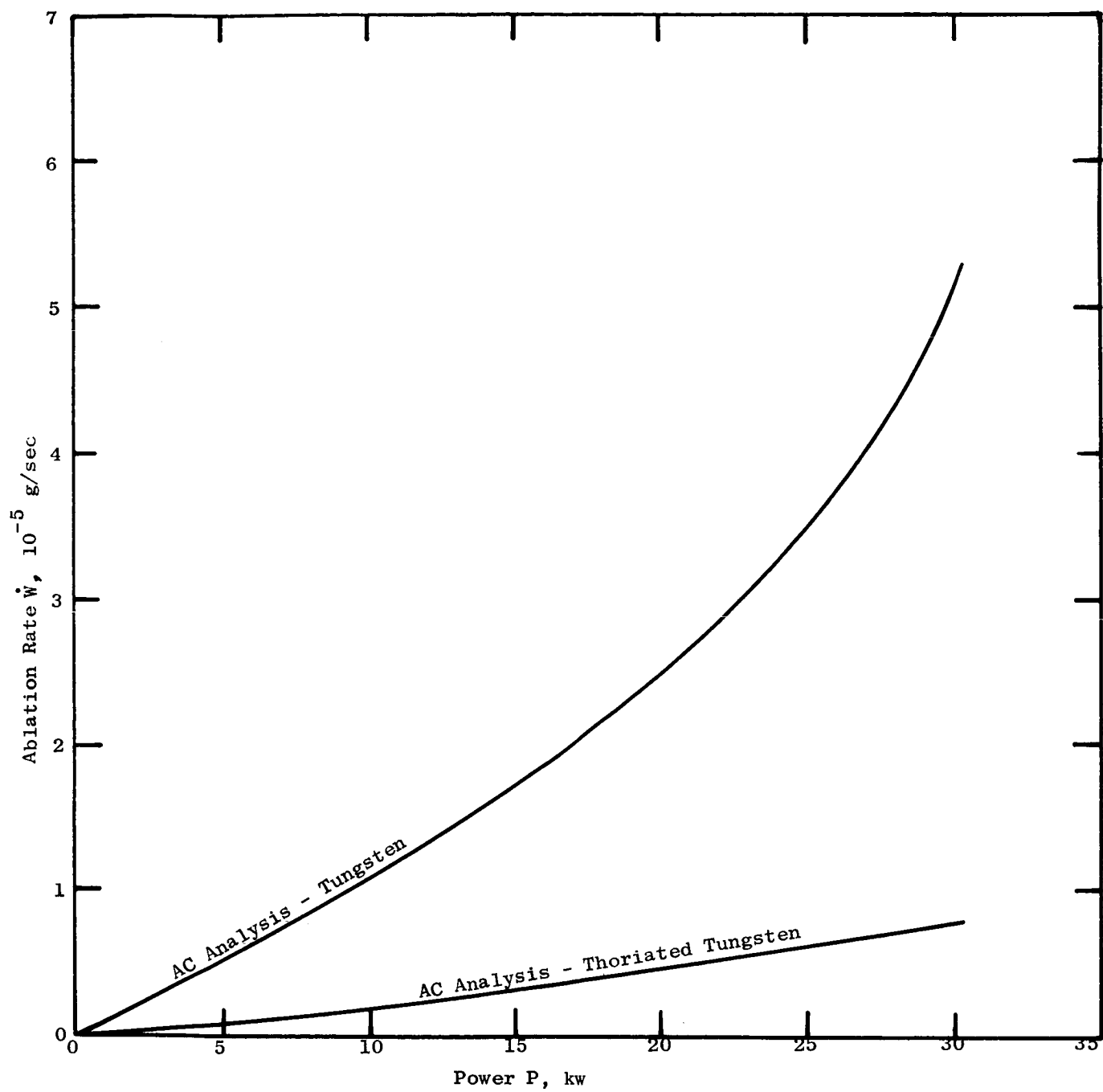


Fig. III.12: Ablation Rates of Tungsten and Thoriated Tungsten Electrodes, Three-Phase Engine, Atmospheric Pressure

Fig.III.13. It can be seen that the ablation rate is somewhat higher for operation at the higher stagnation pressure.

III.2.5 Methods to Decrease Electrode Ablation

When a reliable analysis for electrode ablation is available, possible methods to decrease the ablation rate can be determined. The analysis indicates that ablation rates can be influenced by changes in the materials, the geometry of the electrodes or the operating conditions.

The important characteristics for an electrode material are to withstand high temperatures, to have a high electron emission rate, and a low evaporation rate. The parameter (j_e/w) has been devised to provide a useful comparison between different materials. It will be defined as the Relative Emission Factor, that is

$$\text{Relative Emission Factor} = \frac{j_e}{w} = \frac{A_1 T^2}{C_2} \sqrt{\frac{2\pi Q T}{M}} e^{-\frac{1}{kT} (\phi_o \epsilon - LM)}$$

where

C_2 = constant appearing in the vapor pressure equation, $P_v = C_2 e^{-\frac{LM}{QT}}$

Q = universal gas constant, 8.317 joule/ $^{\circ}$ K

k = Boltzmann's constant = 1.38×10^{-23} joule/molecule

ϵ = charge on an electron = 1.602×10^{-19} coulomb

M = atomic mass of the material, g

A graph of the Relative Emission Factor for tungsten and for tantalum is shown in Fig.III.14. In order to minimize the ablation at a given power level, it is desirable to maximize the Relative Emission Factor. Therefore, as can be seen from the graph, it would be preferable to operate at a low temperature and to use tantalum rather than tungsten as the electrode material. However, in order to achieve desired specific impulse levels with hydrogen as propellant, it is often necessary to operate at a stagnation temperature of about 3600 $^{\circ}$ K. In this case tantalum cannot be used because of its lower melting point.

The effects of changes in electrode geometry and operating conditions have been investigated both experimentally and analytically. For instance, operation at chamber pressures as low as 5 psia has been performed. The experimental results show a slight decrease in the ablation rates which is in agreement with the theoretical predictions.

Another modification to the electrode geometry which is being investigated is to increase the size of the electrode. This procedure decreases the ablation rate because of the increased conduction through the electrode. Therefore, the electrode operates at a lower temperature which decreases the ablation rate. Also, the amount of electrode material has simultaneously been increased so that the

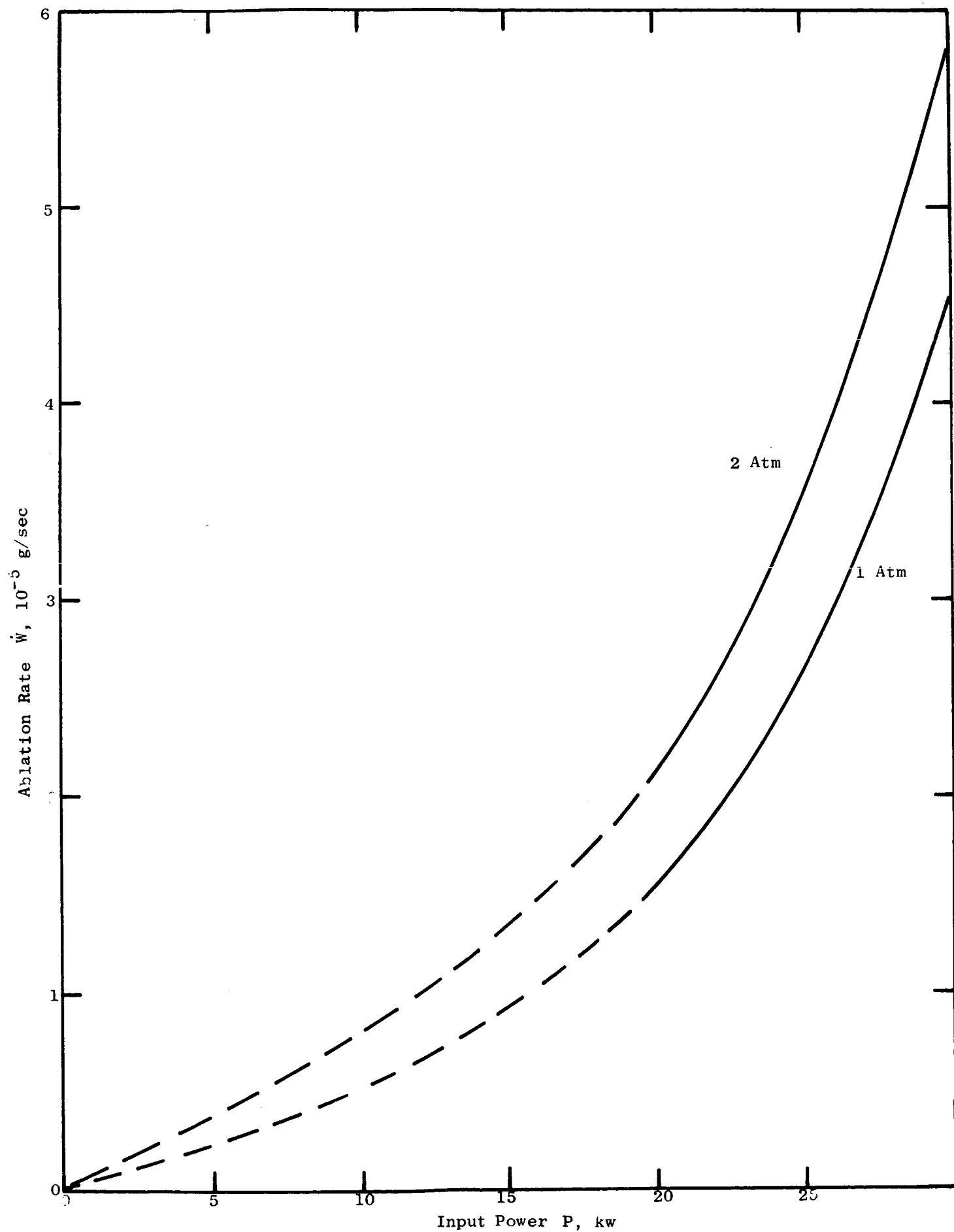


Fig.III.13: Effect of Pressure on Ablation Rate (Tungsten Electrode)

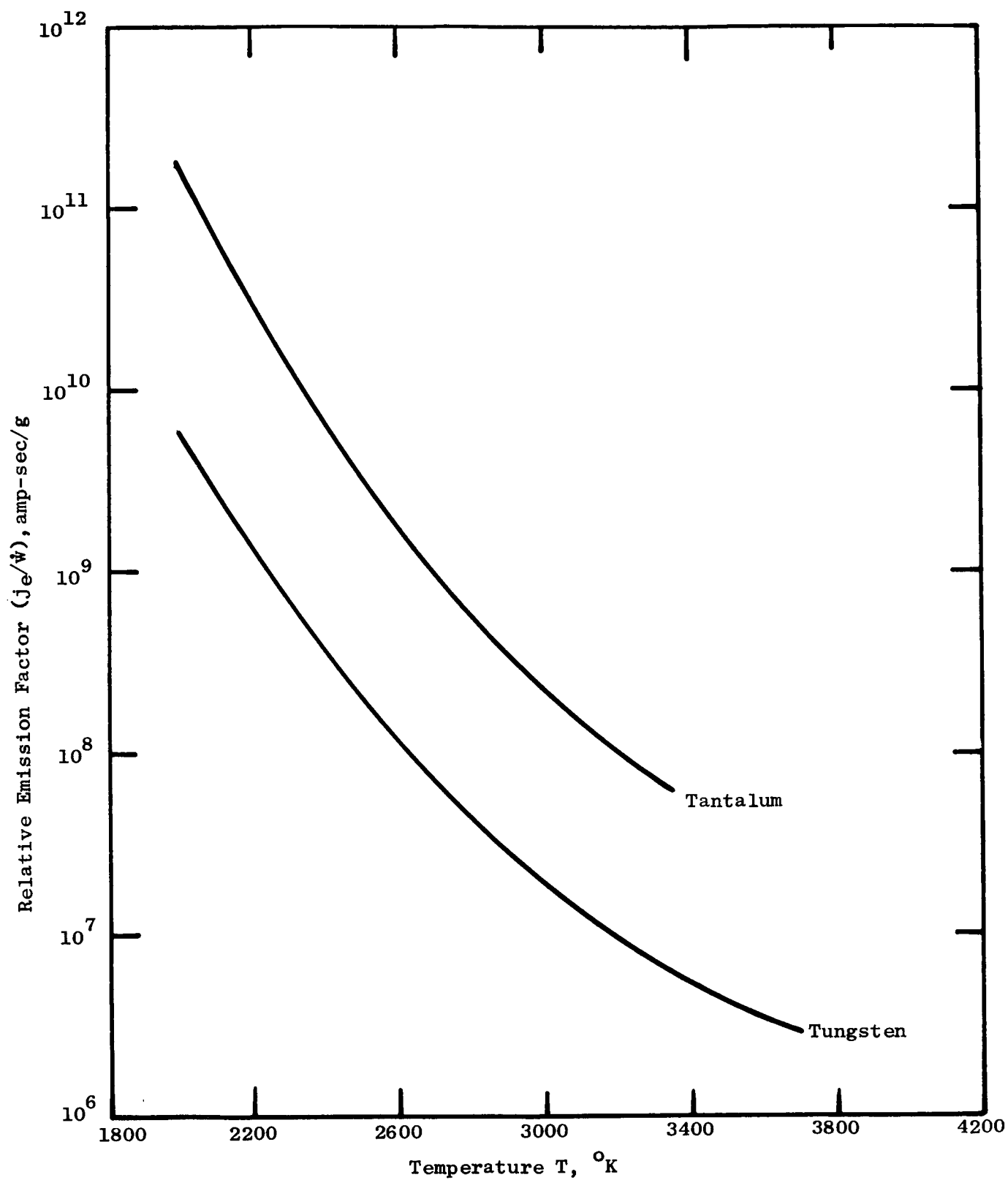


Fig. III.14: Relative Emission Factor for Tungsten and Tantalum

useful electrode operating life has been increased in two ways. The comparison between predicted ablation rates for 1/2 inch and 3/4 inch tungsten electrodes is shown in Fig. III.15.

III.2 Ablation Rates for a 7.5 KW Engine

The ablation rates for the electrodes of a single phase 7.5 kw engine can be analyzed by the same procedures used for the 30 kw engine. The results of these analyses are shown in the section of this report on single phase testing. It can be seen that they demonstrate rather good agreement with the data even at low power levels.

III.4 Conclusions

The theoretical investigation of the ablation phenomenon of electrode material in plasma arc jet engines has yielded valuable information on the parameters most dominantly affecting the lifetime of electrodes. The analytical results have shown good agreement with the ablation rate data measured with the 30 kw three-phase plasma arc jet engine and a 7.5 kw single phase plasma arc jet engine. The most important results are

1. The ablation rate of plasma arc jet engines can be predicted analytically with a fair degree of accuracy.
2. The combined ablation rate of all three electrodes in a three-phase plasma arc jet engine is slightly higher than the ablation rate of the cathode of a dc plasma arc jet engine.
3. The ablation rate of the nozzle of a three-phase plasma arc jet engine is probably less than that of a dc engine whose nozzle functions as the anode.
4. From conclusions 2 and 3 it follows that the three-phase plasma arc jet engine will probably operate with higher performance but with a slightly shorter electrode lifetime than a dc engine of the same power and performance design.

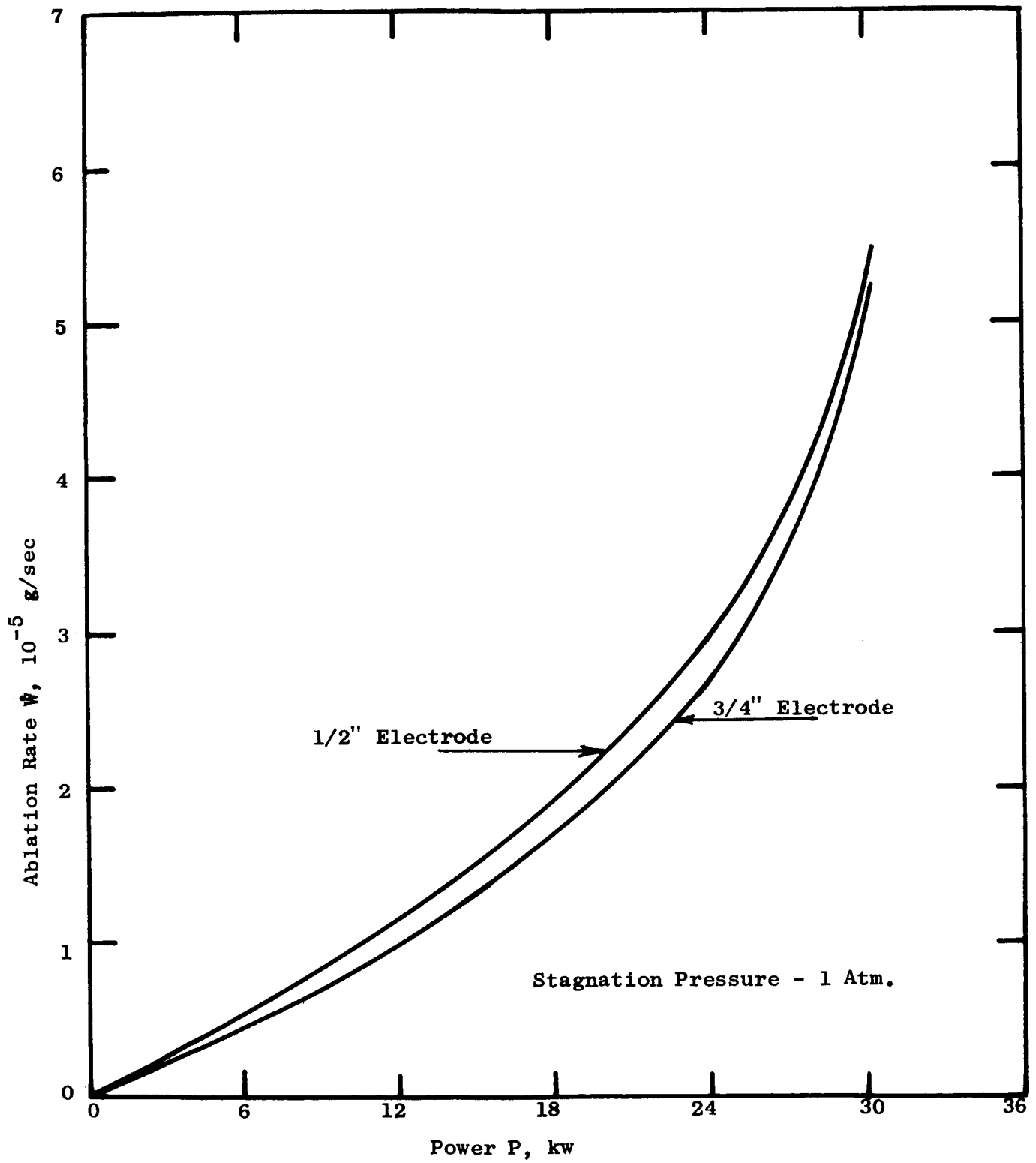


Fig. III.15: Ablation Rates for an AC Arc with Different Size Tungsten Electrodes

APPENDIX IV

IV. SELECTION OF OPTIMUM NOZZLE AND ELECTRODE MATERIALS

IV.1 Testing for Optimum Nozzle Material

In order to arrive at a decision for the selection of the best suited tungsten material for the 30 kw plasma arc jet engine, a comparison of three materials was made. These three materials are:

1. Extruded tungsten with a density of better than 99.3%.
2. 2% ThO₂ - tungsten extruded to a density of better than 99.3%
3. 2% ThO₂ - tungsten sintered

From the operational behavior with respect to arc current, no distinct difference between the three materials was observed. This was rather surprising as it had been expected that the thoriated tungsten would result in higher currents due to the higher electronic emissivity at a given temperature. This was not found to have any effect on the arc operation in the case of the three-phase engine operating with non-thoriated tungsten center electrodes. There was, however, a very distinct difference in the appearance of the nozzle areas that were exposed to the arc.

IV.1.1 Extruded Tungsten

The extruded tungsten nozzles, of which two were tested, showed a very pronounced tendency to experience a high degree of ablation whenever the arc stagnated. The results of these tests, in comparison with the results of the tests with the other materials available, actually raised the question as to whether stagnation of the arc is aggravated by the use of the non-thoriated tungsten material. In the area where the arc stagnated deep, indentations were made by the flow that swept the molten material into the nozzle throat. In case of stagnation the tests had to be terminated because of a sudden rise in the arc chamber pressure and visible signs of ablation.

While nozzles made from one batch of material indicated several small longitudinal cracks forming after the first operation, only a single nozzle of the second batch showed a minor fissure of no consequence. This nozzle never cracked any more despite repeated startups and shutdowns.

IV.1.2 Extruded 2% ThO₂ Tungsten

Nozzles made out of 2% thoriated tungsten behaved quite differently from those made of pure tungsten. Right after the first operation small axial cracks would be visible. These cracks would remain almost of the same size. A nozzle made of this material was cycled 30 times. After inspection no difference from the previous appearance was found. These cracks had no effect on the engine performance so no attempt was made to stress-relieve the nozzle before starting

While large removal of material was found to occur quite often with the non-thoriated tungsten nozzle, stagnation has apparently no detrimental effect on the thoriated tungsten nozzle. Closing of the nozzle throat has never occurred with this nozzle and no indentations were seen in the area of arc attachment.

IV.1.3 2% ThO₂ Sintered Tungsten

The 2% thoriated sintered tungsten performed very well during operation. After the first test run the signs of arc attachment were almost completely absent. However, there were a large number of axial hairline cracks and one circumferential crack. Upon disassembly of the engine the nozzle broke completely along the circumferential crack.

This behavior of the sintered nozzle was not unexpected as during machining the material indicated a tendency to break along the edges.

IV.1.4 Conclusion

Of the three materials the extruded 2% thoriated tungsten was selected as the best suited material for the plasma arc jet engine nozzle at the present time. This material is being selected with the reservation that when a better understanding about the stagnation phenomenon of the arc has been obtained, the non-thoriated extruded tungsten might be considered preferable. At the present time extruded 2% thoriated tungsten has been shown to stand up best in the present engine design. The small axial cracks which occur after the first start-up do not affect the engine performance nor do they deteriorate with time. This nozzle was able to withstand a large amount of thermal cycling without failure.

Sintered thoriated tungsten is not acceptable as a plasma arc jet engine nozzle material as it is highly susceptible to thermal cracking.

IV.2 Testing of Thoriated Tungsten Electrodes in Engine Y16-2

Two percent thoriated tungsten electrodes had previously been tested in Engine Y16-1. In those tests it was found that the ablation rate of thoriated tungsten electrodes was much higher than the ablation rate of non-thoriated pure tungsten electrodes.

When testing a 1% thoriated tungsten electrode in the 7.5 kw single phase engine, ablation rate data were obtained which were considerably below those measured with a non-thoriated tungsten electrode. This difference in ablation rate was found for dc as well as for ac operation. Based on these data it was felt that the earlier measured ablation rates with thoriated tungsten in the Y16-1 engine might have been erroneous and should be rechecked.

The 2% thoriated tungsten electrodes were installed in Engine Y16-2 with a gap of zero setting (see Fig. 3.5), a gap setting that has been found to permit the engine to operate stably at 30 kw with non-thoriated electrodes. The engine achieved a power level of 30 kw at an average current of 116.7 amps ($I_A = 119$ amps,

$I_B = 117$ amps, $I_C = 114$ amps). The power in each line was 9.7 kw, 9.2 kw and 11.5 kw respectively. The engine was operated under these conditions for 3 hours and 19 minutes.

After this run the electrodes were weighed and an ablation rate of 4.43×10^{-5} and 2.93×10^{-5} g/sec for the respective electrodes was determined. The area of arc attachment was rather rugged and very uneven. Balls of metal of various sizes had formed as can be seen in Fig.IV.1. This appearance of the electrodes was quite different from the appearance the electrodes had after only 1 hour operation. At that time only a very small area of arc attachment in the center of the electrodes could be seen.

Comparing the 1 hour run with the 3 hour, 19 minute run it was found that during the last half hour of the long run the engine operated rather unstably with the mode of operation varying almost continuously. During the 1 hour run, on the other hand, the engine operated absolutely stably in the upper power mode. From the visible appearance of the exhaust plume and the signs of arc attachment in the nozzle it can be deduced that the low power mode in Engine Y16-2 is associated with an arc operation completely upstream of the nozzle throat. In the upper power mode the arc is apparently drawn through the nozzle throat. In the low power mode the center electrodes are therefore exposed to much higher temperatures. Thorium, produced from reduction of thoria by tungsten, vaporizes at a high rate and accelerates electrode ablation. The overall high ablation rate during the 3 hour 19 minute run might therefore have to be attributed to the unfavorable operating condition at the end of the run.

The tests of 2% thoriated tungsten electrodes therefore indicated that thoriated tungsten is not as good a material as non-thoriated tungsten for the center electrodes of the three-phase plasma arc jet engine of the present design, and testing of this material was concluded.

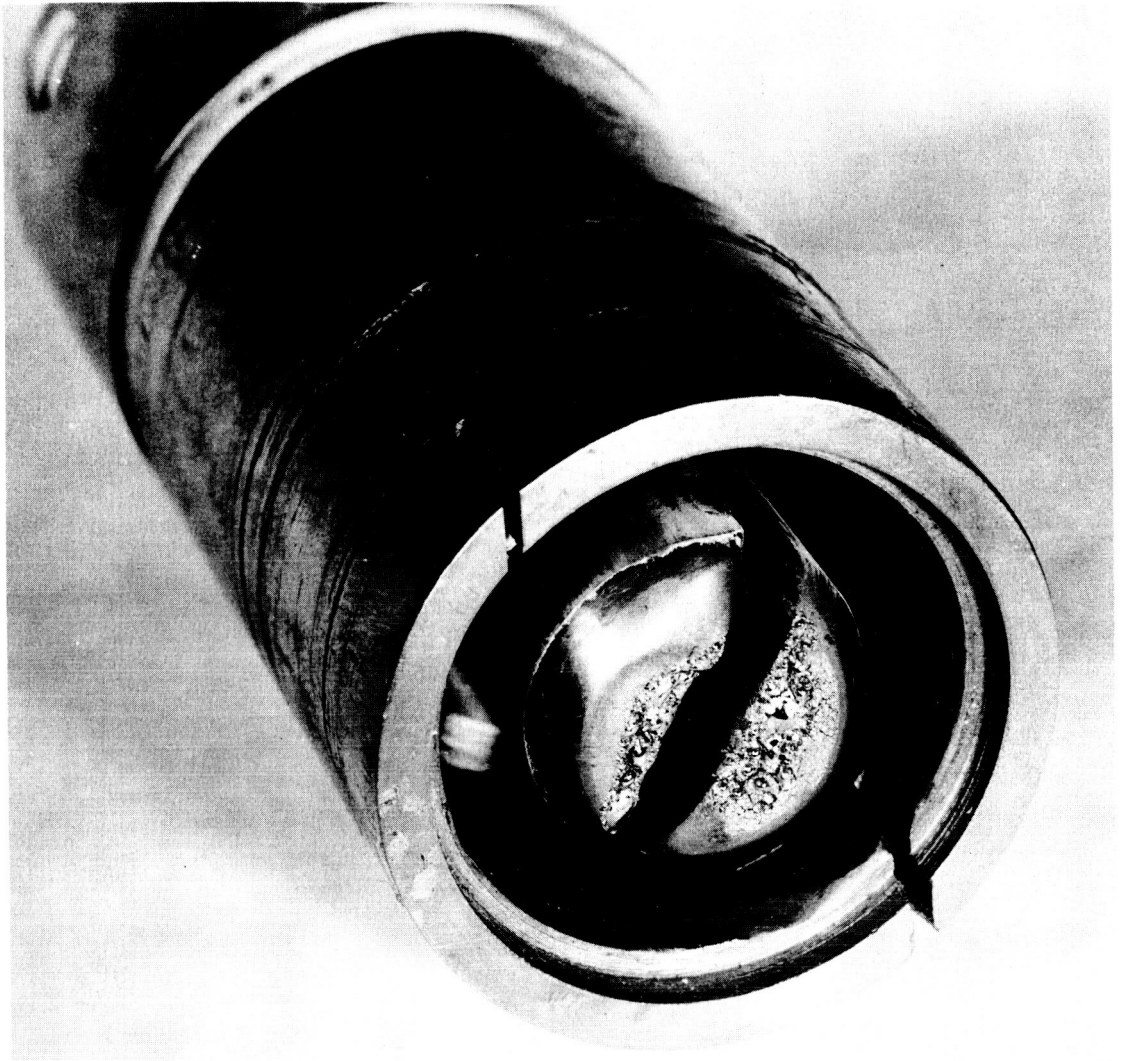


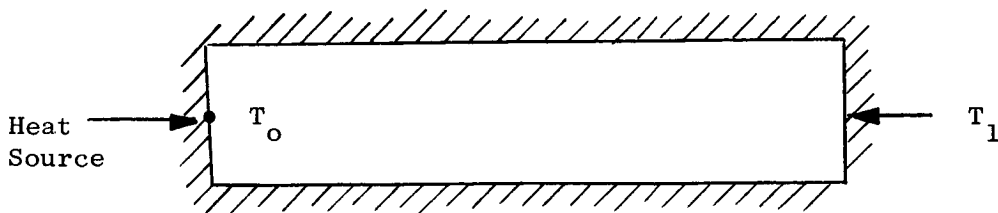
Fig.IV.1: Electrodes of Engine Y16-2 After 3 Hrs. 19 Minutes Operation

APPENDIX V

HEAT CONDUCTION THROUGH THE ELECTRODE

In performing an energy balance at the end of an arc engine electrode, one term that must be considered is the conduction through the electrode. This can be done by assuming a one-dimensional heat flow at the electrode face, and then introducing a correction term to account for the two-dimensional effects. The analysis to determine the correction factor involves solution for the temperature distribution in a rectangle with insulated sides and a heat source at one end. The analysis to determine the correction factor follows:

Let us assume a two-dimensional flow pattern



Let us assume a flow field

$$w = C \ln \sinh \frac{\pi z}{a}$$

Now $\sinh t$ can be expanded into

$$\sinh t = t \prod_{n=1}^{\infty} \left(1 + \frac{t^2}{n^2 \pi^2} \right)$$

so that

$$\begin{aligned} w &= C \left[\ln \frac{\pi z}{a} \cdot \prod_{n=1}^{\infty} \left(1 + \left(\frac{z}{na} \right)^2 \right) \right] \\ &= C \ln \frac{\pi z}{a} + C \ln \left(1 + \left(\frac{z}{a} \right)^2 \right) + C \ln \left(1 + \left(\frac{z}{2a} \right)^2 \right) + \dots \end{aligned}$$

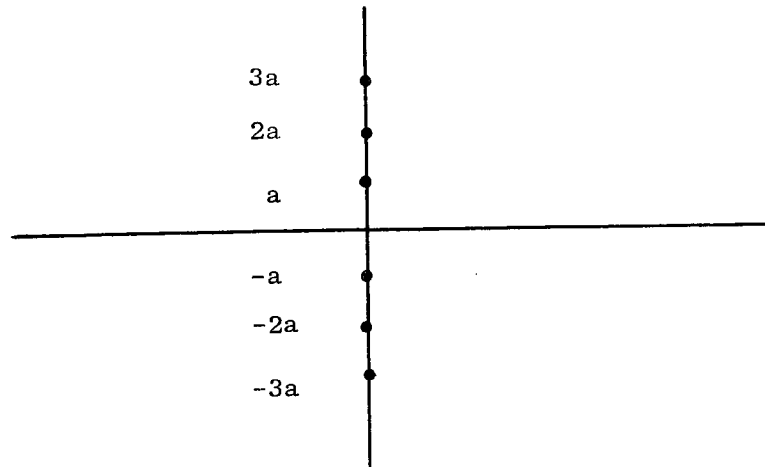
Now

$$1 + \frac{z^2}{n^2 a^2} = \frac{(z + i a n) (z - i a n)}{n^2 a^2}$$

so that

$$\begin{aligned} w = & C \ln z + C \ln (z + i a) + C \ln (z - i a) + C \ln (z + 2 i a) + \\ & C \ln (z - 2 i a) + \dots \\ & + C (\ln \pi/a - \ln a^2 - \ln (2a)^2 - \ln (3a)^2 + \dots) \end{aligned}$$

When a is a constant real number, w is the complex potential due to an infinite number of sources of equal strength $2\pi C$ equally spaced apart by a distance a on the y axis



Because of symmetry there can be no flow across $\pm a/2, \pm 3a/2, \pm 5/2 a, \dots$. For all practical purpose $y = \pm a/2, \pm 3/2 a, \dots$ can be boundaries of the flow field. Returning to

$$w = C \ln \sinh \frac{\pi z}{a}$$

and using the relationship

$$\sinh z = \sinh (x + iy) = \sinh x \cos y + i \cosh x \sin y$$

we have

$$w = C \left(\ln \sinh \frac{\pi}{a} x \cos \frac{\pi}{a} y + i \cosh \frac{\pi}{a} x \sin \frac{\pi}{a} y \right)$$

which becomes

$$w = \phi + i\psi = C \ln \left(\sinh^2 \frac{\pi x}{a} \cos^2 \frac{\pi y}{a} + \cosh^2 \frac{\pi x}{a} \sin^2 \frac{\pi y}{a} \right) \\ - \frac{C}{2} \ln \left(\sinh \frac{\pi x}{a} \cos \frac{\pi y}{a} + \cosh \frac{\pi x}{a} \sin \frac{\pi y}{a} \right) - i(\theta + 2\pi k)$$

In our case

$$\frac{\partial T}{\partial x} \text{ is } \frac{\partial \phi}{\partial x}$$

and

$$\left(\frac{\partial \phi}{\partial x} \right)_{x=ma} = \left(v_x \right)_{\substack{x=ma \\ y=0}} = \frac{C/2}{\sinh^2 \frac{\pi x}{a} \cos^2 \frac{\pi y}{a} + \cosh^2 \frac{\pi x}{a} \sin^2 \frac{\pi y}{a}} \\ \cdot \left(2 \frac{\pi}{a} \sinh \frac{\pi x}{a} \cosh \frac{\pi x}{a} \cos^2 \frac{\pi y}{a} + 2 \frac{\pi}{a} \cosh \frac{\pi x}{a} \sinh \frac{\pi x}{a} \sin^2 \frac{\pi y}{a} \right)$$

which reduces to

$$\left(v_x \right)_{\substack{x=ma \\ y=0}} = \frac{2\pi}{a} \cdot \frac{C}{2} \coth m\pi$$

and

$$\left(\frac{dT}{dx} \right)_{\infty} = \left(v_x \right)_{\substack{x=\infty \\ y=a}} = \frac{2\pi C/2}{a}$$

Now

$$m = \frac{x}{a} = \text{ratio of equivalent source area to electrode area}$$

so

$$m = \frac{A}{A_o}$$

therefore

$$\frac{\left(\frac{dT}{dx}\right)_{ma}}{\left(\frac{dT}{dx}\right)_{\infty}} = \frac{\left(\frac{v}{x}\right)_{x=ma}}{\left(\frac{v}{x}\right)_{x=\infty}} = \coth m\pi = \coth \frac{A\pi}{A_o}$$

Therefore, the correction factor to be applied to the one-dimensional problem is $\coth A\pi/A_o$, so that the conduction term becomes

$$\frac{q}{A} = -k \frac{\Delta T}{\Delta x} \coth \frac{A\pi}{A_o}$$

This term has therefore been incorporated in the energy balance equation used for the ablation analyses.

APPENDIX VI

MAXIMUM HEAT CONDUCTION THROUGH A GAS

In the energy balance equation for an electrode a significant part of the heat input was found to be due to conduction from the hot arc column. Since this conduction term is large, it should be investigated that it does not exceed the maximum conduction possible by the kinetic theory.

From Jeans (Ref. 6, page 47), the maximum energy that can be transferred by gas particles across a distance λ' is given by

$$\bar{q}_{\max} = \lambda' \frac{d\bar{E}}{dz} \quad (1)$$

where λ' is the projection of the free path λ on the z axis and \bar{E} is the energy of a gas particle, $\bar{E} = 3/2 kT$ for a monatomic gas and $\bar{E} = 5/2 kT$ for a diatomic gas without the vibrational energy modes excited.

The maximum energy transferred per unit area is therefore

$$\frac{q}{A} = n \bar{C} \lambda' \frac{d\bar{E}}{dz} \quad (2)$$

where

n = particle density, cm^{-3}

\bar{C} = average particle velocity, cm/sec

For a gas with a Maxwellian velocity distribution

$$\bar{C} = 2 \sqrt{\frac{2 kT'}{\pi m}} \quad (3)$$

where T' is the average temperature in the electrode voltage drop region

$$T' = \frac{T_o + T}{2} \quad (4)$$

from Jeans

$$\lambda' = 1/2 \lambda \quad (5)$$

and assuming

$$dz = \lambda \quad (6)$$

Then equation (2) becomes

$$\frac{q}{A} = n \sqrt{\frac{2 kT'}{\pi m_H}} d\bar{E} \quad (7)$$

For a gas composed of atomic and molecular hydrogen

$$\frac{q}{A} = n_H \sqrt{\frac{2kT}{\pi m_H}} d\bar{E}_H + n_{H_2} \sqrt{\frac{2kT}{\pi m_{H_2}}} d\bar{E}_{H_2} \quad (8)$$

From the thermodynamic relations the dissociation x and the density ρ of the gas are given. Then

$$x = \frac{n_H}{n_H + 2 n_{H_2}} \quad (9)$$

and

$$\rho = n_H m_H + n_{H_2} m_{H_2} \quad (10)$$

where

$$2m_H = m_{H_2} \quad (11)$$

Equations 9, 10, and 11 give

$$n_{H_2} = \frac{\rho}{m_{H_2}} (1 - x) \quad (12a)$$

$$n_H = \frac{\rho x}{m_H} = \frac{2\rho x}{m_{H_2}} \quad (12b)$$

Also

$$d\bar{E}_{H_2} = 5/2 k (T_o - T) \quad (13a)$$

$$d\bar{E}_H = 3/2 k (T_o - T) \quad (13b)$$

Inserting equations (12) and (13) into equation (8) the maximum heat transfer is given by

$$\frac{q}{A}_{\max} = \frac{\rho k (T_o - T)}{2m_{H_2}} \sqrt{\frac{2kT}{\pi m_{H_2}}} \left(6\sqrt{2} x + 5 (1-x) \right) \quad (14)$$

This equation therefore gives the maximum heat conduction in a gas

composed of H atoms and H₂ molecules. This result can be compared with the heat conduction terms used in the ablation analyses. Calculations were made for a few typical cases.

For a 1/2" tungsten electrode in a 30 kw engine:

$$\frac{q}{A} = \frac{k_g (T_o - T)}{d_c} = -1382 \text{ watts/cm}^2$$

$$\frac{q}{A}_{\text{max}} = -1.186 \times 10^{+5} \text{ watts/cm}^2$$

Therefore the calculated value of heat conduction is only about 1% of the maximum possible value according to kinetic theory.

APPENDIX VII

VII. THE PERFORMANCE ANALYSIS OF ENGINE Y16-2

After a thorough analytical study of a 30 kw plasma arc jet engine with respect to overall efficiency had been made, the design of the Y16 engines was based on a weight flow rate of 5×10^{-4} lb/sec and a stagnation pressure of 1 atm. The selection of the stagnation pressure of 1 atm was based mainly on the observation that the ablation rate of electrode material increased with increasing stagnation pressure. Though higher stagnation pressures would improve the overall efficiency of the plasma arc jet engine, the desired long duration operation of the engine made the selection of 1 atm stagnation pressure advisable.

Based on the final Y16-2 nozzle design the performance of the engine was predicted to be

Thrust $T - 0.52$ lb

Specific Impulse $I_{sp} - 1020$ seconds

under the condition of

Propellant Weight Flow Rate $\dot{W} - 5 \times 10^{-4}$ lb/sec

Applied Power $P - 30$ kw

Ambient Pressure $P_a - 1$ mm Hg

VII.2 Accuracy and Applicability of Measured Performance

At the present time the accuracy with which the two performance values are determined are

$$\text{Efficiency} \left[\frac{\Delta \eta}{\eta} \right]_{ab.} = \pm 4\% \text{ absolute}$$

$$\frac{\Delta \eta}{\eta} = \pm 2.45\% \text{ mean}$$

$$\text{Specific Impulse:} \left[\frac{\Delta I_{sp}}{I_{sp}} \right]_{ab.} = \pm 2\% \text{ absolute}$$

$$\frac{\Delta I_{sp}}{I_{sp}} = \pm 1.4\% \text{ mean}$$

While the actual performance of the engine can be greater or less by the above given possible deviations due to the limitations set by the instrumentation, the performance of the engine itself can vary by an even greater amount due to changes in the ambient conditions in which the engine operates. The assumption is made that the ambient pressure in the tank is 1 mm Hg. However, due to intermittent changes in the steam pressure which is used for the vacuum system of the test tank, and the temperature of the exhaust gases, the pressure in the tank can vary by ± 0.5 mm Hg. A short calculation shows that these variations have a major effect on the performance.

The thrust produced by the engine is the sum of the momentum of the gas and the pressure difference across the exit plane of the nozzle. This is expressed by

$$T_2 = \frac{V}{g} \dot{W} + A (p_{ex} - p_a)$$

The nozzle has an expansion ratio of $p_o/p_{ex} = 475$. The exit pressure is therefore

$$p_{ex} = \frac{14.7}{475} = 0.03094 \text{ psia}$$

The ambient pressure is 1 mm Hg

$$p_a = 0.01933 \text{ psia}$$

The nozzle exit area is

$$A_{ex} = 0.986588 \text{ in}^2$$

so that the thrust contribution due to the pressure differential is

$$T_{\Delta p} = 0.986588 \times (0.03094 - 0.01933) = 0.01 \text{ lb}$$

and the specific impulse contribution at a flow rate of 5×10^{-4} lb/sec is

$$I_{sp \Delta p} = \frac{0.01 \text{ lb}}{5 \times 10^{-4} \text{ lb/sec}} = 20 \text{ sec}$$

If the ambient pressure rises to 1.5 mm Hg

$$I_{sp \Delta p} \approx 0$$

If the ambient pressure rises to 2 mm Hg

$$I_{sp \Delta p} \approx -20 \text{ sec}$$

On the other hand if the ambient pressure drops to 0.5 mm Hg the specific impulse contribution increases to

$$I_{sp} \Delta p = 0.986588 \times (0.03094 - 0.00916) = \frac{0.021488}{5 \times 10^{-4}} = 43 \text{ sec}$$

These results are shown in tabulated form in Table 13.

p_a , mm Hg	0.5	1.0	1.5	2.0
I_{sp} , sec	1043	1020	1000	980
$\frac{\Delta I_{sp}}{I_{sp}}$	+0.02254	0	-0.0196	-0.03921
$\frac{\Delta \eta}{\eta}$	+0.045	0	-0.0392	-0.07842
η	40.34	38.6	37.1	35.6

Table 13: Effects of Ambient Pressure on Engine Performance

VII.2 Test Results of the Experimental Performance Envelope Determination

It is rather important to keep the results of the section on accuracy and applicability of measured performances in mind when interpreting the data presented in Table 14. The data were obtained by varying the flow rate and the power to Engine Y16-2 and always returning to the design point of 30 kw and 5×10^{-4} lb/sec flow rate. In Fig. VII.1 only the test data obtained with a flow rate of 5×10^{-4} lb/sec are plotted with the analytically predicted performance curve for this flow rate superimposed. The analytical curve has been bounded by the accuracy limits. As can be seen, except for one data point all test points fall inside of the test accuracy range. The performance map of engine Y16-2 is shown without test points in Fig. VII.2.

Point	Power, P kw	Flow Rate, W lb/sec	Displacement, d mils	Thrust, T lb	Specific Impulse I _{sp} , sec.	Efficiency, percent	Current amps
1	23	5.0 x 10 ⁻⁴					119
2	26	5.0					-
3	30.5	5.025	37.6	0.5085	1012	36.8	128
4	29.8	5.0	37.9	0.5125	1025	38.5	118
5	29.5	5.025	38.1	0.5152	1025	39.1	121
6	25.5	5.0	36.8	0.4977	995	42.4	104
7	29.5	5.0	37.6	0.5085	1017	36.5	130
8	33	5.0	37.9	0.5125	1025	34.8	-
9	28.7	5.0	37.1	0.5017	1003	38.3	122
10	29.2	5.0	37.5	0.5071	1014	38.5	123
11	30.5	5.59	41.2	0.5572	997	39.7	125
12	29.3	5.0	37.3	0.5044	1009	37.9	123
13	29.0	5.0	37.3	0.5044	1009	38.3	-
14	27.1	3.6945	28.3	0.3827	1036	31.9	-
15	28.2	4.552	33.3	0.4503	988	34.4	-
16	28.5	4.926	35.8	0.4841	982	36.4	-
17	29.7	4.926	36.1	0.4882	991	35.6	-
18	27.5	3.842	29.8	0.4030	1049	33.6	-
19	29.5	5.123	37.3	0.5044	985	36.8	-
20	29.7	5.024	37.6	0.5085	1012	37.8	130
21	33	5.024	38.2	0.5166	1028	35.1	-
22	34	5.0	38.6	0.5220	1044	35.0	-
23	29.0	5.0	37.1	0.5017	1003	37.9	-
24	30.2	5.0	37.3	0.5044	1009	36.8	128
25	30.2	5.0	37.2	0.5031	1006	36.6	-
26	30.5	4.975	37.3	0.5044	1014	36.6	-
27	30.5	4.975	37.6	0.5085	1022	37.2	129

Table 14: Test Data of Engine Y16-2 (November 15, 1963) (36.97 mils/0.5 lb)

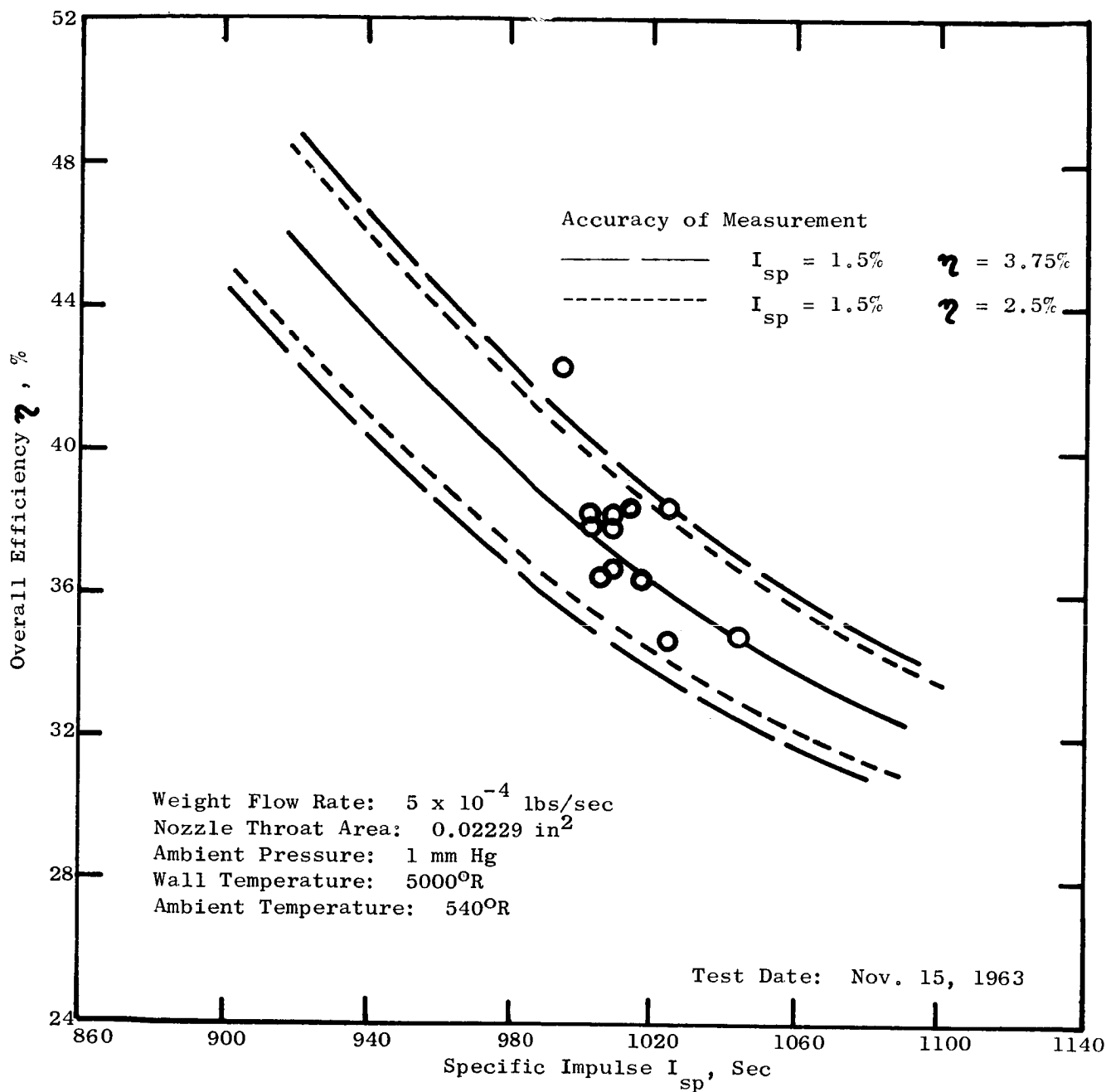


Fig. VII.1: Test Accuracy of Y16-2 Performance Test

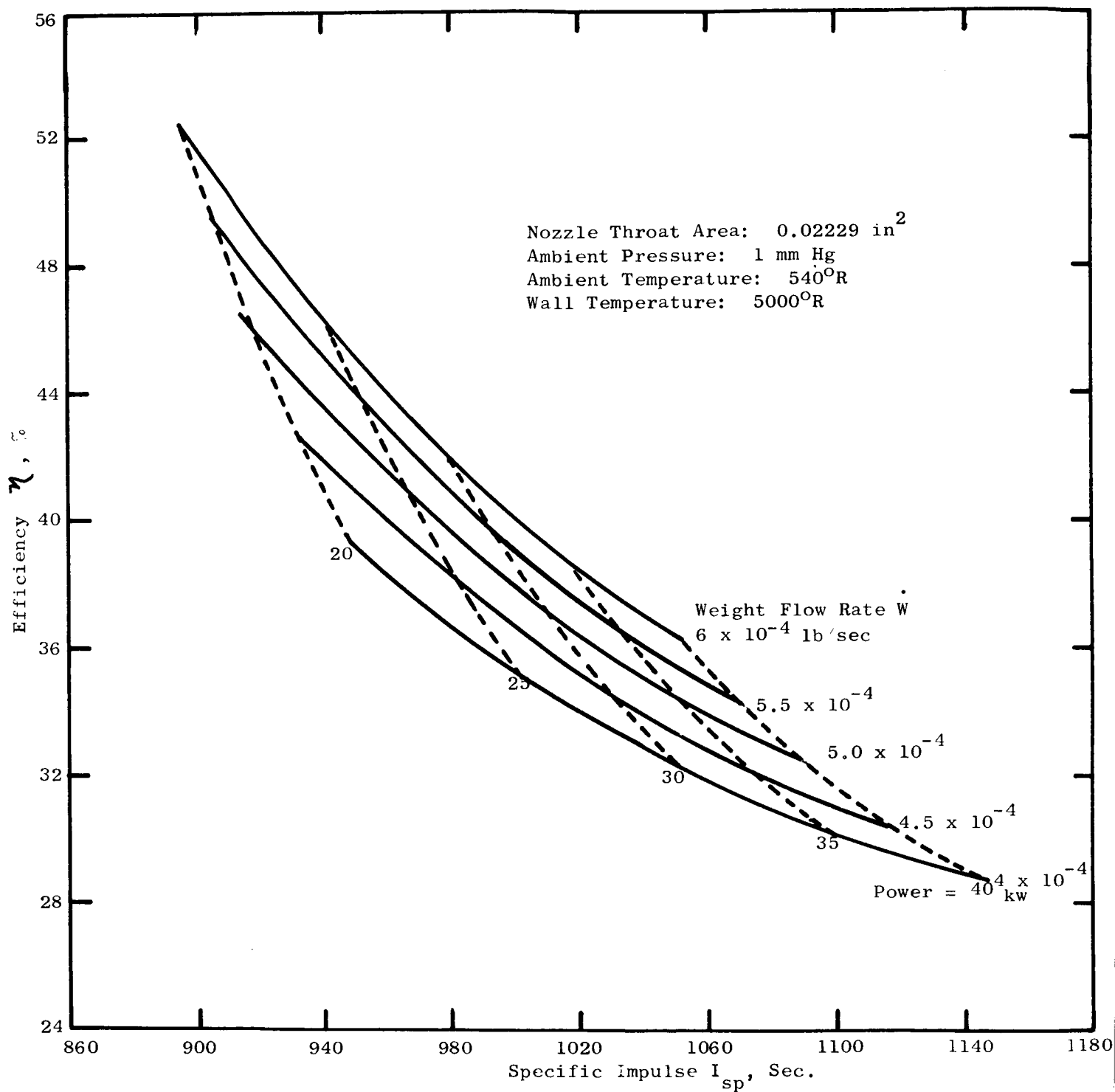


Fig. VII.2: Analytically Predicted Performance of Engine Y16-2 Design

APPENDIX VIII

30 KW THREE-PHASE PLASMA ARC JET ENGINE DESIGN

The present design of the 30 kw three-phase arc jet engine is based on the need for a test engine whose individual components can easily be modified without necessitating the redesign of other parts of the engine. Although the engine design presented in this section is not the optimum design for a flight engine, it proved to be a very convenient design for laboratory investigation.

The materials used in the design of the engine are:

<u>Component</u>	<u>Material Specification</u>
<u>Tungsten:</u>	
Electrodes	Fine grained 99.9% dense
Nozzle	2% ThO ₂ tungsten 99.9% dense
<u>Molybdenum:</u>	
Body	TZM Commercial
Deflector	TZM Commercial
Vortex Sleeve	TZM Commercial
Nut	TZM Commercial
<u>Boron Nitride:</u>	
Insulator	Commercial
Electrode Holder	Commercial
Separator	Commercial
<u>Stainless Steel:</u>	
Electrical Studs	300 Series
Propellant Studs	300 Series
Electrical Seal	300 Series
Swagelok Nut	300 Series
Set Screws	300 Series
<u>Inconel X:</u>	
Main "O" ring seal	Commercial Grade
Electrical "O" ring seal	Commercial Grade

There is a choice of material for the nut as it has been proven that stainless steel 431 or 446 can equally well be employed.

The weld that joins the nozzle to the engine body is made with a molybdenum wire. Neither before nor after the welding operation is a stress relieving operation required.

Assembly of Engine

No special procedures are required for assembly of the engine, but it was found that there exists a preferred way of assembly.

First, the insulator should be assembled permanently with the nut and the two Swagelok fittings. The nut is screwed over the insulator until it reaches the stop. Then it is backed up again by at least 1/2 turn until it is in position where the set-screw holes in the nut are 45° turned from the electrical lead holes in the insulator. In this position four holes, 0.15 to 0.20 in. deep, are drilled into the insulator through the set-screw holes in the nut. The nut and insulator are locked together with the four set-screws. The Swagelok nuts are placed into the insulator and the Swageloks with the metal 'O' rings in place are screwed tight into the nuts. Normally there should be no need for disassembly of this section again.

Next the electrode holder and the vortex sleeve are assembled. The vortex sleeve should fit tightly over the electrode holder. If the sleeve moves freely over the electrode holder a piece of mica can be used to obtain the tight fit.

The electrode holder-vortex sleeve is placed into the engine body making certain that the vortex sleeve and the nozzle body are fitted together correctly. The main 'O' ring is put into place and the insulator is screwed on the body with enough torque to compress the 'O' ring. This initial assembly will fix the relation between the electrode holder and vortex sleeve.

The engine is taken apart again and the electrodes with the separator are installed in the electrode holder. Their position is measured from the inner shoulder of the vortex sleeve. The electrodes are held in place by tightening the two set-screws in the electrode holder.

The deflector and the electrode holder assembly are placed into the engine. The insulator assembly is screwed on the engine body until the 'O' ring has been compressed by more than four mils. It is vitally important to have made sure that the threads in the body and the nut are absolutely clean of all foreign particles and that the threads are well coated with a molybdenum lubricant coat (NEVER-SEEZ is recommended).

The two electrical studs are inserted into the Swagelok fitting and alternately tightened up. The contact of the studs with the electrodes is ascertained by measuring the electrical continuity between the studs and the electrodes.

The Swagelok ferrules are placed over the studs and tightened down by the Swagelok nut.

Disassembly of Engine

Before trying to take the engine apart the joint between the engine body should be thoroughly soaked with penetrating oil. After about ten minutes of soaking the engine can be taken apart easily.

If there is any difficulty in unscrewing the insulator from the engine body the following steps should be taken:

1. Remove the electrical studs
2. Remove the Swagelok fittings

If this does not improve the situation, the problem lies in the screw joint between the engine body and the nut. Only by carefully working back and forth the nut, using plenty of penetrating oil, can the engine be opened up.



REV NO.	TITLE
PARTS LIST FOR	Three-Phase Plasma Arc Jet Engine, Y16
CONT ON SHEET SH NO.	FIRST MADE FOR NASA

SUBSTITUTIONS REQUIRE ENGINEERING APPROVAL

[illegible]PRINTS TO

MADE BY
Robert Richter

APPROVALS

Re-Entry Systems Dept^{DIV. OF}
DEPT

LOCATION

PARTS LIST FOR

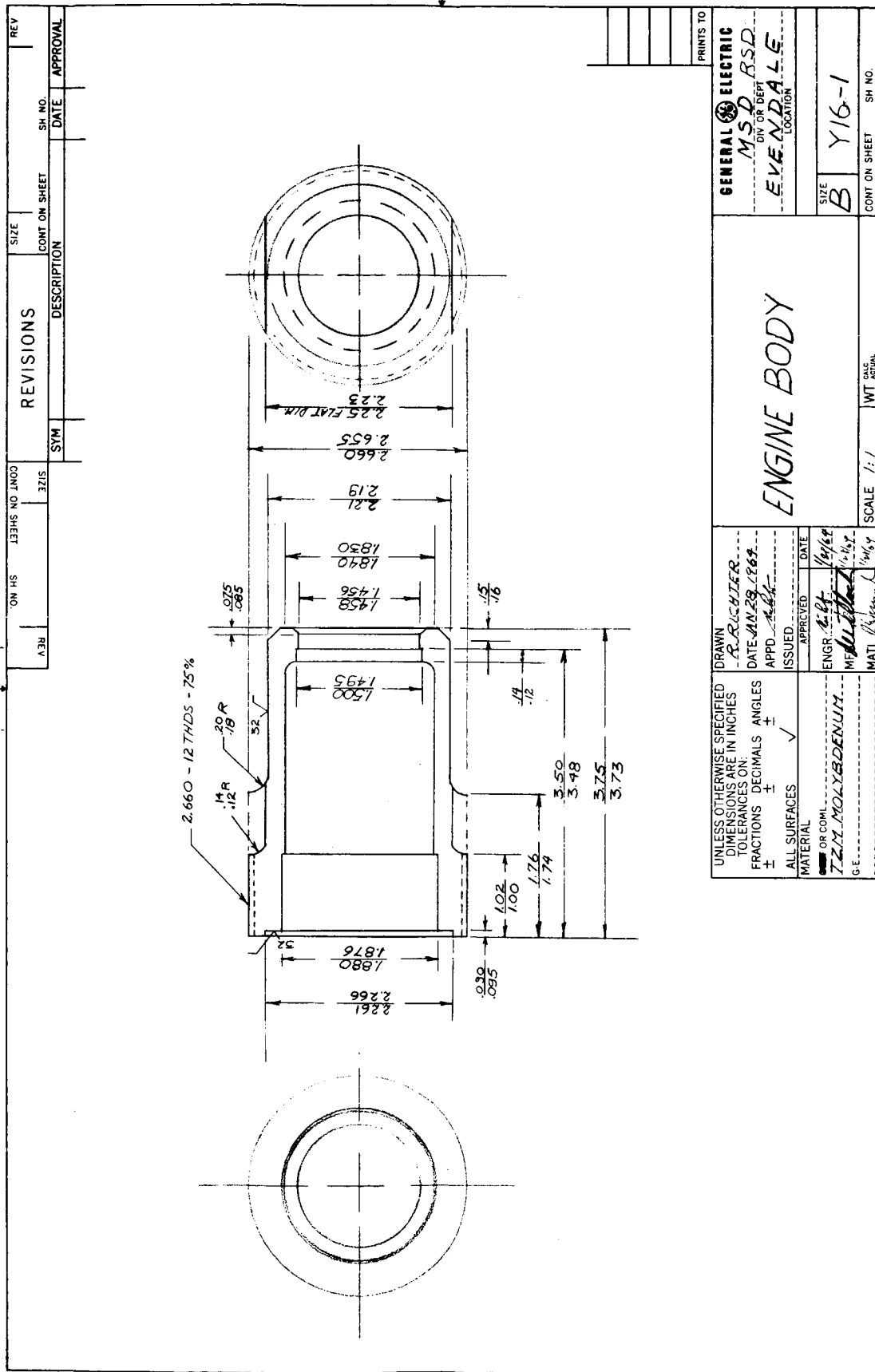
CONT ON SHEET

SH NO.

CODE IDENT NO.

FF-750-L (12-59) Rev.

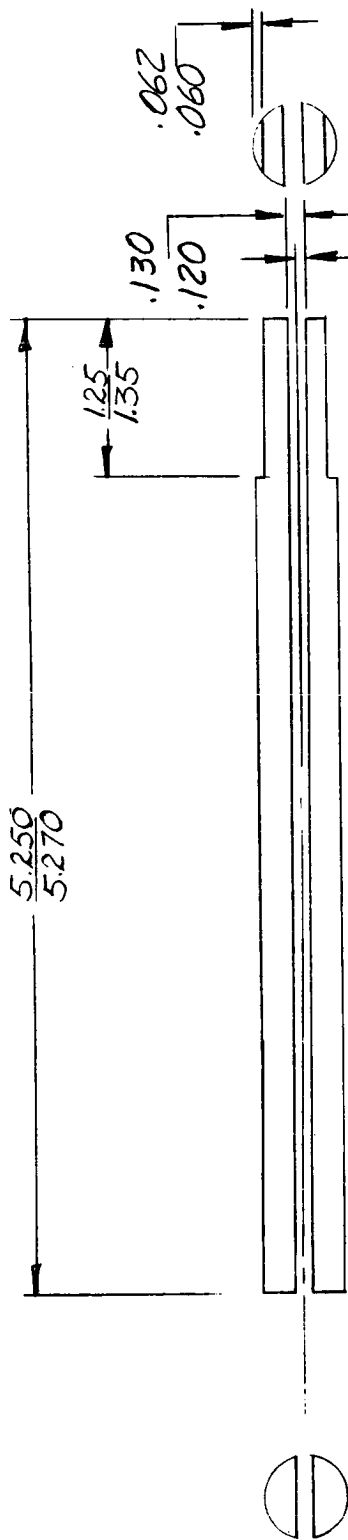
PRINTED IN U.S.A.



REVISIONS		SIZE	CONT ON SHEET	SH. NO.	REV
SYM	DESCRIPTION			DATE	APPROVAL
	2.660- 12 THDS - 75%				
	0.5 0.6				
	1.75 1.85				
	3.005 2.990				
	45°				
	1/4-20 THDS 4 EQ. SP.				
	3/8-16 NC 4 EQ. SP.				

UNLESS OTHERWISE SPECIFIED DIMENSIONS ARE IN INCHES		DRAWN <i>R. RICHTER</i>		DATE <i>2.17.1963</i>	
TOLERANCES ON:		APPROVED		DATE	
FRACTIONS DECIMALS ANGLES		ENGR. <i>RICHTER</i>		<i>10/10/62</i>	
± ± ±		MFG. <i>RICHTER</i>		<i>11/1/63</i>	
ALL SURFACES ✓		ISSUED		MATERIAL	
MATERIAL		G-E		T.Z.M. MOLYBDENUM	
G-E		SCALE 1:1		WT. CALC. ACTUAL	
CONT ON SHEET		NUT		SH. NO.	
SIZE A		Y16-2			
GENERAL ELECTRIC		MSD RSD		EVENDALE	
DIV OR DEPT		LOCATION			

REV		SIZE		CONT ON SHEET		SH NO.	
REVISIONS		SYM		DESCRIPTION		DATE	
APPROVAL							



① SPLIT ELECTRODE MAKE FROM
.500 DIA ROD

PRINTS TO

UNLESS OTHERWISE SPECIFIED DIMENSIONS ARE IN INCHES TOLERANCES ON:		DRAWN <i>Shirley M. Martin</i>		DATE <i>May 2 1963</i>	
FRACTIONS DECIMALS ANGLES + ± ±		APPD <i>Shirley M. Martin</i>		ISSUED <i>Shirley M. Martin</i>	
ALL SURFACES <i>32</i>		APPROVED <i>Shirley M. Martin</i>		DATE <i>5/3/63</i>	
MATERIAL <i>TUNGSTEN</i>		ENGR <i>Shirley M. Martin</i>		MFG <i>Shirley M. Martin</i>	
<i>HIGH DENSITY</i>		MATL <i>Shirley M. Martin</i>		SCALE <i>1/1</i>	
<i>FINE GRAINED</i>		WT CALC		WT ACTUAL	
<i>99.9 DENSE</i>		CONT ON SHEET		SH NO.	

GENERAL ELECTRIC

SPPS

DIV OR DEPT

LOCATION

PLANT

SIZE

A

SH NO.

Y16-5

SCALE

WT CALC

WT ACTUAL

1 DIA^SB, C, & D TO BE CONC. WITH DIA A WITHIN .005 FIR.

<div style="display: flex; justify-content: space-between;"> <div>REVISIONS</div> <div>SIZE</div> <div>REV</div> </div>		SH NO.	
		DATE	
SYM		DESCRIPTION	
CONT ON SHEET		APPROVAL	

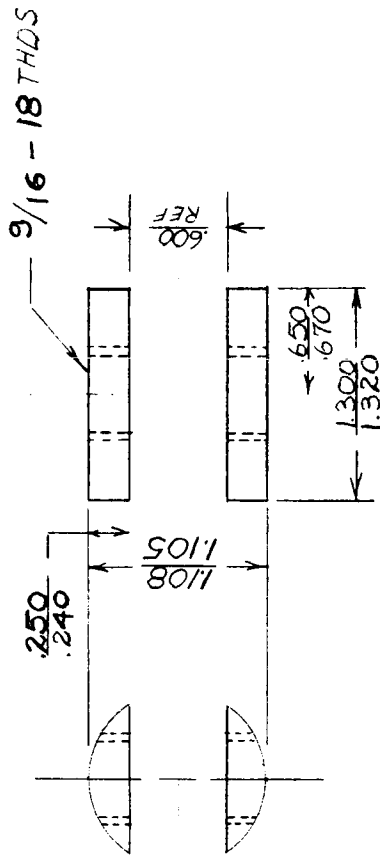
2.125
 2.115
 1.26
 1.24
 .125
 .115
 1.500
 1.498
 DIA A
 1.252
 1.250
 DIA B
 .90 DIA C
 .88
 .040 2 SLOTS
 .030

2. ALL CORNER RADII .00-.02
 1. DIA'S B & C TO BE CONC. WITH DIA A WITHIN .005 FIR.

GENERAL ELECTRIC MSD ASD DIV OR DEPT EVENDALE PLANT LOCATION		SIZE A Y16-7	
VORTEX SLEEVE 30 KW THREE-PHASE ARC JET		CONT ON SHEET SH NO.	
SCALE 1/1		WT CALC ACTUAL	

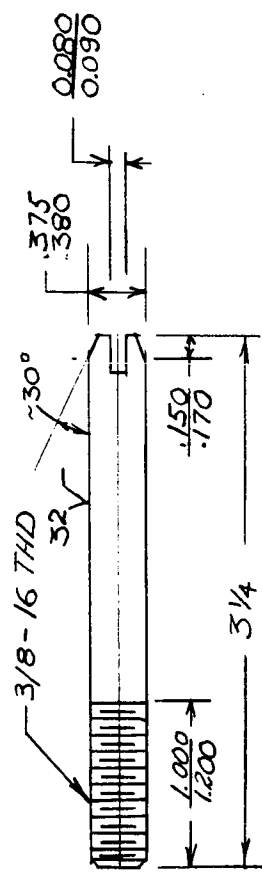
REVISIONS		SIZE	CONT ON SHEET	SH NO.	REV
SYM	DESCRIPTION			DATE	APPROVAL
<div style="display: flex; justify-content: space-between;"> <div> <p>UNLESS OTHERWISE SPECIFIED DIMENSIONS ARE IN INCHES TOLERANCES ON:</p> <p>FRACTIONS DECIMALS ANGLES</p> <p>± ± ±</p> <p>ALL SURFACES ✓</p> </div> <div> <p>MATERIAL</p> <p>GOVT. OR COML. <u>2% THQ. TUNGSTEN</u></p> <p>G-E <u>99.9% DENSE</u></p> </div> </div>					
<p>DRAWN <u>R. RICHIER</u></p> <p>DATE <u>JAN 29, 1964</u></p> <p>APPD <u>WZ</u></p> <p>ISSUED _____</p>		<p>APPROVED _____</p> <p>ENGR <u>WZ</u></p> <p>MFG <u>WZ</u></p> <p>MATL <u>WZ</u></p>		<p>DATE <u>1/25/64</u></p>	
NOZZLE					
<p>GENERAL ELECTRIC</p> <p><u>MSD</u> DIV OR DEPT</p> <p><u>EVEN DALE</u> LOCATION</p>		<p>SIZE <u>A</u></p> <p><u>Y16-8</u></p>		<p>CONT ON SHEET</p> <p>SH NO. <u>1</u></p>	
<p>SCALE <u>1:1</u></p> <p>WT <u>0.130</u></p> <p>ACTUAL</p>		<p>PRINTS TO</p>			

REV		SIZE		CONT ON SHEET		SH NO.	
REVISIONS		DESCRIPTION		DATE		APPROVAL	
SYM							



UNLESS OTHERWISE SPECIFIED DIMENSIONS ARE IN INCHES TOLERANCES ON:		DRAWN R. RICHTER		DATE JUNE 27, 1963	
FRACTIONS	DECIMALS	ANGLES	APPROVED [Signature]	ENGR. RICHTER	DATE 6/27/63
±	±	±	ISSUED	MF [Signature]	DATE 6/27/63
ALL SURFACES	✓			MATL. [Signature]	DATE 6/27/63
MATERIAL					
GOVT. OR COML.					
STAINLESS STEEL 309S					
G-E					
SCALE 1:1		WT. CALC. ACTUAL		CONT ON SHEET SH NO.	
				Y16-9	
				SIZE	
				LOCATION	
				DIV OR DEPT	
				MSD RSD	
				GENERAL ELECTRIC	
				EVENDALE, OHIO	
				PRINTS TO	

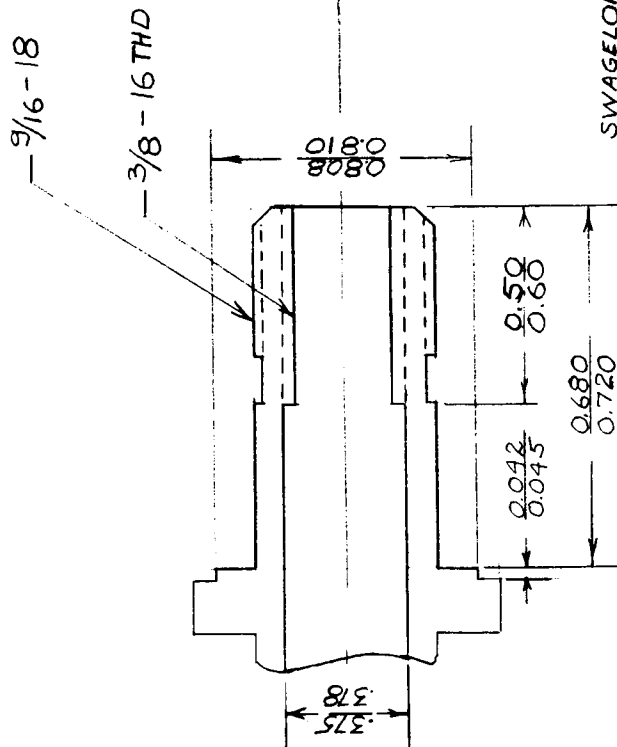
REVISES		SIZE	CONT ON SHEET		SH NO.	RCV
		SYM	DESCRIPTION	DATE	APPROVAL	



UNLESS OTHERWISE SPECIFIED DIMENSIONS ARE IN INCHES TOLERANCES ON: FRACTIONS DECIMALS ANGLES ± ± ± ALL SURFACES ✓ MATERIAL GOVT. OR COML. STAINLESS STEEL G.E. 300 SERIES	DRAWN <i>R. RICHTER</i>	GENERAL ELECTRIC	
	DATE <i>11/19/64</i>	<i>M.S.D. ASD</i> DIV OR DEPT	
	APPD <i>Self</i>	<i>EVENDALE OHIO</i> LOCATION	
	ISSUED	SIZE <i>A</i>	
APPROVED <i>Self</i>		CONT ON SHEET	
ENGR. <i>Self</i>		SH NO.	
MFG. <i>Self</i>		Y16-11	
MATERIAL <i>Self</i>		SCALE 1:1	
WT. CALC		WT. ACTUAL	

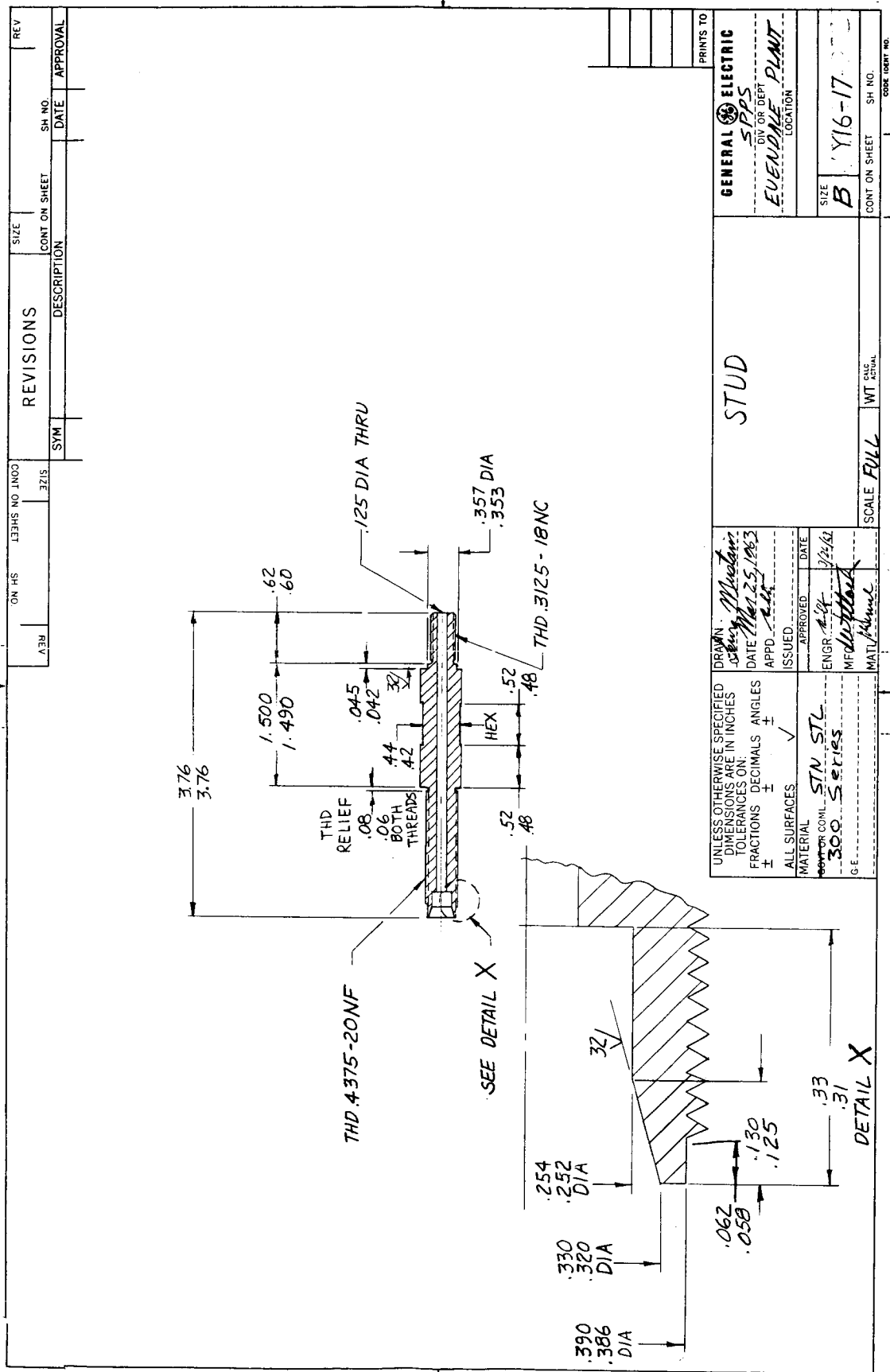
PRINTS TO

REV		SIZE		CONT ON SHEET		SH NO.	
SYN		DESCRIPTION		DATE		APPROVAL	



PRINTS TO

UNLESS OTHERWISE SPECIFIED DIMENSIONS ARE IN INCHES TOLERANCES ON:		DRAWN <i>R. RICHTER</i>		GENERAL ELECTRIC	
FRACTIONS	DECIMALS	ANGLES	DATE <i>JAN 28 1964</i>	MSD	DIV OR DEPT
±	±	±	APPD	<i>Y16-12</i>	LOCATION
ALL SURFACES	✓	ISSUED	ENGR. <i>R. Richter</i>	<i>EKENDALE</i>	
MATERIAL		APPROVED	MFG. <i>W. H. H. H.</i>		
GOVT. OR COM.		DATE	MATL. <i>W. H. H. H.</i>		
STAINLESS STEEL					
G-E 300 SERIES					



REFERENCES

1. Cobine, J. D., and Gallagher, C. J., "New Electrodes for Stabilizing Inert-Gas Welding Arcs", AIEE Transactions, V. 70, 1951, p. 804.
2. Richter, R., "Study of AC Arc Dynamics Stabilization and Starting Criteria", General Electric Company Report No. GE 63FPD283, July 31, 1963.
3. Cobine, J. D., "Gaseous Conductors", Dover Publications, 1958.
4. Somerville, J. M., "The Electric Arc", Wiley, New York, 1959.
5. Kohl, W. H., Materials Technology for Electron Tubes, Reinhold, 1951, p. 457.
6. "Theoretical and Experimental Investigation of Arc Plasma-Generation Technology", ASD-TDR-62-729, Part II, V. 1, Sept., 1963.
7. Jeans, Sir James, An Introduction to the Kinetic Theory of Gases, Cambridge, 1960, p. 47.
8. Vincenti, W. G., Lectures on Physical Gas Dynamics, Stanford Univ. Press, 1961, p. 2.14.